UNIVERSITY OF CALIFORNIA, SAN DIEGO

Influence of atmosphere-ice-ocean interactions on phytoplankton along the coastal Antarctic Peninsula

A dissertation submitted in partial satisfaction of the
requirements for the degree
Doctor of Philosophy

in

Oceanography

by

Mattias Rolf Cape

Committee in charge:

Maria Vernet, Chair
Lihini Aluwihare
Peter Franks
Sarah Gille
Jonathan Shurin

2014

The dissertation of Mattias Rolf Cape is approved, and it is acceptable in quality and form for publication on microfilm and electronically:

_____

_____

_____

_____

_____

Chair

University of California, San Diego

2014

DEDICATION

To Mamma och Pappi,

for always encouraging me to follow my own path,

and teaching me the value of an open mind.

EPIGRAPH

Southwards, a magnificent Alpine country, illuminated by the rising sun,
rose slowly from the sea;
there were mighty fells with snowy crowns and with sharp, uncovered teeth,
around the valleys through which enormous, broad rivers of ice came flowing
to the sea.

—J. Gunnar Andersson

TABLE OF CONTENTS

LIST OF FIGURES

LIST OF TABLES

ACKNOWLEDGEMENTS

This thesis would not have been possible without the continuous support of a tremendous number of individuals through the years, and these meager pages are an attempt to acknowledge all of you. As sure as I have misplaced a certain percentage of my brain while putting together this work, it is also impossible for me to express the depth of my gratitude for all the help, the laughs, shenanigans, discussions, and adventures that have brought me to this point. But, here it goes.

A big thank you to Maria Vernet, my advisor, mentor, and friend, who has guided me through this thesis, months of fieldwork in the Antarctic, and countless scientific meetings in the USA and abroad. From the very beginning she gave me the opportunity to explore my interests in polar research and field work, giving me the freedom to define my own research while always being there to discuss ideas. Her tremendous experience in seagoing polar research has been a source of inspiration, and I'd like to think that I've absorbed a small percentage of that knowledge during my time in her lab. I look forward to more adventures together at the frozen extremes of our planet, or perhaps, sometime, in more tropical locations.

Thank you to my committee for supporting me in this endeavor, and for all the comments during this process. A special thanks goes out to Peter Franks, who through the years has always been available to listen to my questions concerning life and research at SIO. He is a wonderful mentor, passionate about oceanography and genuinely interested in student learning, which is obvious to anyone who has ever taken his classes or met with him. I wish I'd had more time at SIO to extract a bit more of his knowledge, but hope that will come in the future.

One of the primary reasons I started at SIO was because of its community, and there again I have many to thank. Folks at IOD, UCSD Facilities, and the Grad Department were always there to lend a helping hand, be it to fix a freezer, computer,

funding, travel, and so many other daily conundrums we face as grad students. Annika Sanfilippo-Howard was the first to introduce me to research at SIO, for which I'll be eternally grateful. Phil Hastings and the marine vertebrates lab (HJ, Cindy) gave me my start as a wide eyed undergrad, and I'll never forget all the good times keying out fishes, working in the collection, and building GIS databases while listening to Cajun music. Greg Mitchell and the A-team brought me to Antarctica for the first time, encouraged me to keep working in the field, and pick up surfing along the way, both of which were turning points in my life. Corine and Camilla in Maria's lab were so helpful in guiding me through the graduate life while giving me advice for the future and became great friends. I've been lucky to have been a part of the Birch Aquarium at Scripps dive team, an eclectic mix of divers and aquarists all of whom have become both friends and colleagues. Thank you for all the underwater fun, and for putting a smile on my face at every turn.

None of this work would have been possible without the support of the both generous donors (Green Family, Robert Buzelli, Wyer Family), the graduate department, and funding agencies (NSF, NASA) that believed both in my work and our project. Researchers I collaborated with as part of the LARISSA project taught me about a wide array of topics, from geology to glaciology, all of which contributed to this interdisciplinary dissertation. This is also true of my many co-authors, who generously gave their time to improve my thesis chapters.

This thesis is dedicated to my parents, who have shown endless compassion, interest, and support throughout my life. I'll never be able to thank you enough. My whole goofy family has also always been there as a source of laughter and encouragement. The many friends I've made in France, Sweden, at Carlsbad, UCSD, OB, and SIO have all kept me sane, made me laugh, pushed me to keep going with my passions, and helped me put all this work in perspective. A special thanks to Tod Muilenburg who got me

interested in marine science and diving in the first place when I was a high school student. When I started at SIO I was encouraged to talk and work with my fellow students, and that is likely the best advice I ever received. The 2008 BO cohort was an excellent one, and we've had more adventures than pages in this dissertation, some percentage of which involved science. We learned from each other, vented, laughed, and cried, and that has brought us ever closer.

Thank you to one and all, and may the adventures continue.

Chapter 2 was published previously as: Cape, M. R., M. Vernet, M. Kahru, and G. Spreen (2014), Polynya dynamics drive primary production in the Larsen A and B embayments following ice-shelf collapse, *J. Geophys. Res. Oceans*, 119, 572–594. The dissertation/thesis author was the primary investigator and author of this paper.

Chapter 3 is in preparation for publication as: Mattias R. Cape, Vernet, M., Skvarca, P., Marinsek, S., Scambos, T., Domack., E. Foehn winds link climate-driven warming to coastal cryosphere evolution in Antarctica.

Chapter 4 is in preparation for publication as: Mattias R. Cape, Vernet, M. Sensitivity of coastal marine ecosystems to atmospheric processes after ice shelf disintegration.

Chapter 5 is in preparation for publication as: Mattias R. Cape, Vernet, M., Huber, B., Smith, C.R., Ekern, L., Leventer, A. Impacts of ice shelf collapse and sea ice variability on primary production and organic matter export in the NW Weddell Sea.

VITA

2005	National Science Foundation (NSF) Summer Student Fellow, Woods Hole Oceanographic Institution
2005-2006	Undergraduate Research Assistant, Scripps Institution of Oceanography, University of California San Diego
2006	B. A. in Applied Mathematics *magna cum laude* University of California, San Diego
2006	B. S. in Biology: Ecology, Behavior, Evolution *magna cum laude* University of California, San Diego
2006	NSF Summer Student Fellow Scripps Institution of Oceanography University of California San Diego
2006-2008	Staff Research Associate Scripps Institution of Oceanography University of California San Diego
2008-2014	Graduate Student Researcher Scripps Institution of Oceanography University of California San Diego
2014	M.S., Oceanography Scripps Institution of Oceanography University of California San Diego
2014	Ph.D., Oceanography Scripps Institution of Oceanography University of California San Diego

PUBLICATIONS

Gutt, J., M. Cape, W. Dimmler, L. Fillinger, E. Isla, V. Lieb, T. Lundälv, and C. Pulcher (2013), Shifts in Antarctic megabenthic structure after ice-shelf disintegration in the Larsen area east of the Antarctic Peninsula, *Polar Biol*, 36(6), 895–906.

Cape, M. R., M. Vernet, M. Kahru, and G. Spreen (2014), Polynya dynamics drive primary production in the Larsen A and B embayments following ice-shelf collapse, *J. Geophys. Res. Oceans*, 119, 572–594.

ABSTRACT OF THE DISSERTATION

Influence of atmosphere-ice-ocean interactions on phytoplankton along the coastal Antarctic Peninsula

by

Mattias Rolf Cape

Doctor of Philosophy in Oceanography

University of California, San Diego, 2014

Maria Vernet, Chair

Coastal regions of the Antarctic Peninsula (AP) harbor seasonally thriving populations of phytoplankton that contribute significantly to overall Southern Ocean productivity, carbon sequestration via the biological pump, and to the basic survival of higher trophic levels. Although well adapted to their extreme, high latitude environment, phytoplankton are however intimately dependent on variability in the physical environment, which in the last half century has evolved in response to rapid regional climate change. While the impacts of warming on coastal waters have been extensive and well-documented, including the shortening of sea ice seasons, the thinning and acceleration of coastal

glaciers, the freshening of surface water, and the retreat of ice shelves, the consequences of these changes for phytoplankton communities remain largely unknown. In this dissertation I examine the response of phytoplankton to the catastrophic disintegration of the Larsen A and B ice shelves in 1995 and 2002 along the east Antarctic Peninsula (eAP) and the mechanism that control their growth in the newly opened embayment waters. Remote sensing observation, providing a long-term and synoptic view over the eAP marine ecosystem, show that phytoplankton have quickly colonized the formerly dark, ice shelf-covered waters, with rates of primary production rivaling the most productive coastal regions of the Antarctic. The embayments now behave like wind-driven polynyas, whose dynamics are linked to variability in foehn (dry, warm, downsloping) winds resulting from the deflection of synoptic circumpolar westerlies by the AP mountain range. Large-scale fluctuations in climate patterns and synoptic pressure gradients, such as the polarity of the Southern Annular Mode (SAM) and the location of the Amundsen Sea Low (ASL), are critical in determining the frequency of foehn winds, with repercussions on seasonal sea ice cover along the eAP and thereby rates of primary production. Remote sensing and *in situ* observations also demonstrate a strong, persistent cross-shelf gradient in phytoplankton biomass and productivity that is mirrored in the sediments by a gradient in organic matter deposition, implying strong variability in the magnitude of organic matter export out of the euphotic zone across the embayment. These observations are also linked to cross-shelf variability in mixed layer properties, implying spatial heterogeneity in atmosphere-ocean interactions within these systems. These results suggest that atmosphere–ice–ocean interactions control the evolution of the marine ecosystem in the Larsen embayment by impacting phytoplankton processes at the bottom of the food web.

Chapter 1

Introduction

1.1 Background

The Southern Ocean, commonly defined as the region south of the Polar Front, is a critical component of global ocean circulation (Ganachaud and Wunsch 2000), a major site of deep-water formation (Deacon 1933, Orsi et al. 1999), and one of the largest oceanic regions on the planet where macronutrients are underutilized by phytoplankton (a High Nutrient Low Chlorophyll region, or HNLC; Martin et al. 1990). Despite relatively low average rates of net primary production, biological production in the Southern Ocean and the shelf areas around the continent are thought to play a significant role in the drawdown of CO_2 into the deep ocean on the global scale via the meridional overturning circulation (Arrigo et al. 1999, Takahashi et al. 2009). This is especially the case along the continental shelves surrounding Antarctica, where intense phytoplankton blooms and comparatively high levels of primary production occur during the summer (Tréguer and Jacques 1992). At the base of the food web, phytoplankton (particularly diatoms) are also the food source of the Antarctic krill (*Euphasia superba*), themselves the major prey of the charismatic whales in these seas (Hart 1934, Marr 1962). Understanding the

variability of phytoplankton in space and time has therefore long been thought as the key to understanding the Southern Ocean ecosystem.

Of the productive shelf regions, the Antarctic Peninsula (AP), and more precisely the open shelf region of the west Antarctic Peninsula, has been one of the major research foci in recent decades (Ducklow et al. 2007). The Antarctic Peninsula stretches farther north that any other part of the Antarctic, reaching subpolar latitudes near the South Shetland Islands. This leads to a strong N/S climate gradient, and along with its unique oceanographic setting helps make the AP one of the most productive regions in the Southern Ocean (Mitchell and Holm-Hansen 1991, Arrigo et al. 2008). The steep and tall arm of the Antarctic Peninsula also constrains tropospheric circulation, separating the relatively warm and maritime climate on its western side from the cold continental climate of the Weddell Sea to the east (Martin and Peel 1978, King and Turner 2009). Due to these influences, the east coast of the peninsula is approximately 7°C colder than at similar latitudes on the western side (Reynolds 1981), and its shelf tends to be covered by multi-year sea ice even in the summer (Yi et al. 2011).

The Antarctic Peninsula has in the last 50 years undergone rapid regional climate change driven by high rates of atmospheric warming (Marshall et al. 2003, 2006, Vaughan et al. 2003, Steig et al. 2009). This has a resulted in extensive changes in the physical environment, including the acceleration of coastal glaciers (Cook and Vaughan, 2005), changes in the seasonality and decreases in the duration of sea ice (a major structuring force on the Antarctic Peninsula marine ecosystem, Smith et al. 1999, Maksym et al. 2012, Stammerjohn et al. 2008), freshening of coastal regions leading to sea level rise (Meredith and King 2005, Rye et al. 2014) and the deepening of mixed layers (Meredith et al. 2013). A concurrent shift in the Southern Annular Mode (SAM), the dominant mode of southern hemisphere atmospheric variability describing sea level pressure differences between the Antarctic continent and mid-latitudes, towards positive polarity has resulted

in the strengthening of circumpolar westerlies (Marshall et al. 2003, Thompson and Solomon, 2002), with further repercussions on patterns of warming and on the sea ice system (Holland and Kwok 2012). Fluctuations in tropical modes of climate variability, such as El Niño Southern Oscillation, have also been shown to impact processes along West Antarctica and the Antarctic Peninsula specifically (Li et al. 2014, Ding and Steig 2013, Yuan 2004, Stammerjohn et al. 2008).

Because of the close association between environmental fluctuations and biological processes at these high latitudes (Clark et al. 1988, Smith et al. 1999), contemporary research programs have sought to understand the potential consequences of these physical changes on phytoplankton processes, given their importance to the rest of the food web. Along the west Antarctic Peninsula continental shelf, studies have focused on the impact of sea ice changes on patterns of phytoplankton community composition, productivity, biomass, and export out of the surface ocean (Vernet et al. 2008, Montes-Hugo et al. 2009, Ducklow et al. 2007, Smith et al. 1999), providing important insight into the functioning of this ecosystem and the link between climate forcing, water column production, export, and higher trophic levels. By comparison, the eastern coastline of the Antarctic Peninsula has received little attention despite it undergoing extensive physical changes in the last decades.

In 2002, a 3200 km^2 section of the Larsen B Ice Shelf along the Antarctic Peninsula disintegrated in less than one month. This event marked the final chapter in the collapse of the ice shelf, which had started retreating in the 1980s (Scambos et al. 2003). Geological events indicates that it had been present for the last 10,000 years (Domack et al. 2005, Rebesco et al. 2014), tying its retreat to anthropogenic climate change. Although high rates of warming have been noted along large portions of the Antarctic Peninsula, warming along its eastern side bordering the NW Weddell Sea and the Larsen area has been proportionally larger due to the orographic influence of the

Antarctic Peninsula mountain chain on atmospheric circulation patterns (Marshall et al. 2003). Deflection of stronger incoming westerly flow over the peninsula has led to the advection of warm maritime air, further warmed by latent heat release and adiabatic descent from higher atmospheric levels, leading to a foehn effect with warm, dry winds more frequently seen on the east side (Orr et al. 2008, van Lipzig et al. 2008). Extensive melting over the ice sheet caused by these winds is thought to then have contributed to the retreat and collapse of the Larsen B (van den Broeke 2005, Scambos et al. 2003).

While imposing in its rapidity and scale, the disintegration of the Larsen B is not unique along the Antarctic Peninsula, with retreats of two other ice shelves along the eastern Peninsula in the last half century, the Larsen A and Prince Gustav ice shelves (Rott et al. 1996, Cooper et al. 1997, Vaughan and Doake 1996, Skvarca et al. 1999), as well as numerous others along the west Antarctic Peninsula (Cook and Vaughan, 2010). Retreat and removal of ice shelves can have important consequences due to their fundamentally altering physical process in coastal regions. Following ice shelf collapse, acceleration of coastal glaciers has led to increased glacial input into coastal embayments and fjords (Rignot et al. 2004, Shuman et al. 2011, Berthier et al. 2012), further exacerbating the negative ice sheet mass balance noted along the West Antarctic (Rignot et al. 2008). Dark waters previously covered by hundreds of meters of permanent glacial ice are now open to the influence of surface ocean circulation, wind, and the seasonality of sea ice, marking a change in the very coastline of the Antarctic (Ferrigno et al. 2008). With solar irradiance now able to reach surface waters during the austral summer in years of low sea ice cover, primary production becomes possible, along with a possible restructuring of the marine ecosystem in this region.

The breakup of the Larsen A and B ice shelves followed a rapid, intense period of climate warming that is still ongoing and will likely induce the breakup of more shelf area in the future. All these systems—glacial, geologic, biologic, and oceanographic,

continue to evolve responding to the climate forcing and strong inter-system feedbacks. The response of the marine ecosystem, and specifically phytoplankton communities, to this rapid evolution in coastal atmosphere-ice-ocean processes has however not received due attention, with only a select few studies investigating the response of biological communities to this forcing despite the potentially far-reaching impacts of similar ice shelf retreats around the Antarctic continent (Bertolin and Schloss 2009, Peck et al. 2010, Gutt et al. 2011, Sañe et al. 2001). Coastal regions along the Antarctic Peninsula, at the interface between the ice sheet and ocean, have in general remained poorly studied, despite their potentially important role as biological hotspots in the Southern Ocean marine ecosystem (Nowacek et al. 2011, Grange and Smith 2013). The sudden changes in the Larsen A and B systems provide a perfect opportunity for studying the dynamic response of Antarctic systems and polar ocean-ice systems to modern and future warming.

The overarching goal of this dissertation, a component of the larger LARISSA project (Larsen Ice Shelf System, Antarctica), is to understand the response of phytoplankton productivity and biomass to the removal of the Larsen A and B ice shelves, gain insight into the processes influencing their growth in the sea-ice dominated setting of the NW Weddell Sea, and in so doing examine the potential consequences of these biological patterns for higher trophic levels

1.2 Organization of the dissertation

Chapter 2 provides a long-term view of the evolution of the Larsen embayment by analyzing remote-sensing observations of phytoplankton productivity and open water area between 1997 and 2010. These observations are complemented by atmospheric reanalysis model output, which demonstrate the importance of westerly winds in driving opening of the embayment. This chapter was published in 2014 in the *Journal of Geophysical*

Research-Oceans (Cape et al. 2014).

Chapter 3 describes the variability in westerly foehn winds near the Larsen B embayment derived from automated weather stations records. Trends in both surface temperature and foehn frequency are described and linked to climate indices and synoptic circulation. These results are further tied to surface ice sheet melting and the collapse of the ice shelf. The contents of Chapter 3 are in preparation for publication.

Chapter 4 intertwines the analysis of satellite-derived phytoplankton primary production, coastal sea ice cover, and foehn winds to quantify the importance of atmosphere-ice-ocean interactions to phytoplankton dynamics. The contents of Chapter 4 are in preparation for publication.

Chapter 5 reports results from biological, chemical, and physical shipboard sampling of the Larsen A embayment during March-April 2012. Hydrographic patterns observed during the cruise are discussed in context with satellite observations to derive general characteristics of phytoplankton growth and organic matter export. The contents of Chapter 5 are in preparation for publication.

Chapter 6 summarizes findings from the previous chapters and discusses future directions.

Chapter 2

Polynya dynamics drive primary production in the Larsen A and B embayments following ice shelf collapse

2.1 Abstract

The climate-driven collapses of the Larsen A and B ice shelves have opened up new regions of the coastal Antarctic to the influence of sea ice resulting in increases in seasonal primary production. In this study, passive microwave remote sensing of sea ice concentration and satellite imagery of ocean color are employed to quantify the magnitude of and variability in open water area and net primary productivity (NPP) in the Larsen embayments between 1997 and 2011. Numerical model output provides context to analyze atmospheric forcing on the coastal ocean. Following ice shelf disintegration the embayments function as coastal, sensible heat polynyas. The Larsen A and B are as productive as other Antarctic shelf regions, with seasonally averaged daily NPP rates reaching 1232 and 1127 mg C m^{-2} d^{-1} and annual rates reaching 200 and 184

g C m^{-2} yr^{-1}, respectively. A persistent cross-shelf gradient in NPP is present with higher productivity rates offshore, contrasting with patterns observed along the West Antarctic Peninsula. Embayment productivity is intimately tied to sea ice dynamics, with large interannual variability in NPP rates driven by open water area and the timing of embayment opening. Opening of the embayment is linked to periods of positive Southern Annular Mode and stronger westerlies, which lead to the vertical deflection of warm, maritime air over the peninsula and down the leeward side causing increases in surface air temperature and wind velocity. High productivity in these new polynyas is likely to have ramifications for organic matter export and marine ecosystem evolution.

2.2 Introduction

In the past 50 years,the Antarctic Peninsula (AP) has undergone rapid regional climate change, with a warming of both air and sea that has significantly impacted cryosphere dynamics (Vaughan and Doake, 1996, Cook et al. 2005, Marshall et al. 2006, Cook and Vaughan, 2010, Stammerjohn et al. 2012). Stronger westerly winds associated with a positive Southern Annular Mode (SAM) are thought to have contributed to increases in air temperature and meltwater fluxes along the northeast Antarctic Peninsula, ultimately leading to the collapse of both the Larsen A and B ice shelves (Skvarca et al. 1999, Thompson, 2002 , Orr et al. 2004 , Scambos et al. 2004 , van den Broeke et al. 2005). These events precipitated changes in cryosphere-ocean dynamics in the NW Weddell Sea, including the acceleration of coastal glaciers (Rott et al. 2002, Glasser et al. 2011), and possibly changes in coastal ocean circulation and sedimentation rates as well as the opening of large coastal regions to the influence of sea ice.

The Larsen A ice shelf, continuously present since the Little Ice Age approximately 600 years before present after advancing and retreating three times during the

Holocene (Brachfeld et al. 2003), covered approximately 4000 km^2 in 1961 but retreated incrementally until January-February 1995, when the final major collapse of the ice shelf occurred (Rott et al. 1996). The Larsen B ice shelf, which had been present throughout the Holocene (approximately 10,000 years) (Domack et al. 2005), covered 12,000 km^2 in 1963 and continued to advance until the early 1990s (Ferrigno et al. 2008a, Cook and Vaughan, 2010). It then proceeded to retreat much like the Larsen A until 2002 when 3250 km^2 of the ice shelf disintegrated (Scambos et al. 2000, 2003).

The Larsen embayments are now transitioning to a more dynamic state as part of the seasonal sea ice zone (Tréguer and Jacques, 1992). Structuring the timing, magnitude, and spatial extent of blooms, sea ice serves as a major physical forcing on phytoplankton at these latitudes (Smith et al. 1995, Stammerjohn et al. 2012). Once permanently dark waters are now seasonally exposed to the atmosphere and solar irradiance in the absence of heavy ice cover, making phytoplankton growth possible. Within the sea ice zone, primary production can be limited by light (Mitchell et al. 1991), micronutrient availability (Martin et al. 1990b , Boyd, 2004 , Boyd and Ellwood, 2010) or zooplankton grazing (Walsh et al. 2001). Along the coastal Antarctic Peninsula, where macro and micronutrients are thought abundant (Martin et al. 1990a), phytoplankton blooms and spatial gradients in primary productivity may be controlled by water column stability primarily via freshwater input from coastal glaciers and sea ice melt (Smith and Nelson, 1986 , Mitchell et al. 1991 , Tréguer and Jacques, 1992 , Klinck, 1998 , Dierssen et al. 2002 , Garibotti et al. 2003). Shallow summer mixed layers, along with the potential seeding of the water column by sea ice algae as the ice retreats, can enhance phytoplankton growth (Ackley and Sullivan, 1994). Similar dynamics are thought to occur along the eastern Antarctic Peninsula (EAP) where in the absence of the ice shelf, freshwater from the tidewater glacier is expected to spread along the sea surface during the spring and summer, increasing stratification (A. Gordon, personal communication). Melting of

retreating sea ice would reinforce this stratification, and during the period of highest air temperature and incident light in the summer, could be conducive to phytoplankton growth.

Despite extensive seasonal ice cover and relatively low average rates of annual net primary productivity (Arrigo et al. 2008a), biological production in the Southern Ocean is thought to play an important role in the drawdown of CO_2 into the deep ocean via the meridional overturning circulation (Takahashi et al. 2009). This is especially the case along the continental shelves surrounding Antarctica, where intense phytoplankton blooms and comparatively high levels of primary production occur during the summer (Arrigo et al. 2008b). The seasonal presence of phytoplankton as a potential new source of organic carbon marks an abrupt change in the marine ecosystem, which is hypothesized to increase carbon export to the deep ocean and potentially serve as a negative feedback to climate change (Bertolin and Schloss, 2009, Peck et al. 2010, Shadwick et al. 2013).

While the ecological effects of atmospheric warming and changes in the seasonality of sea ice cover are well documented along the open West Antarctic Peninsula (WAP) shelf (Stammerjohn et al. 2008, Vernet et al. 2008, Montes-Hugo et al. 2009), few studies have been undertaken along the AP's eastern coastline (Bertolin and Schloss, 2009, Gutt et al. 2011, 2013, Sañe et al. 2011b, 2012, 2013). These new waters now appear to be biologically active, perhaps contributing significantly to Weddell Sea production on an otherwise ice-covered continental shelf. Sedimentation in the Weddell Sea can be very high (1200 mg C m^{-2} d^{-1}), with as much as 8–15% of daily primary production caught in sediment traps (Froneman et al. 2004). This downward carbon flux depends on grazer community structure and phytoplankton cell-size distribution (Fischer et al. 2002). This new state of the cryosphere along the EAP may therefore have important consequences for habitat use by higher trophic levels and the evolution of the benthic communities below the former ice shelves (Gutt et al. 2011, 2013).

Following the demise of the ice shelves, we hypothesized that the previously ice-covered waters of the Larsen B embayment now support a thriving photosynthetic autotrophic community, with production rates similar to other productive areas of the Weddell Sea. We also expected that sea ice would be a major physical forcing on phytoplankton growth by both limiting the area over which production can occur and temporally constraining production depending on the timing of retreat. In this study we address the follow- ing questions: (1) what are the long-term patterns of phytoplankton production in the Larsen embayments, (2) how do spatial and temporal patterns of phytoplankton relate to fluctuations in sea ice cover and open water area, (3) how do sea ice dynamics relate to atmospheric conditions and climate forcing, and (4) are the Larsen embayments important sites for carbon fixation and potentially export? For this purpose we analyze remote sensing data for ocean color and sea ice concentration combined with atmospheric reanalysis data sets between 1997 and 2011 to describe phytoplankton variability in relation to environmental forcing. In doing so, we give the first estimate of inter-annual water column phytoplankton production for these embayments, thereby evaluating the possible contribution of this new production to carbon export and providing a baseline for future marine ecosystem studies of the NW Weddell Sea.

2.3 Methods

2.3.1 Study area

The Larsen A and B embayments lie in the Northwest Weddell Sea, near the tip of the Antarctic Peninsula. In order to characterize spatiotemporal variability in phytoplankton in this region we considered three sectors (Figure 2.1). These included the Larsen A (4262 km^2) and Larsen B (7473 km^2) embayments separately as well as a larger sector within the coastal Northwest Weddell Sea (91,049 km^2). We defined the western

boundary of these regions by the Antarctic coastline using the most recent Mosaic of Antarctica provided by NSIDC (MOA, http://nsidc.org/ data/moa/, Scambos et al. 2007), modified using a 1997-2011 ocean color composite to account for the further retreat of the ice shelves since the compilation of MOA in 2006. The Larsen A embayment was delimited to the east by a line joining the tip of Cape Longing and Robertson Island, which corresponds approximately to the extent of the ice shelf in 1961 (Ferrigno et al. 2008b). Similarly, the eastern boundary of the Larsen B embayment was defined by a line joining the tips of Cape Framnes and Robertson Island, corresponding to the ice shelf extent in 1995 (Ferrigno et al. 2008a). The NW Weddell Sea region extends from 63.5°S to 68°S and 56°W to the East. Satellite data sets were mapped to an equal-area projection with a pixel size of 1 km^2 encompassing 60° to 68°S and 50°W to 68°W. While the Larsen A ice shelf had retreated almost to its final position by 1997, the start of this study, the Larsen B experienced further retreat in 1999, 2000, and 2002. Presence of this remaining ice shelf is therefore taken into account in the analyses below.

2.3.2 Net Primary Productivity (NPP)

Net primary productivity for the period of October-March 1997-2011 (late spring-early fall, termed seasonal in the remainder of the manuscript) was calculated using satellite-derived daily images of chlorophyll-a and photosynthetically available radiation as inputs into a depth-integrated primary production model (Dierssen et al. 2000). This model uses the structure of the standard Vertically Generalized Production Model (VGPM) (Behrenfeld and Falkowski, 1997) to calculate net primary productivity in the euphotic zone (NPP) based on a photoadaptive variable (P^B_{opt}), daylength (D), surface chlorophyll-a concentration measured via satellite (C_{sat}), euphotic-zone depth (Z_{eu}), and an irradiance-dependent function (F):

$$NPP = P^{B}_{opt} D C_{sat} Z_{eu} F \tag{2.1}$$

Coefficients for the model have been parameterized to field data collected from the West Antarctic Peninsula (Dierssen et al. 2000), with

$$F = \frac{E_d(0^+)}{E_d(0^+) + 11.7} \tag{2.2}$$

$$Z_{eu} = 48.8 C_{sat}^{-0.36} \tag{2.3}$$

$$P^{B}_{opt} = 1.09\, mg\, C\, mg\, chl^{-1}\, h^{-1} \tag{2.4}$$

$E_d(0^+)$ corresponds to satellite-derived photosynthetically available radiation. Daily and monthly maps were generated for further analysis. Details on individual inputs to the model appear below.

We generated a time series of daily, depth integrated NPP by averaging all available cloud-free pixels within each region in daily images. The mean, seasonally averaged proportion of days with valid satellite data within the embayments was 22% with significant inter-annual variability due primarily to variability in sea ice and cloud cover (minimum 0%, maximum 50%). For days with no valid data, linear interpolation using neighboring points was used to estimate NPP. Annual primary productivity was then calculated by integrating the daily time series over the 1 October to 31 March period for each season and within each region. Similarly, total annual primary production was estimated by multiplying the estimated daily depth integrated NPP by daily open water extent, and integrating over each season.

2.3.3 Chlorophyll-a (chl-a)

Daily maps of surface chl-a concentrations were generated from ocean color data collected by MODIS Aqua (R2012.0) and SeaWiFS (R2010.0) and distributed by NASA (http://oceancolor.gsfc.nasa.gov). Chl-a concentrations were calculated using the maximum band-ratio algorithms for MODIS (OC3M) and SeaWiFS (OC4v4) (O'Reilly et al. 1998, 2000). Because extensive changes in the Antarctic coastline due to ice shelf collapse have not been integrated in the standard NASA ocean color processing, land masks erroneously omit valid pixels within approximately 120 km of the coast in regions previously covered by ice shelf. Therefore, we generated images of chl-a concentration at 1 km resolution for the Larsen A and B regions by reprocessing L1A data to L2 using the standard ocean color processing flags in SeaDAS (http://seadas.gsfc.nasa.gov) omitting the land mask. This data set was merged with L2 daily chl-a images using Windows Image Manager (WIM) software (http://www.wimsoft.com) for the wider Antarctic Peninsula to generate daily, regional maps at 1 km resolution over the entire study area.

2.3.4 Photosynthetically Available Radiation (PAR)

PAR was calculated from MODIS and SeaWiFS using standard NASA algorithms. Daily, merged composites at 1 km resolution were generated from both reprocessed L1A and L2 data sets following the processing scheme outlined for chl-a. These images were then spatially binned to 9 km resolution.

2.3.5 Sea Ice Concentration and Open Water Area

As with ocean color processing, standard sea ice products fail to integrate recent changes to the Antarctic coastline caused by the retreat of ice shelves. In this study, daily measurements of sea ice concentration on a 6.25 km grid were calculated from

the 89 GHz channel of the Advanced Microwave Scanning Radiometer-Earth Observing System (AMSR-E) sensor (University of Hamburg, ftp://ftp-projects.zmaw.de/seaice/AMSR-E_ASI_IceConc/tmp_no_landmask/). To complement the time series prior to the launch of AMSR-E in June 2002, we used the lower resolution (12.5 km grid) Special Sensor Microwave Imager (SSM/I) 85 GHz bands. In both cases, sea ice concentration was calculated using the ARTIST (Arctic Radiation and Turbulence Interaction STudy) Sea Ice (ASI) algorithm (Kaleschke et al. 2001; Spreen et al. 2008), which yields ice concentration at higher spatial resolution compared to other standard algorithms (e.g., NASA-Team algorithm).

Previous studies have shown that biases in the calculation of sea ice concentration may result from using different processing algorithms (Andersen et al. 2007). Furthermore, differences in sensor spatial resolution can lead to biases in absolute concentration calculations, particularly near shore where signal from ice-covered land can lead to overestimation of sea ice concentration (Kern et al. 2007; Maaß and Kaleschke, 2010). Instead of using absolute concentration, we calculated open water area based on thresholds of sea ice concentration to estimate the area available for water column primary production. This technique has been used in previous studies and is less sensitive to the algorithm used in the calculation of ice concentration (Comiso and Parkinson, 2008). Because of the different sensor resolutions, we used two different thresholds to estimate open water. Individual pixels were considered open water when sea ice concentration fell below 15% for AMSR-E and 40% for SSM/I. We settled upon different thresholds after comparing the records over the 2002-2011 period of sensor overlap, using the 15% threshold on AMSR-E as a reference data set. We ensured there were no significant differences in seasonal cycles, phase, or amplitude, and that bias between the time series was minimized (see Appendix A). Maps of ice cover processed using this scheme were then used to create time series of daily open water area by summing open water pixels

falling within each region. From these we also created seasonal maps of the total number of open water days by summing the number of days when each pixel could be considered ice-free between October 1 and March 31. Scattered ice floes or very thin ice may still be present in these "ice-free" regions due to ice concentrations falling below the thresholds and errors in the ice concentration algorithm. However, during the periods classified as "ice-free," sufficient open water will always be present to allow primary production.

2.3.6 Reanalysis Products

We obtained numerically analyzed monthly atmospheric data sets from the European Center for Medium-Range Weather Forecasts ERA-Interim data set (EMCWF, http://www.ecmwf.int). The data sets use a horizontal grid spacing of approximately 80 km and include surface wind (at 10 m), surface pressure and temperature (at 2 m) as well as geopotential height at 500 and 850 hPa vertical wind velocities. The pressure surface at 850 hPA corresponds approximately to the summit of the Antarctic Peninsula near the Larsen B embayment. Monthly anomalies for these variables were calculated by subtracting the monthly 1997-2011 climatology from monthly maps. Following the approach of van Lipzig et al. (2008) and others, we reduced the monthly anomaly time series to two composites (averages) for the 8 months with the largest and smallest mean open water areas in the Larsen A and B embayments to describe typical, anomalous atmospheric circulation pat- terns associated with extremes in sea ice cover. We then calculated the difference between high and low composites to identify factors that may contribute to the opening of the embayments.

2.3.7 SAM Index

We used the observation-based index provided by Garreth Marshall (http://www.nerc-bas.ac.uk/icd/gjma/sam.html) to characterize the state of the SAM, a dominant mode of climate variability along the Antarctic Peninsula (Marshall, 2003, 2006). Positive SAM values correspond to negative atmospheric pressure anomalies at high latitudes and positive anomalies at low latitude.

2.3.8 Data Analysis

We used the first (last) date where open water area exceeded 15% of the Larsen A and Larsen B embayment areas for three consecutive days between 1 October and 31 March to identify the opening (closing) date of the embayments. Following Stammerjohn et al. (2008), we defined three statistics: open water duration, open water days, and persistence. Open water duration equates to the number of days between the opening and closing date of the embayment. Open water days refer to the number of days between these dates where open water area exceeds the 15% threshold. Open water days can be shorter than open water duration if sea ice advances and retreats more than once between the opening and closing dates. Persistence was then calculated by dividing open water days by open water duration, which gives the percentage of time the embayments were open within the total open water season. Similarly, we defined the start (end) of the phytoplankton growth period by considering the first (last) date when mean NPP in the embayments exceeded (fell below) 0.5 g C m^{-2} d^{-1} for three consecutive days. This corresponded approximately to the date when chl-a concentration in surface waters exceeded 1 mg m^{-3}. We refer to these dates as defining the timing of phytoplankton blooms in the remainder of this manuscript. Bloom duration corresponds to the number of days between the start and end dates, while bloom days equals the number of days

between bloom start and end where NPP exceeded the bloom threshold. Persistence was calculated by dividing bloom days by bloom duration.

Two transects were also created in the Larsen A (from 60.34°W, 64.627°S to 53.137°W, 65.753°S) and the Larsen B (from 61.549°W, 65.231°S to 52.826°W, 66.698°S) to examine cross-shelf patterns of primary production. NPP along the transect was calculated using a monthly data set by taking a mean and standard deviation of all valid pixels in a 3 x 3 pixel box surrounding each point along the transect. Neighboring transect points were separated by approximately 1 km.

Results are presented as mean $\pm$ one standard deviation unless otherwise stated. The correlation between two variables was calculated using Spearman's Rank-Order Correlation, and reported as ρ(df) = ρ coefficient, p-value, where df = N-2 and N = number of pairwise cases. Simple linear regression was used as a first order estimate of trends in the data, with results presented as b = regression coefficient when significant, $t_{(df)}$ = t-statistic, p-value, where df = N-2 as above. Statistics were calculated using MATLAB Release 2013a (The MathWorks, Inc., Natick, Massachusetts, USA).

2.4 Results

2.4.1 Patterns of Sea Ice and Open Water

Seasonal and Inter-annual Patterns

Larsen A: While the onset of seasonal open water development exhibits little inter-annual consistency, with initial increases occurring anywhere between 2 October (2001–2002) and 13 March (2003–2004), peak values of open water area tend to occur in January before a rapid decline in March (Table 2.1 and Figure 2.2). On average, the embayment opens on November 22 ($\pm$49.01 days) and closes on March 24 ($\pm$6.45 days),

leading to an average open water duration of 87.43±71.45 days. Open water conditions often do not persist throughout a season, with sea ice cover fluctuating rapidly on the time scale of days. An extreme example can be seen in mid-March 2004, when the Larsen A opened to a maximum size of 2400 km^2 (approximately 56% of the total embayment) over 3 days and rapidly closed over the next 3, leading to a 6 day open water season. Mean open water persistence for years when the embayment is open nevertheless remains high (88.87±11.60%). There is no significant trend in embayment opening date ($\rho(8)$ = 20.94, p = 0.38), closing date ($\rho(8) = -0.56$, p = 0.59), or open water duration ($\rho(12)$ = 0.55, p = 0.59) between 1997 and 2011. However, open water duration is strongly negatively correlated with the opening date of the embayment ($\rho(8)$ = 20.98, $p < 0.001$), indicating that long open water duration tends to occur when sea ice retreats early in the season.

Open water area between October and March averages 1092.48 ± 1042.83 km^2 (Table 2.2), with mean seasonal area ranging from 1 km^2 (1997–1998) to 3092 km^2 (2001–2002). Maximum daily open water area also occurred in 2001–2002 (4011 km^2, Figure 2.2), coinciding with the disintegration of the remainder of the Larsen B ice shelf and a low in NW Weddell sea ice cover (Table 2.2). However, several seasons (1997–1998, 2000–2001, 2007–2008, and 2009–2010) saw no significant opening of the embayment, leading to a pattern where sea ice cover and open water alternate over a 1-3 years period. With this high level of inter-annual variability, we find no significant trend in mean seasonal open water area overall ($t_{(12)}$ = 0.51, p = 0.62). Mean October-March open water area is, however, negatively correlated with the opening date of the embayment ($\rho(8)$ = 20.88, $p < 0.01$).

Larsen B: Due to progressive ice shelf retreat, changes in open water area between 1997 and 2002 in the Larsen B embayment account for both changes in sea ice cover and the removal of permanent ice shelf. Opening of the embayment generally occurs

in early November (November 6 $\pm$ 50.68 days) and closing in mid March (February 21 $\pm$ 47.85 days), leading to shorter open water duration than the Larsen A on average (76.50 $\pm$ 69.30 days, Table 2.1 and Figure 2.3). The closing date of this embayment appears far more variable than the Larsen A (February 21 $\pm$ 47.85 days), although this variability is primarily due to one anomalous season (2009–2010). Overall opening dates for the embayment range from September 29 (2001–2002) to March 15 (2003–2004), while closing dates range from 13 October (2009–2010) to 21 March (1998–1999 and 2008–2009). Markedly short open water seasons occurred in 2003–2004 and 2008–2009, when the embayment stayed open only 3 and 5 days, respectively. Much like in the Larsen A embayment, open water conditions are persistent between October and March, averaging 80.25 $\pm$ 20.50%. Neither embayment opening date ($t_{(8)} = -0.29$, $p = 0.78$), closing date ($t_{(8)} = -0.95$, $p = 0.37$), nor open water duration exhibits any significant trend ($t_{(12)} = 0.45$, $p = 0.66$). Like the Larsen A, open water duration is negatively correlated with the opening date of the embayment ($\rho(8) = -0.76$, $p < 0.05$), though the relation is somewhat weaker.

Mean open water area between October and March ranges between 2 km^2 in 2000–2001 and 3343 km^2 in 2004–2005, averaging 1297.82 $\pm$ 1336.69 km^2 overall (Table 2.2). Reversals in sea ice cover over time scales of days-weeks sometimes lead to multiple peaks in open water area (e.g., 2005–2006). Temporal patterns in the Larsen B largely resemble those of the Larsen A, with high interannual variability and coincident peaks and troughs in open water area. One exception occurred in 2002–2003, when the Larsen A and the rest of the NW Weddell Sea opened later in the season but the Larsen B did not (Figure 2.3). There is no significant trend in open water area over the length of the time series ($t_{(12)} = 1.54$, $p = 0.15$), although a general increase is notable between 1997 and 2005 due to the collapse of the remaining ice shelf. There is also no relationship between mean open water area and opening date ($\rho(8) = -0.32$, $p = 0.37$), unlike the

Larsen A.

Spatial Patterns

The dominant cross and along-shore patterns of seasonal open water appear in Figure 2.4. Duration and extent of open water in the NW Weddell as a whole is severely constrained, with ice cover persisting beyond the shelf break between October 1 and March 31 in most years. The longest open water season overall occurred in 2001–2002, when the whole region experienced ice-free conditions lasting over 140 days. Periods of open water exceeding 60 days are generally constrained to the Larsen embayments as well as south along the Larsen C ice shelf and north of James Ross Island. This is in sharp contrast to the WAP, where ice-free conditions persist for >160 days in most years apart from south of Anvers Island.

Open water duration is comparable between the Larsen A and B when considering averages within the embayments (Table 2.1). Overall maximum open water is found within the embayment rather than offshore, where ice cover is less variable and more extensive (Figure 2.4). On average, open water conditions extend approximately 200–300 km offshore on the leeward side of the peninsula. However, open water within these regions is not spatially coherent and highly variable on an inter-annual basis. While ice-free conditions persist embayment-wide in some years (e.g., 1999–2000 in the Larsen A), they can also be restricted to the southern portions of the embayments. For example, open water lasted upward of 160 days offshore of the Drygalski Glacier in the Larsen A during the 2004–2005 season, while areas farther north saw a significantly shorter ice-free season. A similar pattern appears in the Larsen B in 2006–2007, when coastal waters adjacent to the SCAR Inlet, the remaining portion of the Larsen B ice shelf, stayed open for 120 days while areas farther north and offshore stayed ice free for a maximum of 60 days. In other years, ice-free conditions were restricted offshore near the mouth of the

embayments. This occurred both prior to the breakup of the Larsen B (e.g., 1999–2000), but also in subsequent years in both embayments potentially due to the presence of fast ice occupying a configuration similar to that of the former ice shelves (e.g., 2005–2006).

2.4.2 Climate-Atmosphere-Ice Covariability

Monthly surface (2 m) air temperature composites indicate that the NW Weddell Sea tends to be dominated by a different climate regime than the western side of the AP, but that in months with high open water area the maritime climate of the WAP impinges on the northeastern tip of the peninsula leading to higher average monthly temperatures near the freezing point (Figures 2.5a and 2.5b). The strongest warming signal is focused on the eastern side of the peninsula in the Weddell Sea (Figure 2.5c). Composites of surface air temperature anomaly further confirm that a significant temperature difference exists between months of high and low open water area, and that this difference is asymmetrical about the Antarctic Peninsula (Figures 2.5d–f). Months of extensive open water correspond to warmer than usual temperatures along the northeastern AP, while months with low open water are associated with an average temperature anomaly of less than -1.5°C in the same region. This temperature anomaly difference of over 2°C is centered on the Larsen A and B embayments and extends north to the tip of the peninsula (Figure 2.5f). This is in contrast to the northwestern side of the barrier, where along the WAP only small differences in surface temperature anomaly are apparent. Thus to create this strong localization of the temperature anomaly, stronger sea to air sensible heat fluxes within the embayments likely play a role.

Overall these surface temperature anomalies reflect broader changes in atmospheric properties that lead to increased advection of heat to the northeastern side of the peninsula. During months of high open water, the poleward gradients in sea level pressure and geopotential height at 500 hPa, which generate the polar westerlies, are

stronger than during months of extensive ice cover in the embayments (Figure 2.6). The Amundsen Sea Low, a persistent feature in the Amundsen-Bellingshausen Sea sea level pressure, deepens during open water months while higher than usual sea level pressures dominate the South Atlantic. This results in strengthened polar westerlies with larger northerly component of the wind and an anomalous advection of warmer maritime air across the peninsula (Figures 2.7a–c). These zonal anomalies in cross-peninsula winds extend southward over the Larsen C, but vanish beyond -70°S.

Increased cross-peninsula winds during times of extensive open water in the embayments are also coupled with stronger vertical velocities on either side of the barrier, with negative (ascending) and positive (descending) wind anomalies along the WAP and EAP, respectively (Figures 2.7d–f). These anomalies are focused north of -70°S and limited to within approximately 100 km of the coastline. Such conditions are consistent with the presence of föhn winds along the northeastern AP (see van Lipzig et al. (2008) and references therein). Stronger polar westerlies with an increased meridional component favor the orographic lifting of air masses above and across the peninsula rather than their deflection by the high and steep orography of the Antarctic Peninsula mountain range (flow over versus blocked conditions, respectively (Orr et al. 2004)). As air is lifted over the barrier its humidity and temperature decrease, gradually becoming denser than its surroundings. On the leeward side, the air then sinks, warming adiabatically as it descends (Beran, 2013). This increased air movement results in precipitation and cloud cover along the windward side and decreased cloud cover and dry, warm conditions on the leeward side. This mechanism, known as a föhn effect, therefore results from the interaction between synoptic-scale winds and the local topography of the Antarctic Peninsula. While föhn wind events cannot be resolved in the monthly reanalysis data set, the aforementioned patterns are consistent with increased flow-over conditions during months of low-ice cover.

The months with highest (lowest) open water area used in our composites tended to have positive (negative) SAM index values (Table 2.3), suggesting a link between SAM and open water area in the embayments. When considering the whole monthly time series, we find a moderate positive relationship between SAM and open water area (Larsen A: $\rho(82) = 0.34$, $p < 0.01$; Larsen B: $\rho(82) = 0.38$, $p < 0.01$). There is, however, no significant relationship when consider- ing seasonal averages for both variables (Larsen A : $\rho(12) = 0.23$, $p = 0.28$; Larsen B: $\rho(12) = 0.19$, $p = 0.39$). Using lagged correlations between seasonal open water area and a monthly SAM index smoothed with a 5 month running mean, we find instead a strong, significant relationship between mean October–March open water and a SAM index averaged over the preceding June–October (Larsen A: $\rho(12) = 0.60$, $p < 0.05$; Larsen B: $\rho(12) = 0.75$, $p < 0.01$; Figure 2.8).

2.4.3 Primary Production

Temporal Variability

Larsen A: As in other parts of the Antarctic continental shelf, NPP remains low in October even during years of elevated open water area (e.g., 2001–2002), indicative of light limitation during austral spring (Figure 2.2) (Vernet et al. 2012). Rapid increases in NPP above the bloom threshold of 0.5 g C m^{-2} d^{-1} occur during November (on average November 26 $\pm$ 14.83 days) contingent upon the timing of sea ice retreat (Table 2.4). Although most studies along the Antarctic Peninsula have documented a January maximum in NPP rates, maximal values sometimes exceeding 3 g C m^{-2} d^{-1} occur between December and late February in this embayment before a rapid decline below 0.5 g C m^{-2} d^{-1} in early fall (on average March 11 $\pm$ 7.71 days) even during years of extended open water (e.g., 2001–2002, 2008–2009). Duration of the phytoplank- ton bloom is inconsistent from year to year, lasting on average 67.36 $\pm$ 54.26 days. This is

on average shorter than the duration of open water (87.43 days, Table 2.1), although the difference is not statistically significant (p = 0.58). Advance and retreat of sea ice within a season can lead to successive blooms and multiple peaks in NPP (e.g., 2005–2006, Figure 2.2). Overall the seasonal blooms are persistent, averaging 94.25 $\pm$ 8.27% over the 11 year record. Bloom duration is significantly correlated with open water duration ($\rho(12) = 0.95$, $p < 0.001$). However, there is no statistically significant temporal trend in bloom start date ($t_{(7)} = -0.68$, p = 0.52), end date ($t_{(7)}$ = -1.43, p = 0.20) or duration ($t_{(12)} = 0.19$, p = 0.85) over this time span.

Primary production in the embayment is highly variable on an inter-annual basis, with seasonal cycles in NPP apparent only during the years with an extended period of open water (Figure 2.2 and Table 2.2). Rates of daily depth-integrated productivity are high, averaging 806.26$\pm$668.21 mg C m^{-2} d^{-1} over the length of the time series. Seasonally averaged NPP rates range from 0 (e.g., 2007–2008) to 1232 $\pm$ 870 mg C m^{-2} d^{-1} (e.g., 2001–2002, Table 2.2). Similarly, annual productivity averages 83.24$\pm$67.07 g C m^{-2} yr^{-1}, with a low of 0 (e.g., 1997–1998) and a maximum of 200 g C m^{-2} yr^{-1} in 2001–2002 (Figure 2.9). These values are similar to the NW Weddell Sea as a whole, though the interannual variability is much greater due to the higher proportional year-to-year fluctuations in sea ice cover in the smaller embayments. Total primary production averages 0.195 $\pm$ 0.219 Tg C yr^{-1}, with a minimum of 0 (e.g., 1997–1998) and a maximum of 0.679 Tg C yr^{-1} in 2004–2005. On average the Larsen A accounts for 5.29$\pm$4.49% of the calculated total production of the NW Weddell region while representing 4.68% of the surface area (Table 2.2). Annual and total NPP are positively correlated with open water duration ($\rho(12) = 0.89$, $p < 0.001$ and $\rho(12) = 0.91$, $p < 0.001$, respectively) as well as mean seasonal open water area ($\rho(12) = 0.82$, $p < 0.001$ and $\rho(12) = 0.90$, $p < 0.001$, respectively). Timing of embayment opening appears critical for primary production: both annual and total NPP are negatively correlated with day of

opening of the embayment ($\rho(8) = -0.68$, $p < 0.05$ and $\rho(8) = -0.76$, $p < 0.05$). This is likely due to the strong negative relationship between timing of embayment opening and duration of open water conditions (see section 3.1.1 above).

Larsen B: The seasonal cycle of primary production in the Larsen B embayment resembles that of the Larsen A (Figure 2.3). NPP increases above 0.5 g C m^{-2} d^{-1} generally occur in late November (November 18 $\pm$ 12.73 days), reaching maximum values between November and January before decreasing below this threshold in March (March 4 $\pm$ 11.42 days, Table 2.4). Maximum rates of primary productivity can reach upward of 3 g C m^{-2} d^{-1}, with multiple peaks possible during a single season (e.g., 2005–2006). Over the length of the record, phytoplankton blooms last on average 60.93$\pm$55.64 days, with multiple blooms tied to the advance and retreat of sea ice (Figure 2.3). As in the Larsen A, phytoplankton bloom duration is shorter than open water duration (61.64 versus 90.79 days, respectively, Tables 2.2 and 2.4), though the difference is not statistically significant ($p = 0.27$). Blooms are also persistent in years when open water conditions allow phytoplankton growth to occur (97.39 $\pm$ 6.10%), with bloom duration also positively correlated with open water duration ($\rho(12) = 0.91$, $p < 0.001$). There is no trend in bloom start date ($t_{(6)} = 0.84$, $p = 0.43$) or duration ($t_{(12)} = 0.51$, $p = 0.62$) over this time span. There is, however, a significant linear trend in bloom end date, with an observed increase of 2 days per year ($b = 2.0$ d yr^{-1}, $t_{(6)} = 2.65$, $p < 0.05$). This trend is dominated by changes occurring during the period of rapid ice shelf disintegration leading to the 2001–2002 season.

Rates of daily primary productivity are high, averaging 825.82$\pm$699.96 mg C m^{-2} d^{-1} and ranging from 0 to 1127 mg C m^{-2} d^{-1} when averaged seasonally (Table 2.2). Annual productivity is also extremely variable, with an alternating cycle of high and low productivity evident between 1997 and 2011 (Figure 2.9). Annual NPP averages 81.60 $\pm$ 68.06 g C m^{-2} yr^{-1} with a minimum of 0 (e.g., 1997–1998) and a maximum

of 169 g C m^{-2} yr^{-1}, which is similar to both Larsen A and the NW Weddell Sea. While fluctuations in integrated primary productivity generally match dynamics in the Larsen A over the length of the record, an exception occurred in 2002–2003 when a lack of open water led to low seasonal productivity (Table 2.2 and Figure 2.3). Until the 2001–2002 austral summer season, a large portion of the Larsen B was still covered by ice shelf leading to reduced seasonal open water area and corresponding to years of lower total production than in the Larsen A. Following the 2002 disintegration of the ice shelf, total production surpassed that of the Larsen A due to the larger seasonal open water area and equal or higher rates of annual productivity (Table 2.2 and Figure 2.9). Total production was zero in 1997–1998, 2000–2001, 2007–2008, and 2009–2010 due to total sea ice cover and reached a maximum in 2004–2005 (0.818 Tg C yr^{-1}) when both open water area and annual primary productivity rate were at their maximum. Average total production between 1997 and 2011 is 0.254 ± 0.293 Tg C yr^{-1}. This represents $6.83 \pm 7.89\%$ of the total calculated NW Weddell production, whereas the embayment represents 8.2% of the NW Weddell spatially. Like the Larsen A, annual and total NPP are positively correlated with open water duration ($\rho(12) = 0.89$, $p < 0.001$ and $\rho(12) = 0.88$, $p < 0.001$, respectively) as well as mean seasonal open water area ($\rho(12) = 0.79$, $p < 0.001$ and $\rho(12) = 0.91$, $p < 0.001$, respectively). Timing of embayment opening is correlated with annual primary production ($\rho(8) = -0.61$, $p < 0.10$), while total NPP shows no significant relationship with opening date ($\rho(8) = -0.45$, $p = 0.19$).

Spatial Variability

There is a seasonally persistent cross-shelf gradient in daily integrated net primary productivity in both embayments in seasons of extensive open water. Monthly NPP along two onshore-offshore transects through the Larsen A and B during two productive seasons, 2001–2002 and 2004–2005, is depicted in Figures 2.10a–d, with spatially averaged NPP

for the entire time series appearing in Figure 2.10e.

In the Larsen A, transects of NPP show a clear onshore-offshore gradient with low-productivity near the coast and relatively higher productivity 100–150 km offshore (Figures 2.10a and 2.10b). This gradient first becomes apparent in November during the rapid increases in overall NPP and often persists until February. A secondary decline in NPP is sometimes observed beyond 100 km. Daily integrated NPP is consistently lower inshore than offshore, where daily NPP rates reach upward of 4 g C m^{-2} d^{-1} in some instances. Variability in daily depth-integrated productivity is also higher offshore. The 2004–2005 austral summer exhibited the highest rates of NPP observed in the NW Weddell Sea between 1997 and 2011 with a maximum NPP of over 5.5 g C m^{-2} d^{-1} occurring 150 km offshore.

A similar pattern is visible in the Larsen B, with a strong, persistent seasonal gradient present throughout most of the growing season. Until the final collapse in 2002, the remnant ice shelf prevented water column production within roughly 40 km of the coast (Figures 2.10c and 2.10d). Nevertheless, NPP still exhibited a strong cross-shore gradient, starting at the remnant ice shelf and increasing offshore (see Domack et al. 2005). This pattern moved shoreward in subsequent summer seasons after the ice shelf disintegrated. As in the Larsen A, rates of daily integrated primary productivity reach upward of 4 g C m^{-2} d^{-1} approximately 100 km offshore, with maximum rates during the 2004–2005 austral summer.

2.5 Discussion

The once ice shelf-covered Larsen embayments now behave like polynyas (Gordon and Comiso, 1988). Their opening is linked to föhn wind dynamics, whereby westerly winds impinging on the AP are forced over the peninsula, ultimately leading to

warm (>0°C), dry winds blowing down the leeward side onto the coastal NW Weddell Sea (Figure 2.7) (Orr et al. 2008; van Lipzig et al. 2008). As in coastal polynyas, the dynamic export of sea ice out of the embayment due to offshore winds likely plays a major role in open water dynamics. However, because of the warm nature of the winds, no new sea ice forms to provide the necessary sea to air heat flux common in latent heat polynyas. Instead, these regions behave much more like coastal sensible heat polynyas. In the traditional sense, the formation of sensible heat polynyas involves the transfer of heat from the ocean to the ice and atmosphere due to wind-driven convection of warm (> -1.9°C) water to the surface. In this case, the transfer of heat to the sea ice and surface ocean comes from the atmosphere due to the larger temperature gradient between air and sea. Warm surface air temperatures resulting from föhn winds, along with increased heat absorption in low-albedo surface waters during periods of increasing solar radiation, then prevent new ice growth in the embayments. This dynamic coupling between synoptic circulation, local topography, regional weather, and sea ice response make these polynyas unique on the scale of the Antarctic.

Much like the Ross and Amundsen Sea polynyas, the Larsen A and B are seasonally productive regions with daily rates of primary productivity often exceeding 1 g C m^{-2} d^{-1} (Figures 2.2 and 2.3)(Arrigo et al. 2003). Extensive open water is prominent only between October and March and sporadic during austral fall and winter (not shown), with large inter-annual variability in both spatial extent and duration (Figure 2.4). Phytoplankton growth is spatially restricted to a relatively narrow coastal area encompassing the embayments and occasionally a coastal lead extending below 66°S latitude along the Larsen C, with annually persistent sea ice offshore. As special cases of sensible heat polynyas, the Larsen embayments are sites of intense atmosphere-ice-ocean interaction linked to extensive biological activity. As seasonal hotspots of water column production in otherwise ice-covered coastal seas, these areas may therefore play a disproportionate

role in the marine ecosystems of the NW Weddell Sea.

2.5.1 Physical Forcing and Atmosphere-Ice-Ocean Interactions

The Antarctic Peninsula stretches farther north than any other part of the continental Antarctic, reaching subpolar latitudes near the South Shetland Islands, leading to a strong north/south climate gradient. Moreover, the tall arm of the Antarctic Peninsula constrains tropospheric circulation and separates the relatively warm, maritime climate on its western side from the cold continental climate of the Weddell Sea in the East (Martin and Peel, 1978; King and Comiso, 2003). Due to these influences, the east coast of the peninsula is on average 7°C colder compared to similar latitudes on the western side, and its continental shelf tends to be covered by extensive annually persistent sea ice (Kurtz and Markus, 2012).

The strengthening of the polar westerlies and increased frequency of flow-over conditions have been linked to higher incidence of surface melting along the ice shelves, which is thought to have contributed to their collapse (Scambos et al. 2000; van den Broeke, 2005). We show here using ECMWF ERA-Interim reanalysis data sets that periods of low sea ice cover in the Larsen embayments are associated with stronger westerly winds and vertical wind velocities on either side of the AP north of $-70°$S (Figures 2.5–7). Increased advection of maritime air over the AP mountain range and the orographically forced downward motion on the leeward side leads to heating and drying of the air mass (föhn effect), favoring positive temperature and negative humidity anomalies over the Larsen A and B area as observed in the monthly ERA-Interim data set. Such conditions are conducive to both the melting and advection of sea ice along the northeast AP coastline. The spatial extent of the atmospheric warming from this study, approximately 200 km from the coast (Figure 2.5), matches that found by van Lipzig et al. (2008), who used a higher resolution model with 14 km grid spacing to

study the relationship between SAM and surface temperature along the northeast AP. It also resembles the spatial extent of open water area on an interannual basis (Figure 2.4), indicating a potential link between this föhn mechanism and coastal Weddell ice cover. Higher monthly surface air temperature anomalies, as observed in our composites, are consistent with the influence of the polar westerlies on the northeast AP and an increased frequency of föhn winds over the Larsen embayments during months of low ice cover (Speirs et al. 2013). Because föhn winds persist on time scales of hours to several days (Speirs et al. 2010), the monthly anomaly data sets used here are, however, insufficient to resolve individual wind events and the underlying mechanism linking westerly winds and the timing of sea ice retreat and advance.

The months with extensive open water used in our composites are associated with SAM^{+}, and vice versa for ice-covered months (Table 2.3), indicating that both atmospheric conditions and sea ice are sensitive to the state of the SAM. The atmospheric patterns and links between large scale climate and regional atmospheric response described in this study are similar to those found in previous climate studies of the northeast Antarctic Peninsula (Marshall et al. 2006; van Lipzig et al. 2008). While the relationship between climate, atmosphere, ice and ocean presented here appears simple when considering composites based on extremes in open water area, we find only moderate month-to-month covariability between open water area and SAM over the full record and no relationship when correlating October–March averages. Instead, the strongest relationship is found between mean October and March open water area and a SAM index averaged over the preceding June–October (Figure 2.8). While the spring and summer seasons are most relevant in terms opening of the embayment and primary production, processes occurring during the winter may also have an impact on the physical structure of the sea ice. Sea ice in the Larsen embayments is likely composed of a mix of both land-fast ice and pack ice formed by the dynamical compaction of pack ice advected

from the Weddell Gyre and the thermodynamic growth of ice *in situ* (Fraser et al. 2013). While cold, quiescent periods as well as onshore winds during fall and winter months would favor rapid sea ice growth, high temperatures and increased wind stress caused by repeated offshore föhn wind events may serve to weaken the sea ice and precondition it for breakup in later months (Arrigo et al. 1998b; Smith et al. 1999 ; Petrich et al. 2012 ; Fraser et al. 2013).

Regional weather patterns along the northeastern AP are sensitive to synoptic circulation as well as local dynamics via the topographic modification of westerly airflow (Figures 2.6 and 2.7). Furthermore, remote sensing and reanalysis data sets confirm that the region of the NW Weddell Sea showing the greatest atmospheric and sea ice response to changes in climate patterns encompasses the area having already undergone ice shelf breakup (Figures 2.4, 2.5, and 2.7). Comparatively little signal is apparent south toward the Larsen C ice shelf, as discussed in previous studies (van Lipzig et al. 2008). Therefore, although we have shown that both Larsen A and B embayments have experienced large increases in production and display intense sea ice dynamics, we do no expect similar changes to occur adjacent to the Larsen C unless the physical forcing on the ice shelf and coastal ocean changes.

2.5.2 Primary Production

Intense phytoplankton blooms and extreme inter-annual variability characterizes primary production along the coastal NW Weddell Sea. Rates of daily integrated primary productivity are both very high and variable, averaging 806.26 $\pm$ 668.21 and 825.82 $\pm$ 699.96 mg C m^{-2} d^{-1} for the Larsen A and B, respectively (Table 2.2). These remote sensing estimates are comparable to other *in situ* measurements from the Weddell Sea. Using nutrient depletion in surface waters relative to the winter water, Bertolin and Schloss (2009) calculated a mean daily productivity rate of 426.54 $\pm$ 6.63 mg C m^{-2}

d^{-1} for the Larsen A embayment in December 1996 following the breakup of the ice shelf. Other studies from the NW Weddell Sea reported rates of 570 to 1140 mg C m^{-2} d^{-1} offshore of the Larsen Ice Shelf (Hoppema et al. 2000) and 180 $\pm$ 440 mg C m^{-2} d^{-1} in a polynya identified along the Larsen C (Arrigo and van Dijken, 2003). These rates are also similar to the Ross Sea, where average productivity rates ranging between 700 and 1820 mg C m^{-2} d^{-1} have been reported (Smith et al. 2011). Individual seasons can be much more productive, reaching upward of 1232 mg C m^{-2} d^{-1} on average in 2001–2002. Averaged annual productivity rates of 86.36 g C m^{-2} yr^{-1} for the Larsen A and 79.27 g C m^{-2} yr^{-1} for the Larsen B further confirm that these are productive shelf regions of the Antarctic, as these rates exceed those reported for the Weddell Sea as a whole (70.2 g C m^{-2} yr^{-1}, (Arrigo et al. 2008a)) as well as Amundsen Sea and Pine Island polynyas (78.8 and 61.3 g C m^{-2} yr^{-1}, respectively (Arrigo et al. 2012)). These results are also higher than the annual primary productivity estimates for other Antarctic coastal polynyas (Arrigo and van Dijken, 2003). Nevertheless, production in the Larsen A and B is characterized by a signifi- cantly shorter and much more variable phytoplankton growth season and open water duration than these other polynyas (Figures 2.2 and 2.3 and Table 2.2).

Total production reaches a maximum of 0.68 Tg C yr^{-1} in the Larsen A and 0.82 Tg C yr^{-1} in the Larsen B (Table 2.2). These values primarily reflect the small size of the embayment rather than low levels of primary productivity, which can reach as high as 200 g C m^{-2} yr^{-1}. Bertolin and Schloss (2009) calculated a total annual production of only 0.07 Tg C yr^{-1} for their 1400 km^2 region of interest in the Larsen A, indicating that the embayment contributes less to the total Weddell Sea production than its spatial share of the region (0.015% of the mean Weddell Sea production and 0.05% of its surface area). Peck et al. (2010) provided another estimate of the contribution of new open water regions resulting from ice shelf breakup, using the annual productivity value of

176 g C m^{-2} yr^{-1} for Arthur Harbor in the WAP to estimate the size of the carbon pool in coastal waters uncovered following ice shelf retreat. Using this rate, the Larsen A and B would be expected to contribute 0.75 and 1.32 Tg C yr^{-1} of new organic carbon biomass, respectively. While the average rate of annual productivity used by Peck et al. (2010) is representative of productive seasons in the embayments, the study does not take into account sea ice dynamics when calculating total production, leading to a large overestimation of production on an inter-annual basis. The single season estimate by Bertolin and Schloss (2009) on the other hand underestimates total production in this region. Using a longer time series, we find that the embayments' contribution to production scales with their relative sizes (Table 2.2), though the exact percentage can vary drastically due to interannual variability in sea ice cover. This indicates that these regions contribute significantly to the overall production of the NW Weddell Sea.

Constraints on Production Estimates

Our NPP dataset gives insight into the development of the marine ecosystem following ice shelf collapse and serves as the first baseline of primary production for these new expanses of open ocean. Utilizing the large spatial and long temporal footprint of ocean color remote sensing, this study highlights the incredible variability of coastal primary production in the surface waters of the Larsen A and B embayments and the tight link between sea ice dynamics and phytoplankton growth. Limitations of remote sensing prevent the retrieval of data below clouds, near the ice edge and coastline, at depths beyond the reach of satellite sensors, and within and below the ice where high rates of primary productivity have also been measured (Ackley et al. 1979). Algorithms used in calculating chl-a and NPP from satellite remote sensing reflectance have also been shown to underestimate these quantities in the Southern Ocean when compared to *in situ* data sets (Arrigo et al. 1998a; Kahru and Mitchell, 2010). Parametrization of

productivity models based on field campaigns and quantification of error is an active area of research (Campbell et al. 2002; Carr et al. 2006 ; Johnson et al. 2013 ; Marrari et al. 2006). While *in situ* matchups are therefore critical to accurately estimate NPP, not enough are available in this region to ground truth our algorithm primarily due to the harsh weather and sea ice conditions that make the area largely inaccessible to research vessels. While these sources of error likely lead to an underestimate of NPP, the high rates of primary productivity presented in this study nevertheless demonstrate that the Larsen A and B are seasonally important sites of carbon fixation on par with the rest of the Wed- dell Sea, the most productive sea ice zone of the Antarctic (Arrigo et al. 2008a).

Ice-Production Covariability

On average primary production increases gradually starting in November, peaking in January before rapidly decreasing in March, similar to growth patterns reported in the literature for other parts of the Antarctic. Yet the striking seasonal and inter-annual variability in open water area in the Larsen area limits production, leading to rates of annual and total primary production varying by three orders of magnitude (Table 2.2). Thus, although productivity is high, variability in sea ice cover is extreme on an inter-annual basis.

There is no apparent linear trend in open water area nor in the timing of opening and closing over the 14 year record, as reported by Stammerjohn et al. (2012) and others, owing largely to extreme inter-annual variability but also to the relative short length of the time series. Similarly, there was no significant trend in primary production between 1997 and 2011 for either embayment, though increases in both yearly and total NPP are notable in the Larsen B following the last major collapse during the 2001–2002 season. These results, and the relative synchrony between the two embayments, indicate that these previously ice shelf covered coastal marine ecosystems react rapidly to the removal

of permanent ice cover, becoming productive as soon as open water is present, and that ensuing dynamics are highly dependent on atmosphere-ice-ocean interactions.

Like other coastal polynyas, higher rates of phytoplankton primary productivity and longer phytoplankton blooms are associated with longer periods and larger extents of open water, indicating that NPP is sensitive to sea ice dynamics. Furthermore, NPP tends to be negatively correlated with date of opening of the embayment, with earlier openings associated with longer open water seasons and higher rates of productivity in the Larsen A. A similar trend is present in the Larsen B, though the relationship is weak due to the presence of the remnant ice shelf up until 2002 and two anomalous seasons during which the embayment opened early but closed only 3–5 days later (Figure 2.3 and Table 2.1). Nevertheless, this relationship runs contrary to what is observed in the sea ice zone along the WAP, where later sea ice retreat is associated with higher rates of primary productivity and phytoplankton biomass (Vernet et al. 2008). There, later seasonal sea ice retreat is thought to lead to shallower mixed layer depths and stronger stratification during periods of increasing day length and sunlight, favoring higher NPP rates than in years of early retreat. This difference, as well as the strong correlation between NPP and open water area and duration, suggests that melting of retreating sea ice plays a comparatively minor role in stratifying the Larsen embayments, and that a relatively shallow and stable mixed layer is present when open water conditions persist.

Primary Production and Mixed Layer Depth

In the Antarctic and elsewhere, mixed layer depth and the stability of the water column are important parameters thought to influence phytoplankton growth (Hart, 1934; Sverdrup, 1953; Mitchell et al. 1991). While along the WAP the retreat of the ice edge in the spring and summer plays an important role in controlling the spatial distribution and magnitude of phytoplankton bloom on the shelf, the same relationship is not present

along the eastern coastline of the AP. This may in part be due to the significant input of fresh water and ice from coastal glaciers. Removal of the Larsen A and B ice shelves has led to rapid and extensive mass losses in all the tributary glaciers feed- ing the embayments (Scambos et al. 2004; Shuman et al. 2011; Berthier et al. 2012), likely contributing to increased input of fresh water into these constrained coastal systems as both glacial melt and solid ice. This input of melt water into the surface ocean would serve to stabilize the mixed layer after sea ice retreat, while increased solar radiation during ice-free days could further intensify stratification by warming the summer mixed layer. Such conditions could in turn promote phytoplankton growth and high rates of primary productivity (Smith and Nelson, 1985, 1986; Mitchell et al. 1991; Sakshaug et al. 1991; Lance- lot et al. 1993; Dierssen et al. 2002).

Glacial and sea ice melt may also supply iron (Fe) to these waters (Sedwick and DiTullio, 1997; Alderkamp et al. 2012 ; Gerringa et al. 2012 ; Lin and Twining, 2012), which could help sustain the high rates of productiv- ity. Although concentrations of Fe in coastal Antarctic waters are not thought to be limiting (Martin et al. 1990b), sustained production in similar polynya-like systems can be iron limited, particularly at the end of the growth season (Sedwick et al. 2000). Glacial input of micronutrients into coastal waters may therefore serve to prolong phytoplankton bloom duration, primarily by pushing back the date of bloom decline. Further field studies are needed to explore the link between melt water dynamics and phytoplankton growth in the Larsen embayments and along the Antarctic Peninsula in general.

Spatial Patterns of Production

While NPP rates and temporal patterns of bloom development observed along the EAP are comparable to the WAP, the spatial patterns of production are asymmetrical about the peninsula. Maximum values of primary productivity are found near the coast

along the WAP, decreasing offshore to a low away from the continental shelf (Vernet et al. 2008). In this study we observe a recurrent pattern of relatively low NPP near the coast increasing to a maximum 100–150 km offshore (Figure 2.10). Previous studies have noted similar patterns in other parts of the coastal Antarctic. A 2005 cruise to the Larsen B embayment noted low surface (7 m) chl-a biomass near the coast associated with relatively lower sea surface temperature and higher sea surface salinity (A. Leventer, personal communication). In the Mertz Glacier Region, a study found a deeper mixed layer near the Adelie Coast and increased stratification offshore which authors linked to atmospheric forcing (Vaillancourt et al. 2003). Phytoplankton biomass in this case reached a maximum near-shore, though authors found evidence of deep mixing and downward advection of cells in this area, which they reasoned might lead to light limitation and over the long run limit production. In the Amundsen Sea, lower chl-a biomass near the Pine Island Glacier was coupled with deeper mixed layers (Alderkamp et al. 2012). In this case, upwelling of Modified Circumpolar Deep Water (MCDW) at the ice shelf-water interface was implicated and thought to limit bloom formation nearshore.

Depressed chl-a biomass and NPP near the coast in the Larsen embayments may be due to similar forcings, such as stronger wind stress on near shore waters leading to deeper mixed layers, or advection of surface waters off- shore and coastal upwelling. Cold, offshore winds draining from the continent may also have a localized effect near-shore due to the decreasing strength of such winds offshore (Bromwich and Kurtz, 1984), leading to localized coastal convective mixing and sea ice formation. Regardless of the exact mechanisms, the cross-shelf pattern of production is a ubiquitous feature observed on daily, monthly, and seasonal time scales. If seasonally persistent throughout the euphotic zone, this gradient may have implication for sedimentation and the distribution of organic matter incorporated in the sediments.

2.5.3 Primary Production and Climate

Despite relatively low average rates of annual net primary productivity, biological production in the Southern Ocean and the shelf areas around the continent plays an important role in the drawdown of CO_2 into the deep ocean via the meridional overturning circulation (Takahashi et al. 2002, 2009; Arrigo et al. 2008b). Recent studies have, however, identified a decreasing trend in carbon uptake in the Southern Ocean (Wang and Moore, 2012). Because the Larsen A and B embayments were covered by ice shelves for the last 600 and 10,000 years, respectively (Brachfeld et al. 2003; Domack et al. 2005), photosynthetic activity in these areas represents new production and potentially a new sink for CO_2.

Bertolin and Schloss (2009) noted intense photosynthetic activity driven mainly by diatoms coincident with $\%O_2$ supersaturation and depletion of CO_2 in surface waters during a 1996 cruise to the Larsen A, hypothesizing that the Larsen A could potentially be a site of seasonal carbon sequestration. We find that locally this new source of primary production is likely to serve as a significant carbon sink, but that the absolute magnitude of the carbon pool as estimated by total annual production is relatively low on the scale of the Antarctic due to the small size of the embayments and the high level of inter-annual variability (Table 2.2). The recent collapses of the Larsen A and B are representative of ongoing changes in ice shelf influenced systems taking place along the entire AP (Cook and Vaughan, 2010). If the retreat of ice shelves continues along the Antarctic Peninsula and elsewhere in the Antarctic, we expect these new regions to be important sites of local and regional organic matter production and export.

2.5.4 Organic Matter Sedimentation and Spatial Patterns of Production

Phytoplankton growth in the embayments marks a new source of organic matter to the marine ecosystem following ice shelf disintegration. Studies in the Ross Sea have indicated that advection of particulate organic carbon below ice shelves can lead to the establishment of thriving benthic communities (Dayton and Oliver, 1977). In the case of the Larsen B, previous studies based on a 2006–2007 cruise to the Larsen embayments showed that significant organic matter export from the upper water column occurred only following the demise of the ice shelf with only limited input of advected organic matter (Sane et al. 2011a, 2011b, 2013; Gutt et al. 2011). Their evidence included a marked change in the dominance of diatoms instead of sponge spicules in the sedimentary inventory of biogenic silica, significant increases in sediment pigment inventories and "fresh" organic matter based on phaeo-pigment to chlorophyll-a ratios, and increases in diatom frustules.

Based on ^{14}C methods, the authors also calculated a sediment accumulation rate of 0.04 cm yr^{-1} following the collapse, which is very low compared to other glacially influenced coastal systems along the WAP (Boldt et al. 2013). The stations sampled during this survey were, however, located close to the coast within the area last uncovered by the breakup in 2002, and may therefore receive less exported organic matter than offshore due to lower overall rates of overlying water column primary productivity (e.g., Figure 2.10). While three productive seasons occurred prior to their sampling (Table 2.2 and Figures 2.2 and 2.3), sea ice cover limited the length of the potential growth period in all seasons but 2004–2005 when the Larsen B embayment as a whole stayed open for upward of 120 days (Table 2.2 and Figure 2.4). In contrast, the longest open water season in 2005–2006 occurred at the mouth of the embayment rather than inshore.

Spatial variability in both seasonal primary productivity and sea ice cover may therefore affect estimates of sedimentation rates and should be taken into account when looking at changes in organic matter export.

Implications for the Marine Ecosystem

Benthic ecosystems are expected to experience a dramatic increase in the flux of organic matter to the sea floor as a consequence of this new water column production. Food availability via the spatially and temporally irregular export of particulate organic carbon from the euphotic zone can serve to structure benthic ecosystems (Smith et al. 2006; McClintic et al. 2008). Gutt et al. (2011), examining benthic community composition and structure during a 2007 cruise, noted evidence of numerous deep-sea taxa at relatively shallow depths (300–800 m) within the Larsen A and B embayments, which they linked to the oligotrophic conditions prevailing prior to ice shelf collapse. They also noted that while the community composition of macro and megabenthic communities resembled that of non ice shelf covered Antarctic seafloor, species richness and density were lower than other parts of the Weddell Sea shelf. Distance from the former ice shelf edge was also found to be the single strongest environmental correlate with megabenthic community structure, giving further evidence that food availability is a primary factor structuring benthic communities in this region. As noted earlier, the relationship between phytoplankton growth and sea ice is highly dynamic in space and time, with strong cross-shelf gradients in phytoplankton production and extreme inter-annual variability in open water area which will affect the timing, quantity, and spatial distribution of organic matter export. Although studies from the WAP have shown that the link between overlying production and benthic ecosystems can be complex (Smith et al. 2006), we nevertheless expect that spatial and temporal variability in productivity within the embayments will have a large impact on the course of benthic

ecosystem evolution, potentially leading to cross-shelf differences in benthic community characteristics mirroring gradients in production, seasonal open water, as well as the history of ice shelf retreat (see Gutt et al. 2013).

2.6 Conclusions

Daily integrated rates of primary productivity in the embayments can be very high, reaching 1232 mg C m^{-2} d^{-1} in the Larsen A and 1127 mg C m^{-2} d^{-1} in the Larsen B on average during the most productive seasons. Much like in the West Antarctic Peninsula, phytoplankton blooms tend to start in November, reaching a peak in January before rapidly decreasing in March. NPP rates show a seasonally persistent cross-shelf gradient opposite that seen along the WAP, with low productivity inshore and maxima near the mouths of the embayments. Depression of NPP near the coast may be due to a deepening of the mixed layer associated with increased wind-driven mixing, sea ice formation, or upwelling, though the exact mechanism remains unclear. Maximum annual productivity rates of 200 and 184 g C m^{-2} yr^{-1} for the Larsen A and B, respectively, exceed those of other productive shelf waters of the Antarctic, including the Amundsen Sea and the Ross Sea. Yet the embayments are characterized by extreme inter-annual variability, with some years showing no measurable production due to the presence of sea ice.

With the collapse of the Larsen A and B ice shelves, the newly uncovered embayments behave like seasonally productive polynyas. Primary production and sea ice dynamics are closely linked, with earlier embayment opening dates corresponding to longer growth seasons and higher productivity rates overall. Though open water dynamics are highly variable seasonally and inter-annually, opening of the embayments tends to occur in late October and closing in late March. Open water is limited to within

200–300 km of the coast, with annually persistent sea ice farther offshore in the Weddell Sea Gyre. The longest open water periods are confined to the southern portion of the embayments near the termini of major coastal glaciers and remnant ice shelves, though some years show maxima offshore due to the presence of a remnant ice shelf or fast ice occupying a similar configuration. With few exceptions, open water dynamics between the two embayments are remarkably similar indicating that a similar forcing is likely acting on the Larsen region north of 67°S.

While the Weddell Sea generally experiences a cold, continental climate, months of extended open water tend to see a more maritime influence along the northeastern coast of the peninsula. Open water months tend to be associated with stronger westerly surface wind flow across the peninsula. Stronger polar westerlies are consistent with positive phases of SAM and the result of a deepening pole- ward pressure gradient, with negative anomalies in the Amundsen-Bellingshausen region and positive anomalies in the South Atlantic. Wind anomalies also correspond to positive temperature anomalies over the NW Weddell Sea centered on the Larsen A and B embayments. These patterns are consistent with a higher incidence of strong, downsloping föhn winds due to the topographic modification of oncoming westerly flow by the steep and tall orography of the peninsula. Because of the influence of these warm winds on the coastal NW Weddell, and the strong sea ice response, the embayments now appear to function as coastal sensible heat polynyas in which both the wind stress and large temperature difference between air and ice/ocean prevent sea ice growth. Though months of high (low) open water are overall associated with positive (negative) phases of SAM, we find only moderate correlation over the entire monthly time series and no correlation when considering seasonal (October–March) averages. Instead, mean October–March open water area is significantly correlated with average winter-early spring (June–October) SAM index. Periods of positive SAM and strong polar westerlies in the winter may lead

to increased frequency of föhn winds, which may structurally weaken the sea ice and precondition it for breakup in the spring.

There is no significant linear trend in either open water area or primary production over the 14 year time series, owing to the high inter-annual variability and relatively short length of the record. With the removal of ice shelves, these embayments have, however, quickly become productive regions of the Antarctic shelf, some years contributing more to total NPP than their spatial share of the NW Weddell Sea surface area. While the absolute magnitude of this new carbon pool is too low to contribute to car- bon sequestration on a global scale and the inter-annual variability in production is extreme, the presence of this new organic matter in the water column and its sedimentation to the benthos are likely to lead to extensive changes in the regional marine ecosystem of the NW Weddell Sea.

2.7 Acknowledgements

The authors thank the collaborators of the LARISSA project, particularly Arnold Gordon for thoughtful comments on polynya dynamics and Ted Scambos for discussions of föhn winds, Alison Cook for providing the historical ice shelf extent data set, the ocean color community for providing insight into data processing and analysis, and two reviewers for helpful comments on the manuscript. This work was supported by the National Science Foundation Office of Polar Programs under NSF grant ANT-0732983. MRC was also supported by the NSF Graduate Research Fellowship under grant DGE-1144086 and by NASA Headquarters under the NASA Earth and Space Science Fellowship Program–grant NNX12AN48H.

This chapter was published previously as: Cape, M. R., M. Vernet, M. Kahru, and G. Spreen (2014), Polynya dynamics drive primary production in the Larsen A and B embayments following ice-shelf collapse, *J. Geophys. Res. Oceans*, 119, 572–594. The

dissertation/thesis author was the primary investigator and author of this paper.

Table 2.1: Open water characteristics for the Larsen A and B embayments. Opening and closing dates listed as day of the year (DOY), with January 1 = 1 and December 31 as 365 (non-leap) or 366 (leap year). Because seasons span more than one year, the opening and closing dates can exceed 365 or 366. For example, an opening day of January 1 would correspond to day of the year 367 if the prior year was a leap year. A dash (-) indicates no data.

	Larsen A					Larsen B				
Year	Opening (DOY)	Closing (DOY)	Duration (days)	Open water days (days)	Persistence (%)	Opening (DOY)	Closing (DOY)	Duration (days)	Open water days (days)	Persistence (%)
1997-1998	-	-	0	0	-	-	-	0	0	-
1998-1999	336	446	110	84	76	336	445	109	44	40
1999-2000	368	446	78	72	92	283	404	121	64	53
2000-2001	-	-	0	0	-	-	-	0	0	-
2001-2002	275	454	179	179	100	272	421	149	139	93
2002-2003	349	460	111	80	72	-	-	0	0	-
2003-2004	437	442	6	6	100	439	441	3	3	100
2004-2005	279	449	170	152	89	277	438	161	129	80
2005-2006	301	459	158	112	71	278	438	160	116	73
2006-2007	302	446	144	131	91	302	423	121	116	96
2007-2008	-	-	0	0	-	-	-	0	0	-
2008-2009	325	447	122	118	97	333	445	112	104	93
2009-2010	-	-	0	0	-	281	286	5	5	100
2010-2011	296	442	146	146	100	301	431	130	97	75
Mean	326.80	449.10	87.43	77.14	88.87	310.20	417.20	76.50	58.36	80.25
SD	49.01	6.45	71.45	65.31	11.60	50.68	47.85	69.30	56.49	20.50

Table 2.2: Seasonal sea ice and primary production statistics for the Larsen A, Larsen B, and Weddell Sea. Data is presented as mean or mean ± one standard deviation.

	Larsen A (4,264 km^2)				Larsen B (7,473 km^2)				NW Weddell (91,049 km^2)			
		Primary production				Primary production				Primary production		
Year	Open water area (km^2)	daily (mg C m^{-2} d^{-1})	annual (g C m^{-2} yr^{-1})	total annual (Tg C yr^{-1})	Open water area (km^2)	daily (mg C m^{-2} d^{-1})	annual (g C m^{-2} yr^{-1})	total annual (Tg C yr^{-1})	Open water area (km^2)	daily (mg C m^{-2} d^{-1})	annual (g C m^{-2} yr^{-1})	total annual (Tg C yr^{-1})
1997-1998	1	0	0	0	34	0	0	0	1531	490±240	54	0
1998-1999	918	856±580	99	0.128	552	592±272	91	0.059	11726	881±626	134	1.797
1999-2000	1084	884±493	120	0.239	904	880±555	116	0.193	16492	1115±743	191	4.157
2000-2001	3	0	0	0.000	2	0	0	0	1194	415±196	63	0.099
2001-2002	3092	1232±870	200	0.679	2443	1013±737	169	0.458	56327	1162±884	199	12.901
2002-2003	1125	537±398	86	0.151	66	268±141	45	0.004	13102	526±328	78	1.366
2003-2004	118	259±129	42	0.005	84	243±101	43	0.003	3526	440±276	77	0.286
2004-2005	2745	1118±770	177	0.606	3343	1127±867	167	0.818	20571	990±794	167	4.541
2005-2006	1118	747±671	137	0.232	2152	976±843	184	0.607	13791	953±674	169	2.827
2006-2007	1459	486±169	77	0.137	2870	557±285	77	0.335	17920	545±297	93	2.079
2007-2008	5	0	0	0	42	0	0	0	3870	633±660	98	0
2008-2009	1269	797±637	120	0.222	2967	930±759	136	0.673	21565	824±720	153	4.703
2009-2010	20	0	0	0.000	95	0	0	0	2970	313±197	59	0.192
2010-2011	2338	589±395	106	0.323	2617	631±369	114	0.404	20635	656±453	122	3.138
Mean	1092.48	806.26	83.24	0.195	1297.82	825.82	81.60	0.254	14658.48	788.00	118.37	2.763
SD	1042.83	668.21	67.07	0.219	1336.69	699.96	68.06	0.293	14172.06	664.40	50.59	3.365

Table 2.3: The eight October - March months with the highest and lowest open water (OW) areas for the Larsen embayments used in creating composites of ERA-Interim datasets. Bold SAM indices indicate departure from the general trend during high and low open water periods.

High-OW	Date	Dec-2001	Dec-2004	Feb-2005	Jan-2005	Feb-2002	Nov-2001	Jan-2002	Feb-2003	mean
	SAM	1.16	-1.02	1.59	1.07	2.80	2.54	2.22	**-0.98**	1.17
Low-OW	Date	Oct-1999	Dec-2000	Feb-2001	Mar-2001	Oct-2002	Oct-2007	Feb-2008	Feb-2010	mean
	SAM	**3.35**	-2.05	-2.70	-0.57	-5.77	-0.86	**1.09**	-2.12	-1.20

Table 2.4: Phytoplankton bloom characteristics for the Larsen A and B embayments.
Phytoplankton bloom characteristics for the Larsen A and B embayments.

	Larsen A					Larsen B				
				Bloom					Bloom	
Year	Start (DOY)	End (DOY)	Duration (days)	Days (days)	Persistence (%)	Start (DOY)	End (DOY)	Duration (days)	Days (days)	Persistence (%)
1997-1998	-	-	0	0	-	-		0	0	-
1998-1999	335	439	104	100	96	321	420	100	100	100
1999-2000	345	444	99	99	100	314	405	92	92	100
2000-2001	-	-	0	0	-	-		0	0	-
2001-2002	315	442	127	116	91	316	428	113	113	100
2002-2003	355	427	72	71	99	-		0	0	-
2003-2004	-	-	0	0	-	-		0	0	-
2004-2005	320	443	123	121	98	324	439	115	111	97
2005-2006	316	432	117	117	100	310	436	126	126	100
2006-2007	323	431	108	81	75	340	432	92	76	83
2007-2008	-	-	0	0	-	-		0	0	-
2008-2009	346	422	77	77	100	344	438	95	95	100
2009-2010	-	-	0	0	-	-		0	0	-
2010-2011	322	438	116	103	89	313	433	120	120	100
Mean	330.78	435.33	67.36	63.21	94.25	322.75	428.88	60.93	59.50	97.39
SD	14.83	7.71	54.26	50.98	8.27	12.73	11.42	55.64	54.82	6.10

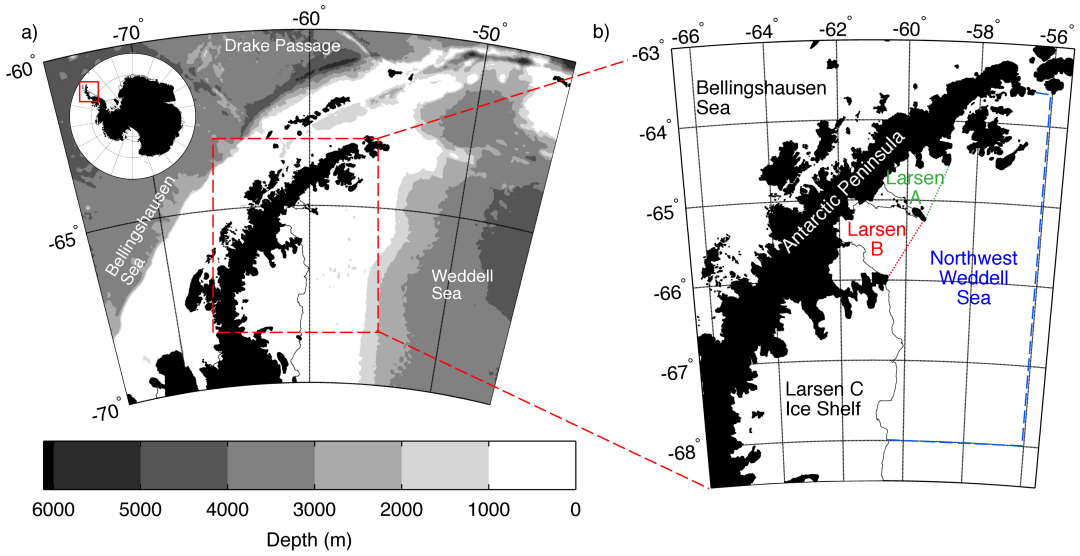

Figure 2.1: Map of the study area depicting (a) the Antarctic Peninsula and (b) the study area along the northwest Weddell Sea. The shelf in this region is 200–300 km wide with an average depth between 500 and 600 m. Areas over which statistics were calculated for the three regions of interest (NW Weddell Sea, Larsen A, and Larsen B embayments) are outlined. Coastlines are taken from Scambos et al. [2007] and bathymetry from Smith and Sandwell [1997].

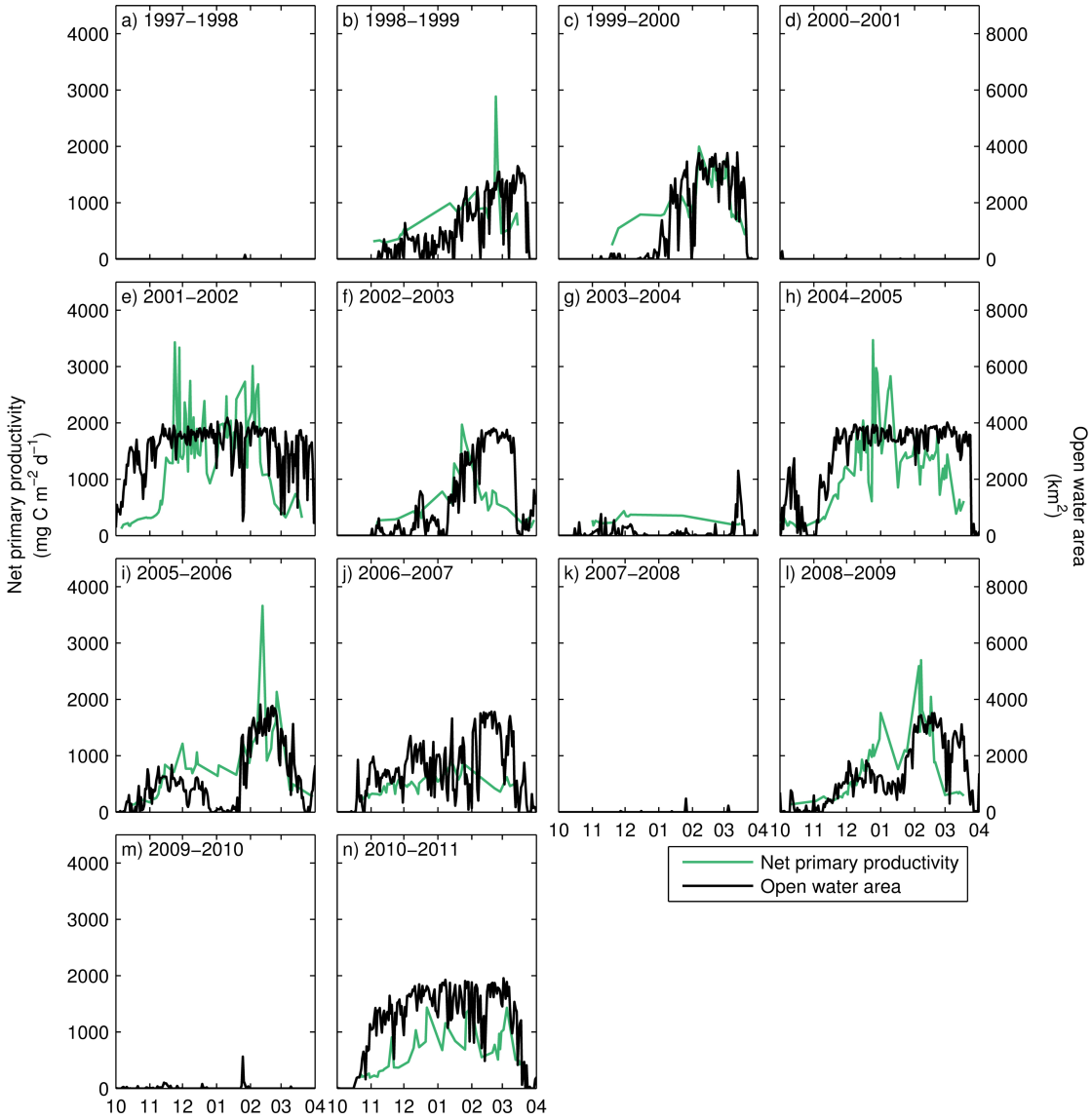

Figure 2.2: Seasonal time series of open water (km^2) area and net primary productivity (mg C m^{-2} d^{-1}) for the Larsen A embayment between 1997 and 2011. Plotted values represent daily averages within the Larsen A region, as indicated in Figure 2.1.

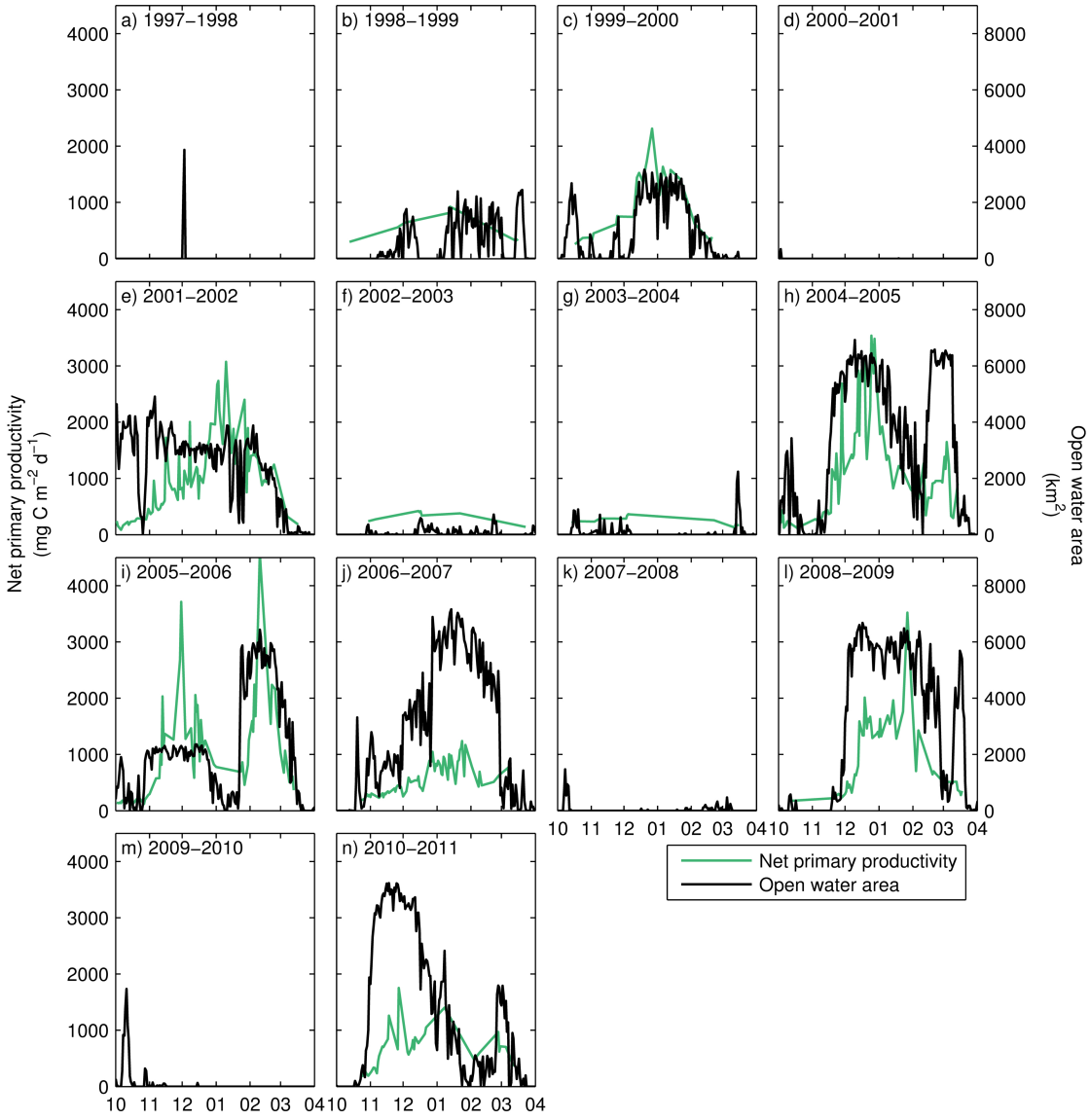

Figure 2.3: Same as Figure 2.2 for the Larsen B embayment.

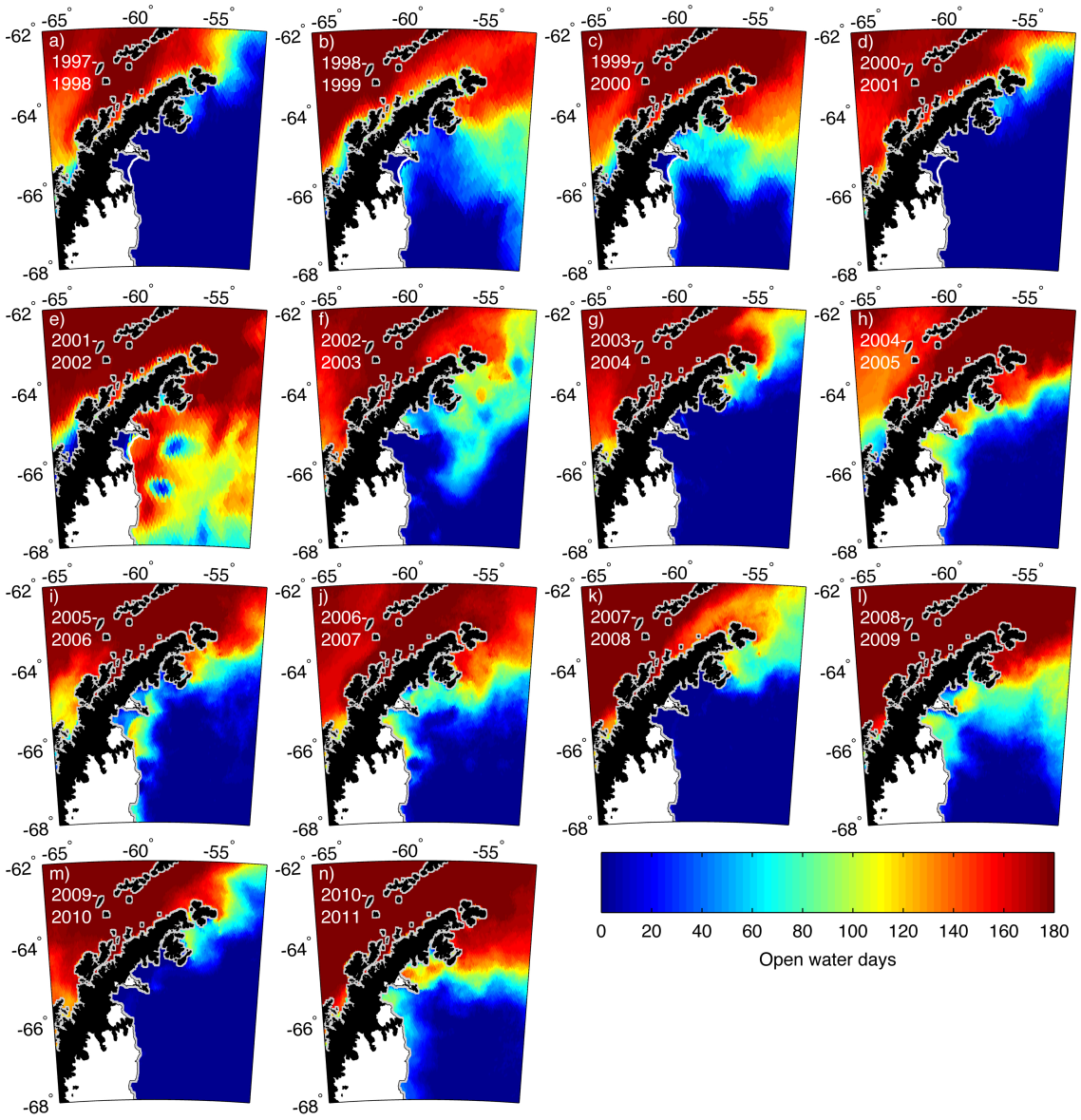

Figure 2.4: Number of open water days, defined as the number of days between 1 October and 31 March of each season when sea ice concentration in each pixel fell below the 40% threshold for SSM/I and 15% threshold for AMSR-E. Pixels within 7 km of the coast have been masked due to potential contamination. The white contour within the Larsen B embayment in (a-e) represents the ice shelf extent prior to the 2002 collapse.

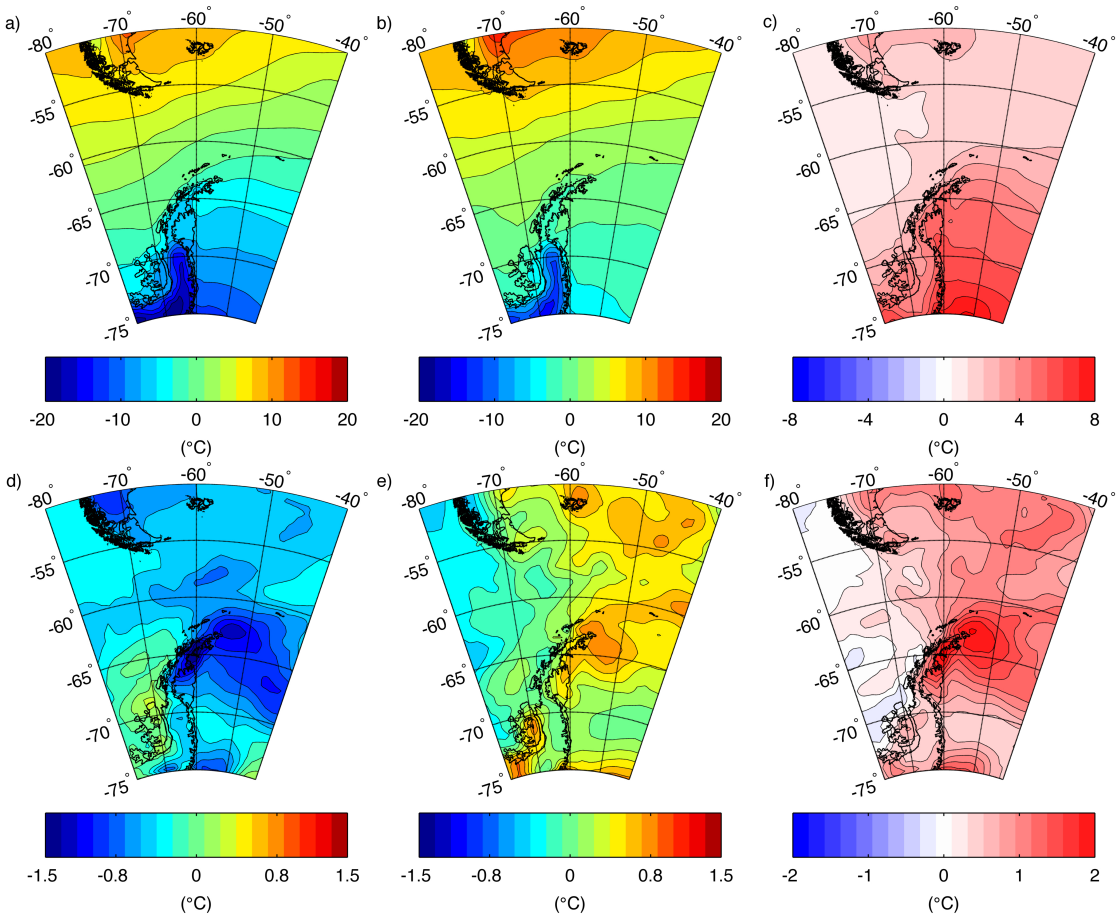

Figure 2.5: Mean monthly surface (2 m) air temperature (°C) composites for the 8 months with the (a) lowest and (b) highest open water areas in the Larsen embayments between 1997 and 2011; (c) difference in surface temperature composites between the high and low open water periods. (d–f) Same as Figures 2.5a–c for composites of monthly surface air temperature anomalies for (d) low and (e) high open water periods, and (f) the difference between composites. Anomalies are calculated by subtracting the monthly 1997–2011 mean from each monthly data set.

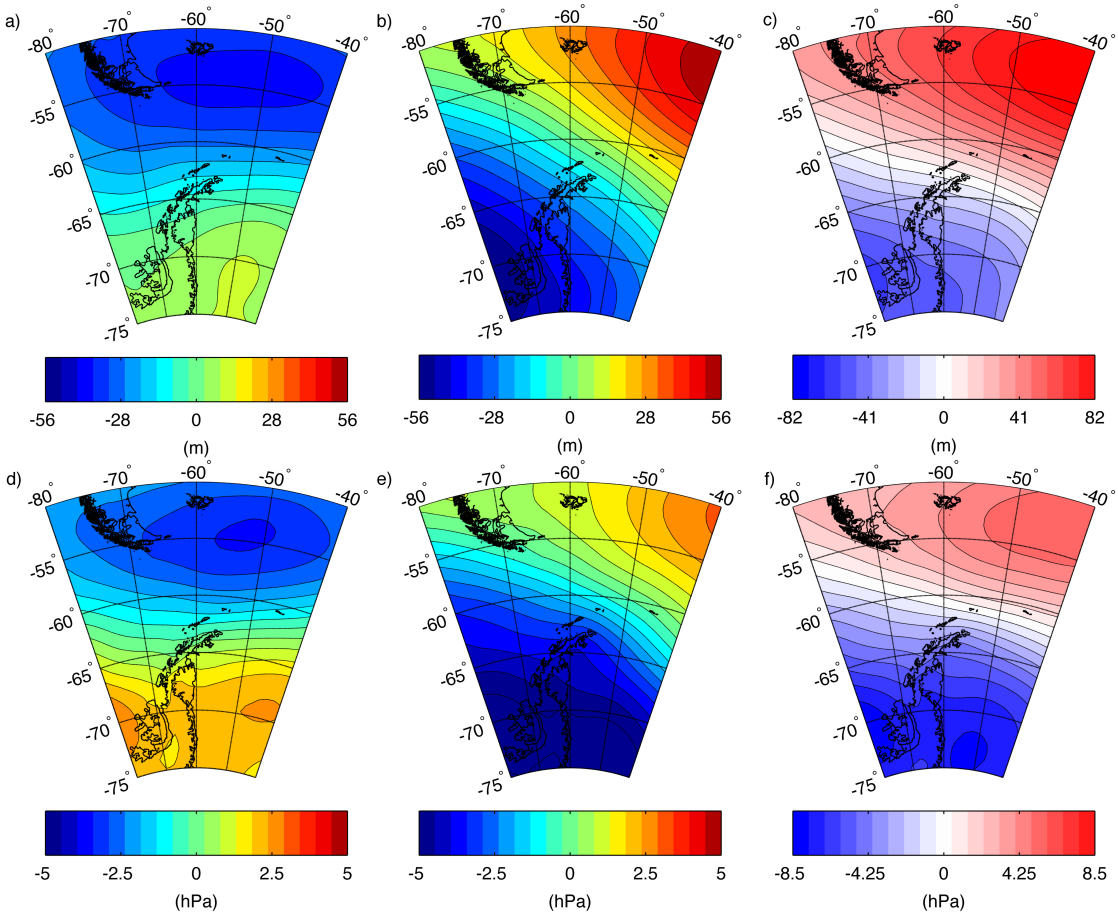

Figure 2.6: Mean monthly 500 hPa geopotential height (m) anomaly composites for the 8 months with the (a) lowest and (b) highest open water areas in the Larsen embayments between 1997 and 2011; (c) difference in mean monthly 500 hPa geopotential height anomaly between the high and low open water periods. (d–f) Same as Figures 2.6a–c for sea level pressure (hPa) for the months with the (d) lowest and (e) highest open water areas; (f) differences between the composites.

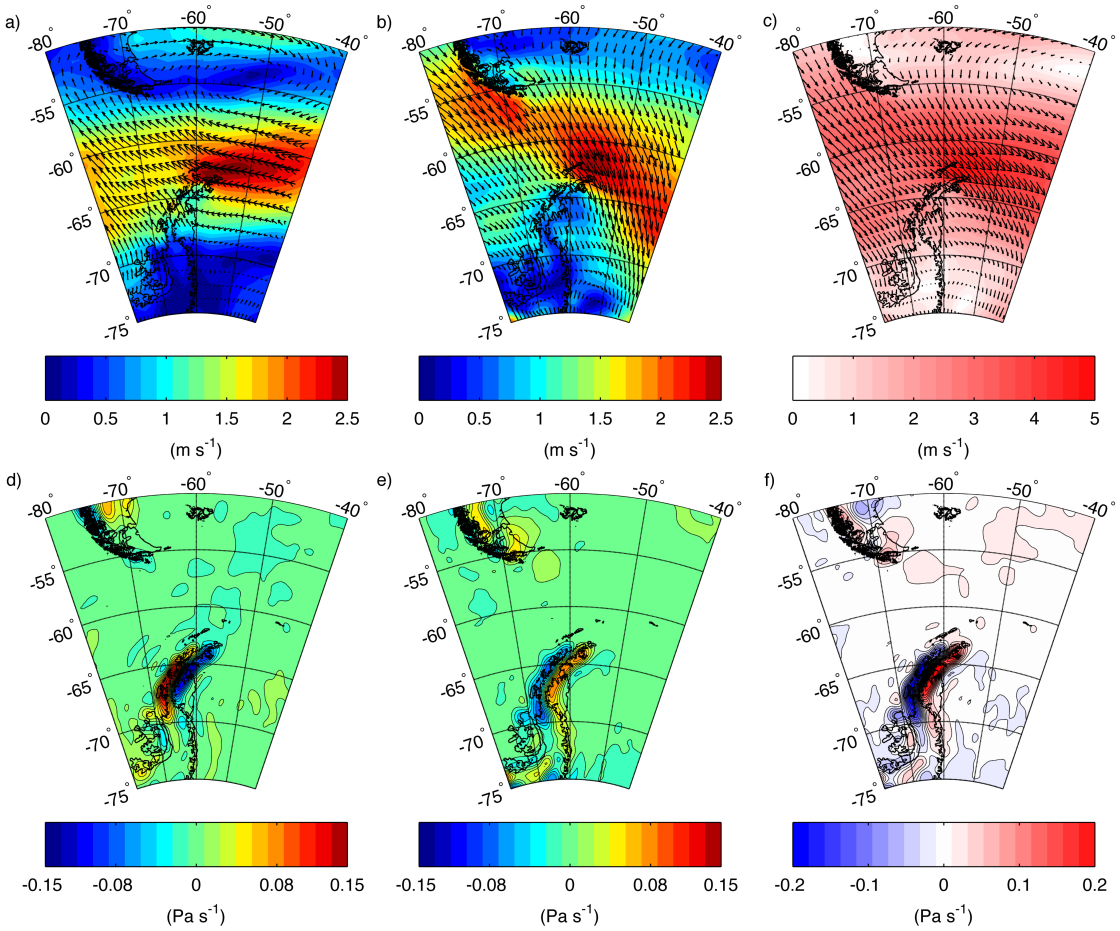

Figure 2.7: Same as in Figure 2.5 for anomalies in (a-c) surface (10 m) wind speed (m s^{-2}, shading) and velocity (arrows) and (d–f) vertical wind velocity at 850 hPa (Pa s^{-1}) for the months with (a and d) the lowest and (b and e) highest open water areas. Differences between the composites appear in Figures 2.7c and 2.7f.

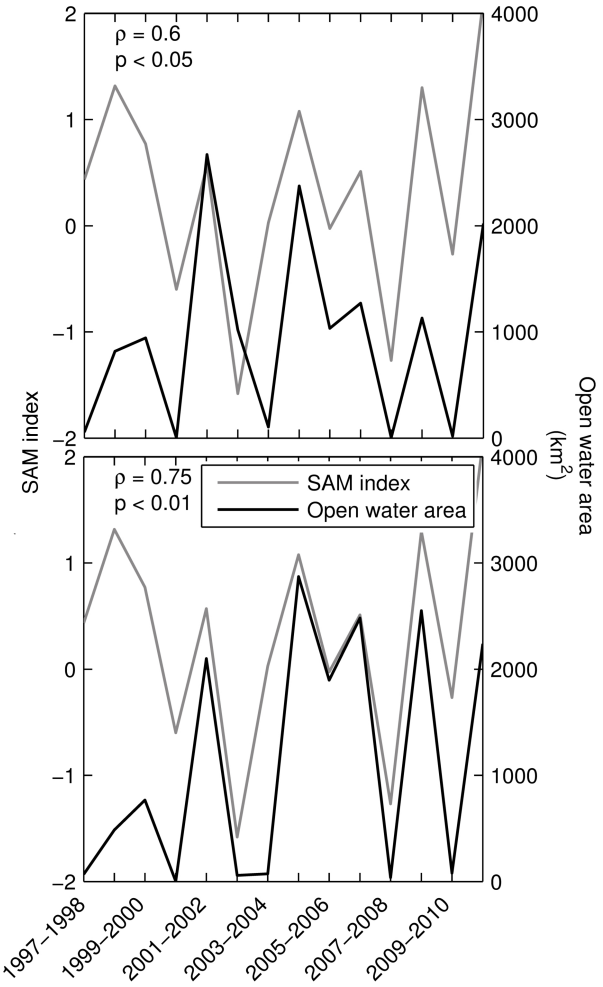

Figure 2.8: Time series of SAM index (black) and mean seasonal open water area (gray) for the (a) Larsen A and (b) Larsen B embayment. The monthly SAM index was smoothed with a 5 month running mean and lagged to find the most dominant cross correlations between SAM and open water area. The strongest correlation was found with SAM leading seasonal open water area by 5 months, corresponding to a June to October mean SAM index and an October to March mean open water.

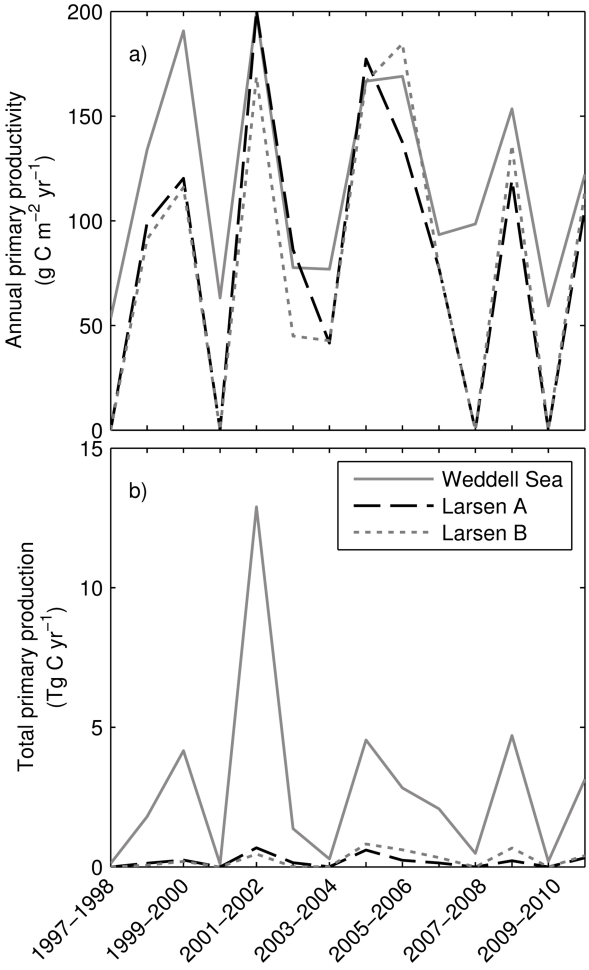

Figure 2.9: Time series of (a) annual primary productivity, calculated as the integral of daily primary productivity rates within the three regions of interest over March to October seasons, and (b) total annual production, calculated by multiplying daily productivity rates by open water area and integrating seasonally.

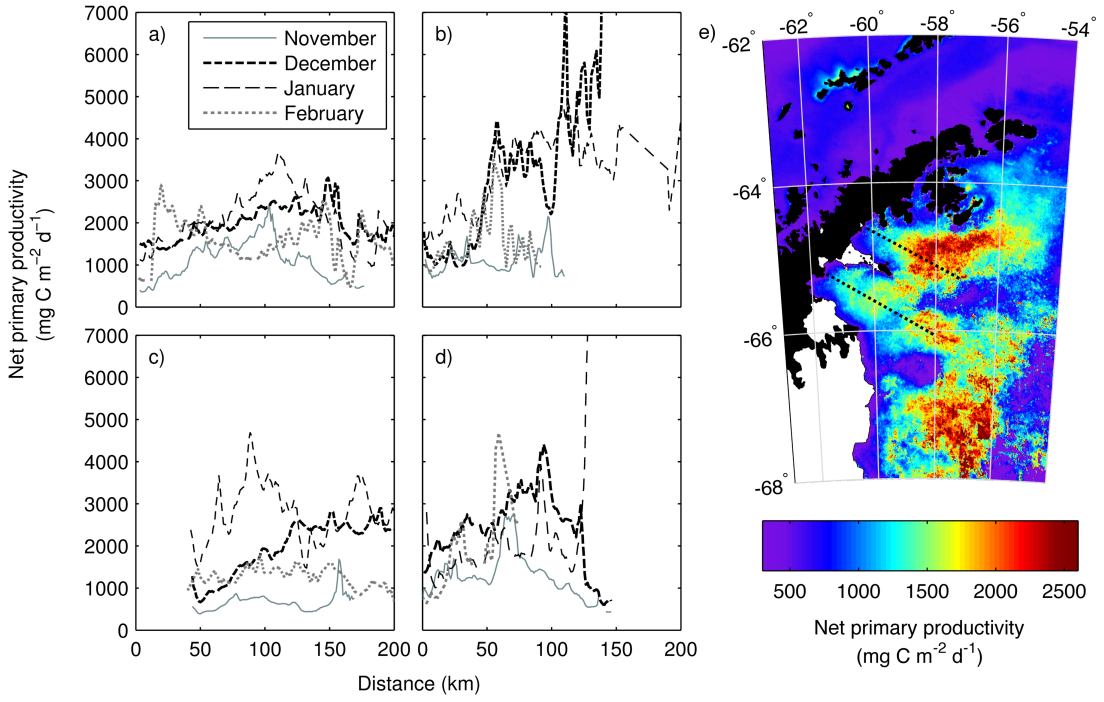

Figure 2.10: November–February, monthly cross-shelf transects of NPP through the Larsen A embayment in (a) 2001–2002 and (b) 2004–2005. Similar transects through the Larsen B for (c) 2001–2002 and (d) 2004–2005. (e) composite (average) of net primary productivity for the full 1997–2011 time series, showing location of transects from (a-d) (black dashed line). The origin corresponds to the Antarctic Peninsula coastline, with distance increasing offshore. Transect points are separated by 1 km and represent an average within a 3 x 3 pixel square along the transect. Lack of data within 40 km of the coastline in Figure 2.10c reflects the presence of the Larsen B ice shelf.

Chapter 3

Foehn winds link climate-driven warming to coastal cryosphere evolution in Antarctica

3.1 Abstract

Rapid warming along the eastern side of the Antarctic Peninsula in the last decades has led to extensive melting on the surface of the ice sheet, precipitating the rapid collapse of the Larsen A and B ice shelves. The warming trend has been attributed to stronger circumpolar westerlies resulting from a shift towards positive SAM polarity, which promotes the flow or warm, maritime air over the peninsula resulting in more frequent strong, warm, downsloping foehn winds in the lee of the mountain range. While the foehn mechanism for warming has been explored in recent literature, long-term observational datasets to test this hypothesis have been lacking from this region of rapid environmental change. In this study we explore trends in surface temperature and long-term variability in foehn winds using a novel, multi-decadal atmospheric weather record

from the Argentinian station Matienzo, located between the Larsen A and B embayments. Records from weather stations installed around the Larsen B embayment provide a spatial context to analyze regional meteorological patterns. Significant warming is found to occur in all seasons at Matienzo, with a maximum increase of +3.71 °C between 1962-1972 and 1999-2010 during the austral winter. Temperature anomalies are significantly positively correlated with anomalies in foehn frequency over times scales of months to years, with a positive trend in foehn frequency shown to occur during the austral summer season. Overall, foehn winds are major climatological features of the weather record demonstrating significant spatial and temporal variability linked primarily to the synoptic circulation and characteristics of the windward atmospheric flow. Foehn frequency and surface temperatures anomalies are strongly correlated with variability in the Southern Annular Mode (SAM) across seasons and on an inter-annual basis, demonstrating the sustained impact of changing climate patterns on the Larsen region. Foehn events are shown to have significant impact on both surface melt of continental ice and sea ice cover variability in the Larsen B embayment, further confirming the importance of these wind patterns to regional atmosphere–ice–ocean processes.

3.2 Introduction

Observations from sparse and often discontinuous meteorological stations collected over the last 6 decades have shown a dramatic increase in near-surface temperature along the Antarctic Peninsula (AP), with rates exceeding those observed both regionally and globally (Bromwich et al. 2013, Vaughan et al. 2003). This trend is part of a greater change in surface conditions ongoing across much of the West Antarctic (Kwok and Comiso 2002, 2012, Steig et al. 2009). However, recent studies have also highlighted the spatial variability in warming across the AP, with some of the strongest statistical trends

occurring over the eastern side of the peninsula (Marshall et al. 2006). Climatologically, the narrow mountain chain of the AP separates a warm, maritime climate along the western coastline from a cold continental climate to the east, leading to an average 5–10 °C temperature difference at similar latitude across the barrier (Martin and Peel 1978, King and Turner 2009). Yet in recent years, rapid warming along this side of the AP has led to major changes in regional climate and ice conditions across the land-ocean continuum, including higher rates of seasonal surface melting on the Larsen A and B ice shelves (van den Broeke 2005, Scambos et al. 2003, Skvarca et al. 1999). The propagation of glacial crevasses caused by the accumulated meltwater load is thought to have caused the dramatic retreat and ultimate structural collapse of these ice shelves in 1995 and 2002 (Scambos et al. 2003), precipitating changes in both cryosphere and ocean as a response to this major disturbance (Rignot et al. 2004, Scambos et al. 2004).

Previous studies have linked this rapid rise in temperature to changes in synoptic circulation and the strengthening of circumpolar westerlies, mediated by changes towards positive polarity of the Southern Annular Mode (SAM) (Marshall et al. 2006), the dominant mode of variability in the southern hemisphere. The mechanism links stronger upwind flow to more frequent advection of warm, maritime air over the peninsula and increases in surface temperature. Examining automated weather sensor (AWS) sensor from the Larsen C, van den Broeke (2005) estimated that the highest modeled long-term melt rates over the Larsen B were associated with northwesterly winds, consistent with this mechanism. Regionally, warming and drying of air as it flows over the lee side of the mountain barrier is thought to be caused by the latent heat release in the form of precipitation or the adiabatic descent of higher-level air towards the surface (Defant, 1951), though the exact causes are event-dependent. This flow pattern, observed in many parts of the world on the lee side of major mountain ranges, is commonly referred to as foehn. Foehn winds are characterized by a dramatic and sometimes prolonged increases

in leeside temperature and decreases in humidity relative to the windward side of a mountain range, with temperature changes in excess of +20 °C over a timescale of hours sometimes observed as these winds gradually replaces cold air masses. Several modeling studies have corroborated this foehn hypothesis for warming, demonstrating that strong westerly flow can lead to foehn-driven warming along the lee side of the peninsula (Orr et al. 2008, van Lipzig et al. 2008). Other authors have observed events *in situ*, describing dynamics associated with specific events and quantifying their contribution to the surface energy budget, demonstrating that foehn events can cause significant and prolonged melt events both within and at the ice surface (Kuipers Munneke et al. 2012, Elvidge et al. 2013, King et al. 2008, Elvidge et al. 2014, Grosvenor et al. 2014, Scambos et al. 2013). Moreover, results from another study analyzing reanalysis datasets has pointed to foehn events as implicated in the regulation of coastal ice cover in the Larsen A and B embayments following ice shelf collapse (Cape et al. 2014).

While the dynamics associated with specific foehn events in the region of the Antarctic peninsula, as well as the surface temperature response to singular events, have therefore been well relatively well described in both modeling and observational frameworks, long-term observations have been lacking, partially owing to the remoteness and general inhospitable climate characterizing this region. Whereas long-term wind patterns have been primarily derived from the Larsen C station assuming similarity in regional weather patterns along the NW Weddell Sea (van den Broeke 2005), eastern AP temperature trends have themselves been computed from the research stations at Marambio and Esperanza, > 100 km north of the region of recent ice shelf collapse (Marshall et al. 2006). Whether observations from these two stations are representative of patterns observed over the former ice shelves remains uncertain.

In this study, we test the foehn hypothesis for warming of the eastern Antarctic Peninsula by analyzing a novel multi-decadal surface atmospheric time series collected

at the Argentinian base Matienzo. In operation since 1961, the base is located on the Seal Nunataks 30 km northwest of Robertson Island between the former Larsen A and B ice shelves, and therefore situated at a critical site bordering areas of recent, rapid and dramatic changes at the atmosphere-ice-ocean boundary. While the early part of the record has been previously analyzed (Schwerdtfeger 1975, 1979), these studies focused on the dynamics of the cold, southerly barrier winds common to this region rather than the impact of foehn events on the regional climate. Using the full, high-resolution record covering two decades of observation between 1962–1975 and 1999–2010, we first describe long-term patterns in surface air temperature and test them against published trends derived from weather stations and reanalysis models. We then present the first long-term analysis of foehn winds in this region by quantifying the frequency, strength and variability of events along the eastern AP. We relate this foehn time series to atmospheric temperatures recorded at the same site, as well as estimates of continental ice melt and sea ice concentration to examine the impact of foehn variability on the coastal cryosphere and ocean. In so doing, we give new insight into the nature of ongoing changes along the Larsen Ice Shelf and possible future trajectories of the atmosphere-ice-ocean system, complementing previous studies of atmospheric dynamics in the region.

3.3 Data and Methods

3.3.1 Weather Station Records and Foehn Detection

Long-term weather records for the northern Larsen ice shelf region in the NW Weddell Sea were collected at the Argentinian station Tienente Matienzo (Figure 3.1, Table 3.1). The base was first established by the Argentinian air force in 1961, with weather data initially collected year-round between 1962 and 1975 and thereafter only during summer months (typically January-March) until 1987 by trained military personnel

of the Servicio Meteorológico Nacional (SMN) under the auspices of the Argentine Air Force and later the Ministry of Defense. Temperature data were collected by precision mercury thermometers calibrated in Buenos Aires prior to deployment and each season when the base was occupied. A new suite of automated sensors installed in 1999 at the same location by members of the Instituto Antártico Argentino extended this record another decade until 2010, when gradual instrument failures brought about by harsh storms ended the time series. The datasets include measurements of temperature, relative humidity, as well as wind speed and direction every 3–6 hours between 1962 and 1987, and every 1.5 hours thereafter.

Automated weather stations components of Automated Meteorology-Ice/Indigenous species-Geophysics Observation System (AMIGOS) (Scambos et al. 2013) and cGPS (Nield et al. 2014) systems further extended *in situ* observations around the Larsen B embayment between January 2010 and January 2013. Installed at sites surrounding and overlooking the Larsen B embayment as part of the LARISSA (LARsen Ice Shelf System, Antarctica) project (Figure 3.1, Table 3.1), these sensors collect data hourly and provide a spatial context for weather patterns and dynamics in this region. Meteorological datasets from the cGPS sensors were downloaded from www.unavco.org. Details regarding the location of the meteorological sensors appear in Table 3.1.

Following previous studies in the Antarctic (e.g. Speirs et al 2010, 2013), we used a semi-automated selection criterion to identify the onset and cessation of foehn events from weather records. Onset was identified as an increase in temperature of 1 $^{\circ}$C per hour, an increase in wind speed above 5 m s^{-1} from a westerly direction, and a decrease in relative humidity of at least 5 % hr^{-1}. Exact wind directions for the foehn events were dependent on the location of the sensor relative to topography. For records with lower temporal resolution (3-6 hours), or during periods when only a subset of sensors were available, the criterion was adjusted and events were classified manually.

All time series were manually quality controlled before analysis. Across the records, this semi-automated approach correctly classified 89% of foehn events, with 8% false positives and 6% events manually added on average. The resulting time series were temporally binned by counting a day experiencing 6 or more hours of foehn conditions as a foehn day. This additional criteria facilitated quantitative analysis and comparison of records. More details regarding the method can be found in Speirs et al. (2013) and Steinhoff et al. (2013).

Monthly time series of temperature and % foehn days (defined as the number of foehn days divided by number of days in the month) were generated by taking the mean and sum of daily observations respectively. Only days and months in which 85% of observations were available were used for higher-level composites.

3.3.2 Atmospheric Models

Atmospheric forecast and reanalysis models were used to describe regional and synoptic patterns contributing to foehn events in the Larsen B area. Archived numerical forecast output from the Antarctic Mesoscale Prediction System (AMPS, Powers et al. 2003) were downloaded from the repository at the National Center for Atmospheric Research (NCAR) covering the Antarctic Peninsula region (grid 6, 3.3 km) as well as the Antarctic continent (Grid 2, 10 km) and used to describe synoptic flow patterns for specific foehn events. This high-resolution model has been shown to adequately reproduce atmospheric patterns associated with foehn events in the Antarctic, including mountain wave effects (Steinhoff et al. 2014). AMPS is initialized twice daily at 0000 and 1200 UTC. To minimize effects of model initialization, only the 12-24 hr forecasts from each initialization were used in this study.

The spatial and temporal characteristics of foehn events over the Larsen area are dependent on patterns of tropospheric flow upwind of the peninsula and their interaction

with the mountain topography (Elvidge et al. 2014). To estimate long-term variability in synoptic flow near the Antarctic Peninsula and thereby characterize the upwind forcing of foehn events over the latter part of the Matienzo record, we obtained numerically analyzed monthly atmospheric datasets from the European Center for Medium-Range Weather Forecasts ERA-Interim dataset (EMCWF, http://www.ecmwf.int). Temperature and wind velocity datasets between the 1000 hPa and 800 hPa model levels at a location approximately 150 km west of Anvers Island and the Antarctic Peninsula (-63.75° lat, -66.75° lon, approximately one Rossby radius from the mountain range) were used to compute the non-dimensional mountain height $\hat{h} = \frac{Nh}{U}$, a quantity used to characterize the response of atmospheric flow impinging upon the peninsula to deflection by the mountain range. Here, N corresponds to the buoyancy frequency of the undisturbed upwind air mass, h is the height of the mountain (approximately 1400 m at the level of the Larsen B embayment), and U the mean-state layer-averaged wind speed component normal to and directed towards the AP (Steinhoff et al. 2014). A theoretical threshold of $\hat{h}$ = 1.1 separates linear flow from non-linear atmospheric flow. In the case of linear flow (high velocity, weak stratification), the presence of the mountain chain represents only a weak obstacle for the incoming flow, and low-level air is easily advected over the peninsula (Durran 1990). In the case of non-linear flow, the mountain range presents a significant barrier to atmospheric flow (e.g. for weak upwind velocities, or strong stratification), potentially leading to blocking of low-level flow, mountain-wave breaking, and leeside hydraulic jumps. The characteristic of the upwind flow, as described by $\hat{h}$, can have important consequences for the strength, frequency, and spatial characteristics of foehn warming over the eastern side of the peninsula. Linear flows have been shown associated with more extensive warming along the lee side, with weaker temperature signatures and more topographic channeling of flow observed for non-linear flows (Elvidge et al. 2014). While only the single record at Matienzo is available prior to 2010, characterizing the

nature of the flow over the peninsula therefore gives insight into the expected spatial variability in foehn winds over the long-term.

3.3.3 Sea Ice Concentration and Continental Ice Melt Detection

In order to quantify the long-term response of the cryosphere to foehn wind events we used satellite-derived datasets of sea ice concentration and continental ice melt events. Daily measurements of sea ice concentration on a 6.25 km grid were calculated from the 89 GHz channel of the Advanced Microwave Scanning Radiometer - Earth Observing System (AMSR-E) sensor (University of Hamburg, ftp://ftp-projects.zmaw.de/seaice/AMSR-E_ASI_IceConc/tmp_no_landmask/). To complement the time series prior to the launch of AMSR-E in June 2002, we used the lower resolution (12.5 km grid) Special Sensor Microwave Imager (SSM/I) 85 GHz bands. In both cases, sea ice concentration was calculated using the ARTIST (Arctic Radiation and Turbulence Interaction STudy) Sea Ice (ASI) algorithm (Kaleschke et al. 2001, Spreen et al. 2008). Mean monthly sea ice concentration was calculated by averaging daily values for each pixel. We generated a monthly time series for the Larsen B embayment by spatially averaging pixel values within an area bounded approximately by the 1963 extent of the Larsen B ice shelf (Figure 3.1, Ferrigno et al. 2008) and binning the daily values to month.

Following the approach of Barrand et al. 2013, we used microwave backscatter measurements from the QuikSCAT (QSCAT) Enhanced Resolution Imagery database for melt detection of continental ice. The dataset consists of daily, enhanced resolution slice-based SIR images between 1999 and 2010, with a pixels size of 2.225 km and an effective resolution of 5 km (Long and Hicks, 2010). We defined melt on a pixel-by-pixel basis, using an austral winter mean normalized backscatter threshold approach to identify whether melt was present or absent each day and in each pixel. Daily detections were then added to yield a time series of monthly melt days covering the Antarctic Peninsula.

For additional details on the method, see Barrand et al. 2013 and references therein. The QSCAT dataset is available for download from the Brigham Young University (BYU) NASA Scatterometer Climate Record Pathfinder (http://www.scp.byu.edu/).

3.3.4 Times Series Analyses

Standard anomaly time series were generated for *in situ* temperature, foehn days, sea ice concentration and surface melt by subtracting climatological means from the monthly time series and diving by climatological standard deviations. The correlation between two time series was then calculated using Spearman's Rank-Order Correlation, and reported as ρ(df), p-value, where df = N-2 and N = number of pairwise cases. Simple linear regression was used to analyze trends in the data, with results presented as b = regression coefficient when significant, t(df)= t-statistic, p-value, where df = N-2 as above. Results are presented as mean $\pm$ 95% confidence interval unless otherwise stated.

3.3.5 Climate Indices

We compared temperature and foehn variability to both the Southern Annular Mode (SAM) and El Niño Southern Oscillation (ENSO), dominant modes of climate variability along the Antarctic Peninsula (Marshall et al. 2003, Ding and Steig 2009). We used the observation-based index provided by Garreth Marshall (http://www.nerc-bas.ac.uk/icd/gjma/sam.html) to characterize the state of the SAM. Positive SAM values correspond to negative atmospheric pressure anomalies at high latitudes and positive anomalies at low latitude. We used the Niño 3.4 sea-surface temperature index, available at http://iridl.ldeo.columbia.edu/docfind/databrief/cat-index.html, to characterize ENSO variability. In order to describe variability in the Amundsen Sea Low (ASL), a persistent low pressure system in the Amundsen and Bellingshausen Seas that has been shown to

significantly affect regional and seasonal patterns of circulation (Hosking et al. 2013), we used the ASL Relative Central Pressure Index, as well as time series of the geographic location of the ASL, available at http://www.antarctica.ac.uk/data/absl/.

3.4 Results

3.4.1 Inter-annual Temperature Variability and Trends

Seasonal and annual temperature time series and trends for the two decades of Matienzo observations are presented in Figure 3.2 and 3.3. There is a significant positive trend for mean annual temperature, with an average warming of 0.85±0.57 °C per decade (Figure 3.2a), which equates to a total warming of 3.35 °C between the two decades of observation. Statistically significant warming has occurred in every season at Matienzo, with the strongest warming occurring during winter months (June, July, August, or JJA, 0.94±0.63 °C per decade, or 3.71 °C average temperature difference, Figure 3.2 and 3.3). Significant positive trends at the α = .05 level are also apparent for the summer (December, January, February, or DJF) and fall (March, April, May, or MAM), with rates of 0.37±0.29 and 0.76±0.63 °C per decade (1.47 and 3.34 °C total difference respectively), while the trend during the spring months of September, October, and November (SON) is relatively weaker though significant at the 0.1 level (0.63±0.65 °C per decade, 2.42 °C difference). Considering only January and February months in the record, which extends the time series by 7 years between 1975 and 1985, yields similar results to the DJF time series, with an estimated rate of 0.32±0.31 °C per decade (1.17 °C average temperature difference between decades). The austral summer season of 2001-2002, when the last major collapse of the Larsen B ice shelf occurred, stands as the warmest season on record, with an average surface temperature of 1.2 °C recorded at Matienzo.

Significant seasonal and inter-annual variability is however also evident. Annual and seasonal time series show strong 2-3 year oscillations in temperature, with mean seasonal temperatures differences between 3–12 °C common from one year to the next (Figure 3.2). While the overall annual and seasonal trends are positive, an apparent cooling trend is also apparent since 2004-2005 during summer and fall, indicating a potential shift in conditions since the middle of the last decade (Figure 3.2a-b).

3.4.2 Foehn Winds and Regional Climate

Case Study - March 25-28 2012

Figure 3.4a shows a characteristic signature of foehn wind events in the Larsen B region. This strong event, lasting from March 25 to March 28, 2012, was recorded at all meteorological stations operating near the embayment up to 100 km away from the continent, at 450 m elevation on the Flask Glacier, as well as onboard the Nathaniel B. Palmer 60 km offshore of the Larsen A embayment during the NBP12-03 cruise. Onset of the wind event was marked by a rapid increase in wind speeds to 10-15 m s^{-1} and a concurrent shift to a westerly direction. Surface temperatures around the embayment increased from an average of -10 °C to +10 °C and remained elevated for 12-24 hours even upon relaxation of the winds, while relative humidity dropped below 50%. By comparison, the meteorological record at Duthier's Point, situated at a similar latitude at the entrance of Andvord Bay on the west side of the AP, shows only weak variability during the same period. The timing of onset and cessation of this wind event was variable across sites, with some weather stations lagging others by 2-6 hours. Delay between stations may reflect differences in the location of the stations relative to the coast (e.g. Foyn Point is both closer to the coast and more sheltered than the Robertson Island station), and the relative time taken by the winds to destroy any cold pools of air pushed

against the eastern side of the AP mountain range (Schwerdtfeger 1975). Decreased cloud cover over the eastern side of the AP was also apparent (i.e. foehn clearance, Hoinka 1985), with evidence of cap clouds over the ridge as well as rotor and lenticular clouds downstream from the mountain range (Supporting Figure B.1, Duran and Klemp 1983). Foehn cessation was marked by a rapid change in wind direction to southerly winds, as a strong low pressure center over the Weddell Sea advected cold, continental air along the mountain range to the Larsen area, leading temperatures to drop to below -20 °C and to rapid sea ice formation (not shown)

The synoptic atmospheric pattern associated with this surface warming is characterized by a strong meridional and cross-peninsula pressure gradient due to a low pressure center in the southern Bellingshausen Sea and 10–15 m s^{-1} westerly airflow impinging on the mountain range (Figure 3.4b and Supporting Figure B.2). The non-dimensional mountain height for this event was 1.7 for a mean upwind wind direction of 277°, indicating that non-linear flow behavior was likely on the lee side of the mountains. During this period, the AMPS forecast for March 26, 2012, 12:00 UTC presents evidence of low-level blocking and mountain wave activity, with warm air aloft advected down towards the surface of the Larsen B embayment and elevated surface wind velocities along the lee slope and up to 100 km from the continent (Figure 3.5 and Supporting Figure B.3).

Foehn Winds as Major Features of the Eastern AP

Foehn events such the one in Figure 3.4 and 3.5 are commonly observed in the Matienzo record and, along with strong topographically driven southerly barrier winds (Schwerdtfeger 1975), distinguishing features of the wind patterns in the region. Ranging in length from several hours to occasional weeks (Figure 3.6a), these events often occur in rapid successions, with extended periods showing sustained elevated surface temperatures

and wind speeds. These winds demonstrate considerable seasonal variability, occurring on average between 5% and 25% of the months with maxima in the fall (SON) and minima in the summer (DJF) (Figure 3.6b). In extreme cases, foehn conditions can dominate monthly weather patterns with over 80% of the monthly record classified as foehn days, such as during October–December 2001, or can alternatively be completely absent (for example December–February 2001, not shown). These patterns are consistent over time, as there is no significant difference in monthly climatological foehn frequency between the two decades. Variability in monthly foehn frequency is related to the both the position and strength of the Amundsen Sea Low (Figure 3.6b). Foehn frequency across both decades appeared most sensitive to the latitudinal position of the low-pressure center ($\rho(10) = -0.90$, $p < 0.01$ and $\rho(10) = -0.85$, $p < 0.01$ for 1962-1972 and 1999-2010 respectively) as well as its relative strength ($\rho(10) = -0.95$, $p < 0.01$ and $\rho(10) = -0.85$, $p < 0.01$), although significant correlation was also found for longitude and absolute central pressure (not shown). Maximum foehn frequency lags both minimum central pressure and latitude by one month.

Significant inter-annual and inter-decadal variability is observed over the two decades of observations (Figure 3.6c). While during 1962-1972 the record shows mainly negative anomalies in foehn days, with sporadic months of increased foehn frequency, 1999-2010 is characterized by more sustained periods of positive anomalies, particularly early in the record. The years 1999, 2000, and 2001 stand out, with long periods of positive anomalies in % monthly foehn days occurring in concert with major retreat events of the Larsen B ice shelf. Wavelet analysis of the foehn time series further support these observations, showing higher periodicity in the 1.5 to 4 year modes between 1999 and 2010 compared to 1962-1972, when significant variability occurred mainly at periods of 1 year or less (Supporting Figure B.4).

Unlike the temperature time series, a weakly positive trend in monthly % foehn

days is found only in the summer (slope = 0.37 $\pm$ 0.4 % yr-1, p = 0.072, Figure 3.7), dominated by higher frequency and variability in the early part of the 2000s. Similarly to the temperature record, a decreasing trend in foehn frequency also appears present after the middle part of the decade in DJF as well as MAM (not shown).

Relationship to Temperature and Regional Climate

By advecting warm, dry air to a region that is otherwise governed by a cold, continental climate, foehn events significantly moderate regional climate. For the strongest foehn events in the winter and fall, surface temperature changes recorded around the Larsen embayment can exceed +30 °C, with periods of above freezing conditions lasting days even in mid winter (Figure 3.5a). Characteristics of atmospheric temperature and wind during period foehn and non-foehn conditions are shown for Foyn Point, a meteorological station located well within the Larsen B embayment at the base of the lee side slope (Figure 3.8). Analysis of observations during non-foehn periods shows that Foyn Point is generally a low wind speed site, dominated by weak westerly through much of the year (Figure 3.8c, f, i, l). Across all seasons, atmospheric temperatures during foehn events are significantly elevated relative to outside of these periods, with temperatures on average reaching or exceeding the freezing point (Figure 3.8a, d, g, j). As expected, winds during foehn event tend to originate from the west, with high wind speeds much more frequent relative to normal conditions. These general foehn characteristics hold for the entire sensor network analyzed in this study, though the various sites differ widely in the average atmospheric conditions they are exposed to. For comparison, the station at Robertson Island (ROBI) is generally characterized by much stronger southerly winds outside of foehn events, likely an indication of the site's greater exposure to barrier winds and circulation associated with open shelf conditions (Supporting Figure B.5) As observed in Figure 3.8, the overall effect of foehn winds on average seasonal temperature

is strongest during fall and winter, with every 1% increase in the frequency of foehn days equating to a 0.292 ± 0.166 °C rise in surface air temperature during winter (Figure 3.9c). During the summer months, when cyclonic activity around the peninsula is generally lower due to the movement of the Amundsen Sea Low towards the peninsula, which leads to a northward movement of storm tracks (Hosking et al. 2013), and average surface temperatures at Matienzo closer to the freezing point (Supporting Figure B.6), foehn winds tend be less frequent and their impact less dramatic ($+0.129 \pm 0.097$ °C $\%^{-1}$). Rates in the fall and spring lie between these two extremes (0.236 ± 0.162 and 0.243 ± 0.155 °C $\%^{-1}$ respectively). All regression slopes are significant at the $\alpha = 0.01$ level.

Anomalies in surface air temperature and monthly foehn event frequency are highly correlated throughout the record ($\rho(312) = 0.58$, $p<0.01$, Figure 3.6c), implying a strong influence of foehn winds on regional conditions across the northern Larsen Ice Shelf area.

Synoptic Drivers of Regional Variability

As observed in Figure 3.6, foehn events are highly variable within and between seasons, with ultimate effect on surface conditions dependent on the large-scale atmospheric flow. Elvidge et al. 2014 showed that upwind tropospheric flow velocity and direction can have a major impact on the horizontal scale of the warming, with linear upwind flow leading to extensive warming and high winds speeds across the entire northern Larsen C ice shelf and non-linear flows favoring more topographically constrained gap flows and a smaller horizontal extent of influence. While the March 25–28 event was recorded across the Larsen embayment, AMPS forecast output indicates that significant channeling of flow may have occurred (Supporting Figure B.3), with near-surface high velocity jets focusing the wind energy on the lee side of the peninsula. Observations from the NBP12-03 cruise support this prediction, with wind velocities decreasing by 20–30

m s^{-1} over the span of < 10 km during the March 2012 foehn event, despite observations of sustained high temperature and decreased relative humidity along the cruise track (not shown). This complex spatial response of surface conditions across the northern Larsen Ice Shelf regions is further reflected in the LARISSA weather station network, with some locations showing dramatic changes in temperature with little change in wind speed in response to the same foehn event (Supporting Figure B.7).

To investigate the temporal variability in regional upwind flow conditions between 1999 and 2010 and identify general patterns associated with foehn winds using the single record at Matienzo we isolated the time periods identified as foehn events from the observational network to explore large-scale flow variability using the ERA-Interim reanalysis dataset. Figure 3.10a shows a histogram of the non-dimensional mountain height $\hat{h}$ for all recorded foehn events, a proxy for the expected linearity of the incoming tropospheric flow. A majority of foehn events were characterized by non-linear upwind flow, indicating that along the NW Weddell Sea, high spatial variability in wind speeds and warming across the ice shelves and embayment are likely common, as observed in March 2012. Linear events with $\hat{h}$ <= 1.1 account for less than 10% of all observations, implying that conditions leading to an extreme spatial extent of melt over the Larsen area are uncommon. Instead, foehn flow is expected to be highly spatially variable, likely characterized by significant jets and gaps. Higher variability in $\hat{h}$ is found for northwesterly wind directions between 275° and 300° (Figure 3.10b). For wind directions below 275°, upwind flow tends to be linear or weakly non-linear. Synoptic atmospheric patterns show that foehn conditions tend to be associated with well-developed low-pressure systems in the Amundsen-Bellingshausen Sea and a strong meridional pressure gradient (Figure 3.6b), occasional with strong blocking highs situated in the South Atlantic (not shown, Massom et al. 2006, 2008), leading to westerly advection of relatively warmer maritime air across the AP and the Larsen region. However, a wide array of

synoptic configurations appear to lead to foehn events, with slight differences in the position of weather systems potentially having large impacts on the direction of the incoming flow, the degree of linearity, and ultimately the surface manifestation of these winds on the lee side of the peninsula.

We examined climatic sources for this variability by considering the contribution of SAM and ENSO to synoptic wind patterns and regional wind response over the northern Larsen region (Figure 3.6c). Overall foehn frequency shows an upward trend between 1962 and 2010 coincident with the positive shift in the SAM over the same period. Between 1962 and 1972, the foehn and SAM time series are only weakly though significantly related ($\rho(175) = 0.249$, $p < 0.01$), with few periods of synchrony between the two records. This changes for the most recent decade of 1999-2010, when the two time series are more strongly correlated ($\rho(139) = 0.448$, $p < 0.01$). Considering seasonal averages of both time series, the SAM and foehn time series appear highly correlated over all seasons, with highest correlation in the fall ($\rho(9) = 0.91$, $p < 0.01$) and weakest in the summer ($\rho(9) = 0.52$, $p <0.10$), while SAM and surface temperature are similarly correlated over all seasons but the summer (DJF, $\rho(9) = 0.37$, $p = 0.24$, Table 3.2). There was no relationship between the Nino3.4 index and either foehn or temperature.

Impacts on the Cryosphere

To gain more information regarding the spatial context of this relationship and the possible contribution of foehn events to surface ice melt, we correlated the foehn anomaly time series with melt estimates for the continental ice surface derived from QuikSCAT. Over the ice sheet, significant positive correlation between wind and melt anomalies are observed predominantly along the eastern coastline of the peninsula north of the Crane Glacier, which feeds the Larsen B embayment (Figure 3.11b and Supporting Figure B.8). The relationship between the two time series is strongest over the Seal Nunataks, where

Matienzo is located, as well as along the northern end of the Larsen A to Cape Sobral and Cape Longing ($\rho(130) = 0.507$, $p < 0.01$). This relationship weakens farther south over the SCAR inlet, the Jason Peninsula, and the Adie and Cabinet Inlets. There is no significant relationship between the two variables over the Larsen C.

3.5 Discussion and conclusions

Using two decades of weather observations collected from the Base Matienzo, located between the former Larsen A and B ice shelves, we explored the hypothesis that foehn winds, resulting from the interaction of synoptic westerly flow with the steep and tall Antarctic Peninsula orography, fundamentally impact both the regional climate and cryosphere dynamics over the coastal NW Weddell Sea. As described in previous studies, we find that the eastern AP has on average experienced a sustained and significant increase in atmospheric temperatures, with warming evident in all seasons and on an annual basis at Matienzo. The significant rates of warming described in this study, ranging from 0.37 to 0.94 °C per decade (Figure 3.3), are far higher than the global average and are some of the highest measured across the Antartic continent, exceeding trends recently described at Byrd Station (Bromwich et al. 2013). It is also notable that these rates also comparable to those measured at the Argentinian station at Marambio farther north in the NW Weddell Sea, which has frequently been used as the reference station for the eastern AP (Marshall et al. 2006). In the latter case, only summer and annual trends were found significant however. The positive trend reported in this study in spring and summer is particularly noteworthy, given the potential impact of extended periods of > 0 °C temperatures on ice sheet melt.

Foehn events are common atmospheric phenomena along the lee side of the AP that have a dramatic impact on surface conditions. Because of the generally cold,

continental climate that dominates the Weddell Sea, foehn winds serve to moderate surface conditions, often leading to extended periods of dramatic warming lasting up to several days (Figure 3.6a). As observed in the McMurdo Dry Valleys (Speirs et al. 2013, Steinhoff et al. 2014), foehn events tend to occur in groups rather than singletons (Figure 3.6a), with sustained events associated with positive anomalies in both atmospheric warming as well as surface ice sheet melt (Figure 3.6, 3.9, 3.11). Seasonal surface temperature are very sensitive to the frequency of foehn events, with the highest rates of warming for a 1% change in seasonal foehn frequency occurring in the winter and spring (slope = 0.29 and 0.24 $^{\circ}$C $\%^{-1}$ respectively, Figures 3.8, 3.9a). This is a result of both the colder temperatures encountered during these seasons, and the larger magnitude of the temperature changes associated with these events. Considering the two decades of observation, positive monthly anomalies in surface air temperatures are strongly correlated with increased frequency of foehn winds, further implying a regulatory mechanism between wind events and surface conditions (Figure 3.9b). Wavelet analysis of the foehn record also indicates a change in periodicity over the two decades observation, with more sustained anomalies over the latter decade, particularly between 1999 and 2002 (Figure 3.6c). A positive trend in the frequency of summertime foehn frequency is also apparent, significant due to the potentially dramatic impact of extended melt periods on the cryosphere (Figure 3.7, Supporting Figure B.4). These results further reinforce previous findings from the Larsen C (van den Broeke 2005), showing that higher frequency of foehn winds leading up to the 2001-2002 season had a dramatic impact on surface conditions, likely contributing to the retreat and collapse of the Larsen B ice shelf as posited in earlier work (Marshall et al. 2006).

Variability in the Southern Annular Mode is strongly linked to foehn variability, with positive SAM associated with warmer temperature and more frequent foehn winds (Figure 3.6c, Table 3.2). This strong relationship holds over all seasons but the summer,

for which comparatively weaker correlations between temperature and SAM are found (Table 3.2). Monthly time series provide a complementary outlook on the link between surface warming and climate patterns, with variability in SAM, foehn events, and temperature closely associated over the entire time series, although the relationship is stronger in the decade between 1999 and 2010 (Figure 3.6, 3.9). Particularly notable are the large synchronous excursions associated with periods of retreat and collapse of the Larsen B ice shelf in 1999, 2000, and 2002 (Figure 3.6), as well as seasonal minima in coastal sea ice concentration (e.g. 2004-2005, Figure 3.11, Cape et al. 2014). These observations, along with a positive trend in foehn frequency dominated by low frequency and variability between 1972 and 1987 and large positive anomalies between 1999 and 2002 mirroring temperature increases during summer, are consistent with the foehn hypothesis for eastern AP warming (Marshall et al. 2006). Yet the instrumental record is also characterized by high variability both across and within seasons. In the summer and specifically, a significant downward trend in temperature and foehn frequency is apparent in the last decade (Figure 3.2b-c, 3.7). This cooling trend is corroborated by a temperature history derived from isotope analyses of an ice core collected on the Bruce Plateau above the Larsen B embayment (Zagorodnov et al. 2012), which shows a maximum in temperature between 1995 and the early 2000s followed by a rapid decrease. These observations may indicate a return to more dominant cold, continental conditions characteristics of the early decade, which may have important ramifications for the integrity of the ice sheet in this northern AP region.

We find that monthly foehn variability is driven by changes in the latitudinal position and strength of the Amundsen Sea Low, a dominant pressure pattern in the Amundsen-Bellingshausen Seas (Figure 3.6b). This result is intuitive, given the importance of the meridional pressure gradient in generating foehn winds (Elvidge et al. 2014). Similarly, processes outside the Antarctic, such as the position of the South

Atlantic anticyclone, also likely play a determining role in wind variability along and across the AP and may explain some of the variability observed in regional circulation patterns (Lübbecke et al. 2014). During the anomalous 2001–2002 and 2004–2005 austral summers, for example, a blocking high-pressure system in the South Atlantic was implicated in the extreme weather felt across the entire Antarctic Peninsula, contributing to strong anomalies in sea ice cover and sustained positive anomalies in foehn frequency and surface temperatures over the Larsen area (Figure 3.6c, Massom et al. 2006, 2008). While affecting windward atmospheric patterns, strong cross-peninsula flow can also have a significant impact on atmospheric circulation over the Weddell, with cyclogenesis in the lee of the AP further reinforcing the dominant southerly flow, as observed in March 2012 (Figure 3.4, Turner et al. 1998, Lubin et al. 2008, King and Turner 2009). The effect of westerly flow on mean surface temperature and foehn frequency is therefore complex, involving atmospheric dynamics on both sides of the AP as well as variability across several spatial scales.

The strong offshore foehn wind storms are clearly an important component of circulation patterns experienced in the vicinity of the Larsen B and are significant for surface conditions, yet their characteristics are highly variable, with some events leading to widespread heating over > 100 km from the mountain range and others localized only to the base of the glaciers feeding the Larsen B embayment with only brief and minor changes in temperature (e.g. Figure 3.4, Supporting Figure B.7). This variability is captured across our sensor network, which serves to highlight the importance of placement of automated weather stations in the study of such phenomena (Grosvenor et al. 2014). Elvidge et al. (2014) attributed similar variability in Larsen C foehn events observed between November 2010 and February 2011 to dynamic interactions between incoming flow and the peninsula mountain range. In that case, aircraft and modeling observations identified mesoscale foehn jets, resulting from the flow of air through gaps in

the AP topography, channeling higher level flow towards the surface of the ice shelf, with adjacent wake regions characterized by weaker winds but higher temperatures. Given the gap-flow mechanism underlying the genesis of foehn winds, the authors remarked that relatively weak cross-peninsula or even along-peninsula flows could potentially lead to foehn events and localized surface warming. Linearity of the flow, a function of wind characteristics and synoptic pressure system organization, as well as wind direction were found to affect both the vertical and horizontal source of air, the lee side extent of both winds and temperature increases over the ice shelf, and the physical mechanism responsible for warming of the air mass as it passes the peninsula (i.e. latent heating, sensible and radiative heating, or isentropic drawdown, Elvidge 2013). Similar findings have been described for the McMurdo Dry Valleys (Speirs et al. 2012, Steinhoff et al. 2014). In the Larsen A and B area, we find that recorded wind events are associated with a broad distribution of flow linearities resulting from a wide range of synoptic-scale patterns and wind directions (Figure 3.10). However, non-linear flow patterns tend to dominate, occurring in over 90 % of foehn events. This is consistent with the surface expression of foehn events as observed by the observational network, with a wide range of wind and temperature responses recorded across the embayment for a single event (Figure 3.4a and Supporting Figure B.7). This preponderance of non-linear flows may explain the melt signatures observed via satellite over the Larsen C, which show melting typically limited to a narrow region adjacent to the AP mountain range (Barrand et al. 2013).

The implications of higher surface temperatures, and as demonstrated in this study foehn frequency, for cryosphere dynamics in the region are apparent when comparing these records with QSCAT derived surface melt observations. High correlation between backscatter estimates of surface melt and foehn events are found along the coastal Larsen A and B embayments between the Crane Glacier in the south and James Ross Island

in the north (Figure 3.11). In an effort to quantify the physical mechanism for melting, Elvidge (2013) showed using modeling results that large downward solar radiation due to clear sky conditions (i.e. foehn clearance, Supporting Figure B.1) and sensible heat fluxes from air to ice are responsible for warming of the ice surface during foehn events, with the highest rates of melt induced by strong, linear foehn events. More recently, results from Grosvenor et al. (2014) showed that shortwave input dominated the melting signal resulting from foehn conditions. While foehn winds therefore appear to significantly contribute to surface melt in this region, this relationship does not hold south over the Larsen C despite field observations of foehn events (Elvidge et al. 2014). These observations are in general agreement with other studies that noted a rapid latitudinal decrease in surface melt south of the Larsen B region, attributed to the dominance of cold, continental conditions (Grosvenor et al. 2014). This seemingly arbitrary geographical divide may nevertheless be a result of differing interactions between incoming atmospheric flow and the mountain chain as the relative heading of AP changes (from approximately 30° to 50° at the level of the SCAR Inlet ice shelf). This further highlights the importance of both the physical setting and wind direction in determining lee-side response, as observed in the variability of weather records across the embayment to a seemingly uniform synoptic upwind forcing (e.g. Supporting Figure B.7). While the Matienzo time series has shed light upon both causes of warming in the rapidly changing Larsen A and B region as well as the link between climate change and surface weather response, it may however not be representative of foehn variability farther south. Due to the importance of these winds in shaping the physical environment over the Larsen Ice Shelf region, it is important to gain a better understanding of the long-term dynamics of these winds over the Larsen C using long-term observational platform such as the Larsen C AWS to predict future evolution of the cryosphere in this region (Grosvenor et al. 2014).

The retreat and collapse of the Larsen A and B ice shelves in the last three

decades demonstrated the power of gradual changes in air temperature and atmospheric circulation on cryosphere dynamics, quickly becoming a powerful example of the impact of climate change on polar regions (van den Broeke 2005, Scambos et al. 2003, Domack et al. 2005). Observations of structural ice shelf characteristics using satellite imagery of the region have indicated that the time span between 1962 and 1986, corresponding to the early decade discussed in this study, corresponded to a period during which the Larsen B ice shelf was likely in steady state (Scambos et al. in prep). Weather records during this period are likewise relatively consistent, with little to no trend in either foehn or temperature (Figure 3.2). Conversely, increased sheer zone stress and fracturing was evident on the ice shelf surface between 1986 and 1998, implying a rapid change in conditions during that time. The dramatic collapse in 2002 as then the concluding chapter of a long chain of events linking atmospheric trends to gradual breakdown of the structural integrity of the ice shelf. Unfortunately, this critical period in the evolution of the ice sheet is missing from the Matienzo weather record due to constraints on budgets, equipment, and manpower. Patterns in both temperature and foehn discussed in this study are however consistent with these observation, particularly considering summer trends and the large positive anomalies observed between 1999 and 2002 (Figure 3.2b, 3.7). While observations between 1987 and 1998 may never be recovered, the Matienzo record could be used link extensive *in situ* observations to high-resolution models in an effort to reconstruct this period of dynamic change and better constrain the mechanisms responsible for ice shelf collapse (e.g. Bromwich et al. 2013). Given the widespread thinning and retreat of ice shelves across the Antarctic Peninsula and the continent as a whole (Cook and Vaughan et al. 2010), this in turn could shed light on the potential future of other ice shelves in regions of rapid warming.

3.6 Acknowledgements

The authors wish to acknowledge Argentinian scientists, staff, and military members responsible for the establishment and maintenance of the weather station at Matienzo, Matthew Lazarra and the staff of the Antarctic Meteorological Research Center at the University of Wisconsin Madison for assistance with automated weather station data processing and for always being available to answer questions, Gunnar Spreen for continued support and update of the sea ice dataset, the captain and crew of RVIB *Nathaniel. B Palmer* as well as Raytheon Polar Services technicians for assistance with instrument deployment during NBP1001 and NBP1203. Discussions with Peter Franks led to new ideas that significantly contributed to this work. Kevin Manning provided valuable input for the analysis of AMPS forecasts, while Johanna Speirs and Andrew Elvidge gave helpful advice for the analysis of foehn wind events. This work was supported by the National Science Foundation Office of Polar Programs under NSF grant ANT-0732983. MRC was also supported by the NSF Graduate Research Fellowship under grant DGE-1144086 and by NASA Headquarters under the NASA Earth and Space Science Fellowship Program–grant NNX12AN48H.

This chapter is in preparation for publication as: Mattias R. Cape, Vernet, M., Skvarca, P., Marinsek, S., Scambos, T., Domack., E. Foehn winds link climate-driven warming to coastal cryosphere evolution in Antarctica.

Table 3.1: Automated weather station information. ID correspond to names in Figure 3.1, while sensor platform distinguishes between cGPS stations, AMIGOS sensors, and the permanent base at Matienzo.

ID	Sensor platform	Name	Latitude	Longitude	Elevation (m)	Earliest Data	Latest Data
DUPT	cGPS	Duthiers Point	-64.80	-62.82	57	2009 Apr 03	2014 Aug 28
ROBI	cGPS	Robertson Island - Cape Marsh	-65.25	-59.44	127	2010 Feb 06	2014 Aug 28
CAPF	cGPS	Cape Framnes - Jason Peninsula	-66.01	-60.56	121	2010 Feb 18	2014 Aug 28
FONP	cGPS	Foyn Point	-65.25	-61.65	114	2010 Feb 07	2014 Aug 28
FLSK	AMIGOS	Flask Glacier	-65.75	-62.90	450	2010 Feb 06	2014 Jul 11
SCAR	AMIGOS	SCAR Inlet	-65.80	-62.00	54	2010 Feb 16	2014 Aug 28
MTZO	station	Matienzo	-64.98	-60.07	25	1962 Jan 1	2010 Dec 31

Table 3.2: Seasonal correlation of average foehn frequency and temperature with SAM and Nino3.4 indices. Significance at $\alpha = 0.1$ is indicated by *, while significance at $\alpha = 0.05$ or below is indicated by **.

Observation	Season	SAM (ρ)	Nino3.4 (ρ)
Foehn (%)	DJF	0.52*	-0.38
	MAM	0.91**	-0.39
	JJA	0.63**	-0.41
	SON	0.67**	-0.48
Temperature (°C)	DJF	0.37	-0.25
	MAM	0.73**	-0.3
	JJA	0.76**	-0.24
	SON	0.82**	-0.27

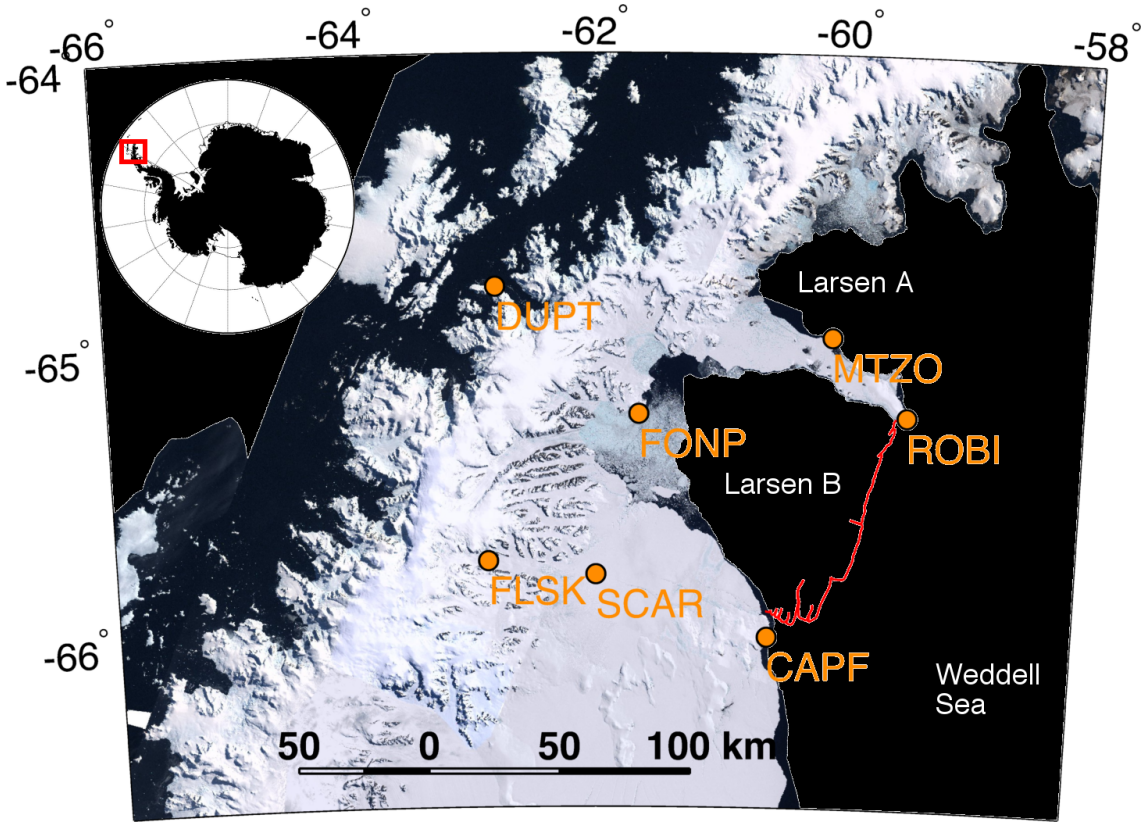

Figure 3.1: Map of the northern Antarctic Peninsula, showing locations of weather sensors used in this study. The maximum extent of the Larsen B ice shelf in the 1960s over which sea ice averages were computed is indicated by a grey line Further information regarding the weather stations appears in Table 3.1.

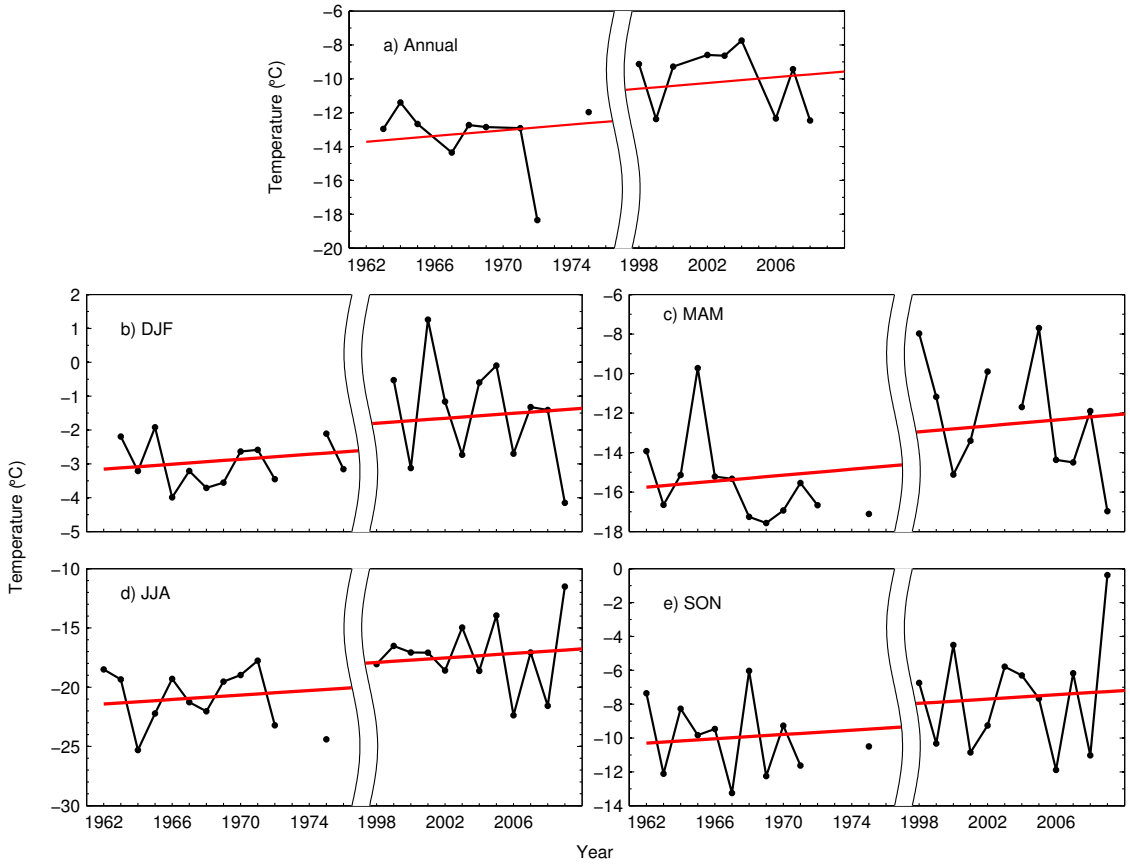

Figure 3.2: Temperature time series for Matienzo between 1962 and 2010. Mean a) annual and b-e) seasonal temperature time series. Red line denotes linear trend in the data. Only months in which 85% of daily observations were available were used in this analysis.

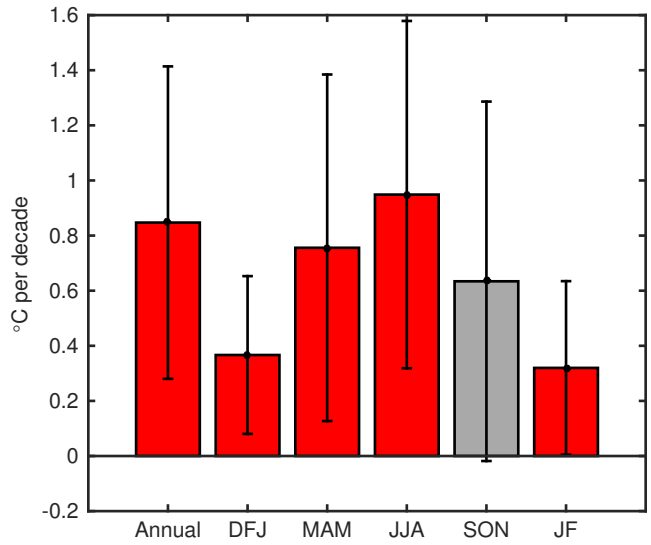

Figure 3.3: Summarized linear trends in annual and seasonal temperature at Matienzo between 1962 and 2010. JF denotes the January-February average. Vertical bars represent the 95% confidence intervals on the slopes. Red color denotes statistically significant trends at the $\alpha = 0.05$. Note that the SON trend is significant at the $\alpha = 0.1$ level

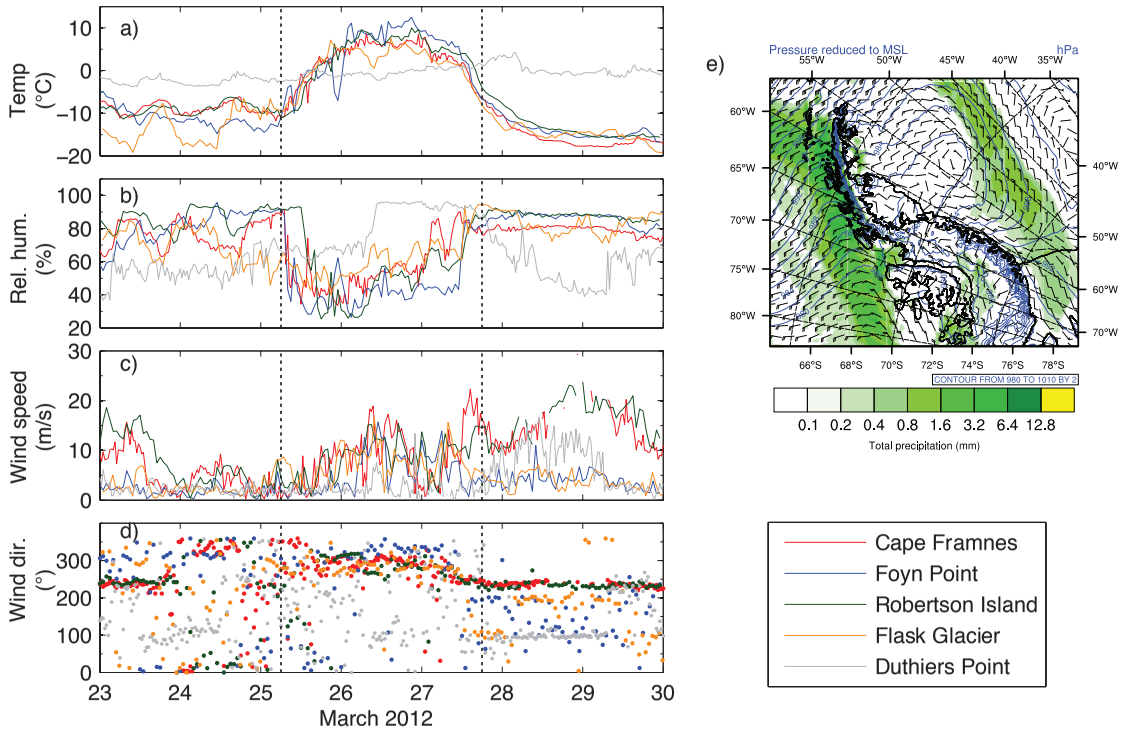

Figure 3.4: Meteorological characteristics during a March-April 2012 foehn event. Time series of (a) temperature, (b) relative humidity, (c) wind speed, and (d) wind direction for weather stations at Capes Framnes, Foyn Point, Robertson Island, and Flask Glacier along the eastern AP, and at Duthier's Point on the West Antarctic Peninsula. b) AMPS forecast for March 26, 2014 at 12:00 UTC, showing sea level pressure (blue lines), wind vectors (black arrows) and total precipitation (shading) during the same event.

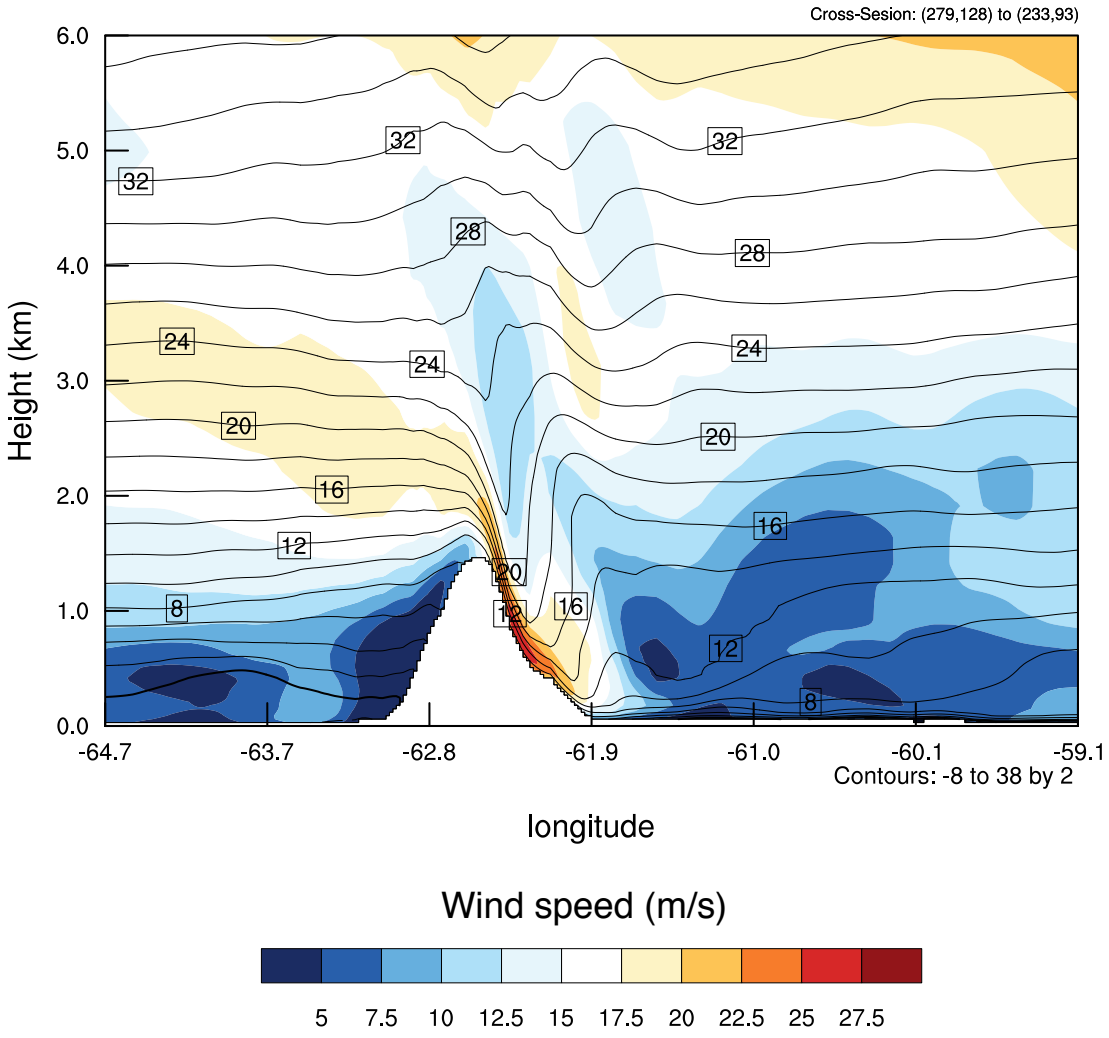

Figure 3.5: Vertical cross-section of potential temperature (°C, black isotherms) and horizontal wind speed (m s^{-1}, shading) along the transect shown in Figure 3.1 for the March 26, 2014, 12:00 UTC forecast. Data derived from AMPS.

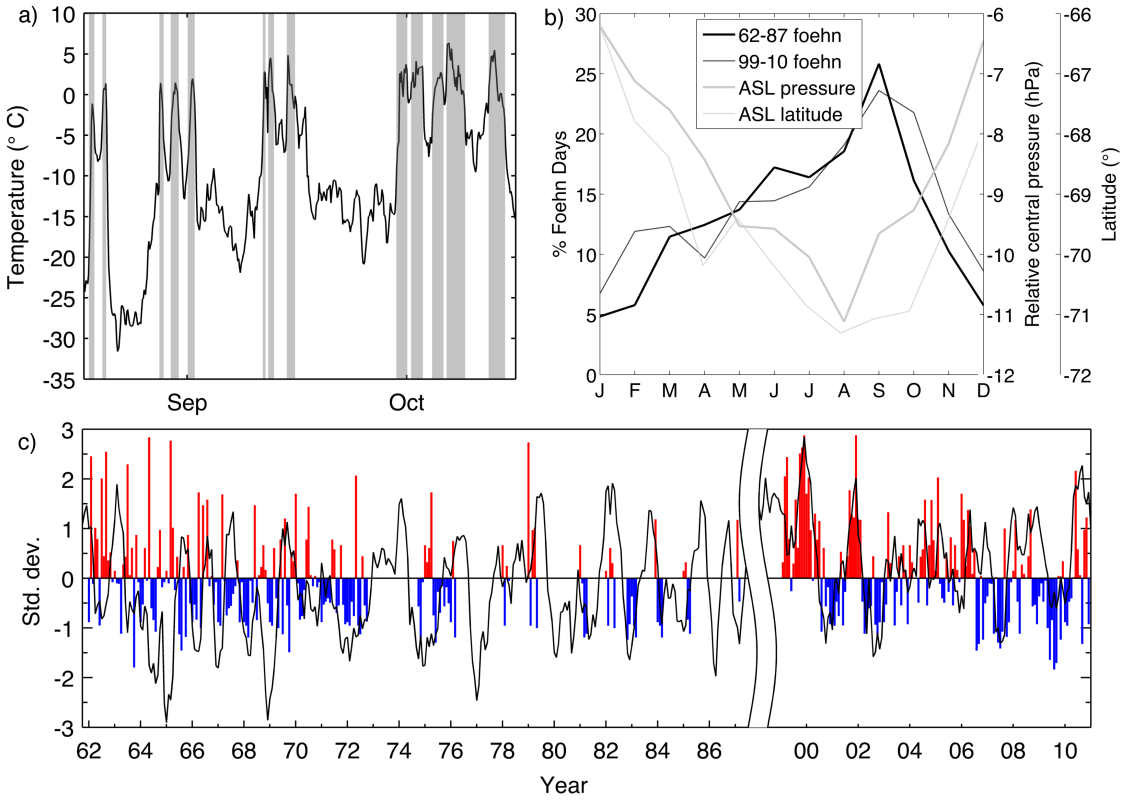

Figure 3.6: Temporal characteristics of foehn events. a) time series of Matienzo temperature between August 17 and October 15, 2004, with shading corresponding to identified foehn events b) seasonal cycle of mean monthly foehn frequency for each decade between 1962–1987 (black solid) and 1999–2010 (black dashed, as well as Amundsen Sea Low relative central pressure (grey solid) and latitude (grey dashed). c) time series of monthly standard anomaly in foehn frequency, with positive anomalies in red and negative anomalies blue. Black line corresponds to the SAM index, smoothed using a 5-month moving average. Note break in time series between 1987 and 1999.

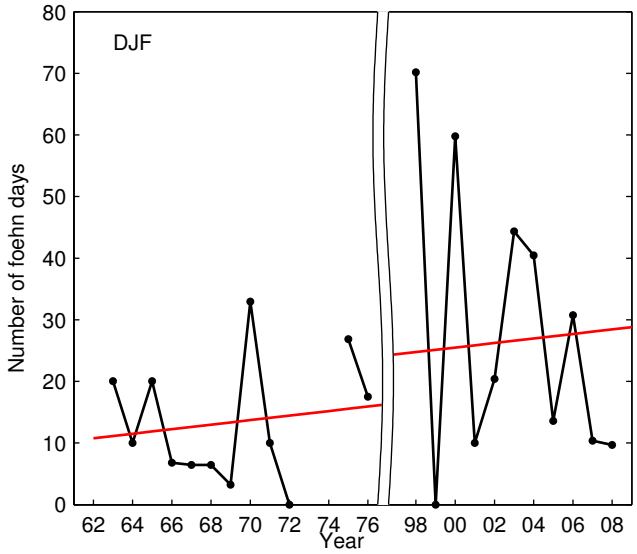

Figure 3.7: Seasonal foehn day time series for Matienzo between 1962 and 2010 for the summer season. Points represent sum of foehn days during DJF. Red lines correspond to linear trend. Only months in which 85% of daily observations were available were used in this analysis.

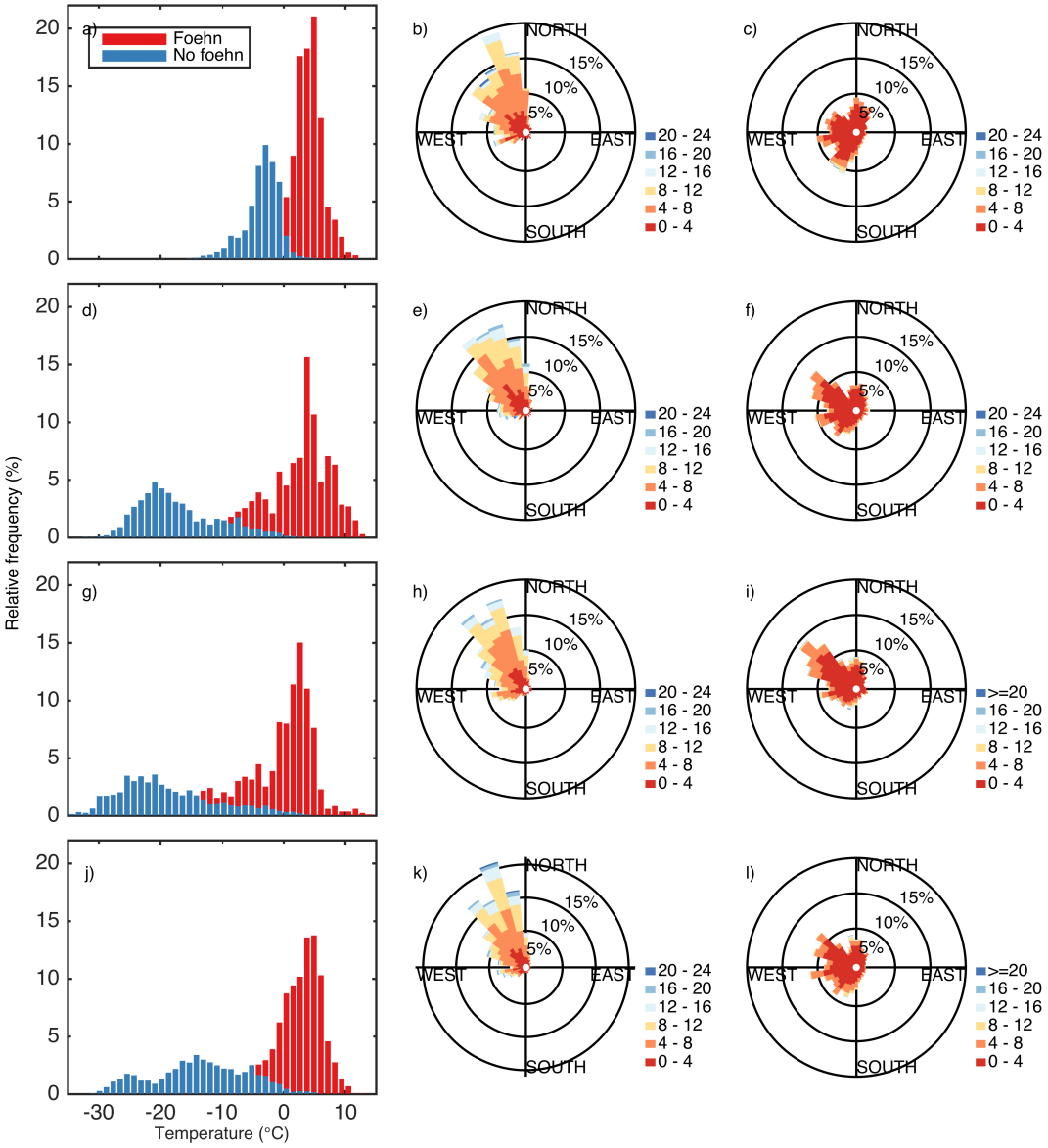

Figure 3.8: Characteristics of air flow at Foyn Point (FONP) during periods of foehn and non-foehn conditions for (a–c) summer (DJF), (d–f) fall (MAM), (g–i) winter (JJA) and (j–l) spring (SON). The first column shows frequency histograms of temperature observations for foehn and non-foehn conditions, the second column wind speed and direction during foehn events, and the third wind speed and direction during non-foehn conditions. Wind speed is indicated by colors, with units of m s-1. Frequency of observation is calculated relative to observations collected during foehn or non-foehn periods separately.

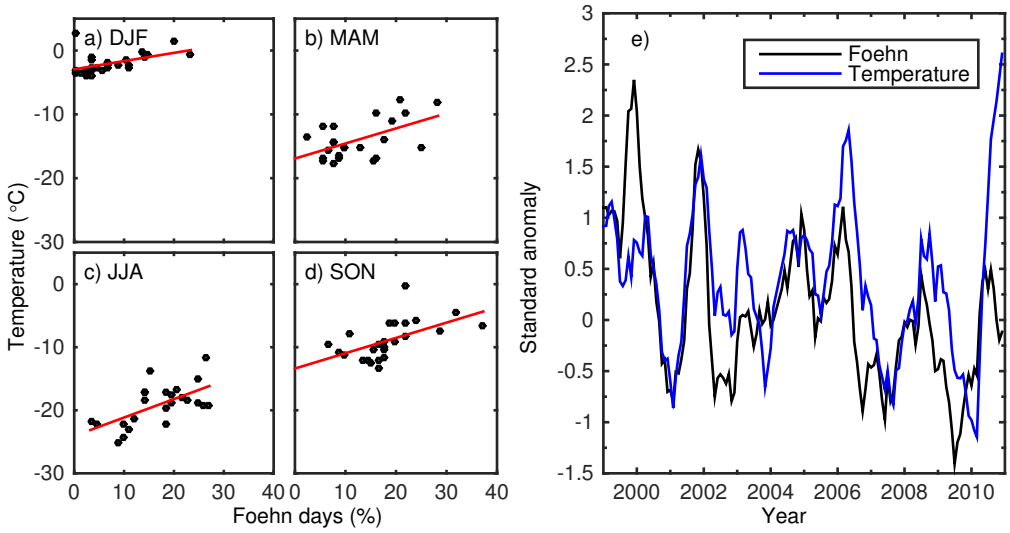

Figure 3.9: The relationship between mean seasonal temperature and foehn frequency for Matienzo for (a) summer, (b) fall, (c) winter, and (d) spring. Red line show linear trend in the data. b) Time series of standard anomalies in foehn frequency (black) and temperature (blue) between 1999 and 2010. Time series are smoothed with a 5 month moving average.

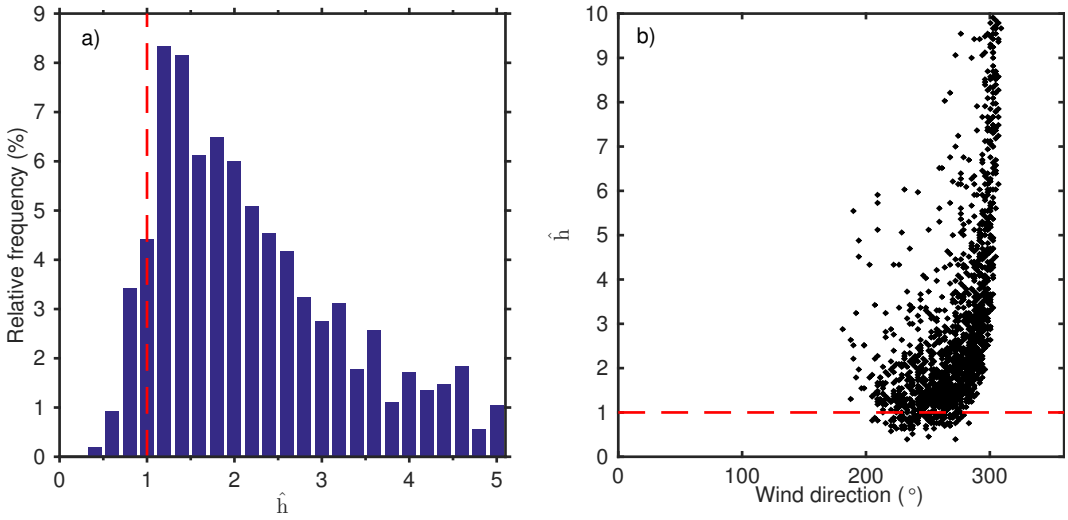

Figure 3.10: a) histogram of non-dimensional mountain height, $\hat{h}$, for all foehn events between 1999 and 2010 computed at location 150 km west of the Antarctic Peninsula (-63.75° lat, -66.75° lon). Only $\hat{h}$ values below 5 are shown (80% of all occurrences). b) scatterplot of wind direction averaged between the 1000 and 800 hPa ECMWF model levels (approximately 200–1000 m) versus non-dimensional mountain height for foehn events, calculated at the same point as a). Red vertical (a) and horizontal (b) lines correspond to the theoretical threshold of $\hat{h}$=1.1 separating linear from non-linear flow.

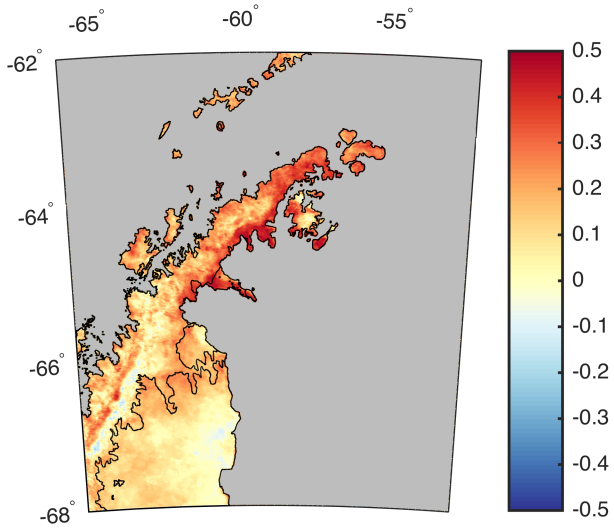

Figure 3.11: spatial correlation (ρ) between the foehn anomaly time series and backscatter-derived melt over land. Significance of correlation (p-value) is shown in Supplemental Figure 3.8

Chapter 4

Sensitivity of coastal marine ecosystems to atmospheric processes after ice shelf disintegration

4.1 Abstract

Primary production in the Larsen B represents a new source of organic carbon to the marine ecosystem of the NW Weddell Sea in the last 12,000 years. Using the abrupt collapse of the Larsen B ice shelf in 2002 as a model system for coastal Antarctic regions, we show that the climate-mediated changes in wind patterns and atmospheric temperature which contributed to ice shelf collapse along the east Antarctic Peninsula, now control inter-annual variability of phytoplankton biomass and primary production in the newly opened polynya by regulating the timing of sea ice retreat and the extent of open water area in this region. Following polynya opening, feedbacks between atmosphere and ocean further amplify the effect of wind forcing on the cryosphere. Given these close ties between atmospheric processes and phytoplankton growth, further warming in the

region may have important consequences for the future of this coastal system and other ice-shelf dominated regions farther south.

4.2 Introduction

The abrupt collapse of the Larsen B ice shelf in 2002, which exemplified the effects of climate change on the cryosphere in the popular and scientific literature, provides a natural laboratory to explore physical-biological relationships and the evolution of polar marine ecosystems in the face of climate change. Present for the last 12,000 years (Domack et al. 2005, Rebesco et al. 2014), the Larsen B retreated starting in the 1960s and finally disintegrated in February/March 2002, with 3250 km^2 of floating ice lost in a few weeks (Scambos et al. 2003). Unlike other regions of the Antarctic, where ice shelf retreat has been linked to the increased advection of warm ($\sim$1.2 °C) circumpolar deep water (CDW) to the ice front (Jacobs et al. 2011, Rignot et al. 2014, Dutrieux et al. 2014), the collapse was associated with rapid increases in atmospheric temperature (van den Broeke et al. 2005). Warming along the east Antarctic Peninsula (eAP) has been linked to a shift towards positive polarity of the Southern Annular Mode (SAM) and a concomitant strengthening of circumpolar westerlies, favoring the advection of warm maritime air over the Antarctic Peninsula (AP) mountain range and the genesis of strong, warm, and dry downsloping foehn winds over the Larsen Ice Shelf (Marshall et al. 2006,). Atmospheric teleconnections from the tropics, which have been shown to significantly impact atmospheric patterns over the West Antarctic Ice Sheet, may also have contributed to this increased northwesterly advection (Ding and Steig 2013, Li et al. 2014). Warm foehn winds moderate climate along the eAP, which is otherwise dominated by steady southerly winds and a cold continental climate that promotes sea ice growth and deep winter mixing (Martin and Peele 1978, Schwerdtfeger 1975). A recent study

has lent further support to this foehn hypothesis for ice shelf collapse, noting sustained periods of foehn winds and positive anomalies in atmospheric temperatures preceding major 20th century retreat events of the ice shelf (Cape et al. submitted). Prolonged melt seasons and melt-driven fracturing of an already weakened structure due to atmospheric forcing, thereby contributed to the demise of the ice shelf (Scambos et al. 2003).

Biological processes are intimately tied to the physical environment and their functioning both directly and indirectly structured by the extreme seasonality in atmosphere-ocean processes (Eicken 1992, Clarke 1988). Changes in the phenology of major seasonal transitions in the physical environment, such as the advance and retreat of sea ice, could therefore have far-reaching effects on the marine ecosystem ranging from local processes (food availability for higher trophic levels) to global responses (CO_2 sequestration via the biological pump, Sarmiento et al. 2004, Hoegh-Gulberg and Bruno 2010). While negative consequences tend to be emphasized on a global scale, the consequences of marine ecosystems evolution under continued warming could be positive for some species (Smetacek and Nicol 2005, Montes-Hugo et al. 2009). Long-term observations of direct impacts of climate-driven changes on biological systems are however limited in this extreme and remote environment, and the range of consequences of warming on the Antarctic marine ecosystem remain poorly constrained.

The Larsen B embayment is undergoing intertwined physical and biological evolution that are unique in their magnitude and their rate of change, yet also representative of the changes ongoing across the coastal Antarctic. Now an active coastal polynya following ice shelf retreat (a coastal region of open water otherwise surrounded by sea ice), the Larsen B embayment is a site of active seasonal water column primary production during periods of open water (Cape et al. 2014), marking an abrupt and exceptional shift in the previously oligotrophic, chemosynthesis based ecosystem characterizing the sub-ice shelf environment throughout the Holocene (Domack et al. 2005, Gutt et al.

2011). The embayment is now also subject to the seasonality of sea ice cover, whose dynamics have undergone significant regional changes as a result of variability in surface ocean heat uptake and atmospheric circulation (Stammerjohn et al. 2008, Holland et al. 2014). Removal of ice shelf buttressing has led to increases in coastal glacier velocities and increased glacial ice and meltwater discharge into coastal regions, as observed in the Amundsen Sea (Rignot et al. 2008, Jacobs et al. 2011, Stanton et al. 2013), contributing to sea level rise and further precipitating negative trends in ice sheet mass balance in the region (Scambos et al. 2004, 2011, Berthier et al. 2012, Shuman et al. 2011). While providing an opportunity to investigate the particular disturbance of ice shelf removal on the evolution of coastal Antarctic systems, the collapse of the Larsen B also gives us the ability to test the importance of various physical forcings on phytoplankton processes at the bottom of the food web, as these changes in both cryosphere and atmosphere are likely continue in the future (Cook and Vaughan, 2010, Rignot et al. 2014).

Using satellite records of phytoplankton biomass and primary productivity, sea ice concentration, and a long-term meteorological record located at a critical site between the former Larsen A and B ice shelves, we show that atmospheric processes responsible for the collapse of the Larsen B now control inter-annual variability in marine ecosystem processes following ice shelf disintegration. The timing of sea ice retreat, the length of the growth season, and the seasonal area of the new coastal polynya are intricately tied to foehn winds, ultimately controlling phytoplankton biomass and seasonal primary productivity rates in the region. In this way, waters previously protected from atmospheric forcing by the ice shelf are now subject to variability in atmospheric circulation associated with a changing climate, and the development of the marine ecosystem constrained by physical forcing on phytoplankton at the base of the food web.

4.3 Methods

Foehn events were quantified from automated weather time series collected between 1999 and 2010 at the Argentinean Base Teniente Matienzo. The base is located on the Seal Nunataks at 25 m altitude at the northern edge of Larsen B embayment (Figure 4.1a). The records consist of measurements of temperature, relative humidity, wind speed and direction. Following Speirs et al. 2012, we identified the initiation of foehn events using a semi-automated algorithm by their characteristic signature of rapid increases in temperature ($\frac{dT}{dt}$ = 1 °C hr^{-1}), decreases in relative humidity ($\frac{dRH}{dt}$ = -5 % hr^{-1}), and strong wind gusts from a generally westerly direction (wind speed >= 5 m s^{-1}, between 240 and 300 °). Cessation of wind events consisted of a return to pre-foehn conditions. For time periods when the full suite of sensor was unavailable, foehn events were primarily identified by their temperature signature. The time series was then quality controlled manually. We classified days experiencing 6 or more hours of foehn conditions as "foehn days", and further composited the daily dataset to month by summing the number of foehn days occurring within a calendar month and calculating a % monthly foehn frequency by dividing by the total number of days in the month.

A continuous, daily resolution sea ice concentration dataset for the period of interest was generated by concatenating records derived from the Advanced Microwave Scanning Radiometer-Earth Observing System (AMSR-E, 6.25 km grid) and Special Sensor Microwave Imager (SSM/I, 12.5 km grid). Sea ice concentration was calculated using the ARTIST (Arctic Radiation and Turbulence Interaction STudy) Sea Ice (ASI) algorithm (Klaeschke et al. 2001, Spreen et al. 2008), processed without any land masking to account for the gradual retreat of the Larsen B ice shelf (Cape et al. 2014). The AMSR-E dataset is available at ftp://ftp-projects.zmaw.de/seaice/AMSR-E_ASI_IceConc/tmp_no_landmask/. The daily sea ice concentration record was further binned to month by

averaging daily values for each pixel. A spatial average over the Larsen B embayment was also computed by averaging pixels within the 1963 extent of the Larsen B ice shelf (Ferrigno et al. 2008, Figure 4.1a).

Monthly mean net primary productivity (mg C m^{-2} d^{-1}), monthly integrated productivity per unit area (g C m^{-2} $month^{-1}$) and total monthly production (Tg C $month^{-1}$) for the Larsen B embayment as a whole were derived from daily ocean color time series of photosynthetically available radiation (PAR) and chlorophyll-a (chl-a) collected by MODIS Aqua (r2012.0) and SeaWiFS (r2010.0). Level 1 and 2 ocean color datasets were downloaded from http://oceancolor.gsfc.nasa.gov/ and processed using SeaDAS (http://seadas.gsfc.nasa.gov/). Surface chl-a concentration was used as a proxy for phytoplankton biomass. A modified version of the standard Vertically Generalized Production Model (VGPM) tuned to data from the AP was used to compute productivity (Dierssen et al. 2000). For days with no valid data, linear interpolation using neighboring points was used to estimate NPP. Monthly mean productivity per unit area was calculated as the mean of all pixels within the Larsen embayment as defined above. Monthly production per unit area was calculated by integrating mean daily values over each month. Similarly, total production was estimated by multiplying daily net primary productivity by open water area, derived from sea ice concentration, and integrating over each month. Details of the processing scheme for ocean color datasets and productivity models can be found in Cape et al. (2014). Annual rates were estimated from available ocean color data by assuming a growth season extending from October 1 to March 31 and integrating monthly time series.

Sea surface skin temperature at 60 m resolution within the polynya was calculated from the thermal infrared bands of the Landsat 7 Enhanced Thematic Mapper Plus (ETM+) downloaded from http://glovis.usgs.gov. A threshold on band 4 was used to identify regions of open water. Thermal infrared bands were calibrated and converted to

SST using standard routines outlined in the Landsat 7 Science Data User's Handbook (http://landsathandbook.gsfc.nasa.gov/pdfs/Landsat7_Handbook.pdf).

We quantified the relationship between time series using the non-parametric Spearman's Rank-Order Correlation. Associations between two variables were also quantified using simple linear regression, with results presented as b = slope, r^2, p-value.

4.4 Results and discussion

4.4.1 Polynya production and atmospheric variability

The time series of satellite-derived productivity and foehn frequency at Matienzo demonstrate a remarkable association between physical forcing and rates of integrated phytoplankton productivity in the Larsen B polynya on a number of time scales. Foehn winds in this region are highly variable on a monthly and inter-annual basis, with large excursions in monthly foehn frequency apparent over the span of 2–6 months (Figure 4.1b). Monthly anomalies in integrated primary productivity rates mirror this pattern, with periods of positive productivity anomaly either directly following or occurring in concert with increased foehn frequency in the region. This pattern is also observed when considering other proxies for phytoplankton growth, such as chl-a biomass or mean productivity rates (Figure 4.1c). While significant scatter is still evident in the monthly datasets, annually integrated primary productivity rates for the Larsen B shows a strong relationship with the number of foehn events, particularly considering a lagged relationship between winds and productivity rates. A doubling of foehn frequency during the winter and early spring (Jun–Nov) tends to be associated with almost an octupling of seasonally integrated primary productivity during the subsequent growth season (Oct-Mar, $b = 3.98$, $r^2 = 0.48$, $p < 0.05$, Figure 4.1c,).

Although surrounded by the extensive grasp of the thick Weddel Sea ice cover

and bathed in a continental climate for most of the year (King and Turner 2009, Yi et al. 2011), the Larsen B polynya can seasonally become a haven for microbial communities. With rates of annual primary productivity rivaling other productive polynyas of the coastal Antarctic, such as the Ross Sea, Amundsen, or Pine Island polynyas (up to 200 g C m^{-2} yr^{-1}, Figure 4.1c, Figure 4.2, Arrigo et al. 2003), the Larsen embayment is a hotspot of productivity bordering the oligotrophic Weddell Sea Gyre. Typical patterns of phytoplankton biomass in the Larsen B appear in Figure 4.2a. A well-developed bloom is apparent in the polynya, with maximum biomass of up to 14 mg m^{-3} near the center of the embayment and decreasing biomass near-shore and along the ice-edge. Similar patterns can be observed in the Larsen A polynya to the north, with significantly lower concentrations apparent along the coastal western AP at this time.

Maxima in total production tend to occur between December and February at the peak of seasonal melt and light availability, with blooms beginning in October and November following sea ice retreat (Figure 4.2b). Coastally trapped by offshore pack ice, phytoplankton bloom development in surface waters shows a characteristic signature similar to other polynyas and coastal marine ecosystems. Yet these patterns are highly fluid and far less predictable than for other Antarctic polynyas on an inter-annual basis, with timing of sea ice retreat and advance often severely limiting or even preventing phytoplankton growth (summers of 2000–2001, 2007–2008 and 2009–2010 in Figure 4.2b). As a result, the timing of peak total production also shows significant inter-annual variability tied to the timing of opening of sea ice and the length of open water conditions, with early opening coupled with longer ice-free seasons and higher rates of productivity. This relationship between productivity and sea ice dynamics becomes apparent when considering rates of total production integrated over the entire embayment, with high rates of total production preferentially occurring during months of low sea ice concentration (Figure 4.2c).

The inherent variability in this system and seemingly strong association between physical processes and microbial growth rates are evidence for a highly dynamic system. By influencing both the area available for surface phytoplankton growth and the rates of productivity, foehn winds and sea ice synergistically control patterns at the bottom of the food web. An understanding of the underlying dynamics is however needed to better predict the future evolution of this new marine coastal ecosystem.

4.4.2 Foehn winds drive variability in sea ice cover

Sea ice cover in the Larsen B embayment can be highly variable, with multiple instances of advance and retreat within a single season, unlike the west Antarctic Peninsula, which experiences seasonally persistent ice-free conditions at similar latitudes between October and March (Stammerjohn et al. 2008). In 2004-2005, the first opening of the Larsen B embayment occurred in early October, followed by subsequent retreats in November and February after periods of increased ice cover (Figure 4.3). Periods of strong foehn wind forcing, identifiable by temperature and relative humidity signatures, accompanied these transitions, with multiple events occurring in rapid succession. Models and limited aircraft observations of specific events have shown that these winds have a profound effect on the temperature regime of the region (Elvidge et al. 2014, King et al. 2008, Orr et al. 2008); the predictions are supported by our recent field measurements of rising temperatures of up to 20 °C for periods of up to 7 days between October and March 2004-2005 (Figure 4.3f). Periods of low and increasing sea ice concentration during this season are associated with relaxation of westerly wind flow over the AP and reduced foehn frequency, with a return of cold southerly flow.

Decreases in sea ice concentration that characterize the inter-annual variability discussed above are consistently associated with periods of sustained foehn events, suggesting that foehn wind variability drives seasonal sea ice variability in the spring

and summer (Supporting Figure C.1). Time series of average sea ice concentration within the Larsen B embayment derived from satellite show that anomalies in monthly foehn frequency between 1999 and 2010 are strongly negatively correlated with sea ice concentration, a proxy for sea ice cover, with positive anomalies in wind events associated with negative anomalies in sea ice concentration (Figure 4.4a, $\rho(139) = 0.57$, $p \ll 0.01$). This relationship holds even through the fall and winter (April–September), though variability in sea ice concentration is far less pronounced due to the overall lower atmospheric temperatures encountered during these seasons (Supporting Figures C.1 and C.2). Powerful wind forcing from warm, dry foehn winds on coastal sea ice cover is often succeeded by a hiatus in foehn events and persistence open water over time scales of weeks to one month before gradual increase in sea ice concentration linked to either *in situ* ice growth or shoreward advection of the pack ice.

The spatial extent of foehn influence along the NW Weddell is best illustrated by the correlation map between monthly time series of foehn frequency anomaly and monthly anomalies of satellite-derived sea ice concentration (Figure 4.4b). Significant correlations are evident from the tip of the AP and south along the eastern side of the peninsula to the Larsen C ice shelf, with positive foehn wind anomalies associated with decreased sea ice cover (correlations of $\rho(139) < -0.3$ and $\rho(139) > 0.3$ are significant at $p < 0.01$, see also Supporting Figure C.2). The area of strongest negative correlations between the Matienzo wind record and sea ice northeast of the AP corresponds to a region of broad northwesterly wind intensification associated with southeastward advection of sea ice during periods of positive SAM, further demonstrating a link between large scale flow, regional foehn dynamics, and sea ice processes (not shown). Offshore near the shelf break we find little to no relationship between foehn wind events and sea ice concentration, consistent with the presence of extensive and persistent sea ice in the Weddell Sea Gyre. The relationship is also comparatively weak along the western AP

north of 64°S, increasing southward, where a significant positive correlation may indicate increased ice compaction in the region resulting from more frequent low-level westerly wind (Stammerjohn et al. 2008b). The spatial footprint along the eAP derived from this correlation map is consistent with previous modeling results and limited aircraft observations of foehn events in the region (Orr et al. 2008, van Lipzig et al. 2008, Elvidge et al. 2014). Given the particular spatial signature, foehn winds resulting from increased westerly flow may also have contributed to the negative trend in sea ice concentration observed in the NW Weddell Sea prior to ice shelf collapse (Stammerjohn et al. 2008).

Foehn winds serve as a major control on landscape variability following ice shelf removal, with frequency of foehn events the major factor controlling open water area and ultimately productivity. These regional results further support previous studies highlighting the strong link between large-scale wind forcing and sea ice processes (Holland and Kwok, 2012) Although the strength of the association between foehn winds and sea ice concentration is modest, reaching a maximum of $\rho = -0.62$ along the tip of the AP and averaging between 0.3 and 0.5 elsewhere along the coastal NW Weddell, the analysis above does not take into consideration the impact of other dominant regional atmospheric circulation patterns, such as the strong southerly winds commonly observed in the region (Schwerdtfeger, 1975), or the structural properties of the sea ice itself, which would have important consequences for both the growth and seasonal decay of sea ice and its response to intermittent foehn forcing (Weeks, 2010)

4.4.3 Complexity in atmosphere–ice–ocean processes

The strong association between wind forcing and coastal physical and biological processes in the Larsen B polynya, exemplified in Figure 4.1 and Supporting Figures C.1 and C.2, does not account for the absolute magnitude of the sea ice response to a given succession of foehn events, which can be variable on both seasonal and yearly time

scales. For example, periods of suppressed sea ice cover in the embayment tend to be shorter between April and September rather than October to March due to the overall colder temperatures encountered during these months. The impact of foehn winds is instead greater in the summer, when seasonal temperatures are near 0 °C. Nevertheless, the fall and winter months likely play an important role in determining the magnitude of the impact of foehn events in the spring and summer sea ice cover (e.g. Figure 4.1b)

Foehn eventscan influence sea ice though a combination of dynamic and thermodynamic processes by impacting structural properties of the ice and its motion (Holland and Kwok, 2012). Between 1999 and 2010, seasons with enhanced October–March sea ice concentration followed months of reduced wintertime foehn activity and a relatively stable sea ice cover and vice versa ($b = -6.99$, $r^2 = 0.38$, $p < 0.05$, e.g. 2000, Figure 4.1, Supporting Figures C.1, C.2). Extended periods of calm wintertime conditions would be conducive to the growth of fast ice in the embayment, potentially leading to thicker ice during the spring–summer transition and limiting the impact of even strong and frequent foehn events. Conversely, winter seasons characterized by dynamic changes in ice cover and sustained wind events, as observed during 2004, may precondition the ice for breakup in the spring for even limited wind forcing. This preconditioning mechanism is likely implicated in the spring of 2005, when only half of the Larsen B embayment opened following a quiescent winter and fall despite periods of strong, sustained spring foehn events that raised surface temperatures to 5–10 °C for up to 24 hours (not shown). Melt ponds on the fast ice surface across the embayment, as observed in the November 13, 2005 image captured by MODIS Terra (Supporting Figure C.4), is nevertheless further evidence of the widespread and prevalent impact of these winds on even thick ice cover.

Secondary forcing mechanisms and feedbacks between atmosphere, ice, and ocean, likely play an important role in regulating temporal patterns in primary production in this region. Increases in open water area during periods of foehn events, as well as

the presence of melt ponds on the sea ice surface, would promote greater surface heat absorption during periods of high solar heating thereby accelerating decay and melt of sea ice (Perovich et al. 2008). Increased surface ocean heat uptake after initial sea ice retreat is likely particularly important to reinforce the short-term impact of foehn winds events, particularly during calm summers (e.g. 2006–2007, Supporting Figure C.1). High meltwater input into coastal region due to glacial drainage from the ice sheet and glaciers would further reinforce enhanced heat uptake in the mixed layer by lowering surface water salinity and increasing stratification, conditions ideal to reduce light limitation and enhance growth rates in phytoplankton (Mitchell and Holm-Hansen 1991). High-resolution satellite images of sea surface temperature (SST) derived from Landsat 7 provide evidence for this mechanism, showing gradients in SST of up to 3 °C across the open embayment with maxima near-shore and patterns of circulation consistent with meltwater drainage from coastal regions and sea ice melt offshore (Figure 4.5). Further field studies of the Antarctic marginal ice zone are necessary to parse the competing influence of atmosphere and ocean on sea ice processes and exchanges at the atmosphere-ocean boundary.

Sea ice is an important component of Southern Ocean primary production by acting as a persistent habitat for microbial communities and a seed for ice-edge blooms during sea ice retreat (Garrison et al. 1986, Smith and Nelson, 1986, Legendre et al. 1992). The physical characteristics of the sea ice have major consequences for physico-chemical exchanges between ice and the surface ocean. Variations in sea ice temperature, salinity, and porosity affect circulation within the sea ice brine channels (Golden et al. 1998), controlling exchanges of nutrients with the underlying ocean (Tison et al. 2008). This may have important consequences for sea ice microbial communities throughout the year, and therefore photosynthetic rates, biomass and carbon export to the deep ocean in this sea-ice dominated ecosystem (Saenz and Arrigo 2014). Meltwater input

via glacial discharge and sea ice decay may also resupply surface waters with iron and other micronutrients, relieving possible iron limitation and helping to sustain high phytoplankton growth rates (Hawkings et al. 2014, Stibal et al. 2012, Bhatia et al. 2013). Moreover, higher temperatures due to increased surface heat absorption during periods of ice melt may further affect the physiology of phytoplankton, while high cell concentrations in surface waters may serve as a positive biological feedback to water temperature and the physical system (Manizza et al. 2005). These intertwined processes linking atmospheric variability to cryosphere dynamics can facilitate the high rates of productivity observed in this polynya.

The satellite and *in situ* weather data analyses have uncovered the mechanism underlying the evolution of this coastal Antarctic system following abrupt disturbance and the powerful connections between regional atmospheric circulation and primary producers through sea ice dynamics. Foehn events are necessary catalysts for sea ice retreat and thereby phytoplankton production in the Larsen B embayment and along the coastal eAP, though not always sufficient to maintain open water conditions for extended periods of time. Theoretical arguments and limited *in situ* sampling also point to the importance of atmosphere-ice-ocean feedbacks in regulating polynya dynamics. Yet years after the collapse of the Larsen B, these winds continue to play a major role in shaping the environment of the NW Weddell Sea. While the proximal reasons for the upward atmospheric temperature trend and sea ice dynamics are therefore resolved, the ultimate causes for these large-scale variations in synoptic circulation and teleconnections that lead to regional foehn variability remain poorly understood and limited to broad correlations (Stammerjohn et al. 2008, Ding and Steig 2013, Li et al. 2014). Similarly, linear approximations of physical-biological interactions, as utilized in this study, present difficulties due to the often complex and non-linear mechanisms underlying ecosystem dynamics (Hsieh et al. 2005). Nevertheless, this work highlights clear connections

between these different components of the earth system, further supporting the importance of integrated approaches to the study of natural systems.

We've presented new evidence for mechanisms linking atmospheric processes to cryosphere dynamics and the base of the Antarctic food web in a region of rapid environmental change, thereby providing a bottom-up view of the potential evolution of this system under continued atmospheric forcing. While presenting the particular case of the collapse of the Larsen B, this study highlights the sensitivity of biological processes to abrupt environmental change, providing a seldom-described example of ecosystem boom in the face of warming in high latitude oceans. As polynyas and coastal regions play a disproportionate role in the Antarctic marine ecosystem (Tréguer and Jacques 1992, Arrigo et al. 1998), our results have important implications for carbon cycling in these productive regions.

4.5 Acknowledgements

The authors thank Randie Bundy for suggestions that led to improvements of this manuscript, and Ken Mankoff for giving advice on the processing of Landsat images. This work was supported by the National Science Foundation Office of Polar Programs under NSF grant ANT-0732983. MRC was also supported by the NSF Graduate Research Fellowship under grant DGE-1144086 and by NASA Headquarters under the NASA Earth and Space Science Fellowship Program–grant NNX12AN48H.

This chapter is in preparation for publication as: Mattias R. Cape, Vernet, M. Sensitivity of coastal marine ecosystems to atmospheric processes after ice shelf disintegration.

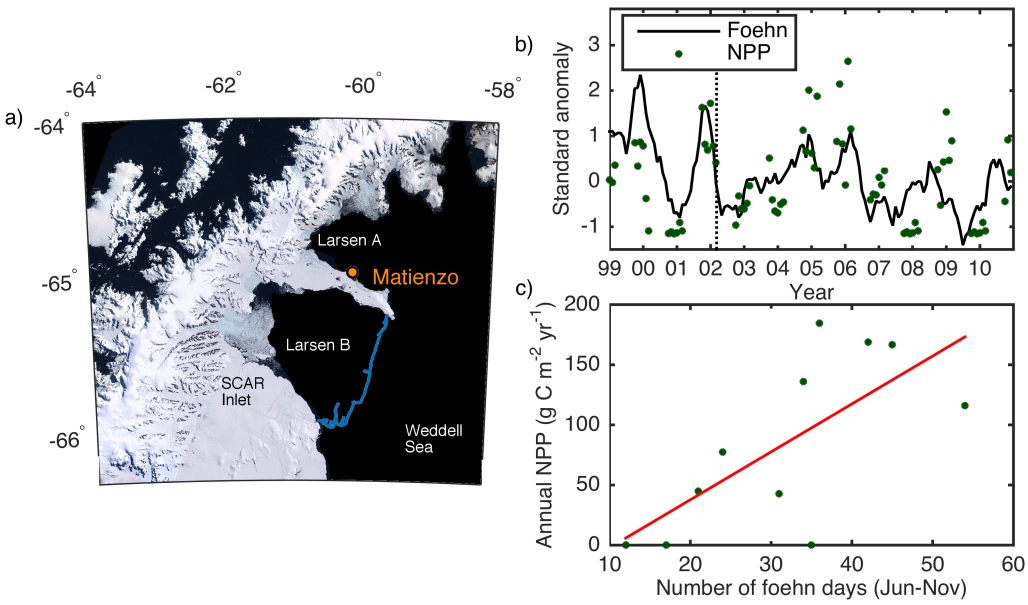

Figure 4.1: Correlation between rates of phytoplankton primary productivity and wind forcing in the Larsen B embayment a) map of the northern Antarctic Peninsula, showing locations of the Base Matienzo. The maximum extent of the Larsen B ice shelf in the 1960s over which sea ice and productivity statistics were computed is indicated by a blue line. b) relationship between anomalies in monthly rates of integrated productivity (green circles) and time series of anomalies in monthly foehn frequency (black line) between 1999 and 2010. The foehn time series has been smoothed with a 5-month moving average. The dashed vertical line corresponds to the 2002 collapse of the Larsen B ice shelf. Positive anomalies in the years leading up to ice shelf collapse are indications of a productive system despite the presence of the ice shelf. c) scatterplot of total number of foehn days between June and October of each year and annually integrated water column primary productivity (g m^{-2} yr^{-1}), estimated from the subsequent October–March growth period. Red line indicates best linear fit to the data.

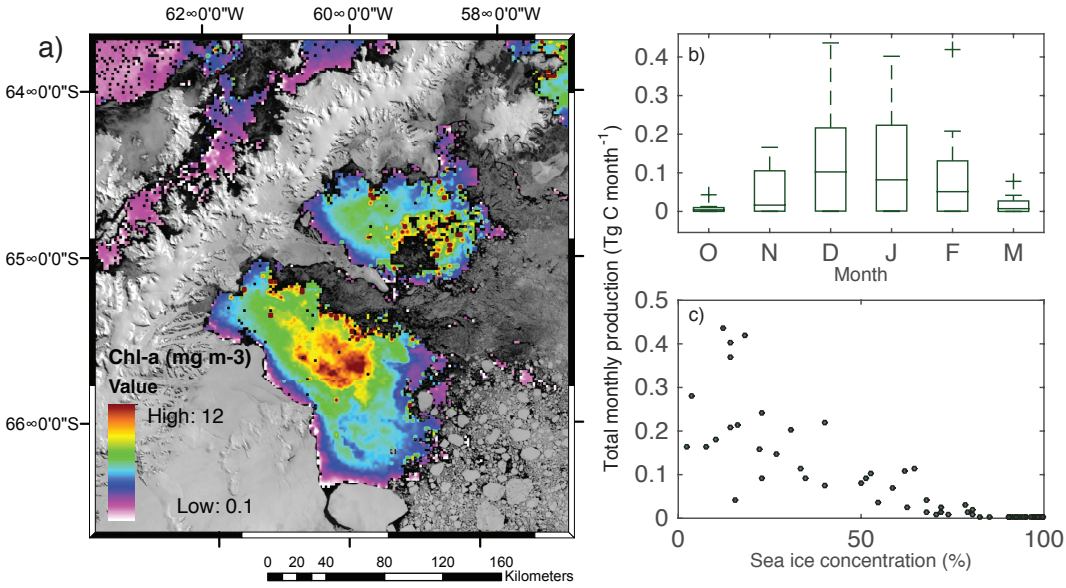

Figure 4.2: Influence of foehn winds on open water area, biomass, and total production in the Larsen B. a) Typical patterns of phytoplankton biomass and sea ice distribution during open growth periods along the eAP, as observed on November 29, 2004 by the MODIS Terra sensor. Color shading corresponds to chl-a concentration. The image of the Larsen region is courtesy of the NSIDC (http://nsidc.org/data/iceshelves_images) b) Seasonal cycle of total monthly phytoplankton production within the Larsen B embayment, with monthly statistics calculated over the 1999–2010 period. Horizontal lines correspond to the minimum, 25th percentile, median, 75th percentile and maximum value from bottom to top, with plus signs corresponding to outliers in the dataset c) relationship between total monthly production rates and sea ice concentration, pointing to the importance of open water area for embayment productivity.

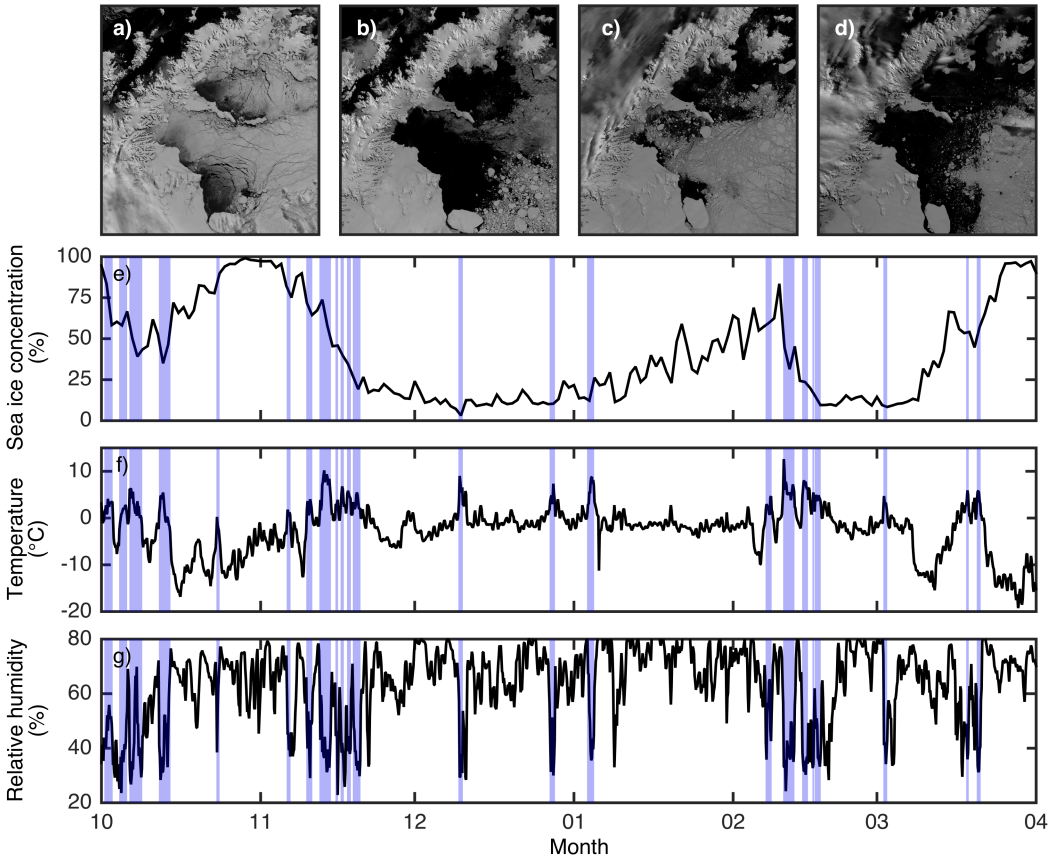

Figure 4.3: Seasonal progression of sea ice cover and meteorological conditions for the 2004–2005 growth season. Images of surface conditions collected by MODIS Terra are shown for a) Oct. 30, 2004, b) Nov. 15, 2004, c) Jan 8, 2005, and d) Apr. 2, 2005 e) Time series of sea ice concentration between October 1 2004 and March 31, 2005, with foehn events (corresponding to periods of high temperature and low relative humidity) highlighted in blue f) same as e) for atmospheric temperature at Matienzo g) same as e) for relative humidity at Matienzo.

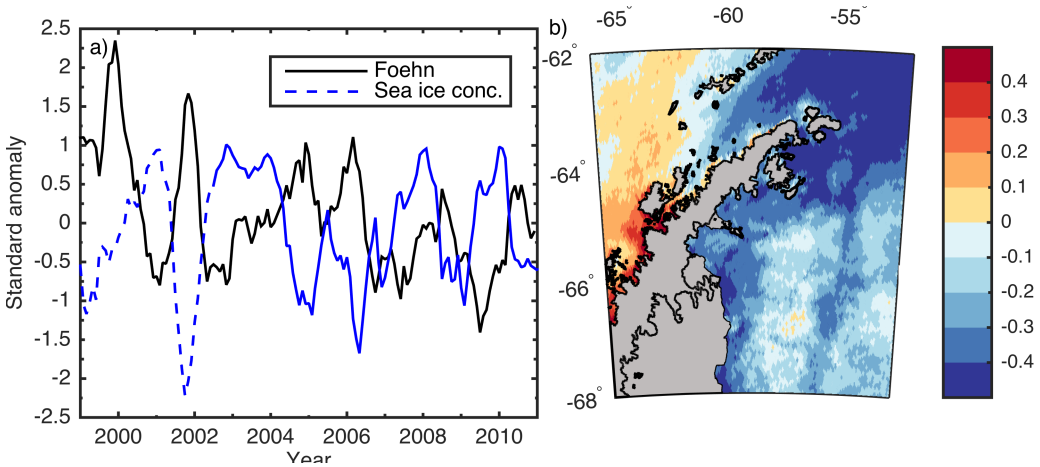

Figure 4.4: Influence of foehn wind frequency on eAP sea ice concentration. a) time series of standard anomalies in monthly sea ice concentration (blue) averaged over the Larsen B embayment and monthly foehn frequency at Matienzo (black). Dashed line represents SSM/I record, while solid corresponds to AMSR-E. b) spatial correlation (ρ) between monthly anomalies in foehn frequency recorded at Matienzo and sea ice concentration derived from satellite. Correlation coefficients above 0.3 and below -0.3 are significant at the 1% level (Supporting Figure C.3).

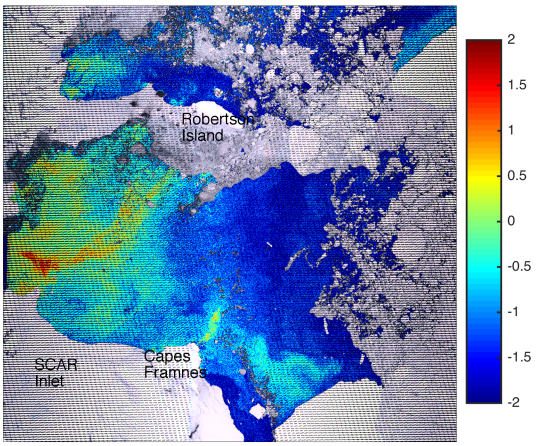

Figure 4.5: Composite of true color image and sea surface temperature from Landsat 7 EMT+, collected on January 7, 2007. The Landsat image was downloaded from http://glovis.usgs.gov/ and processed using ENVI.

Chapter 5

Impacts of ice shelf collapse and sea ice variability on primary production and organic matter export in the NW Weddell Sea

5.1 Abstract

Previous satellites observations have noted that the Larsen A polynya has become a hotspot of primary production following ice shelf disintegration, with variability in both temporal and spatial patterns of phytoplankton growth tied to variability in atmosphere–ice interactions and strong surface biological gradients apparent across the shelf. In this study, samples collected from the polynya during the austral fall of 2012 were analyzed to examine underlying physical processes responsible for this cross-shelf gradient in phytoplankton production. Water column and benthic observations were also used to complement previous surface observations in order to test the spatial and temporal

persistence of phytoplankton patterns since the opening of the embayment. Hydrographic sampling indicated the presence of high phytoplankton biomass sub-surface, with chl-a concentrations reaching a maximum of 8.8 mg m^{-3} near the entrance of the embayment. This deep chl-a and biomass maximum, located at the nutricline, below the mixed layer and in most cases below the euphotic zone, extended from the ice edge offshore to within 10 km of the coastline, with low chl-a concentrations observed both near-shore and underneath the pack ice. Seasonal productivity calculated from a nutrient drawdown method ranged from 495 to 811 mg C m^{-2} d^{-1}, consistent with previous observations, with lower productivity also noted below the pack ice and near-shore. These patterns coincided with a trend of stronger stratification offshore resulting from sea ice melt at the surface. Regional wind patterns served as significant forcing on mixed layer processes, with cold, southerly winds impacting phytoplankton concentrations, nutrient availability in the mixed layer, as well as stratification. Higher sediment pigment inventories offshore relative to inshore mirrored surface phytoplankton patterns, implying persistent gradient in organic matter export out of the euphotic zone. This multi-pronged approach shed light on important patterns of primary production in a new open water region, with implications for other Antarctic regions experiencing unprecedented warming

5.2 Introduction

Antarctic phytoplankton, microscopic drifters of the southern seas, thrive in an environment characterized by continual physical change, from the extensive advance and retreat of sea ice, the seasonal mixing and stratification of surface waters, to cycles of continuous day and night at this southern end of the planet (Smith et al. 1995). Well adapted to their extreme environment, phytoplankton communities, primarily dominated by large diatoms and the prymnesiophyte *Phaeocystis antarctica* (El-Sayed and Fryxell,

1993), are an essential link between the inorganic constituents of the ocean and the rest of the food web. They have therefore been a focus of ecological studies since the first exploratory expeditions of the 1800s, from Charles Wilkes's first descriptions of diatom-stained ice in 1845 to John Hart's classic studies on phytoplankton during the Discovery investigations between 1925–37 (Hart, 1934) and the contemporary long term ecological project at Palmer Station (Ducklow et al. 2013). Resilient to the vagaries of their environment with seasonal cycles timed with major physical transitions in both cryosphere and ocean (Eicken, 1992), phytoplankton communities are however not entirely immune, with alterations in microbial processes having far-reaching impacts on the rest of the ecosystem (Smetacek and Nicol 2005, Montes-Hugo et al. 2009).

Warming of the atmosphere and changes in wind patterns across the West Antarctic have led to extensive changes in the cryosphere and ocean (Marshall et al. 2006, Pritchard et al. 2009). These include the retreat of major glaciers (Rignot et al. 2014), advection of warm, deep water masses near the boundaries of the ice sheet (Jacobs et al. 2011), and alterations in the seasonal timing of sea ice advance and retreat (Stammerjohn et al. 2008, 2012). These observations have prompted concern regarding the fate of the Southern Ocean marine ecosystem (Smith et al. 1999, Smetacek and Nicol 2005, Schofield et al. 2010), which serve as breeding and feeding ground for both ecologically and economically important species. Given the importance of phytoplankton to ecosystem dynamics, a key question in contemporary research has therefore been the impact of climate change on these microscopic organisms.

The retreat and final collapse of the Larsen A and Larsen B ice shelves in 1995 and 2002 (Rott et al. 1996, Skvarca et al. 1999, Scambos et al. 2003) has become a captivating example of climate change in the Antarctic. Occurring over the span of 4-5 decades, the retreat of these ice shelves proceeded in abrupt increments and was caused by increases in surface temperatures along the eastern Antarctic Peninsula (eAP)

which led to sustained surface melting on the ice surface and weakening of the ice shelf (Scambos et al. 2003, Cook and Vaughan 2010). The newly opened embayments, and the previously dark and oligotrophic waters below the extinct ice shelves (Brachfeld et al. 2003, Domack et al. 2005), are now part of the Antarctic sea ice zone (Tréguer and Jacques, 1992), and thereby subject to the seasonal and inter-annual variability in sea ice cover, which has itself shown marked changes in seasonality in this region of the Antarctic (Stammerjohn et al. 2008). Retreat of ice shelves along the Antarctic Peninsula has been suggested as a potential boon for phytoplankton, with increased open water area leading to higher production and net drawdown of CO_2 in Antarctic coastal waters (Peck et al. 2010). The collapse of the Larsen A and B ice shelves, occurring during the satellite era, provide a model system to test this hypothesis and investigate the consequences of ice shelf collapse, and resulting changes in atmosphere-ice-ocean processes, on the marine ecosystem.

Unlike the marine ecosystem of the west Antarctic Peninsula, the NW Weddell is typically covered by sea ice year-round at similar latitudes. The Weddell Sea is known as one of the most productive regions of the Antarctic (Arrigo et al. 2008), dominated by production at the ice edge, within the ice, and in coastal polynyas (El-Sayed and Taguchi 1981, Smith and Nelson 1986, 1990, Arrigo et al. 2003). As a result of colder climate, brine rejection, and perennial sea ice cover, the water column is generally well mixed and nutrients are present in high concentrations (Smith and Nelson 1990). A previous satellite-based study in the Larsen area has shown that removal of the ice shelves precipitated a dramatic increase in primary production in the region, with overall rates rivaling the most productive coastal areas along the continent (Cape et al. 2014). Sea ice cover was also shown as the primary factor controlling production, due to the high variability in seasonal and inter-annual cover driven by a generally cold, continental climate (Schwerdtfeger et al. 1975, Martin and Peel 1978). For the higher trophic levels

of both water column and benthos, this increase in upper water column organic matter production marks an abrupt ecological transition that may fundamentally alter the food web in the region (Gutt et al. 2011, 2013). Recent sampling, though limited, suggests that organic matter input to the benthos via advection was low prior to ice shelf removal (Sañe et al. 2011). Yet work in the Ross Sea suggests that phytodetrital advection can also be spatially variable, leading to the establishment of thriving benthic communities in even permanently dark waters (Dayton and Oliver 1977). Because of the harsh climate, extensive sea ice, and remoteness of the region, biological observations in the Larsen region have been very limited (Bertolin and Schloss 2009, Sañe et al. 2011, Gutt et al. 2013). In order to understand post ice-shelf ecosystem forcing, it is however, essential to evaluate phytoplankton growth dynamics with respect to the physical and chemical environment, and to quantify the *in situ* flux of organic matter to the seafloor.

Ice shelf retreat, glacier acceleration, and changes in the phenology of sea ice transitions are continent-wide phenomena that are likely to continue in coming decades. Understanding the impact of these processes on the bottom of the food web is therefore necessary if we are to predict the range of impacts of these physical changes on the marine ecosystem, and ultimately the biological carbon pump. The collapse of the Larsen ice shelves provides a valuable opportunity to explore the response of Antarctic physical–biological processes, as well as test ecological theory of succession and community evolution as a response to abrupt disturbance (Gutt et al. 2011, 2013). Based on a previously published remote-sensing study (Cape et al. 2014), we hypothesized that *in situ* patterns of phytoplankton growth in the Larsen A embayment would show strong cross-shelf gradients associated with gradients in both nutrient distributions and physical water column structure, with coastal regions generally showing lower biomass and rates of production than farther offshore. We also hypothesized that these gradients would be persistent on time scales ranging from years to decades, implying high spatial variability

in organic matter export to the benthos across the shelf leading to a larger inventory of sediment phytodetritus offshore. To test these hypotheses and identify underlying causes for patterns in biological production, we analyzed water column and sediment datasets from a cruise to the Larsen A embayment. In order to give context to cruise results, interpret findings, and relate to previous studies, we also extended analysis to include satellite datasets of ocean color and sea ice concentration. By exploring multi-proxy estimates of phytoplankton processes in this traditionally under-sampled region, and in so doing evaluating patterns of biological production and export over time scales of days to decades using sediment proxies, we provide a comprehensive map of the evolution of this region from a bottom-up perspective, giving insight into the response of coastal systems to a changing Antarctic environment.

5.3 Methods

Data was collected between March 11 and April 19, 2012 during the NBP1203 cruise aboard the RVIB Nathaniel B. Palmer as part of the collaborative LARISSA (Larsen Ice Shelf System, Antarctica) project. Hydrographic stations were occupied along the NW Weddell Sea continental shelf and within the Larsen A embayment within a region bounded by 65.1°S, 63.3°N, 61°W, and 65°W. Additional samples were collected via small boat near Robertson Island, 65.25°S, 59.37°W. While relatively open water conditions were encountered between March 11 and March 27th enabling extensive water column sampling, the onset of cold southerly winds on March 28th, 2012 due to the presence of a strong low pressure system in the Weddell Sea led to both rapid sea ice advance and formation within the embayment, deep mixing and the homogenization of water column properties (see Section 3.1 and 3.2 below). Hydrographic datasets presented below therefore focus on stations sampled prior to March 28th. Five sites

designated as biological process stations were also sampled intensively along a cross-shelf transect through the Larsen A embayment and on the continental shelf to link long-term phytoplankton observations derived from remote sensing and the benthic sediments (see below), as well as other components of the marine ecosystem (Figure 5.1). The three innermost stations, G-I, were located within the coastal area covered by the Larsen A ice shelf prior to the 1995 collapse (Skvarca et al. 1999, Ferrigno et al. 2008), while stations J and K represented shelf stations outside of the embayment.

A Conductivity, Temperature, Depth (CTD) rosette equipped with 24, 10-L Niskin bottles, a Sea-Bird 911plus CTD, a WETLabs ECO fluorometer, a Biospherical Instruments photosynthetically available radiation (PAR) sensor, a Sea-Bird dissolved oxygen sensor, and a WETLabs transmissometer was used to collect water samples for physical, chemical and biological analyses. Samples were generally collected at 12 depths between the surface and 10 m above the bottom, with higher frequency sampling in the euphotic zone (see below for definition). For surface mapping, samples were also collected at 7 m depth using the ship's underway flow-through system, equipped with a SeaBird SBE-45 conductivity sensor, a SeaBird 3-01/S temperature sensor, a WETLabs AFL Fluorometer, a WETLabs C-Star transmissometer, and an oxygen optode. pCO_2

Mixed layer depth for each CTD cast was calculated using a density difference criterion by estimating the depth at which potential density anomaly was 0.03 kg m^{-3} higher than at a surface reference value measured at 10 m (Dong et al. 2008). The euphotic zone depth (Z_{eu}) was defined as the depth at which downwelling PAR reached 1% of its value just below the surface (Kirk, 1994). To derive Z_{eu}, the diffuse attenuation coefficient of downwelling PAR (K_d) was first calculated by fitting an exponentially decreasing function to each CTD cast,

$$E_z = E_0 e^{-K_d z} \tag{5.1}$$

Where E0 is the irradiance below the surface, z corresponds to depth (positive downwards), and Ez is the irradiance at depth. K_d was then used to calculate the depth of the euphotic zone Z_{eu} by solving

$$Z_{eu} = \frac{ln(0.01)}{K_d} \tag{5.2}$$

Because phytoplankton in the Southern Ocean have been shown to photosynthesize below the traditional 1% light level due to their low-light adaptation (Smith et al. 1996), the depth of the the 0.1 % light level was also derived for reference.

Chlorophyll-a (chl-a) was estimated fluorometrically as a proxy for phytoplankton biomass using a chlorophyll acidification method (Holm-Hansen et al. 1965). Water samples (50–2000 ml) were filtered onto a 25 mm membrane filter (GF/F) and frozen at -80 °C. The filters were then extracted in 90% acetone for 24 hours while stored at -20 °C. Chlorophyll fluorescence was measured using a digital Turner Designs 10-AU fluorometer, calibrated with pure chl-a extracted from Anacystic anidulans (Sigma Co.) with concentration measured spectrophotometrically (Jeffrey and Humphrey, 1975). Size-fractionated chlorophyll was measured following the same method using 0.2, 1.0, 3.0, 5.0, 10.0 and 20.0 μm membrane filters (Osmonics). The 0.2 μm fraction was used to estimate total chl-a concentration, while chl-a concentration in other size fractions were calculated by subtracting concentrations retained on larger filters. Depth-integrated chl-a was calculated by integrating chl-a concentrations within the top 100 m of the water column. Fluorometers on the CTD and underway sensors were also calibrated against extracted samples ($r^2 = 0.97$, $p < 0.01$).

Nutrient concentrations were determined by flow injection analysis (FIA) using a Lachat Instruments Quikchem 8000 Autoanalyzer. Samples were collected directly from the Niskin bottles; samples not processed at time of collection were frozen and stored at -20 °C until analysis (usually for a few days). If frozen, samples were carefully

defrosted in warm running water for 1 h. The phosphate method was a modification of the molybdenum blue procedure of Bernhardt and Wilhelms (1967), in which phosphate was determined as a reduced phosphomolybdic acid employing hydrazine as the reductant. The nitrate + nitrite analysis used the basic method of Armstrong et al. (1967), with modifications to improve the precision and ease of operation. Sulfanilamide and N-(1-Napthyl) ethylenediamine dihydrochloride reacted with nitrite to form a colored diazo compound. For the nitrate + nitrite analysis, nitrate ($NO3^{-}$) was first reduced to nitrite ($NO2^{-}$) using a cadmium reduction column and imidazole buffer as described by Patton (1983). Nitrite analysis was performed on a separate channel, omitting the cadmium reductor. The silicic acid method was based on that of Armstrong et al. (1967) as adapted by Atlas et al. (1971). Addition of an acidic molybdate reagent formed silicomolybdic acid which was then reduced by stannous chloride. Ammonium was determined by a modified indophenol blue method modified from ALPKEM RFA methodology which references Methods for Chemical Analysis of Water and Wastes, March 1984, EPA-600/4-79-020, "Nitrogen Ammonia", Method 350.1 (Colorimetric, Automated Phenate).

Water column primary production was estimated using a nitrate drawdown method following Jennings et al. (1984) and Hoppema et al. (2002), which estimates nutrient consumption in the surface as the difference between surface concentrations (averaged within the mixed layer as defined above) and maximum concentration observed in the deeper waters beneath (Hoppema et al. 2007). Nutrient concentrations were normalized to a constant value of salinity to account for dilution processes which may impact nutrient measurements. Productivity is then estimated using the Redfield ratio (Redfield et al. 1963, C:N = 6.6 mol / mol), which has been shown to be appropriate for coastal waters of the NW Weddell Sea (Hoppema and Goeyens 1999). Production calculated in this way represents seasonal production until the time of sampling, integrated since the time of first sea ice retreat. This method does not take into account advective properties of the

system.

Total dissolvable iron (TDFe, weak acid labile, pH = 1.8) measurements were made using a chemiluminescent FIA method according to King and Barbeau (2007; 2011). Briefly, samples were acidified to pH 1.8 with Optima-grade HCl (Fisher Scientific) immediately after collection without any filtration. This mild acidification releases any acid-labile iron into solution. Prior to analysis, samples were filtered through 0.4 μm polycarbonate track-etched filters (Whatman) under vacuum on an acid-cleaned Teflon filter rig (Savillex). 20 mL aliquots of each sample were then placed in separate 60 mL LDPE bottles (Nalgene) and all the iron in the samples was reduced to iron(II) after 12 hours (overnight) with a 2 μmol L^{-1} sulfite addition. Samples were then analyzed via FIA after pre-concentration on a conditioned NTA Superflow resin (Qiagen). Each sample was run in triplicate, with an average blank of 0.02 nmol L^{-1} (n = 72) and a detection limit of 0.07 nmol L^{-1} (three times the standard deviation of the blank). This method gives accurate results for both SAFe (S1 and D2) and GEOTRACES (GS) consensus samples. Values obtained for S1 (0.11 $\pm$ 0.02 nmol L^{-1}, n = 39), D2 (0.93 $\pm$ 0.07 nmol L^{-1}, n = 36), and GS (0.51 $\pm$ 0.02 nmol L^{-1}, n = 12) compare well to the most recent consensus values (http://es.ucsc.edu/ kbruland/GeotracesSaFe/kwbGeotracesSaFe.html).

Sediment cores from the upper 10 cm of the sediment column were collected with a megacorer to characterize long-term patterns of organic matter deposition across the continental shelf and test hypotheses derived from water column and satellite observations. Megacore samples were sectioned into 0.5 cm intervals from surface to 2 cm depth and 1 cm thereafter to 10 cm. From each section, an approximately 3 cm^2 sub-sample for pigment analysis was taken from the interior of the core to minimize artifacts arising from exposure to light and oxygen. Sub-samples were stored in the dark in glass scintillation vials and frozen at -80 °C prior to freeze-drying. This method has been shown to adequately preserve sediment pigments for long-term storage (Reuss and Conley

2005). After weighing, sediment sub-samples were taken for fluorometric pigment analyses and stored at -20 °C. Fluorometric analyses took place on the ship following the procedures described for waters samples, with extraction time increased to 48 h. Pigment concentrations were then normalized to the weight of dried sediment, with final units of μg pigments g^{-1} sediments ($\mu g\ g^{-1}$).

To complement surface sediment pigment analyses we analyzed images collected at comparable depths (423–686 m, Table 5.2) during seafloor photosurveys at each biological process station to estimate surface phytodetritus cover. Images representing 3 m^2 of the seafloor were collected using a yoyo camera system equipped with a 10.2 megapixel Nikon D-80 Camera and Ocean Imaging Systems 3831 Strobe (200 @-S) set to trigger 2.5 m above the sea floor. Digital images were color corrected using Adobe ImageReady based on *in situ* photographs of a color chart. Details on instrumental setup and sampling strategy can be found in Grange and Smith (2013). Following their methods, 25 random images from each transect were chosen from each station and processed using an automated algorithm to isolate regions of the benthos covered by phytodetritus. Images were scaled in ImageJ using 10 cm reference lasers and gridded with an area per point of 900 cm^2. An area of 1.8 m^2 (1.5 x 1.2 m) at the center of each image was retained to minimize vignetting effects at the edges. RGB images were imported into Matlab and converted to HSV (hue, saturation, value) color space. Pixels with phytodetritus were then isolated by using thresholds on hue ($16 < \text{hue} < 119$), which proved sufficient to distinguish organic matter from background sediments. Percent organic matter cover was then computed by dividing the number of pixels identified as phytodetritus by the total number of pixels analyzed. Because data within transects were not normally distributed we used the non-parametric Kruskal-Wallis test to test whether phytodetritus distributions across stations came from the same distribution, and a multiple comparison test with p-values adjusted with a Bonferroni correction to test for differences between stations.

Seasonal and inter-annual patterns of sea ice cover and water column primary production at the process stations were quantified using satellite datasets of sea ice concentration and ocean color. Sea ice concentration between 1997 and 2012 was derived from the passive microwave sensor SSM/I (85 GHz bands, 12.5 km grid, 1997-2012), using the ARTIST Sea Ice (ASI) algorithm (Kaleschke et al. 2001, Spreen et al. 2008). Net primary productivity (mg C m^{-2} d^{-1}) for the same period was calculated using daily images of chl-a and PAR as inputs into a version of the depth-integrated Vertically Generalized Production Model (VGPM) parameterized to field data collected from the Antarctic Peninsula (Behrenfeld and Falkowski, 1997, Dierssen et al. 2000). Additional details on the sea ice and ocean color data processing can be found in Cape et al. (2014). Time series of net primary productivity and sea ice concentration for the biological process stations were derived by spatially averaging datasets within a 15 x 15 km area centered over each station. This area was chosen to relate surface processes with patterns observed in the benthos, given the potentially strong impact of advection on settling organic matter (Siegel et al. 2008). Total production (Gg C yr^{-1}) for all stations was then calculated by multiplying the daily productivity (mg C m^{-2} d^{-1}) by the open water area estimated from sea ice concentration, and then integrating over the growth season (October–March of each year).

5.4 Results

5.4.1 Hydrography

Hydrography across the embayment along one of the primary cruise transects from the pack ice to the coast is presented in Figure 5.2. Lower surface salinity was found offshore within and on the western edge of the pack ice, reaching a minimum of 33.31 under the thick sea ice cover and increasing shoreward to a maximum of 33.99 near

the Drygalski Glacier (Figure 5.2b). While potential temperature across the Weddell Sea during the March-April cruise was generally low, a similar gradient in surface conditions is present ranging from -1.81 °C at the surface under the sea ice to a maximum of -1.58 °C nearshore (Figure 5.2d). Inshore stations were thermally stratified, while the presence of warmer water at 30–50 m depth, along with colder, lower salinity water above, indicates recent surface melt and potentially cooling at the sea ice stations. At depth, warm intrusions of modified Weddell Deep Water (WDW, -1.45 °C, 34.54 salinity) are apparent in the offshore stations between 300-400 m and extend to within 40 km of the coastline near the bottom. At offshore stations 8-11, located within 1 km of each other, the intrusions are transient in space and time and associated with flow velocities up to 15.9 m s^{-1} towards the NW in the temperature maximum layer (Figure 5.3c). The water mass is also evident in T/S space, identified by as spike in temperature below the 27.75 kg m^{-3} isopycnal (Figure 5.2c). Patterns within the embayment at the innermost stations adjacent to the Drygalski Glacier indicate the presence of a colder, fresher layer of water laying above near bottom saltier shelf water at the fringe of the Greenpeace Trough (Figure 5.3d), potentially a result of interaction between deep waters and the Drygalski Glacier (Figure 5.2 c–d, Figure 5.3). This layer is easily visible along both isobaths and isopycnals, spreading NW along the trough and associated with high velocities (maximum 11 cm s^{-1}, Figure 5.3).

Mixed layers depths across the transect were shallow, averaging 17.82 $\pm$ 4.6 m, with minima at stations 13 and 17 (12 and 11 m respectively) and maxima at stations 9 and 15 (24.5 and 23.5 m respectively, Table 5.1). Buoyancy frequency, a metric for the strength of stratification, showed stronger stratification offshore between stations 7 and 15 in the sea ice influenced zone (N = 17.5 $\pm$ 2.6 cycles hr^{-1}) than at stations within 30 km of the inner embayment (stations 17-18, N = 6.0 $\pm$ 1.5 cycles hr^{-1}). Euphotic zone depths calculated with both 1% and 0.1% thresholds were much deeper than the

mixed layer depth at all stations, averaging 50.6 $\pm$ 19.08 m under or near the pack ice edge (stations 7-10) and 34 $\pm$ 4 m within the embayment. Although variable across the stations, the low diffuse attenuation K_d (0.118 $\pm$ 0.037 m^{-1}) indicates a clear water column through the sampling region.

5.4.2 Nutrients, productivity, and phytoplankton biomass

A strong drawdown of nitrate and silicate is apparent in the top 40 m across all stations (minimum 11 and 28.7 μM respectively), indicative of diatom growth, with rapid increases in concentrations to 31 and 70 μM below the nutricline (Figure 5.4). Concentrations of phosphate followed those of nitrate (not shown). Surface nitrate and silicate concentrations were higher both under the sea ice and near-shore, with a minimum near the entrance of the Larsen A embayment. A concomitant maximum in ammonium between 58 and 59 °W was also found at the surface, indicative of heterotrophic activity. Nitrite concentrations were generally highest at the surface, reaching upwards of 0.12 μM, and decreasing exponentially below. Sub-surface maxima were however also present, corresponding to deep chl-a maxima (see below). Total dissolvable iron (TDFe) measured at four stations along a transect towards Robertson Island showed high concentrations at the surface ranging from 30.27 nmol L^{-1} in open water conditions to 97.29 nmol L^{-1} in the proximity of icebergs grounded near the tip of the island. Concentrations in sea ice cores were even higher, averaging 161.9 $\pm$ 6.9 nmol L^{-1} . Nitrate to phosphate (N:P) and silicate to nitrate (Si:N) removal ratios across the embayments averaged 15.5 $\pm$ 1.3 and 2.2 $\pm$ 0.3 in waters shallower than 100 m, ranging from 15.4 to 17.8 for N:P and 1.681 to 2.675 for Si:N.

Total phytoplankton biomass, estimated from chl-a concentration, showed a strong cross-shelf gradient reminiscent of physical and chemical properties, with low water-column concentrations offshore under sea ice cover (0.28 mg m^{-3}, Figure 5.5)

increasing to a sub-surface maximum at station 15 near the entrance of the embayment (8.88 mg m^{-3} at 31 m, station 15), and decreasing again shoreward. Concentrations under the ice were uniformly low. The deep chlorophyll maximum (DCM) was a persistent feature across the Larsen A embayment, becoming broader near-shore and near the ice edge (between 10–50 m depth). DCM depth was consistently at or below the euphotic zone depth and well below the mixed layer depth (Table 5.1). This sub-surface maximum in chl-a was also associated with the nitracline, and found above a minimum in beam transmission (not shown), which points to a concomitant deep maximum in particulate concentration. Depth-integrated chlorophyll between 0–100 m followed the same pattern as the biomass maximum layer, with highest concentrations at station 15 (300 mg m^{-2}) and decreases both near- and offshore (Figure 5.5b).

Although surface chl-a concentrations were overall low relative to the sub-surface, patchy regions of high biomass (maximum of 1.5 mg m^{-3} near shore) were encountered, with peaks in chl-a generally associated with a strong draw-down of pCO_2 implying high seasonal autotrophic production in surface waters (Figure 5.6). Regions of low pCO_2 and low-chla near the entrance of the Larsen A embayment, corresponding to regions of high surface ammonium, are also evidence for past production in surface waters. Primary productivity rates derived from surface nutrient drawdown also suggest a relatively productive season across sampling stations, with average productivity rate of 667.3 $\pm$ 105.1 mg C m^{-2} d^{-1} estimated for 2011-2012 (Table 5.1). Minima in productivity were encountered near shore at stations 17 and 18 (543 and 596 mg C m^{-2} d^{-1} respectively) as well as within the pack ice (station 7, 495 mg C m^{-2} d^{-1}), with productivity rates between these geographic extremes ranging between 602 and 811 mg C m^{-2} d^{-1}.

Large cells generally dominated phytoplankton communities across the embayment within the euphotic zone (Figure 5.7). The highest chl-a concentrations in surface waters were generally associated with nano-and micro-phytoplankton, with the > 20 μm

size fraction dominating at most sampling stations and depths. Stations near the coast also saw a significant pico-plankton contribution to total chl-a. This pattern generally holds at the deep chlorophyll maximum layer between 25 and 40 m apart at the coastal stations. Below the euphotic zone, small cells in the 0.2-3 μm contributed up to 65% of total chl-a, although this pattern was highly variable between stations. The patterns observed agree with microscopy analyses, which showed the numerical dominance of the pennate diatom *Fragilariopsis obliquecostata*, a common and sometimes dominant species associated with both sea ice and ice edge regions, across the embayment at both surface and DCM (51–110 μm apical length, A. Leventer unpublished, Garrison et al. 1987, Cefarelli et al. 2010).

5.4.3 Atmospheric impact on water column properties

Sampling in the Larsen embayment occurred at the end of the growth season and during the period of sea ice advance over the region. Foehn winds, characterized by strong (20-30 m s^{-1}), dry winds out of the west, raised surface air temperatures from -12 to +10 °C for 3 days and briefly led to the melting and further advection of sea ice out of the embayment, leading to a maximum increase in mixed layer temperature of +0.08 °C while not significantly affecting mixed layer depth (not shown). This event was followed by the return of strong, cold southerly winds characteristic of the region. The consequences of these winds on water column stratification between March 26 and March 28, 2012 are presented in Figure 5.8. Prior to the cold wind event (station 18), surface waters were relatively warm (-1.63 °C) and fresh (34.1), with a marked drawdown of surface nutrients relative to below the euphotic zone. A clear deep chl-a maximum of up to 1.56 mg m^{-3} is also apparent at 34 m. As the southerly winds set in, the mixed layer deepened progressively from 30 m to 60 m, with a marked decrease in temperature to the surface freezing point (-1.8 °C) and increases in salinity accompanying rapid sea

ice formation. Chemical and biological gradients were thereby homogenized with the deepening of the mixed layer, with increases in nitrate apparent within the top 12 m (dNO3 = +7 μM) and a rapid disappearance of the DCM below due to vertical mixing. Sustained winds would lead to the final seasonal closure of the embayment and the shoreward advection of Weddell Sea Gyre pack ice.

5.4.4 Remote sensing

The timing of sea ice retreat and advance during the 2011-2012 sampling season was spatially variable across the continental shelf and amongst process stations. Stations J and K were characterized by an earlier seasonal opening (December 29 and December 9, 2011 respectively) than the two near-shore stations G-H, which saw sea ice retreat on February 2 and 7, 2012, yielding a significantly shorter open water season for the latter three sites (51, 55 days for G, H and 76, 63 for J, K, Figure 5.9, Table 5.2). Station I opened up later in the season on February 16, 2012, following the second major sea ice decrease over stations G and H, with a total open water season of 34 days. Opening of stations G-I coincide with a shoreward advance of the pack ice over stations J and K and the end of open water conditions at the peak of the growth season. The pack ice would later retreat over Station J for another 11 days before finally advancing for the remainder of the fall and winter.

Satellite ocean color images of the region showed a relatively constrained growth season due to the presence of sea ice, with surface chl-a concentrations averaging 0.2 mg m^{-3} (0-1.72 mg m^{-3}) throughout the season (not shown). Average daily productivity at the stations featured a clear cross-shelf gradient, with average values of 367.1 and 449.3 mg C m^{-2} d^{-1} neashore (G, H, respectively), and 704.5 and 655.7 mg C m^{-2} d^{-1} on the shelf (J, K, Table 5.2). Net primary productivity at station I was intermediate between the inshore and offshore stations. Maximum and daily productivity rates at stations G–H

ranged from 250 to peak values of 600 mg C m^{-2} d^{-1} (not shown). Stations J and K, open during the typical peak of the growth season between December and January and the period of maximum light, were statistically similar, displaying higher daily rates ranging from 250 mg C m^{-2} d^{-1} early and late in the season to a maximum of 2500 and 1500 mg C m^{-2} d^{-1} in late February respectively. Annual and total production followed the same spatial gradient, with annual rates of 61.6–69 g C m^{-2} yr^{-1} and total rates of 9.0–9.7 Gg C yr^{-1} at J and K compared to < 23.4 g C m^{-2} yr^{-1} and < 3.5 Gg C yr^{-1} at the inshore sites. Total rates were lowest at station I due to the overall shorter open water season experienced at this site.

Considering all years between 1997 and 2012, the 2011–2012 season ranks as below average in productivity (Figure 5.10). In turn, total annual productivity rates can exceed 50 Gg C yr^{-1} offshore (Station K, 2001-2002) and 23 Gg C yr^{-1} nearshore (Station G, 2001-2002). Maxima in production occurred during the 2001-2002 season and the final collapse of the Larsen, and a temporally and spatially extended open water season over the entire NW Weddell Sea. Two to three year cycles in productivity are apparent in total production rates, with numerous years showing no measureable surface productivity in surface waters due to the presence of sea ice (Figure 5.10a). Despite this temporal variability, the spatial gradient in productivity remains relatively constant across the time series, with the offshore stations consistently more productive, but also more variable due to the higher range of productivity rates encountered, than near-shore stations from year to year (Figure 5.10b).

5.4.5 Sediments

Down-core pigment concentration, which represents the integration of past primary production and export in overlying waters over decadal time scales, tend to be high in this area, with the highest concentrations found near the surface and decreasing

concentrations down-core due to a combination of enhanced modern deposition and pigment degradation processes (Figure 5.11a). A notable exception appears at station J, where pigment concentrations reach a maximum in the 1-2 cm depth range exceeding pigment concentration at all other stations and with decreases both above and below (maximum 54.1 μg total pigments g^{-1} dry sediment), possibly indicating enhanced water column production and sediment over that depth and time interval. Overall, pigment patterns follow gradients observed in the ocean color dataset, with higher concentrations found at stations J and K (maximum 70.7 μg total pigments g^{-1} dry sediment) rather than closer to shore. Near the bottom of the cores (6-8 cm), station I appears to retain higher concentrations of pigment than cores collected at other stations. The timing of retreat of the ice shelf in 1995 can be teased out from the profile at the innermost station G, which shows a rapid decrease in pigment concentrations below 5 cm, and negative chl-a fluorescence noted during analysis, indicative of inorganic sedimentation (Sañe et al. 2011). While pigment concentrations remained high throughout the megacores at all other stations, complementary sampling of longer kasten cores at the same sites showed pigment concentrations also decreasing to zero at or just below the 10 cm horizon (not shown). Spatial heterogeneity in benthic organic matter deposition is also apparent in the offset between replicate cores collected from a single megacorer drop.

Considering averages taken over the entire depth of sediment cores yields similar results (Figure 5.11b). There is a clear spatial gradient in sedimentary pigment accumulation, with lowest concentrations found nearshore (1.1–4.1 μg g^{-1} total pigments) and highest offshore (12.4–27.2 μg g^{-1} total pigments). These results are insensitive to the depth of averaging, with qualitatively similar patterns observed when considering only the first depth, the top 5 cm, or whole-core inventories as shown. Phaeo : chl-a ratios are high in the sediment relative to the overlying water column due to enhanced degradation of chl-a to phaeophytin in the sediments (Figure 5.5c). Highest values are

found at station G, with ratios ranging from 3.7 to 16.0, and lowest values at J, where phaeo:chl-a ranged from 1.3 to 8.7. These lower values are indicative of fresher organic matter offshore relative to more degraded pigments nearshore.

Photographic surveys of the seafloor provided further evidence for persistent cross-shelf gradients in water column organic matter production and export (Figure 5.12). Lowest benthic phytodetrital cover was found within the embayment at station G (mean 34%), increasing linearly across the biological stations to a maximum at station K (mean 78% cover). Phytodetritus cover across the shelf was significantly different amongst the biological stations ($\chi^2 = 85.27$, $p \ll 0.01$), with phytodetritus cover at each station significantly different from all but neighboring stations (e.g. G is different from I-K, Supporting Table D.1).

5.5 Discussion

The Larsen A polynya occupies a narrow region of the continental shelf seasonally swept by sea ice, constrained offshore by the perennial sea ice of the Weddell Sea and landward by both the tall mountain range of the Antarctic Peninsula and its ice sheet, which makes its environmental setting distinct from the marine ecosystem of the western Antarctic Peninsula (King and Turner, 2009). It is under the influence of multiple physical stressors, including variable sea ice cover, fluctuating light availability, and the force of the powerful southerly winds characteristic of the Weddell Sea interior (Schwerdtfeger 1975). Yet despite its location in this inhospitable environment and its small size, the polynya remains a hotspot of productivity on par with other well-studied systems (Arrigo et al. 2003, 2012). We explored *in situ* patterns of biomass and productivity during NBP1203 to test hypothesis derived from satellite observations and explore physical forcing on phytoplankton growth within this system.

Following 34–76 days of open water conditions in the Larsen A region, distributions of water column biological and chemical properties observed during NBP1203 point to a relatively productive season within the embayment and on the shelf. High chl-a and particulate biomass was observed sub-surface in a maximum layer located between 10 and 50 m depth and extending from the coastline to the ice edge, with chl-a concentrations reaching 8.88 mg m^{-3} near the entrance of the embayment and decreasing both near- and offshore (Figure 5.5). Net primary productivity rates computed from surface nutrient drawdown also showed relatively high average rates ranging from 500 mg C m^{-2} d^{-1} inshore and beneath the ice to a maximum of 811 mg C m^{-2} d^{-1} at station 12 (Table 5.1). Productivity rates derived from satellite ocean color, though consistent with these rates, underestimated mean productivity compared to nutrient drawdown methods at overlapping stations (G = station 17, K = station 8, Table 5.1, 5.2). Previous estimates of productivity within this system are therefore likely also underestimated (Cape et al. 2014). Satellite phytoplankton biomass estimates were, on the other hand, only representative of surface measurements collected by the ship's flow-through system. These showed relatively low and steady concentrations throughout the embayment, reaching a maximum between 0.2-1.7 mg m^{-3} chl-a. Comparing these estimates indicates that for 2011-2012, a growth season characterized by variable ice cover across the continental shelf and several episodes of advance and retreat of sea ice at stations occupied during NBP1203 (Figure 5.9), integrated phytoplankton biomass in the euphotic zone was severely underestimated by satellite techniques, yet representative of observations collected in the top 10 m of the water column (Figure 5.6). These results are not surprising given the well-known inability of satellite techniques to sense deep biomass maxima and data processing issues under clouds and near the ice edge (Arrigo et al. 1998, Blondeau-Patissier et al. 2013). Yet cross-shelf biological gradients observed both in the water column and the sediments showed remarkable similarity to long-term satellite observations (Cape et al.

2014), indicating that while the magnitude of phytoplankton biomass, and potentially production, may be underestimated in this complex and remote sea ice zone, gradients derived from these remote sensing techniques are more than simply artifacts of optical methods. Instead, these patterns are representative of integrated processes linking the retreat of sea ice to surface autotrophic production, and ultimately particulate export.

5.5.1 Phytoplankton heterogeneity and nutrient limitation

Previous studies have shown that the Larsen A polynya is highly productive, with maximum rates rivaling other productive regions of the Antarctic (Arrigo et al. 2008, Cape et al. 2014). Others have shown that while the sea ice zone (SIZ) is one of the most productive regions in the Weddell Sea (Garrison et al. 1987, Smith and Nelson 1990, Hoppema et al. 2000), the NW Weddell is only moderately productive with daily production rates ranging between 180 and 580 mg C m^{-2} d^{-1} (El Sayed and Taguchi 1981, Jennings et al. 1984). Maximum phytoplankton biomass of 8.88 mg chl-a m^{-3} and seasonal production estimated from surface nutrient drawdown of 667.3 $\pm$ 105.06 mg C m^{-2} d^{-1} reported in this study for 2012-2012 corroborate these previous estimates, and are consistent with measurements along the coastal Antarctic as a whole (Table 5.1, Vernet et al. 2008, Arrigo et al. 2008, Arrigo et al. 2012). Satellite observations between 1998 and 2012 suggest that productivity rates during the 2011-2012 season across the biological sampling stations were below average relative to the full time series (Figure 5.10). This was likely due to the relatively short length of ice-free conditions across the embayment and the late opening of much of the polynya. This suggests that while the observed patterns of growth across the embayment may be representative of mean conditions, the absolute magnitude of both productivity rates and biomass derived *in situ* may be underestimate., Bertolin and Schloss (2009), for example, found deep chl-a maxima of upwards of 14.24 mg m^{-3} offshore of Robertson Island and near the 1995

extent of the former ice shelf.

Comparing profiles of nitrate across the offshore–onshore transects to profiles collected south of James Ross Island during a January 2010 NBP1001 cruise (not shown) to the Weddell Sea shows a stark contrast between nutrient distributions during periods of relatively open water, such as the 2011-2012 season, to periods of complete ice cover (Supporting Figure D.1). In 2010, anomalously persistent sea ice over the NW Weddell Sea prevented the opening of coastal waters entirely, hampering water column production and leading to relatively uniform water column physical and chemical properties. Although the previous austral summer season 2009-2010 was characterized by extensive open water and high rates of primary production (Cape et al. 2014), no chemical signature of this production remained the following year in either nutrients or pCO_2 ($pCO_2 > 400$ μatm at SST, not shown), implying wintertime homogenization of water column properties due to deep convection. This implies that the observed nutrient deficiency in surface waters was the result of summertime biological activity during the 2011-2012 season, rather than a relic of autotrophic production from a previous year.

Size fractionated chlorophyll as well as microscopy analyses showed that phytoplankton communities across the sampling region were dominated by large diatoms > 5 μm, including sea ice associated species of the genus *Fragilariopsis*, at both surface and deep chlorophyll maximum (A. Leventer unpublished, Lizotte et al. 2001, Cefarelli et al. 2010). Significant contributions from pico- and nano-plankton to total biomass were however, also seen throughout the water column (> 50% in some samples, Figure 5.7), highlighting the importance of these size fractions in waters typically assumed to be diatom-dominated (Hewes et al. 1985). Dominance of sea ice associated species points to the importance of sea ice processes, including seasonal melt in the spring and summer, in shaping phytoplankton community composition in surface waters of the Larsen A polynya (Ackley and Sullivan, 1994). These findings are further corroborated by previous surface

sediment analyses (Buffen et al. 2007), which show diatom assemblages consistent with a sea-ice dominated regime in the Larsen A.

The removal of surface nutrients by sinking as a result of biological activity has been proposed as the major mechanism leading to the formation of deep chlorophyll (and biomass) maxima in the ocean (Hodges and Rudnick 2004, Huisman et al. 2006). The temporal evolution of these layers is dependent on both the timescale of sinking particles and the upward flux of nutrients (Huisman et al. 2006). While macro-nutrient concentrations in surface waters, as well as pCO_2 measurements, suggested a large drawdown due to biological activity, macro-nutrient concentrations did not reach limiting levels. Indeed, dissolved nutrient ratios of N:P = 15.5 $\pm$ 1.2 and Si:N = 2.2 $\pm$ 0.3 are on par with and above those of the Redfield ratio of 16 and 1 (Redfield 1958, Turner 1998). Similar ratios have been found in the Ross Sea for blooms dominated by diatoms (Smith and Asper 2001). Low surface phytoplankton biomass and high nutrient concentration may however be an indication of micronutrient limitation (Martin et al. 1990). While TDFe in surface waters measured near Robertson Island was high, implying a sufficient water column iron inventory, these concentrations may not be representative of the rest of the embayment. Advection of sea ice out of the Larsen B embayment led to the presence of multiple icebergs near Robertson Island at the time of sampling, which may have significantly affected surface iron concentrations (Lin and Twining, 2012). The analysis of samples collected for trace metal analysis from a subsequent cruise in 2013 aboard the RV *Araon* (Korean Polar Research Institute, South Korea) will help shed light on the distributions and bioavailability of iron in this system, and the contributions of both sea ice and glacial melt to micro-nutrient inventories across polynya waters.

5.5.2 Impacts of physical and chemical gradients on phytoplankton growth

Processes controlling phytoplankton growth in the Southern Ocean include those that affect physiological processes, such as temperature, light, and nutrients, and those that control phytoplankton distributions, including grazing, advection, sinking, and mixed layer processes (Smith et al. 2008). Conditions experienced during NBP1203 can give insight into the importance of these various mechanisms in controlling the patterns observed in the water columns and over the long term in the sediments.

While the onset of adverse weather conditions limited sampling of phytoplankton communities at the end of the growth season (Figure 5.8), the inshore transect between stations 7 and 18 as well as the biological patterns derived from both satellite and sediment sampling across the offshore transect between biological stations G–K imply strong control of patterns of both phytoplankton production and export by physical processes. Although sampled over the course of 14 days, the stations occupied during NBP1203 represent a gradient of conditions associated with variability in atmospheric processes and sea ice cover. Offshore stations within the pack ice, covered at least 30 days by thick sea ice cover, are representative of conditions encountered late in the fall or earlier winter, while inshore stations beyond the ice edge, characterized by extensive open water until the time of sampling, are reminiscent of patterns of observed late in the summer prior to sea ice advance. Datasets from the two major transects between stations 7 and 18 as well as G–K are considered in concert below to examine major processes responsible for the patterns observed during sampling.

Light availability

Light availability serves as a major control on patterns of phytoplankton bloom development and rates of primary productivity, and in these coastal waters is mediated by the magnitude of incident irradiance, sea ice cover, mixed layer processes, as well as concentration of both suspended organic and inorganic particles in the upper water column (Smith et al. 1996). These processes in turn can affect the physiology and growth characteristics of phytoplankton.

In this region of perennial ice cover, sea ice dynamics plays an important in determining the light field in the water column. The seasonal timing of opening of the embayment showed high spatial variability, with stations located on the shelf opening earlier than those within the limits of the former Larsen A ice shelf (Figure 5.9, Table 5.2). Earlier opening at the shelf stations J and K allowed phytoplankton exposure to longer day lengths during the optimal months of December–February (Vernet et al. 2010), likely contributing to the higher daily rates of satellite-derived productivity observed at the stations relative to inshore. The patterns observed over 2011–2012 via satellite are representative over the long-term, coinciding with observations of higher overall polynya productivity in years of earlier opening and longer ice-free periods (Cape et al. 2014). Conversely, because offshore stations J and K, as well as stations 7–11, experience earlier advance of sea ice in February relative to those within the embayment with complete cover at the time of sampling, phytoplankton biomass and productivity were comparatively lower at these sites than at the ice edge or inshore (Figure 5.5, Table 5.2). The pack ice offshore was also characterized by thick and highly ridged sea ice, with mixed glacial ice and icebergs, often covered by 20–50 cm of snow, leading to high surface albedo and limiting light penetration into the euphotic zone (Brandt et al. 2005).

At the ice edge stations 12–18, where sea ice concentration between March 11 and March 26 remained below 70% (Figure 5.6a), the DCM was observed between 31

and 42 m, below a shallow mixed layer (11–23.5 m) as well as at or below the euphotic zone depth (Table 5.1). Phytoplankton in the Southern Ocean are known to be low-light adapted, capable of photosynthesizing below the depth of 1% surface irradiance (Smith et al. 1996). Mixed layer processes, which regulate the light field experienced by phytoplankton, can also play a major role in governing rates of production depending on the difference between the timescales of mixing and biological photoadaptive processes (Cullen et al. 1986). In this case, particulate and chl-a maxima were found below the mixed layer, implying a relative stable environment up until the deep mixing event (Figure 5.8). Although light levels measured at the DCM were low (1.03–14.6 μEinstein m^{-2} s^{-1}), high concentrations of water column chl-a potentially indicate a suitable environment for phytoplankton growth. Yet while active photosynthesis has previously been associated in DCMs with enhanced dissolved oxygen (DO) concentrations, profiles show that in this case the DCM instead co-occurred with the chemocline, with higher DO in the overlying mixed layer (8.13–8.58 ml L^{-1} surface). Upcoming quantification of variable fluorescence and photosynthetic rates at these stations will shed light on the physiological state of phytoplankton in these deep layers, and whether these populations were growing or simply remnants at the end of the growth season.

Meltwater, stratification and mixing

Vertical water column stability has long been suggested as a major structuring force on phytoplankton growth and primary production (Hart 1934, Sverdrup 1953, Mitchell and Holm Hansen 1991). In the Southern Ocean, solar heating during austral summer and melt of both glacial ice and sea ice are thought to significantly contribute to the development of a stable surface mixed layer (Deacon 1937, Smith and Nelson 1986, Dierssen et al. 2002, Vernet et al. 2008). While the highest phytoplankton biomass was found beneath the mixed layers during the cruise, mixed layer processes in this region

of persistent barrier wind flow may still play a large role in determining the seasonal progression of phytoplankton blooms as well as long-term patterns of production in the embayment.

While a surface low salinity layer was apparent across the embayment, waters below or near the pack ice were both fresher and colder than inshore marking a strong gradient from the ice edge to the continent and implying high surface meltwater contribution from the sea ice offshore (Figure 5.2). This pattern, commonly observed near the ice edge of the Weddell Sea and other regions of the Antarctic (El Sayed and Taguchi, 1981), may be the result of earlier sea ice retreat nearshore relative to offshore. Near the ice edge, surface freshening led to water column stability despite surface temperature inversions. On the other hand, higher salinities near the coast point to a decreased influence of sea ice in this region, as well as a relatively lower contribution of glacial ice and melt to surface freshening. There is likely a high degree of inter-annual variability in stratification patterns within the embayment associated with variability in atmospheric processes, the position of the pack ice, and the time of open water exposure within the embayment (Cape et al. in prep). Examination of stable oxygen isotopes (δ^{18}O) samples will further shed light on sources of meltwater in the water column, allowing the discrimination of meteoric and glacial sources.

The cross-shelf gradients in salinity and temperature were paralleled by a gradient in the strength of surface stratification, estimated by the buoyancy frequency N (Table 5.1), with weaker stratification found at inshore stations 17 and 18 (10–30 km from the coast) relative to 7–15 (30–150 km). Weaker stratification nearshore, if persistent throughout the season, may be the result of more frequent convective mixing in these coastal waters. Katabatic winds draining from the Antarctic Peninsula plateau, which are thought to significantly affect surface atmospheric and oceanic processes up to 20–30 km from the coast (Bromwich and Kurtz 1984), may be the cause of this weaker inshore

stratification, preventing the establishment of a stable mixed layer. This may have negative consequences for phytoplankton, leading to the advection of phytoplankton below optimal depth horizons and the dilution of water column phytoplankton communities (Smith et al. 1996). However, as observed during this project, convective overturning of the water column resulting from advection of cold air to the Larsen area can also lead to the replenishment of surface nutrients (Figure 5.8), or during periods of high surface phytoplankton biomass could serve to relieve light limitations and decrease density-dependent processes such as grazing (Behrenfeld 2014). Occasional wind-induced mixing during the growth season could therefore also enhance phytoplankton production and biomass in surface waters. While the recent installation of meteorological stations around the periphery of the Larsen B embayment and the analysis of a long-term time series at the Argentinian Base Matienzo has shed light on the impact of wind forcing on this region (Cape et al. in prep), significant uncertainty still remains as to the horizontal extent of such coastal winds over the embayment, and therefore the impact of wind stress on both sea ice and water column away from shore. The cold southerly winds experienced during NBP1203 resulted from a strong low-pressure system in the Southern Weddell, and therefore affected the entire region. A better spatial understanding of wind stress over the embayment, and its impact on both mixed layer processes and circulation are needed to disentangle the various processes at play in the region.

In other parts of the Antarctic, basal melt of ice shelf and glaciers due to interactions with warm Circumpolar Deep Water (CDW, 1.8 °C) advected across the shelf has significantly contributed to the negative ice sheet mass balance trend observed in recent years (Pritchard et al. 2009, Jacobs et al. 2011, Rignot et al. 2014). In these systems, meltwater emanating from the glacier face is injected into surface waters, significantly affecting stratification and micronutrient availability (Alderkamp et al. 2012, Gerringa et al. 2012). In the Weddell Sea, this core CDW is present near the shelf break, over

200 km from the Antarctic Peninsula Coastline, and therefore not available to contribute to the basal melt of ice shelves (Gordon 1998). While intrusions of relatively warmer Weddell Deep Water above the *in situ* freezing point were observed in the offshore stations 7-13 (Sigma = -1.45 °C, salinity = 34.54), this water mass was not found at the innermost stations, potentially limited in its distance of intrusion by a rise in bathymetry and topographic steering of deep currents at the southern entrance of the embayment near Robertson Island (Fig 5.2, 5.3). Variability in synoptic circulation over the Weddell Sea, which would influence the gyre and thereby circulation patterns, may affect the horizontal displacement of these intrusions over longer time-scales.

The ambient profiles along the inner portion of the embayment near the Drygalski glacier contain a thick layer of relatively colder, fresher water above the *in situ* freezing temperature between 225 and 500 m depth. This layer is also evident when looking along both deep isobaths and isopycnals (Figure 5.3) with a cold, fresh signature propagating from the Drygalski towards the NE along the Greenpeace Trough. We attribute this difference in the coastal profiles to glacial meltwater input, whereby water masses interacting with the glacier face both freshens and cools relative to water along the outer portions of the embayment. Although this points to the influence of ice-ocean interactions within the embayment, the input of meltwater in this case appears diffuse through the water column, and limited to deeper waters below the pycnocline. At the time of sampling, glacial melt therefore seemed to have little impact on surface physical and biological processes. Yet these processes are likely subject to significant interannual variability (Dinniman et al. 2011), and additional field sampling is needed to constrain melting rates along the glacier face, circulation patterns and residence times of deep waters near the glacier, as well as seasonal changes in the distribution of meltwater throughout the water column to better constrain the impact of ice-sheet-ocean interactions on mixed layer processes.

5.5.3 Sediments: integrators of upper ocean processes

Observations collected during NBP1203 provide a snapshot of both patterns and processes at play within this coastal polynya. The mechanisms linking physical dynamics to patterns of phytoplankton bloom development can occur on a wide range of both spatial and temporal scales (Haury et al. 1978, Levin 1992), and are difficult to resolve during short-term oceanographic sampling in such a remote environment. Nevertheless, salient patterns of phytoplankton production have emerged from this multi-pronged approach that begin to describe the evolution of these systems following ice shelf removal and give insight into the mechanism leading to these patterns.

Consistent spatial gradients in phytoplankton biomass and production previously observed over 15 years via satellite were also observed *in situ*, with significant biological structure and spatial gradients in both chemical and physical properties evident in the water column (Cape et al. 2014, Figure 5.2, 5.4). These patterns are further mirrored in the sediments, whose memory extends far beyond the reach of both oceanographic sampling and ocean color satellites (Figure 5.11, 5.12). Sediment pigments inventories, measured using a fluorometric technique, were at a minimum near-shore at station G, with concentrations increasing to a maximum in sediments collected on the shelf at stations J and K. Analysis of photographic survey collected near core collection sites showed the same pattern (Figure 5.12), giving an independent verification of pigment patterns. Lower phaeo : chl-a ratios at shelf stations also indicate less degradation at these sites relative to G and H and potentially a more abundant and regular supply of organic matter from above (Figure 5.11c). These observations lend weight to the notion that previously described patterns of water column production are reflected in persistent cross-shelf gradients in organic matter burial in this region over years to decades, implying a relationship between overlying production, export, and burial (see Pike et al. 2008 and reference therein).

Examination of down-core sediment concentrations nevertheless points to vari-

ability in spatial and temporal patterns of sediment organic matter accumulation and thereby overlying production. While all cores show a pattern of enhanced pigment concentration at the surface with rapid decreases below, typical of recent deposition and lower degradation (Figure 5.11, Leavitt 1983, Leavitt and Hodgson 2001), pigments at station J reach a maximum downcore between 1-3 cm depth, indicative of enhanced recent relative to both the present and to other stations. Interpretation of these sediment patterns, though relatively straightforward in an average sense, is complicated by the many processes impacting organic matter sedimentation, export, and in the case of pigment analyses preservation in the sediments, including lateral advection, grazing, and sediment chemistry (Siegel et al. 2008, Leavitt 1983, Leavitt and Hodgson 2001). Examination of other proxies, such as sediment diatom concentration or particulate organic carbon, may shed light on the nature of this variability and strengthen our understanding of patterns observed in this region. Considering the modern setting, the patterns observed at J and K are likely dominated by Weddell Sea pack ice dynamics rather than ice shelf and subsequently coastal polynya processes, as observed in G-I.

Retreat of the Larsen A occurred in stages (Skvarca et al. 1999, Ferrigno et al. 2008), with waters over the outermost station I exposed in 1989 and the innermost stations G and H in 1995. Profiles at station G, which featured a sharp exponential decrease in pigment concentrations to noise levels below 5 cm depth, are indicative of a period of suppressed organic matter input to the sediments prior to the collapse of the ice shelf (Sañe et al. 2011). While not present in the other megacore profiles, this same pattern of exponential decrease was evident in deeper kasten cores taken at stations H and I, with pigments concentrations reaching noise level at or just below 10 cm (not shown). This implies that the megacore profiles across all stations represent recent organic matter deposition within the last 25 years. Assuming that the timing of ice shelf retreat over the biological process stations can be gleaned from pigment concentrations (Sañe et al.

2011), an average rate of sediment accumulation can be calculated from the profiles. At stations G, 5 cm of accumulation over 20 years implies an accumulation rate of 2.5 mm yr^{-1}, with a corresponding rate of 4 mm yr-1 for stations H and I based on 25 years of accumulation. Although representing only a coarse approximation, given the high temporal and spatial variability observed in overlying production (Figure 5.10, Cape et al. 2014), these estimates are consistent with rates observed in other glacier influenced coastal systems along the Antarctic Peninsula, including productive coastal fjords (Boldt et al. 2013). Further quantification of accumulation rates across these stations using isotope methods (^{210}Pb) are necessary to be able to compare sites and gain more insight into temporal variability in organic matter export and its relationship to water column processes.

5.5.4 The biological pump and benthic foodbancs

Input of organic matter to the benthos in the Larsen A embayment is a new phenomenon on the timescale of hundreds of years (Brachfeld et al. 2003), and therefore marks an abrupt disturbance for benthic communities. We've demonstrated that sediment pigment inventories across stations located within the limit of the former ice shelf fall below detection limits within 10 cm of the surface, indicative of the depth horizon for ice shelf breakup. Sediment pigment inventories and photographic survey suggest a strong gradient of increasing organic matter (food) input away from shore, while remote sensing observation point to high spatial variability in primary productions across the embayment as well as high inter-annual variability in surface production, with 2–3 year cycles of heavy sea ice suppressing water column production (Figure 5.10, Cape et al. 2014). Similar variability in food input to the benthos is thought commonplace on the Antarctic continental shelf (Ducklow et al. 2008, Smith et al. 2008).

It has long been postulated that the evolution, diversity, and community structure

of faunal benthos on the Antarctic shelf have been shaped by the advance and retreat of ice shelves during glacial/interglacial periods (Gutt, 2000; Clarke and Johnston, 2003; Glover et al. 2008). In particular, the highly oligotrophic conditions under Antarctic shelves are posited to cause local extinction of typical shelf fauna, yielding drastic reductions in faunal diversity and selecting for deep-sea taxa adapted to very low food availability (Dayton and Oliver, 1977; Clarke and Johnston, 2003). Benthic colonization following ice-shelf retreat is thought to be extremely slow, requiring millennia for some foundation species (e.g., hexactinellid sponges, Gutt, 2000). The structure and development of benthic communities beneath Antarctic ice shelves remain poorly studied (Bruchausen et al. 1979), particularly in light of ice-shelf retreat. Patterns observed in the Larsen B embayment following ice shelf collapse seems to support this notion, indicating only weak changes in benthic community composition in the last twelve years (Gutt et al. 2011, 2013). In the case of the Larsen A, the significant variability in food input to the benthos measured across multiple proxies may however, affect the interpretation of benthic ecological patterns observed in these formerly ice-shelf dominated regions, particularly if near-shore stations serve as the reference point. Upcoming analyses of benthic communities across the biological processes stations sampled during NBP-1203 will start giving insight into the processes regulating community composition and the evolution of these systems (Srsen et al. in prep).

5.5.5 Phytoplankton and a changing cryosphere

The recent collapse of the Larsen A and B ice shelf in 1995 and 2002 are two dramatic examples of changes ongoing across the atmosphere–ice–ocean continuum in the Antarctic as a result of climate change (Domack et al. 2005, Rignot et al. 2014, Pritchard et al. 2009). A major question at the center of contemporary ecological research, in the Antarctic and elsewhere, concerns the consequences of climate change

on biological communities from individual species to ecosystems (Smetacek and Nicol 2005). In the Antarctic, ecological dynamics are intimately tied to variability in the cryosphere (Eicken et al. 1992) and the two must be considered in concert to untangle the natural variability in populations and the possible effects of environmental change.

Following ice shelf collapse, the Larsen A embayment has undergone rapid physical change similar to other Antarctic coastal systems, including the acceleration of coastal glaciers feeding the coastal zone and the resulting increased input of glacial ice and melt into coastal waters (Rignot et al. 2004, Berthier et al. 2012), as well as changes in sea ice dynamics modulated by atmospheric processes (Stammerjohn et al. 2008, Cape et al. in prep). On the whole, ice shelf collapse has led to the blooming of a new sea ice zone ecosystem in a region historically distinguished by perrenial sea ice cover, now characterized by rates of primary production consistent with other highly productive coastal Antarctic systems (Arrigo et al. 2008, 2012, Vernet et al. 2008). Results from hydrographic sampling and benthic analyses provide one of the first confirmations of patterns previously observed via satellite, confirming that cross-shelf gradients in primary production appear persistent and strongly correlated with distributions of organic matter on the benthos.

In this system, the timing of opening of the embayment is critical in determining the overall seasonal productivity of the polynya, affecting the area of ocean available for primary production, surface water temperatures, light availability, and the duration of open water conditions (Cape et al. 2014, Cape et al. in prep). This is a common characteristic of polynyas and other coastal regions across the Antarctic (Arrigo et al. 2003, 2012, Alderkamp et al. 2012). Inshore stations G-I, within the former embayment, are frequently covered by fast ice at the onset of spring (not shown), while offshore stations J and K on the shelf are influenced by Weddell Sea pack ice dynamics. This difference may explain differences in timing of retreat experienced across these stations. High phyto-

plankton biomass and productivity in this system is likely sustained by relatively shallow mixed layers resulting from both glacial and sea ice melt input into the water column as well as heat absorption during periods of open water (Figure 5.2). While relatively low surface phytoplankton biomass combined with high nutrients concentrations were found in surface waters, potentially indicating micronutrient limitation of phytoplankton growth (Martin et al. 1990), low surface pCO_2 measurements and high ammonium concentrations point to high seasonal primary production in surface waters and active heterotrophic activity. Satellite records from this region also indicate a potential for high biomass and productivity in surface waters, reaching 30 mg m^{-3} and > 4 g C m^{-2} d^{-1} respectively during the most productive seasons (Cape et al. 2014). Conditions experienced during NBP1203, with a prominent DCM within the polynya, may be more indicative of late summer communities rather than average conditions.

Hydrographic sampling confirm the importance of ice melt for the stratification of surface waters and likely the seeding of surface phytoplankton communities during sea ice retreat (Ackley and Sullivan 1994). Glacial melt, only evident below the mixed layer, seemed to play a lesser role in stabilizing the water column (Figure 5.2, 5.3). Given the importance of glacial ice melt as a mechanism for ice shelf collapse (Scambos et al. 2003), this weak influence of glacial melt may not be representative of other season, when surface air temperatures on this side of the peninsula are warmer and open water seasons longer. In addition to its effects on stratification, meltwater from glaciers can be a significant source of iron to coastal systems, fueling phytoplankton blooms (Alderkamp et al. 2012, Gerringa et al. 2012). Total dissolvable iron concentrations exceeding 30 nmol L^{-1} in iceberg-influenced waters near the coast of Robertson Island indicate high iron input into surface waters, though may not be representative of regions further removed from the coast. We expect that on an inter-annual basis, ice edge processes as well as glacial discharge dynamics play a major role in shaping not only the physical

environment but also chemical gradients in the water column. Atmospheric processes, including wind induced mixing in this region generally dominated by a cold continental climate and southerly winds, also likely play a significant role in shaping the environment for phytoplankton (Figure 5.8).

Polynyas are thought to contribute significantly to the overall productivity of the Southern Ocean, as well as to the drawdown of atmospheric CO_2 via the biological pump (Arrigo et al. 1999). While the absolute magnitude of the seasonal organic carbon pool in this area is relatively small, given the small region occupied by the polynya (Cape et al. 2014), pCO_2 measurements below 156.8 μatm in surface waters attest to this potential for carbon sequestration in surface waters (Figure 5.6). Organic matter export patterns inferred from sediments indicate a strong cross-shelf gradient in export, likely the product of patterns of overlying production and advection during sedimentation (Siegel et al. 2008). No significant trends in either length of the open water season or rates of primary production are present since the collapse of the ice shelf, due to the high inter-annual variability characteristic of this system and the relatively short length of observational time series. Nevertheless, this drastic increase in water column production marks an abrupt transition, which may have dramatic repercussions for higher trophic levels. Ice sheet retreat and collapse, while an ominous sign of the overwhelming human impact on natural environments, may in fact facilitate the creation of new ecosystems in the cold reaches of the Weddell Sea.

5.6 Acknowledgements

The authors thank Pavica Srsen for help with the processing of yoyo images, Amber Lancaster for helping with chlorophyll analyses on the cruise, Randie Bundy for analyzing the iron samples, Gunnar Spreen for continued support with the processing

of sea ice datasets, and the LARISSA group as a whole for many fruitful discussions that led to the development and refining of several ideas presented in this study. Katie Haman filtered and analyzed a great majority of the chlorophyll samples while always keeping a smile on her face (and a passive aggressive note in hand), for which I am greatly indebted. We also acknowledge the captain and crew of the RVIB *Nathaniel B. Palmer* and Lockheed Martin support personnel for facilitating sampling during NBP1203. Some figures were created using Ocean Data View (Schlitzer, R., Ocean Data View, http://odv.awi.de, 2014).This work was supported by the National Science Foundation Office of Polar Programs under NSF grant ANT-0732983. MRC was also supported by the NSF Graduate Research Fellowship under grant DGE-1144086 and by NASA Headquarters under the NASA Earth and Space Science Fellowship Program–grant NNX12AN48H.

This chapter is in preparation for publication as: Mattias R. Cape, Vernet, M., Huber, B., Smith, C.R., Ekern, L., Leventer,, A. Impacts of ice shelf collapse and sea ice variability on primary production and organic matter export in the NW Weddell Sea.

Table 5.1: Buoyancy frequency of the pycnocline (N), mixed layer depth (MLD), euphotic zone depth (Z_{eu}), diffuse attenuation coefficient of PAR (K_d), depth of chl-a maximum (DCM), and net primary productivity (NPP) at stations sampled along the transect shown in Figure 5.2. Euphotic zone depth and K_d for stations sampled at night were not calculated (indicated by a dash). Stations for which no chl-a max was present are also indicated by a dash.

Station	N (cycles hr^{-1})	MLD (m)	K_d (m^{-1})	$Z_{eu1\%}$ (m)	$Z_{eu0.1\%}$ (m)	DCM (m)	NPP (mg C m^{-2} d^{-1})
7	15	20.5	0.063	73	110	-	495
8	18	15.5	0.106	44	65	34	679
9	22	24.5	0.161	29	43	21	633
10	18	15.5	0.081	57	85	-	803
11	20	18.5	-	-	-	44	602
12	16	20.5	0.144	32	48	42	811
13	14	12.0	-	-	-	39	678
14	20	21.0	-	-	-	40	782
15	16	23.5	-	-	-	31	718
17	5	11.0	0.120	38	57	34	543
18	7	13.5	0.150	31	46	34	596
Mean	15.5	17.8	0.118	43.38	65.07	35.44	667.30
SD	5.2	4.6	0.037	16.41	24.62	6.93	105.06

Table 5.2: Seasonal sea ice and primary production statistics for the biological process stations over the 2011–2012 austral summer season estimated via satellite. Opening and closing dates listed as day of the year (DOY), with January 1 = 1 and December 31 as 365 (non-leap) or 366 (leap year). Because seasons span more than one year, the opening and closing dates can exceed 365 or 366. For example, an opening day of January 1 would correspond to day of the year 367 if the prior year was a leap year.

		Sea Ice			Primary Production		
Station	Depth (m)	Opening (DOY)	Closing (DOY)	Length (days)	Daily (mg C m-2 d-1)	Annual (g C m^{-2} yr^{-1})	Total annual (Gg C yr^{-1})
G	431	403	454	51	367.1	21.3	2.1
H	686	399	454	55	449.3	23.4	3.5
I	574	412	446	34	462.7	42.1	2.0
J	600	333	409	76	704.5	69.0	9.7
K	431	345	408	63	655.7	61.6	9.0
Mean	544.4	378.4	434.2	55.8	527.9	43.5	5.3
SD	111.5	36.5	23.7	15.5	144.7	21.7	3.8

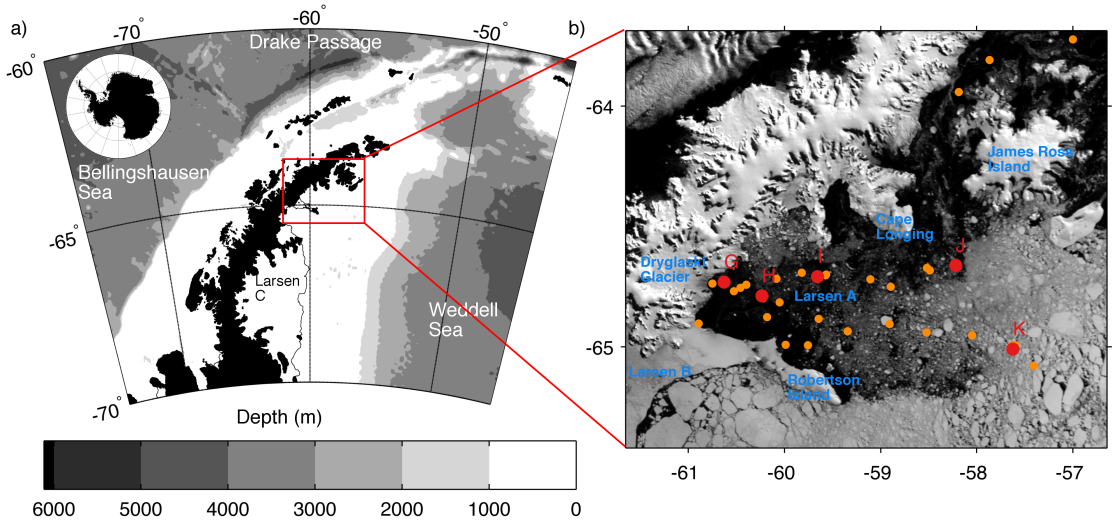

Figure 5.1: Map of the study area, depicting a) the Antarctic Peninsula and b) the area of the NW Weddell Sea sampled during NBP12-03. Orange dots represent sampling stations occupied during NBP1203, and red dots the location of biological process stations. The background image was taken by MODIS-Terra on March 24, 2012 (http://nsidc.org/data/iceshelves_images), showing representative sea ice conditions encountered during the first half of the cruise.

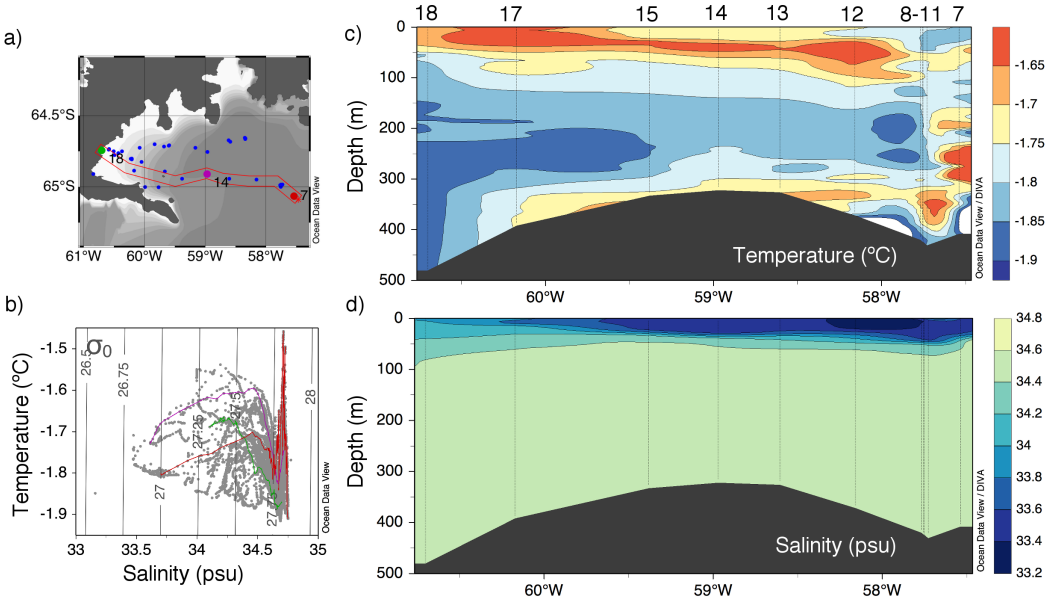

Figure 5.2: Physical structure of the water column encountered during NBP1203. (a) map of sampling stations, showing transect occupied between March 19 and March 27, as well as stations highlighted in Figure 5.2b. (c) potential temperature–salinity diagram for all stations (grey dots), with contours corresponding to isopycnals. Colored lines highlight stations indicated in Figure 5.2a. (c) potential temperature section along the transect indicated in Figure 5.2a. Vertical lines indicate CTD profile locations, with CTD number listed above (d) same as Fig 5.2b for salinity. Note that the high temperature signal at depth in Figure 5.2c was also associated with a salinity maximum at depth.

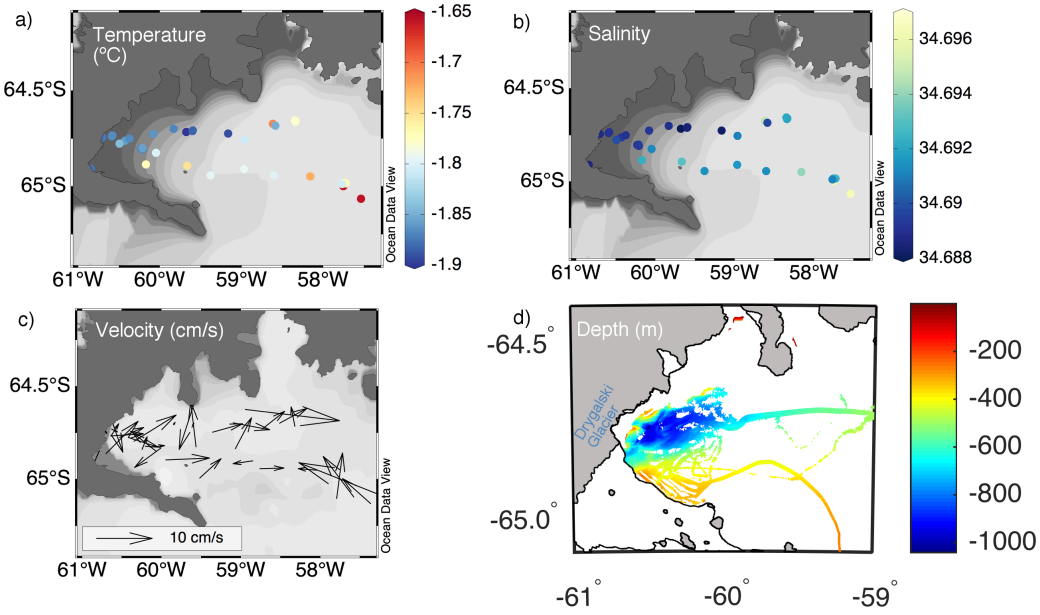

Figure 5.3: Isosurface patterns along the σ_Θ = 27.8 kg m^{-3} isopycnal at the core of the temperature minimum layer observed in coastal stations. Panels show (a) potential temperature, (b) salinity and (c) velocity of the water mass. (d) bathymetry of the Larsen A embayment derived from shipboard multibeam, showing the Greenpeace Trough as a deep depresssion in the bathymetry between 800 and 1000 m depth. The approximate location of the Drygalsky Glacier is also indicated in blue. Multibeam bathymetry was downloaded from http://www.marine-geo.org/portals/gmrt/.

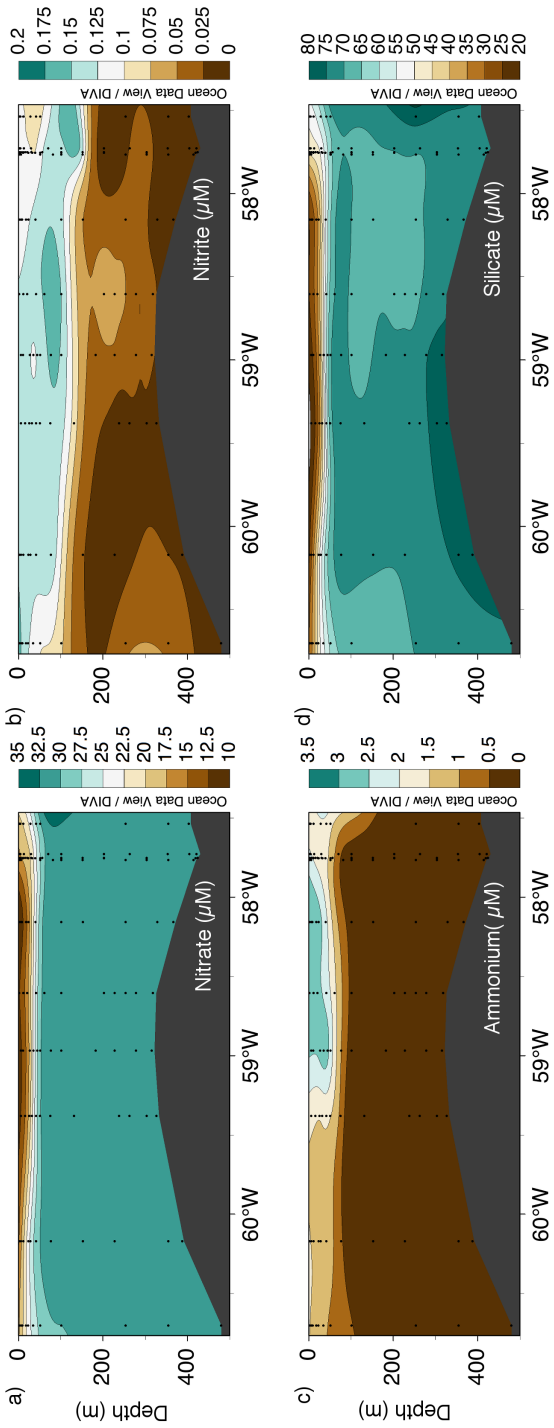

Figure 5.4: Sections of (a) nitrate, (b) nitrite, (c) ammonium and (d) silicate along the transect shown in Fig 5.2a. Closed circles indicate sampling depths.

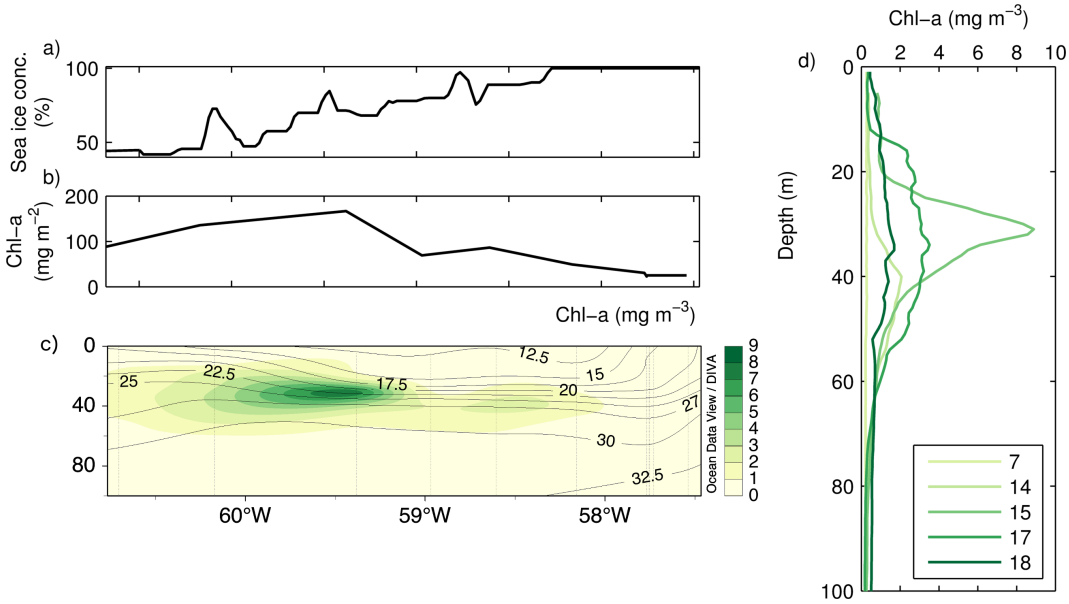

Figure 5.5: Phytoplankton and sea ice distribution across the transect shown in Figure 5.2a, with (a) sea ice concentration derived from a March 24, 2012 SSM/I sea ice concentration image. (b) chl-a biomass in Figure 5.3c integrated between the surface and 100 m. (c) section of chl-a, with contours corresponding to isolines of nitrate. Vertical lines represent CTD station, as shown in Figure 5.2c. (d) chl-a profiles at stations across the transect shown in Figure 5.3c.

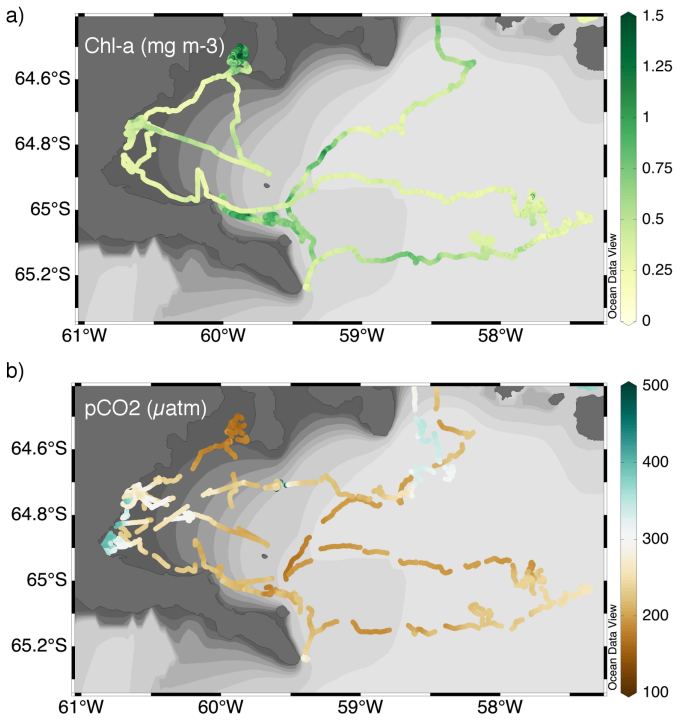

Figure 5.6: Surface patterns (a) chl-a and (b) pCO_2 pressure at SST along the cruise track, sampled at 7 m depth from the ship's flow-through system.

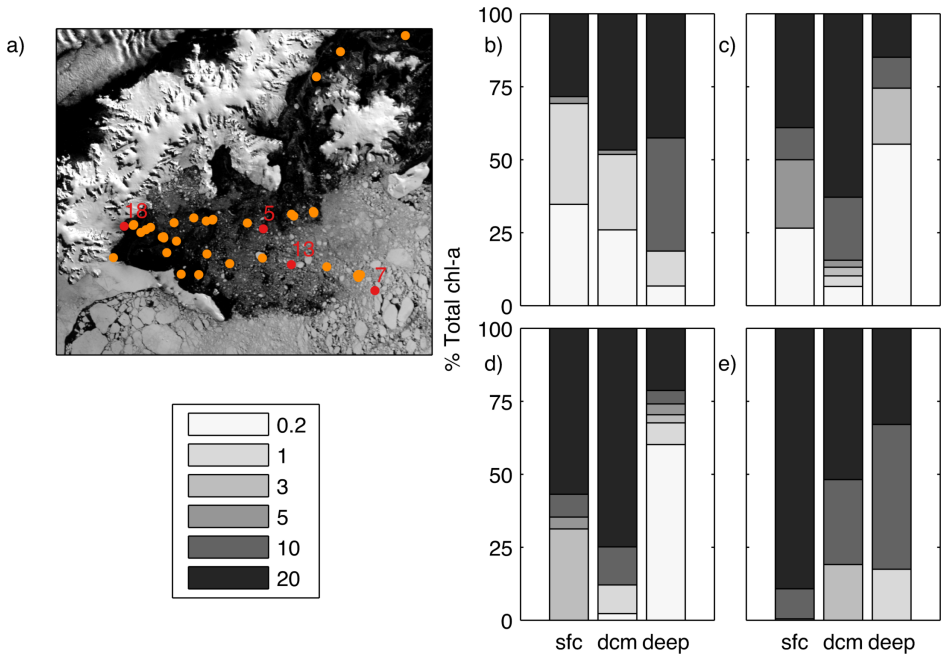

Figure 5.7: Phytoplankton community composition derived from size fractionate chl-a. (a) map of sampling stations, with station shown in Figure 5.7 (b–d) highlighted in red. Size fractionated chl-a for (a) station 5 (b) station 7 (c) station 13 and (d) station 18. Contributions were calculated by diving size fractionated chl-a by total chl-a, measured on the 0.2 μm filter.

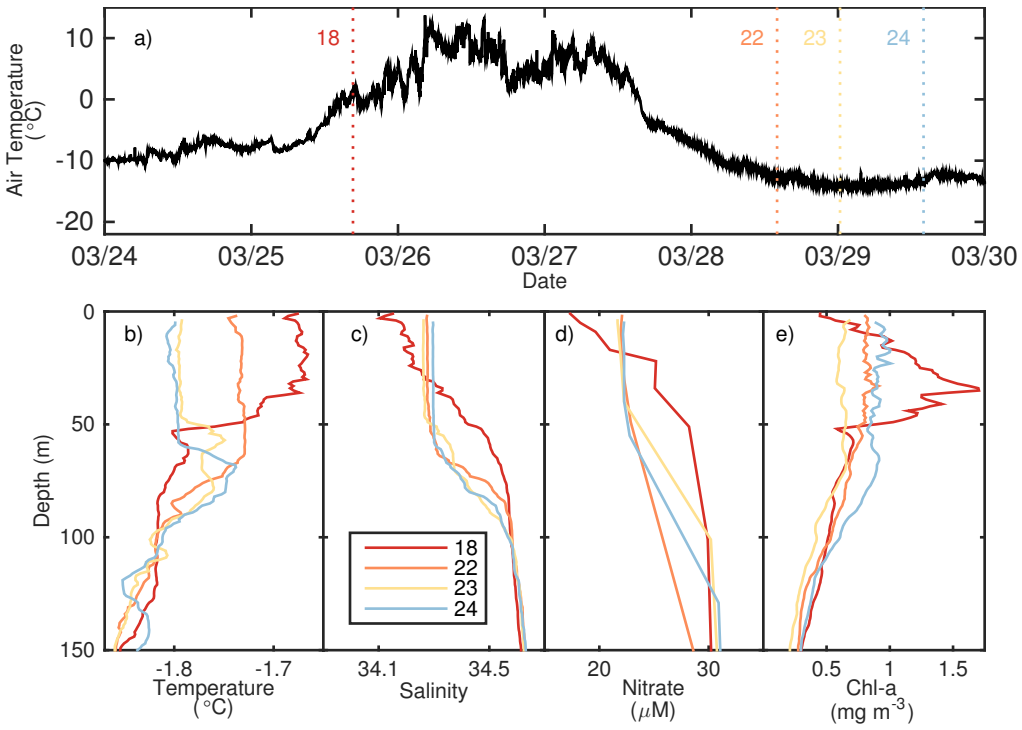

Figure 5.8: Time series of temperature and water column properties showing (a) air temperature as measured on the ship, with salmping time CTD stations indicated by dashed vertical lines, as well as (b) potential temperature (b) salinity (c) nitrate and (d) chl-a at stations located near the Drygalski Glacier. Station 18 was sampled prior to the onset of strong, cold southerly winds over the NW Weddell Sea.

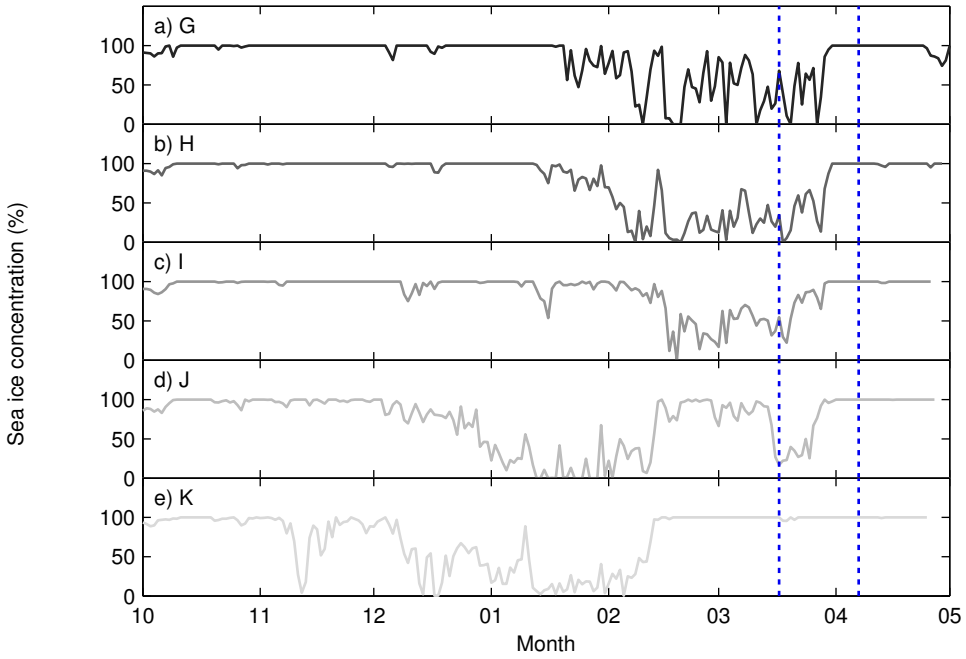

Figure 5.9: Time series of sea ice concentration at the biological process stations between October 1, 2011 and April 30, 2012. Blue vertical bars delimit sampling period within the embayment. Colors corresponding to the stations are maintained in Figure 5.10–5.12.

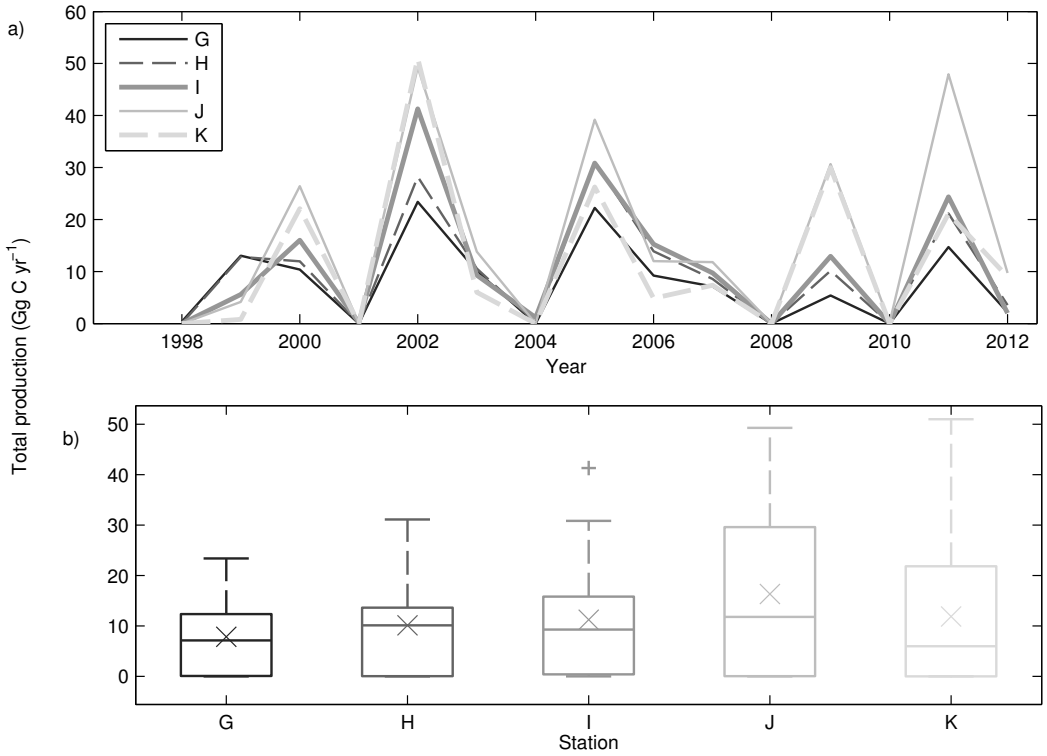

Figure 5.10: (a) time series of total production for biological process stations indicated in Figure 5.1a for 1997–2012. (b) box plot summarizing time series presented in (a). Box edges correspond to 25th percentile, the median, and 75th percentile of observational from bottom to top, and the cross to the mean. Outliers in the data are shown as plus signs.

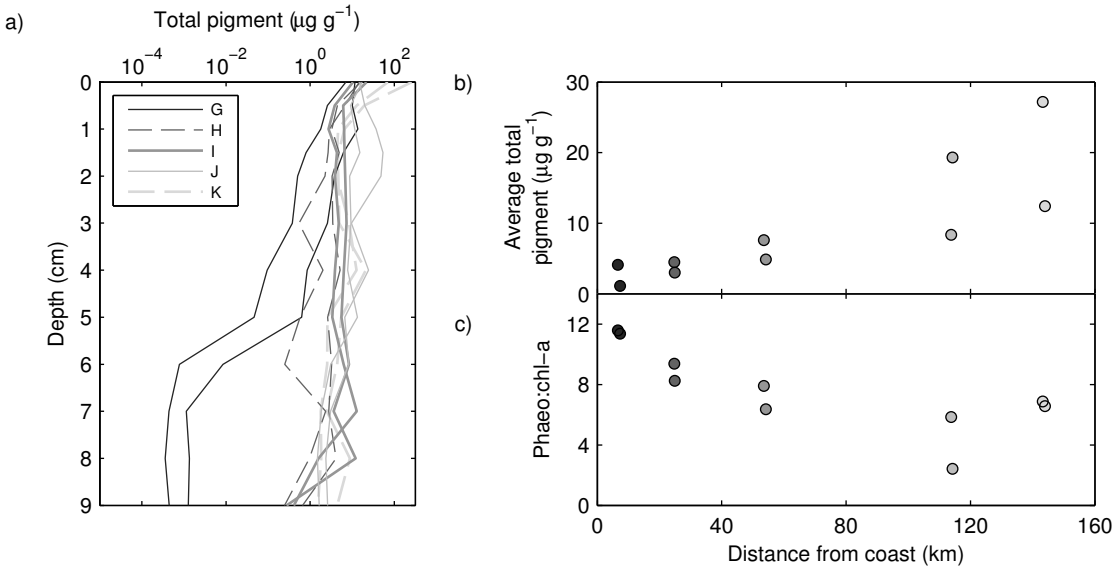

Figure 5.11: (a) total pigment concentration (phaeo + chl-a) for megacores collected at biological process stations. (b) average total pigment concentration in the cores computed from Figure 5.11a. (c) average phaeo : chl-a ratio in the cores.

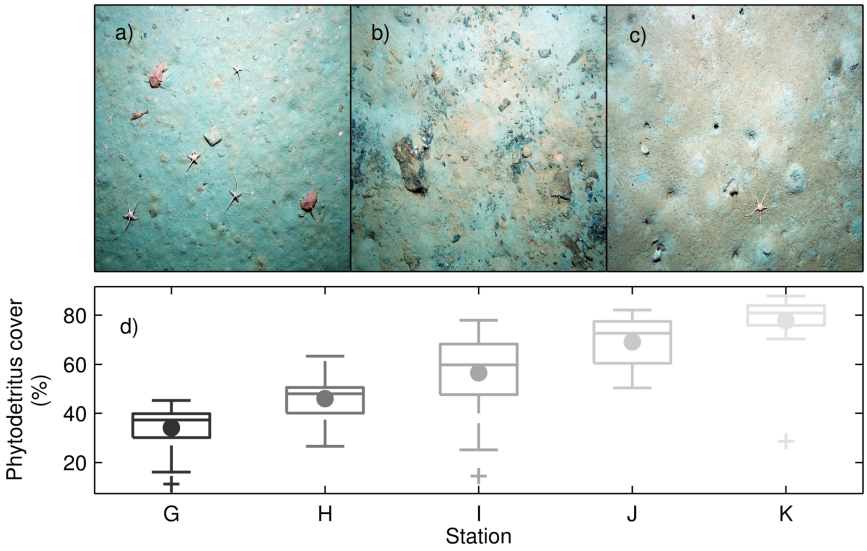

Figure 5.12: Representative yoyo camera image of the seafloor collected at station (a) G (b) I and (c) K, showing phytodetritus as a brown layer. (d) summary statistics of percent phytodetritus cover calculated from seafloor images, with box edges corresponding to the 25th and 75th percentile, the centerline to the median, and the filled circle to the mean. Extreme values are shown as the whiskers and plus signs.

Chapter 6

Conclusions and future direction

Changes in atmospheric circulation and regional climate warming led to the collapse of both Larsen A and B ice shelves in 1995 and 2002 respectively, precipitating changes in the cryosphere-ocean dynamics in the NW Weddell Sea, Antarctica. These include the acceleration of coastal glaciers, changes in freshwater fluxes and ocean circulation, and the opening of large coastal regions to the influence of sea ice. The seasonal presence of phytoplankton as a potential new source of organic carbon marks an abrupt change in the marine ecosystem, which may potentially increase carbon export to the deep ocean and serve as a negative feedback to climate change. This dissertation has helped shed light on the impact of ice shelf removal on phytoplankton biomass and primary production by examining the Larsen A and B embayment as model systems for other Antarctic regions. Following disintegration, the embayments have become new wind-driven polynyas, sites of significant water column primary production in an otherwise sea ice-dominated region of the NW Weddell Sea. The description of both physical and biological patterns and processes at play in these polynyas involved a combination of techniques meant to overcome the ever-present conundrum of sampling in remote, high latitude environments and constrain the system on a number of spatial

and temporal scales, from satellite remote sensing, automated weather sensor analysis, hydrographic sampling, to analysis of sedimentary pigments.

Chapter 2 examined long-term patterns of phytoplankton primary production and open water dynamics in the Larsen embayments using passive microwave remote sensing of sea ice concentration and satellite ocean color imagery. The Larsen A and B were shown to function as wind-driven polynyas, with productivity rates comparable to other well-known productive Antarctic shelf regions such as the Ross Sea or the Amundsen Sea indicating a rapid response of phytoplankton to disturbance. Re-processing of ocean color images over regions previously covered by ice shelves (categorized as land and therefore omitted in the standard NASA processing) provided the first time series of phytoplankton production following ice shelf disintegration in the Antarctic. Maximum productivity rates were consistently measured 50-100 km away from the coastline. This led to the hypothesis that organic matter export to the benthos would show significant cross-shelf variability, with low rates near the coastline and higher rates near the entrance to the embayments. Temporal variability in these systems was high due to high inter-annual variability in both the timing of embayment opening as well as the absolute extent of sea ice cover. Stronger northwesterly winds were shown to favor negative anomalies in sea ice concentration in the NW Weddell, implying a continued influence of foehn winds on cryospheric processes. Periods of open were also associated with a positive SAM index, linking synoptic-scale circulation patterns to regional sea ice responses, a mechanism previously connected to ice shelf collapse.

Given the relationship between atmospheric circulation and sea ice retreat derived in Chapter 2, Chapter 3 explored automated weather sensor records from stations installed on the periphery of the Larsen B embayment to quantify foehn wind frequency and variability. These winds had previously been observed only in a number of isolated cases, or inferred from modeling results. Long-term observational evidence to test

hypotheses linking large-scale circulation to regional warming and surface melting were largely non-existent. Two scales of observations were considered, including a long-term record from an Argentinian research station located north of the Larsen B embayment covering two decades of observations between 1962-1972 and 1999-2010, as well as shorter but more numerous records spanning 2010-2013 derived from automated weather stations installed on the periphery of the Larsen B embayment. These stations provided a spatial context to the long-term analysis. Warming trends between the two decades of observation are significant across all seasons as well as annually, in some cases exceeding maximum rates recorded elsewhere across the Antarctic. The weather records also showed that westerly foehn winds are characteristic and common wind patterns over this region, associated with dramatic surface warming on time scales ranging from days to years. In particular, strong, sustained positive anomalies in foehn frequency were associated with all the major retreat events of the Larsen B ice shelf in the 20th century. They exhibit significant seasonal variability associated primarily with the position of the Amundsen Sea Low, and are therefore sensitive to the meridional pressure gradient as well as the strength and direction of the westerly winds. Over longer time scales, foehn winds as well as higher surface temperatures were also found to be positively correlated with SAM, lending supporting to the hypothesis that large-scale forcing of westerly flow affects regional patterns of circulation near the Antarctic Peninsula, leading to higher rates of warming along the eAP relatively to windward side of the mountain range. This is the first concrete evidence linking *in situ* observations to hypothesized mechanisms of warming in this region. Statistical analyses also indicated a clear link between foehn warming and satellite-derived surface ice sheet melt, providing further evidence for the role of westerly winds in causing the ultimate collapse of the Larsen B ice shelf. These results identified foehn winds as linking atmospheric warming to ice sheet processes, leading to the hypothesis that they also serve as a major forcing on sea

ice, and thereby primary production within the Larsen polynyas. Rapid transition in the structural characteristics of the Larsen B occurred between1986 and 1998 following a period of steady state condition. Because of the strong trend in surface temperature, and in some cases foehn winds, between the two decades of observation, it would be of interest to use these observations in a modeling framework to reconstruct the missing decades of surface conditions in order to gain a better understanding of the impact of atmospheric forcing on cryosphere processes during that time. Similar approaches have been employed elsewhere in the Antarctic (Bromwich et al. 2013). This time series of identified foehn events could also be used in concert with high-resolution atmospheric models to gain a better understanding of the dynamics leading to temporal and spatial variability in foehn winds as well as the role of synoptic atmospheric configuration in forcing westerly winds.

Chapter 4 tested the hypothesis derived from Chapters 2 and 3 linking foehn winds to sea ice dynamics and ultimately net primary production. Foehn frequency is correlated with both rates of primary productivity as well as total magnitude of production, implying an effect on both physiological rates as well as total area available for autotrophic production to occur. Comparison of sea ice concentration time series and foehn frequency showed that winds serve as a major forcing on sea ice, particularly within $\sim$100 km of the coastline. This spatial signature is consistent with previous modeling results. Periods of sea ice retreat were consistently associated with increased foehn frequency, even during winter months. A major conclusion of this chapter is that the atmospheric forcing responsible for ice shelf collapse now continue to shape the evolution of the coupled sea ice-ocean system, with repercussions for phytoplankton processes. While feedbacks between atmosphere, ocean, and sea ice are likely responsible for maintaining open water conditions after cessation of westerly winds, these were not quantified in this study but rather inferred from satellite observations. Significant uncertainty exists

in high latitude systems regarding surface fluxes despite their importance for both the physical environment and biological communities (Bourassa et al. 2013). Chapter 3 showed that surface atmospheric response to foehn winds can be heterogeneous over the Larsen region depending on the linearity of the upwind forcing. Evidence of surface melt ponding on the ice sheet and coastal sea ice surface serves as further evidence for the variable extent of warming along the surf. Yet comparatively little is known regarding the horizontal extent of such winds beyond the coastline, or the effect of these winds on structural properties of the sea ice such as porosity. However, datasets presented in this chapter suggest a strong influence of winter foehn on the integrity of the ice cover and subsequent breakup in the spring. Year around observation of atmosphere, sea ice, and ocean in the Larsen embayment, which could feasibly be accomplished using ice buoys commonly deployed in the Arctic, would shed light on the physical processes at play in this region and serve as a first step to constrain interactions between physical components of these coastal systems.

In chapter 5 we link previous remote sensing observations to water column processes by analyzing datasets collecting on a cruise to the Larsen A area in 2012. High phytoplankton biomass was observed sub-surface in a deep chlorophyll maximum (DCM) layer along a spatial gradient with minima near shore and under the offshore pack ice, and a maximum near the entrance to the embayment. Relatively high seasonal primary productivity rates, derived from surface nutrient depletion methods, followed the same gradient, confirming previous long-term satellite observations presented in Chapter 2. Sediment pigment inventories as well as surface phytodetritus covered estimated from sea floor photographic transects suggested a link between water column production and patterns of organic matter export. Although this study could have benefitted from the addition of sediment trap data, which were deployed but never recovered due to the advance of the pack ice, the novel multi-proxy approach employed in study provides several

independent lines of evidence for the presence of a strong cross-shelf gradient followed ice-shelf removal. Physical and chemical gradients suggest a strong influence of sea ice on both stratification and phytoplankton community composition. Atmospheric processes were also shown to impact mixed layer processes, with cold winds events leading to deep mixing, the dilution of phytoplankton communities, and the injection of nutrients to surface waters. We hypothesize that the consistent depression of phytoplankton biomass and primary production observed near-shore may be the result of the influence of coastal atmospheric processes, such as katabatic winds, which would disproportionately impact mixed layer processes within 10-30 km of the coast. Physical observations collected continuously at the surface on previous cruises to the Larsen A show colder, more saline water near-shore even during periods of calm conditions across the region, potentially an indication of small-scale sea ice formation. Nevertheless, significant uncertainty also remains in our understanding of ocean circulation in this region, which could certainly play a role in the patterns we observed. Analysis of historical ADCP and LADCP data could shed light on this issue. With greater understanding of the offshore behavior of coastal winds and near-shore circulation, coupled physical-biological models could be employed to gain insight into the processes underlying the patterns observed via satellite and *in situ*.

This dissertation as a whole provides an assessment of patterns of phytoplankton biomass and primary production in a region of the Antarctic undergoing rapid climate change. A major strength of this dissertation results from the analysis of datasets across the atmosphere-ice-ocean continuum on a number of spatial and temporal scales, which helped to constrain both patterns and processes at play in this region. While the life of phytoplankton are intimately linked to the physical environment, so is our ability to access and study these remote settings. Long-term observations in the Southern Ocean, particularly in the sea ice zone, are rare given the harsh conditions faced by

both instruments and researchers. Due to the advance and retreat of sea ice, and the movement of icebergs in coastal regions, seasonal and inter-annual observations of the euphotic zone are for example largely non-existent, and their attempt often considered too costly and risky in a funding framework. Our understanding of processes affecting phytoplankton and organic matter export is therefore limited to few, well-studied regions (Ross Sea, Amundsen Sea, west Antarctic Peninsula), usually sampled at the height of austral summer. This can present significant challenges however, given the high variability inherent in the coastal Antarctic marine ecosystem (Ducklow et al. 2007). Given these difficulties, greater collaboration, both international and inter-disciplinary, will be critical in the future to better constrain processes at play in this critical region of the globe in order to ultimately understand the potential evolution of this marine ecosystem in the face of climate change.

Appendix A

Supporting information for Chapter 2

Auxiliary material for this article contains descriptions of comparisons between SSM/I and AMSR-E-derived open water area for the Larsen A and B embayments as well as the NW Weddell Sea over the June 2002-March 2011 period of sensor overlap. Times series of open water area derived from sea ice concentration were analyzed for bias due to the different resolutions and grid sizes of the two sensors and products. Datasets of sea ice concentration were identically computed using the ARTIST sea ice algorithms as outlined in the Methods, and a threshold was applied to the datasets to classify pixels as open water or sea ice covered. Because of the higher resolution of the AMSR-E products, a standard 15% open water threshold was used on this datasets to create a baseline against which to compare SSM/I-derived open water areas. We varied this threshold on SSM/I sea ice concentration and compared the resulting time series of open water area so as to minimize the difference between estimates (computed as sum of square error between daily values). Further comparisons were computed using linear correlation and spectral analysis methods.

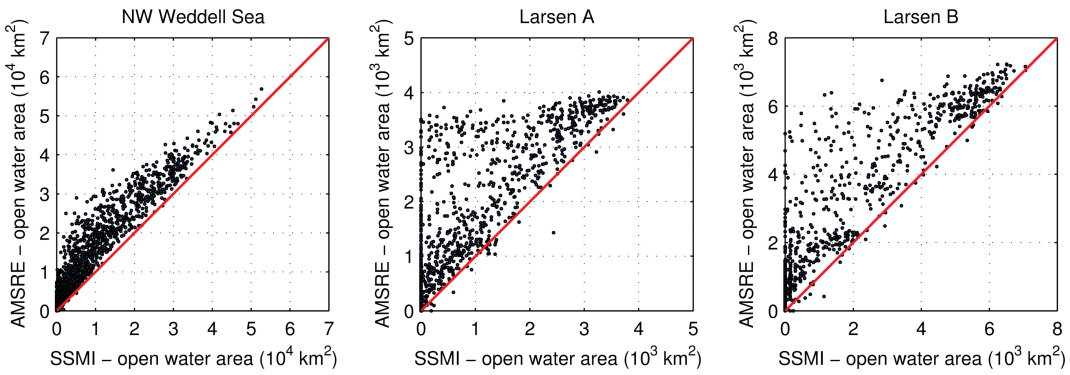

Figure A.1: Comparison of daily open water area calculated using a 15% sea ice concentration threshold on pixels for both AMSR-E and SSM/I over the 2002-2011 period of sensor overlap for the Larsen A, Larsen B and Weddell Sea regions. Open water area calculated using the AMSR-E time series is consistently higher for all areas. Red line shows 1:1 relationship.

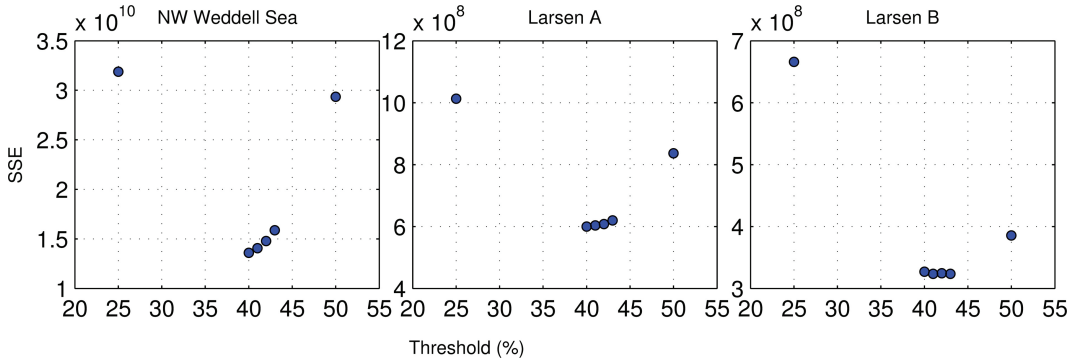

Figure A.2: Sum of squared error (SSE) between the open water time series calculated using a 15% concentration threshold on AMSR-E and varying thresholds on SSM/I. A minimum is reached at a 40% sea ice concentration threshold for the Larsen A and Weddell Regions and 41% for the Larsen B region.

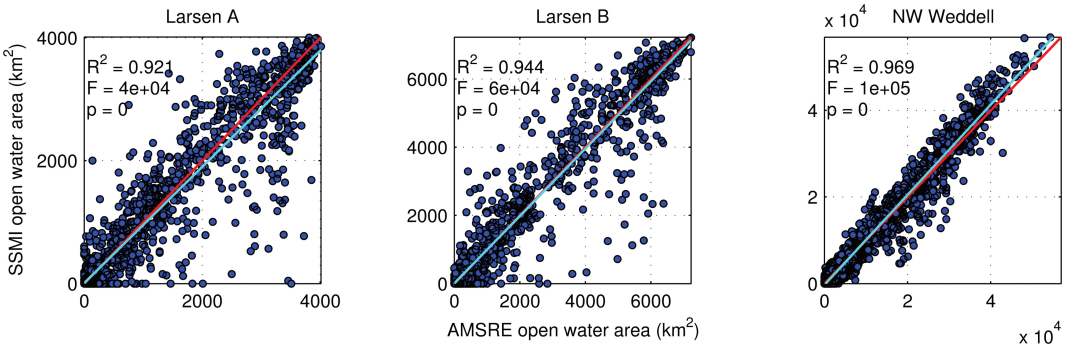

Figure A.3: Comparison of daily open water area calculated using a 15% concentration threshold on AMSR-E pixels and 40% threshold on SSM/I over the 2002-2011 period of sensor overlap for the Larsen A, Larsen B and the Weddell Sea. Red line shows a 1:1 relationship and the cyan line represents the best fit line to the data.

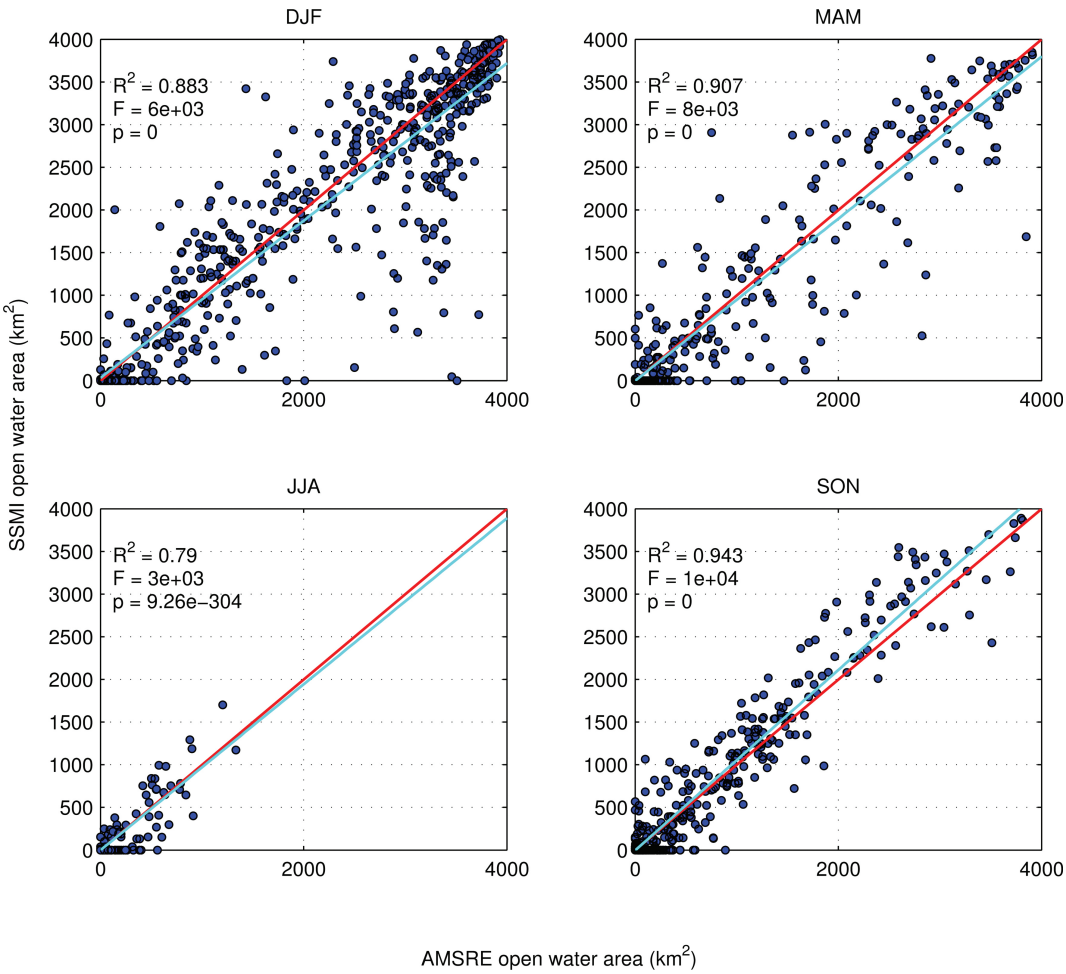

Figure A.4: Comparison of daily open water area calculated using a 15% concentration threshold on AMSR-E pixels and 40% threshold on SSM/I over the 2002-2011 period of sensor overlap for the Larsen A separated by season. Red line shows a 1:1 relationship and the cyan line represents the best fit line to the data. DJF = December, January, February; MAM = March, April, May; JJA = June, July, August; SON: September, October, November.

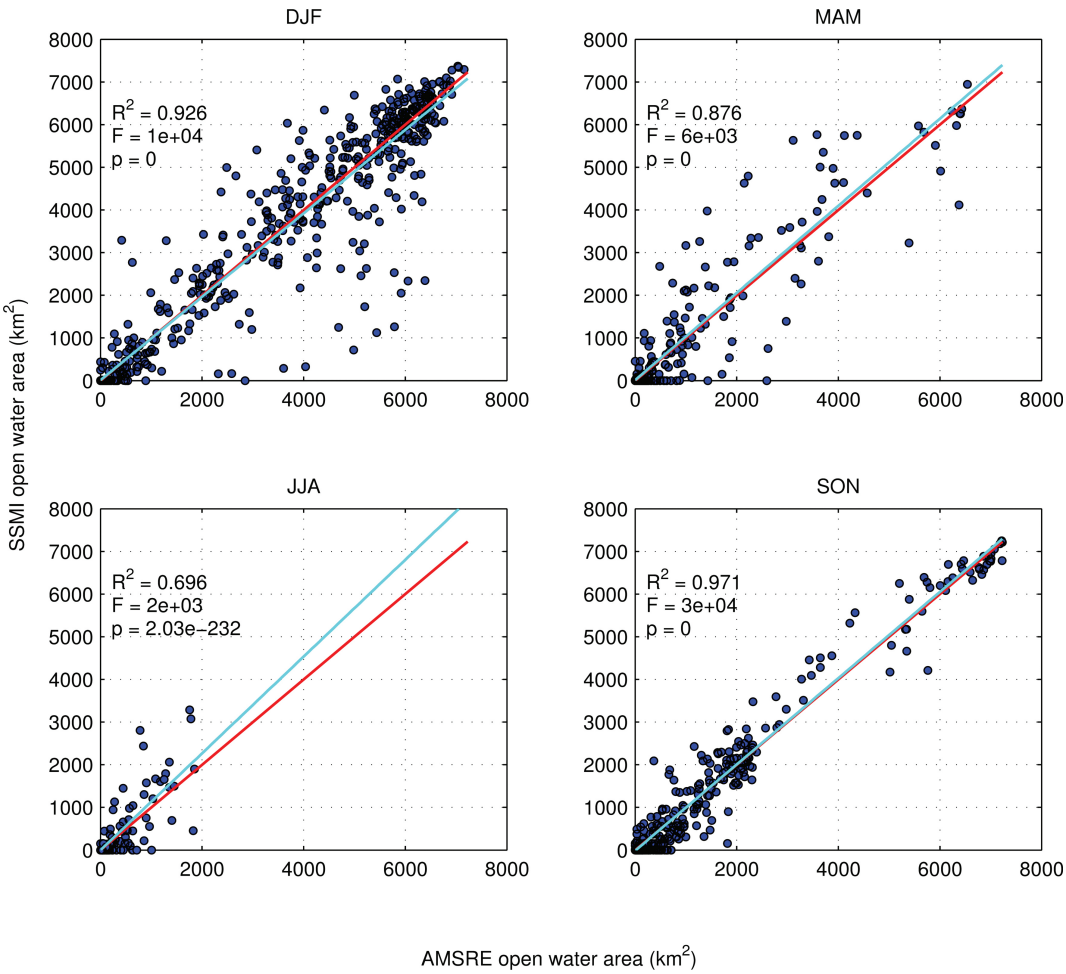

Figure A.5: Same as Supporting Figure A.4 for the Larsen B region.

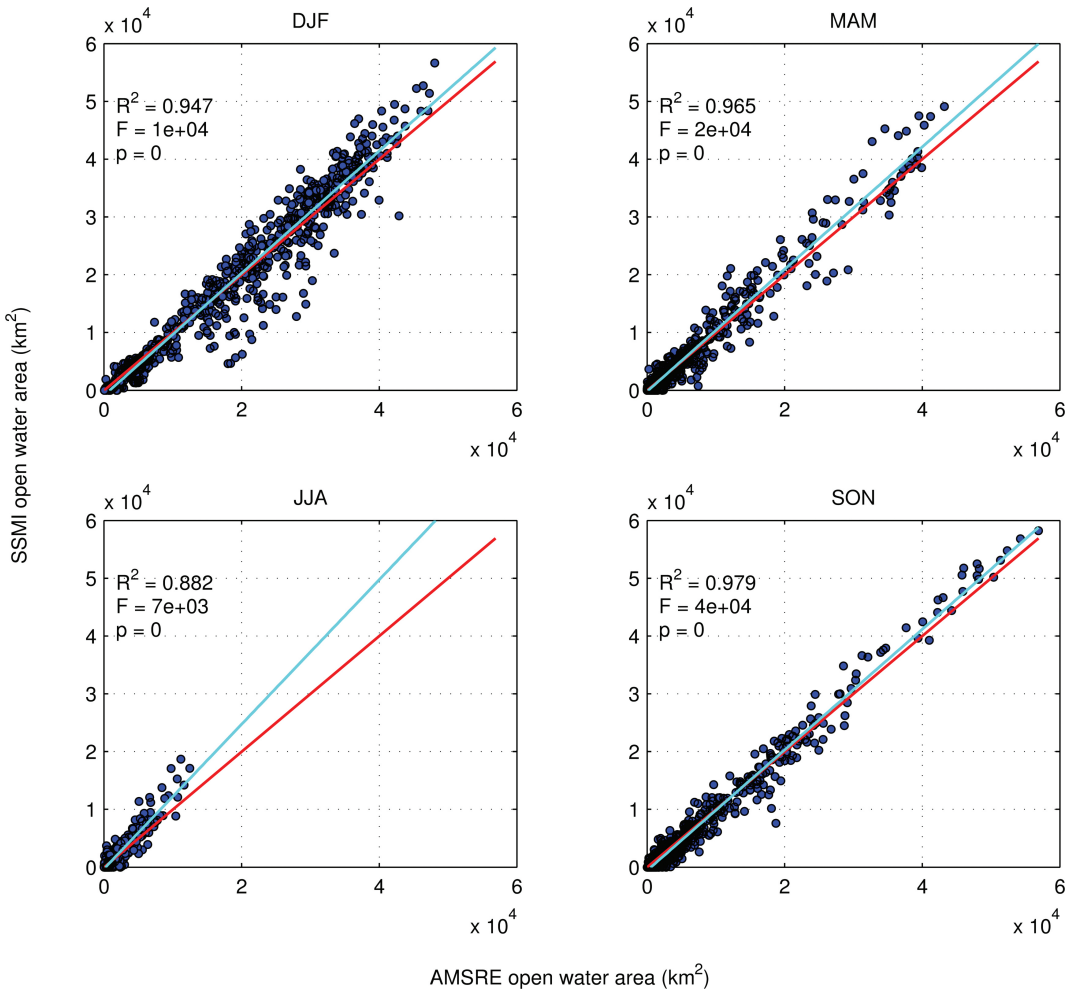

Figure A.6: Same as Supporting Figure A.4 for the Weddell region.

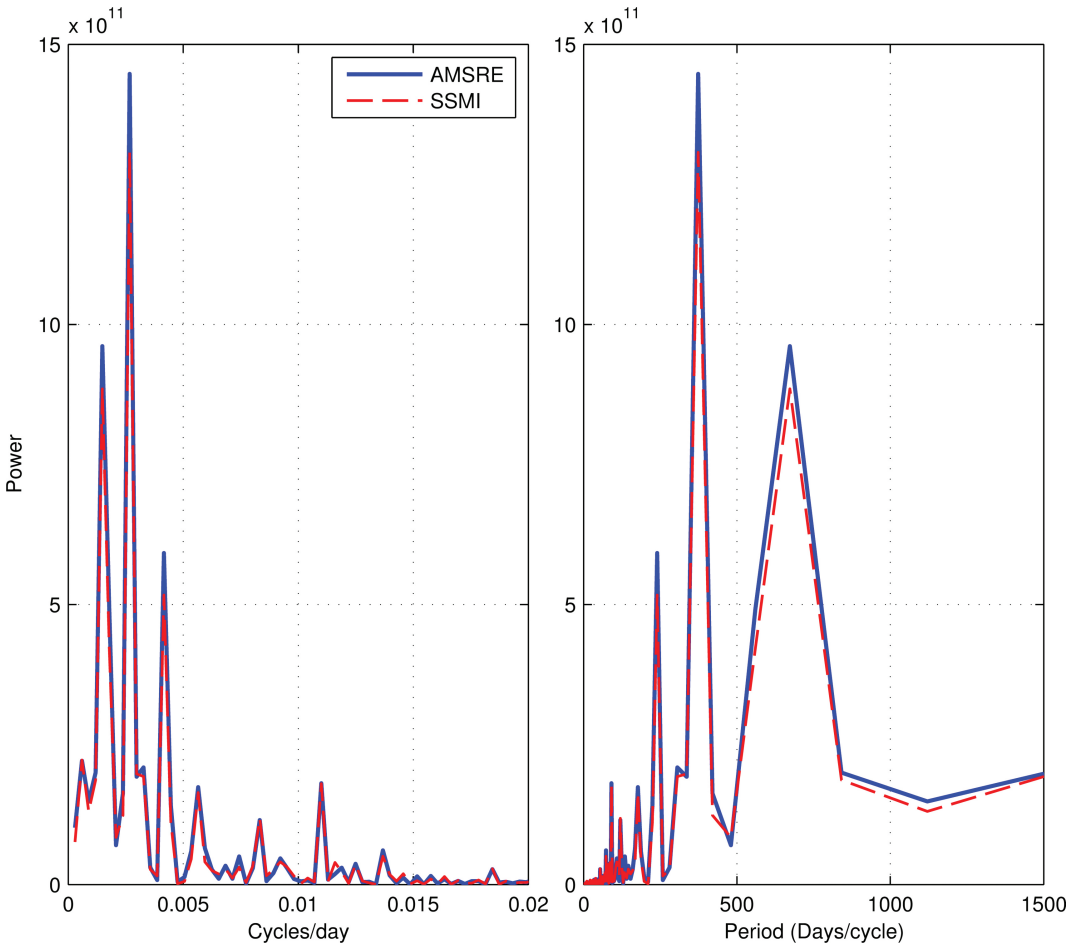

Figure A.7: Periodogram of Larsen A daily open water time series computed using a 15% threshold on sea ice concentration for AMSR-E (blue) and 40% threshold on SSM/I pixels (red). A subset of the curves is shown. Period = 1/frequency.

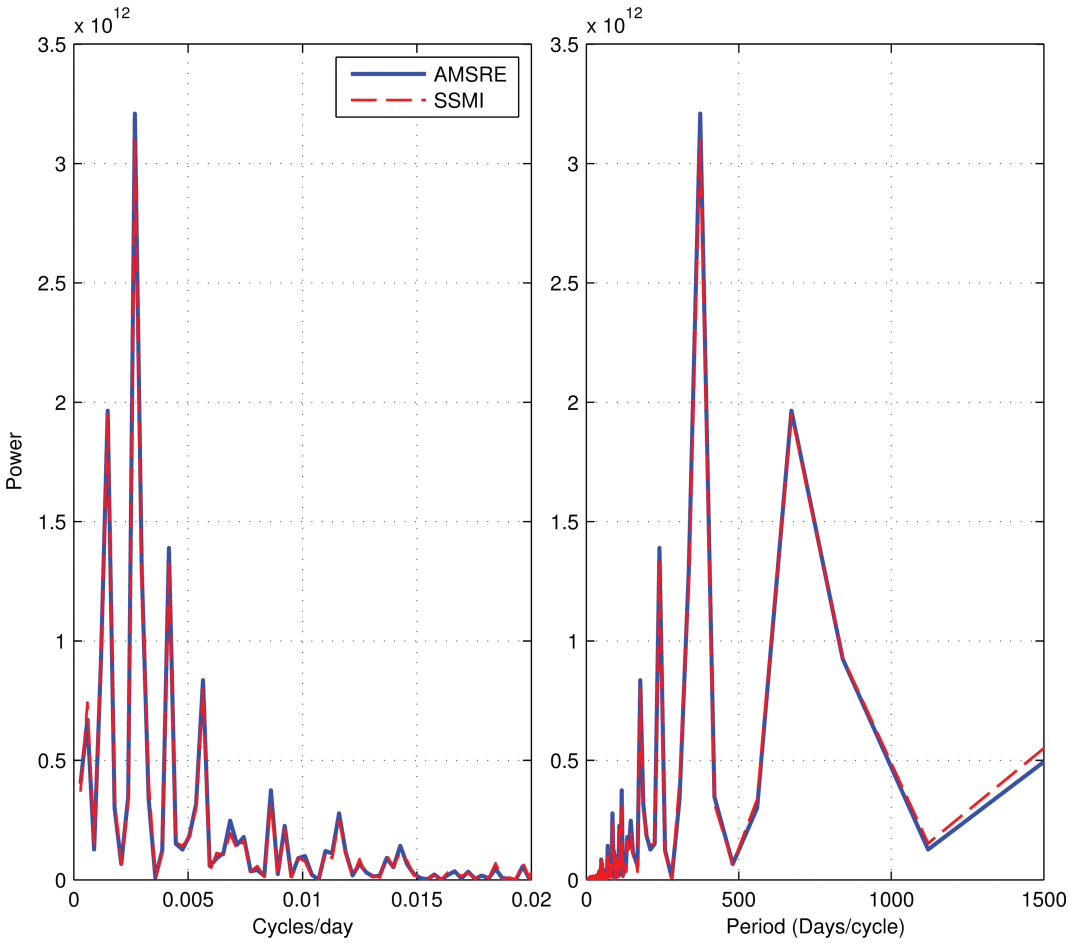

Figure A.8: Same as Supporting Figure A.7 for the Larsen B.

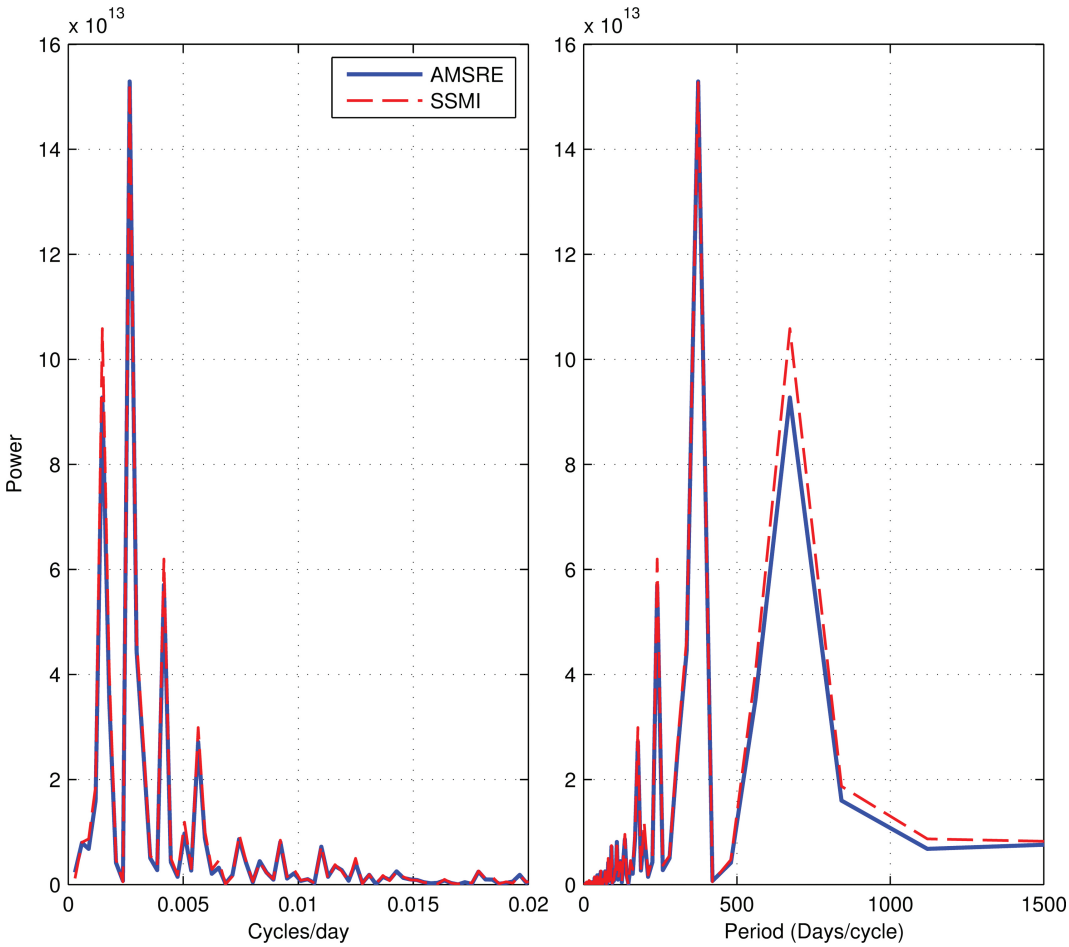

Figure A.9: Same as Supporting Figure A.7 for the Weddell region.

Appendix B

Supporting information for Chapter 3

Figure B.1: Image captured on March 26, 2012 during the NBP12-03 cruise in the Larsen A embayment showing atmospheric patterns associated with a strong foehn event. Cap clouds are visible over the mountains, with possible rotor clouds in the foreground and lenticular clouds above. Foehn clearance appears as a break in the clouds in the lee of the peninsula. Strong winds led to melting and advection of sea ice previously covering the embayment.

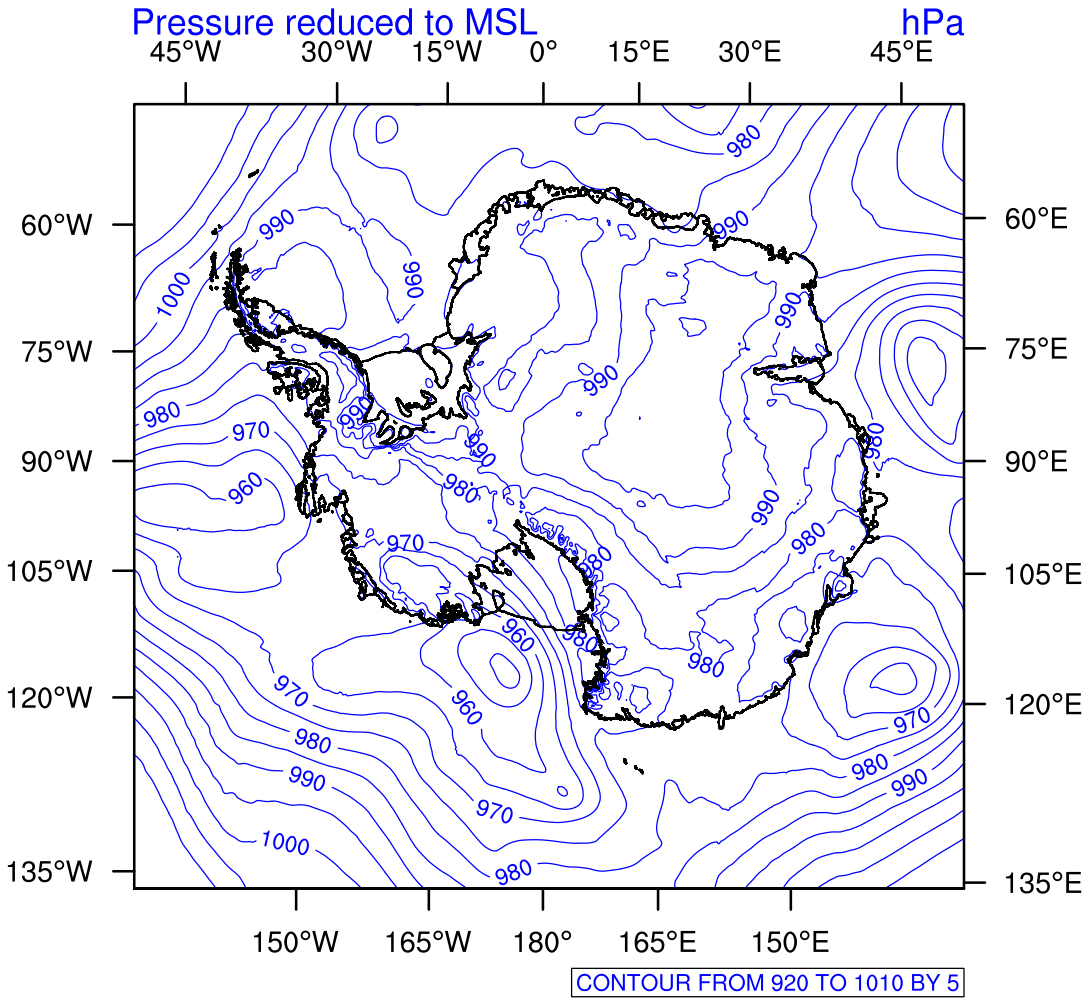

Figure B.2: AMPS forecast for March 26, 2014 at 12:00 UTC, showing sea level pressure (blue lines) across the Antarctic.

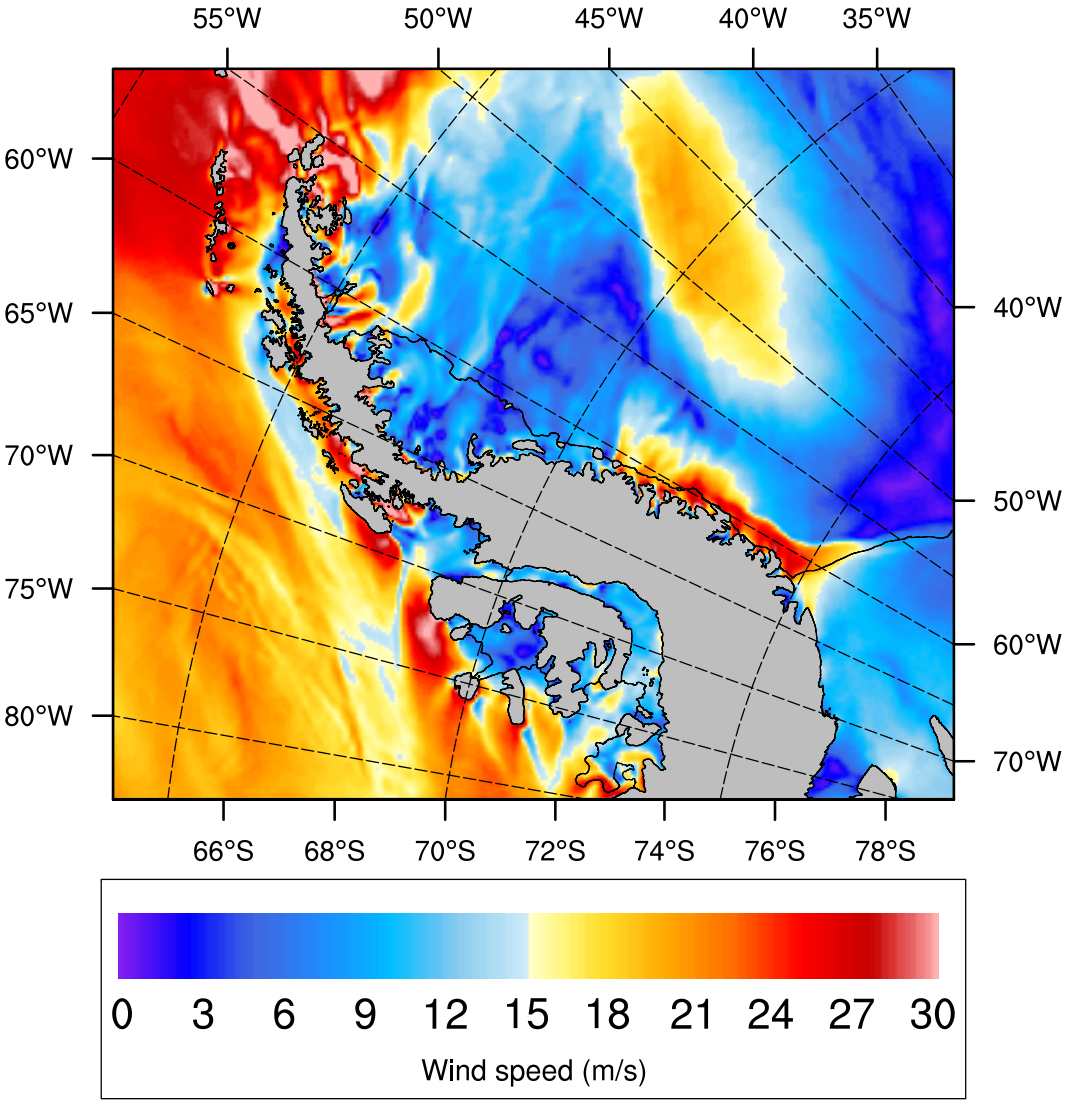

Figure B.3: AMPS forecast for March 26, 2014 at 12:00 UTC, showing surface wind speed (m s^{-1}). Only forecast data over the ocean and ice shelves is displayed. Narrow regions of high velocity winds are visible over the Larsen B embayment.

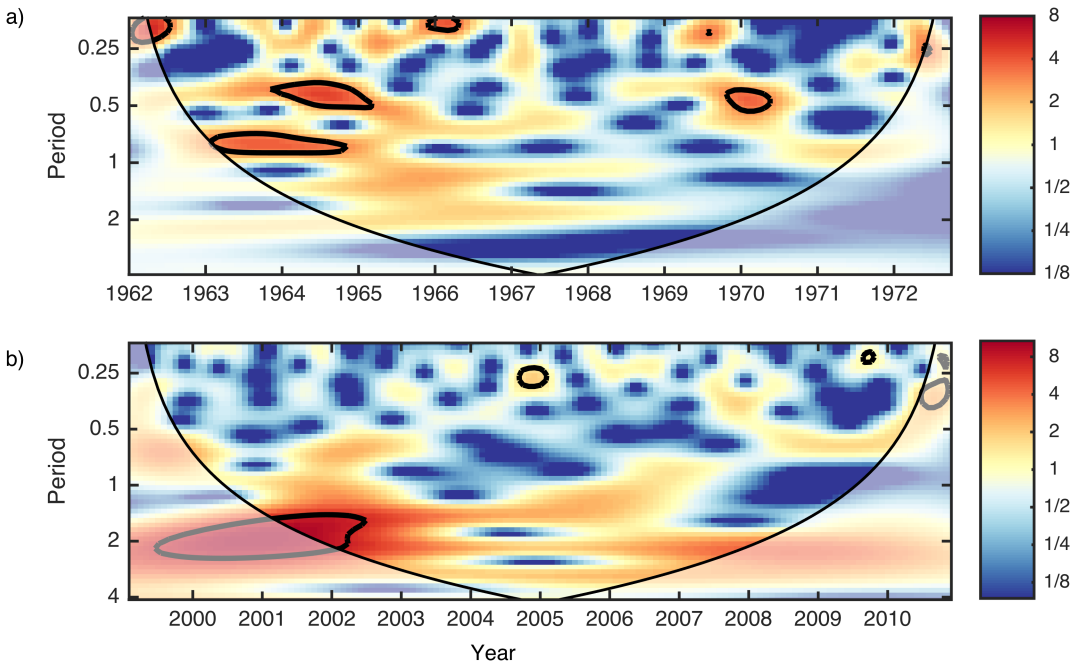

Figure B.4: Wavelet power spectrum of the foehn anomaly time series between a) 1962 and 1972 and b) 1999 and 2010. Colors indicate power. Shaded portion of the plots indicate the cone of influence, delimiting the region not influenced by edge effects. The continuous Morlet wavelet function was used in this analysis.

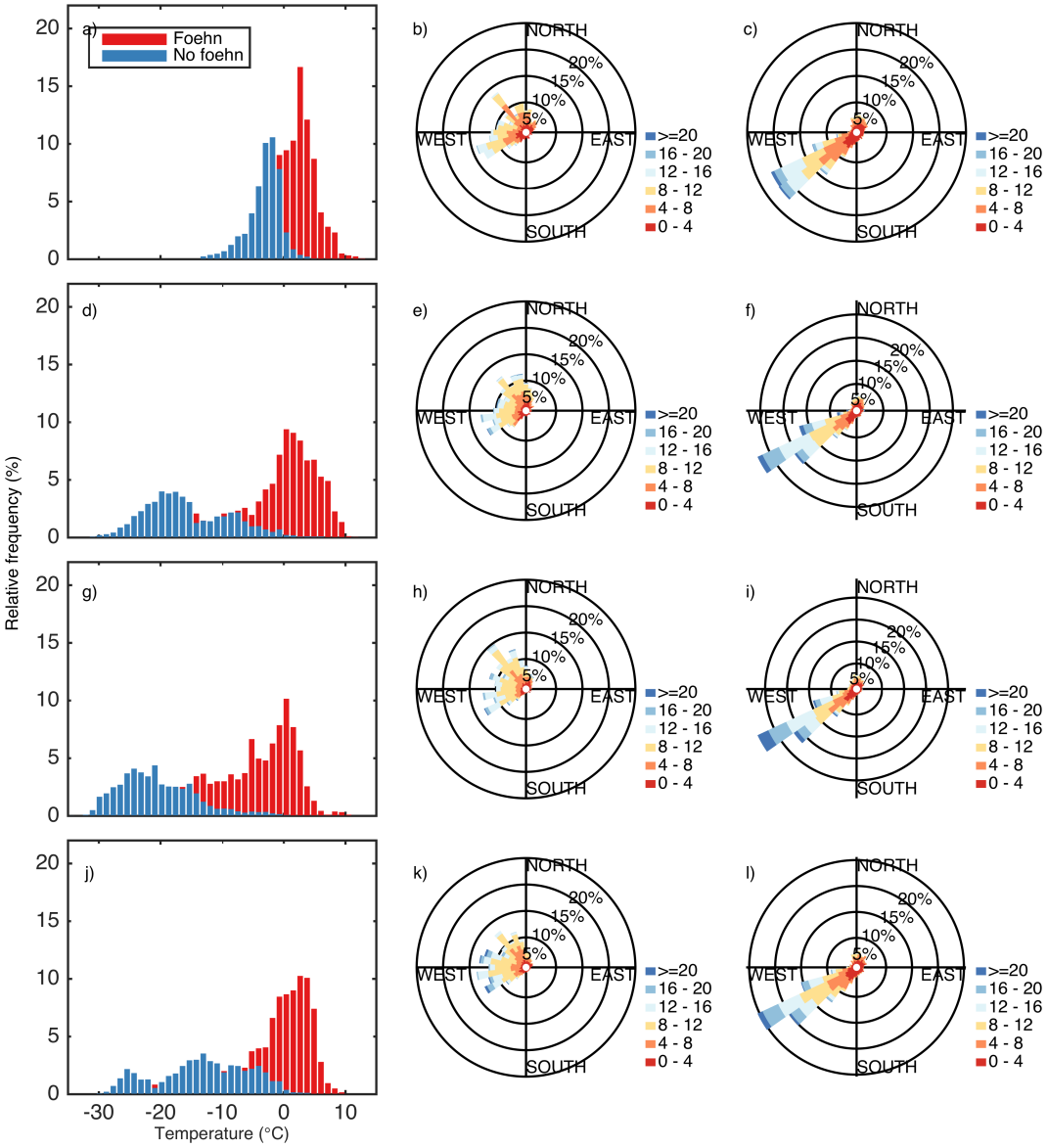

Figure B.5: Same as Figure 3.8, for the Robertson Island weather station. Strong, south-westerly winds dominate atmospheric flow at this location under normal conditions.

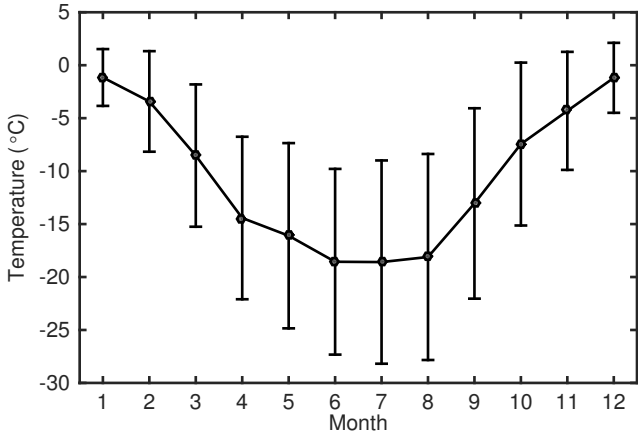

Figure B.6: Monthly climatology of surface temperature at Matienzo between 1962 and 2010. The horizontal line represents mean conditions, with vertical bars corresponding to ± 1 standard deviation about the mean.

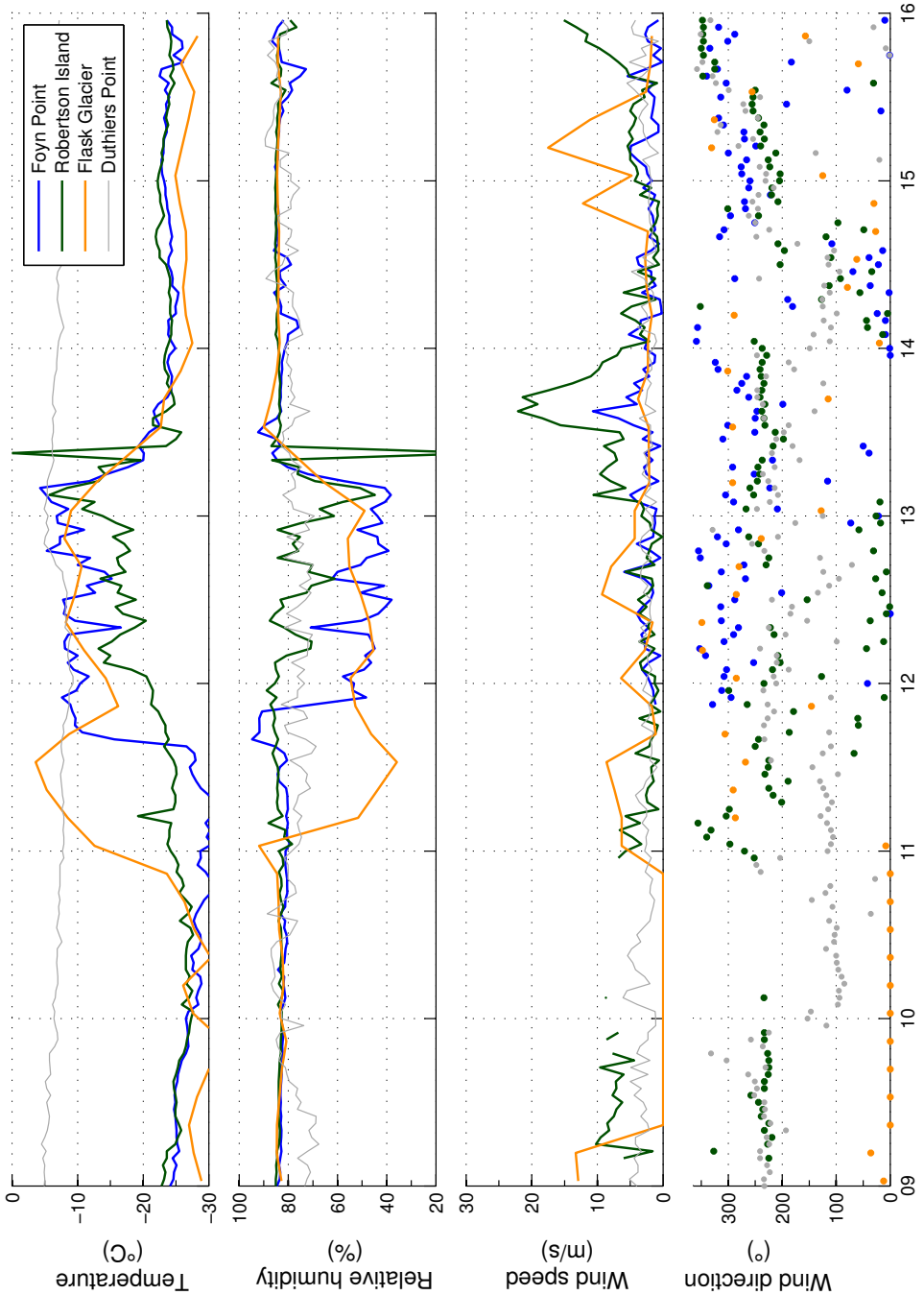

Figure B.7: Same as Figure 3.4a for a June 2011 foehn event.

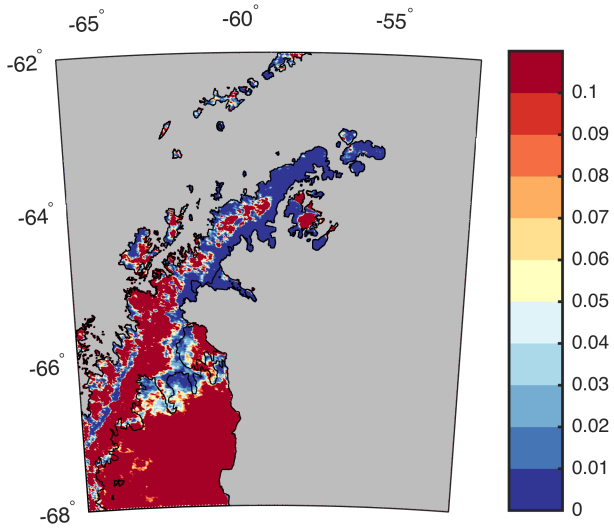

Figure B.8: Significance (p-value) of spatial correlation between monthly ice melt anomalies and monthly foehn frequency anomalies.

Appendix C

Supporting information for Chapter 4

Table C.1: Results from multiple comparison tests of phytodetritus cover across the process station.

Station 1	Station 2	p-value
G	H	0.33
G	I	< 0.01
G	J	< 0.01
G	K	< 0.01
H	I	0.45
H	J	< 0.01
H	K	< 0.01
I	J	0.15
I	K	< 0.01
J	K	1

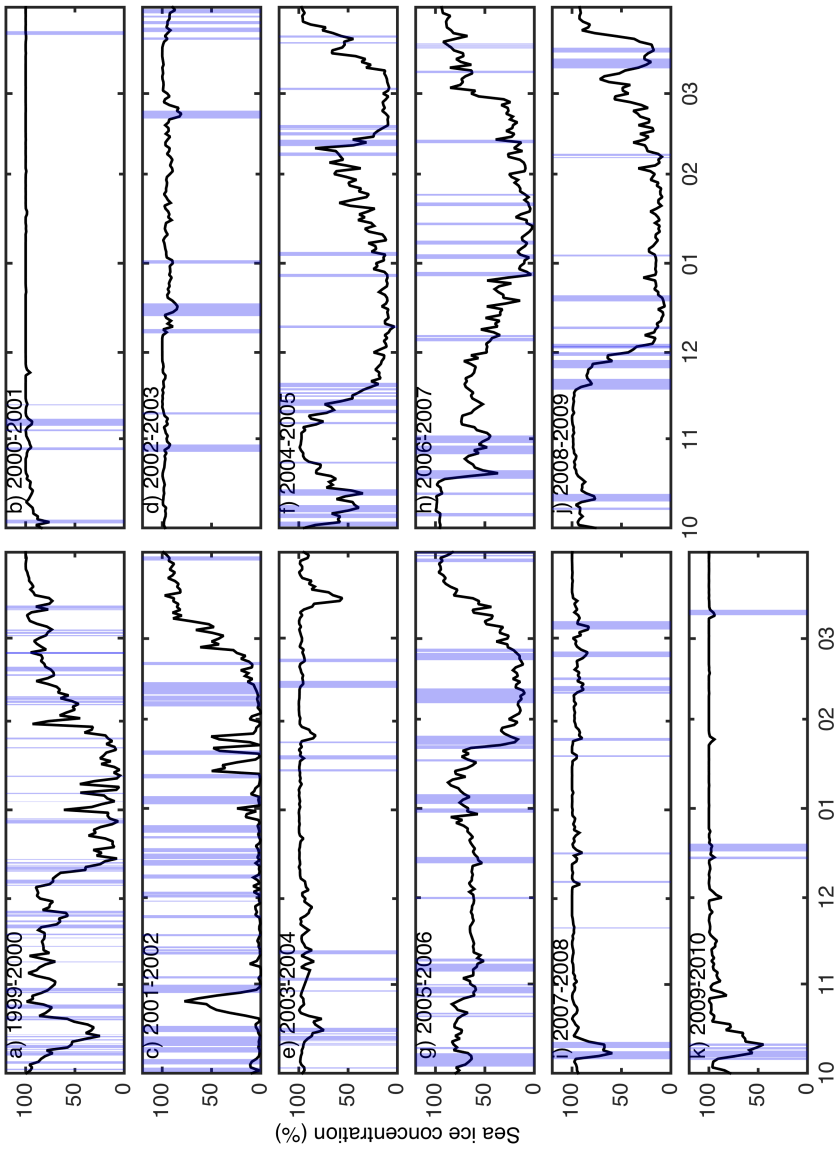

Figure C.1: Seasonal time series of sea ice concentration averaged within the Larsen B embayment between October 1 and March 1 of each year. Foehn events are highlighted in blue.

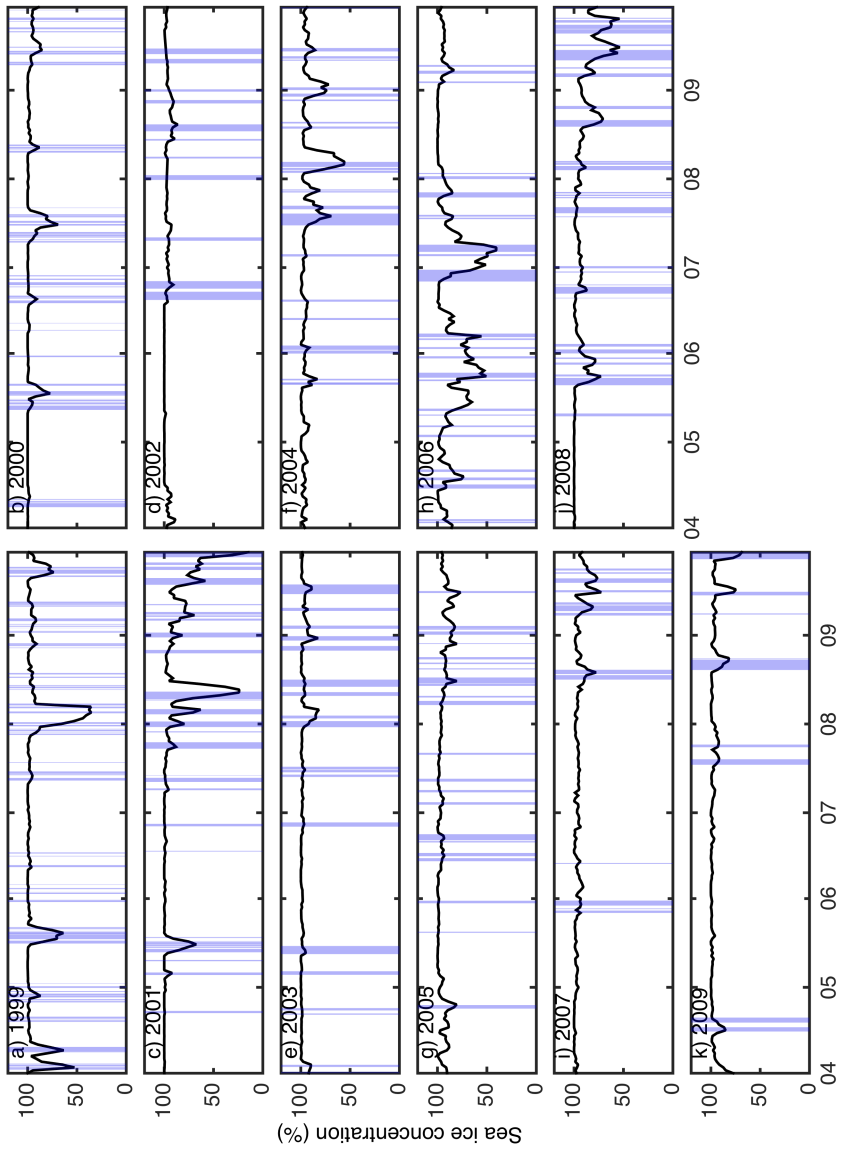

Figure C.2: Same as Supporting Figure C.1 for months between April 1 and September 30 of each year.

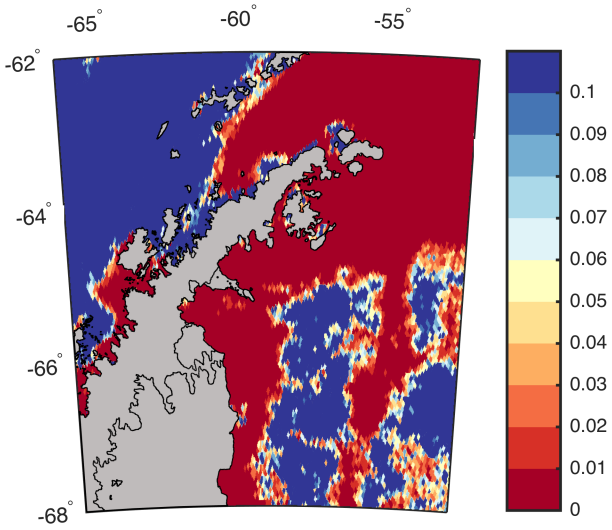

Figure C.3: Significance (p-value) of spatial correlation between sea ice concentration and the Matienzo foehn record as shown in Figure 4.4.

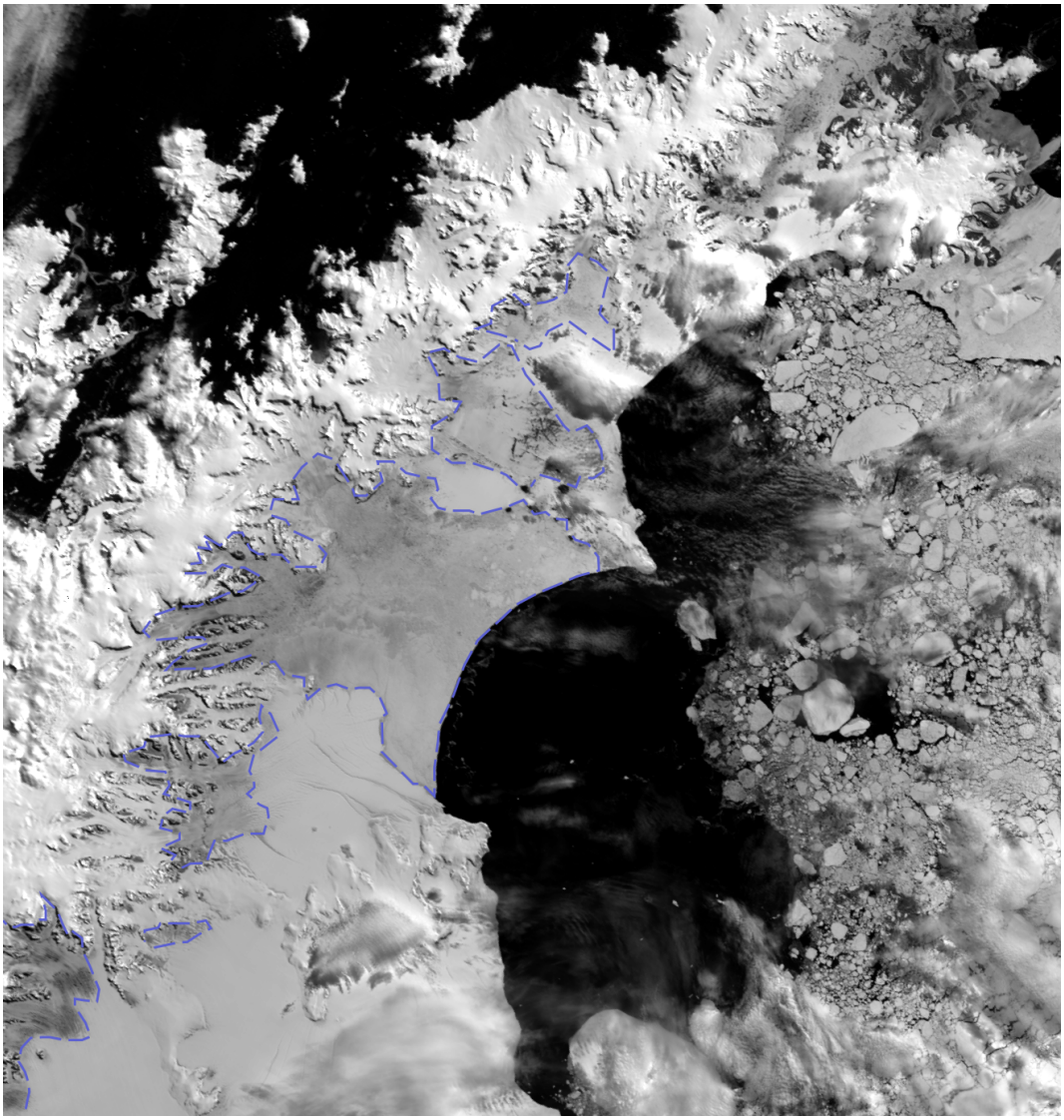

Figure C.4: Surface conditions along the eAP following a sustained foehn event as captured by MODIS Terra on November 13, 2005. Melt ponds, visible as dark patches along the coast, are outlined in blue.

Appendix D

Supporting information for Chapter 5

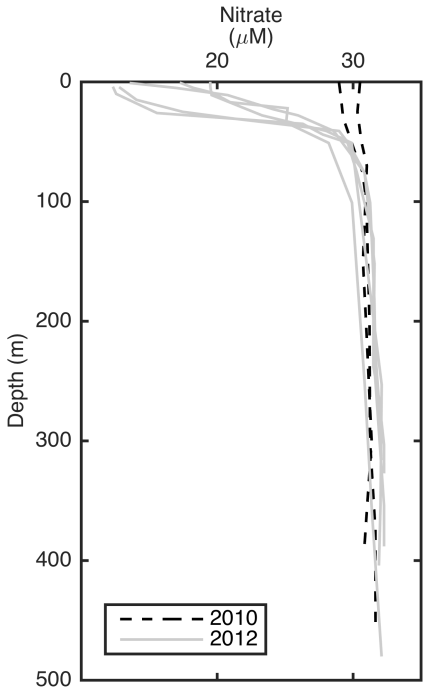

Figure D.1: Profiles of nitrate measured in the Larsen A embayment region in 2010 (NBP1001) and 2012 (this study).

Bibliography

[1] S. F. Ackley, K. R. Buck, and S. Taguchi. Standing crop of algae in the sea ice of the Weddell Sea region. *Deep Sea Research Part A. Oceanographic Research Papers*, 26(3):269–281, 1979.

[2] S. F. Ackley and C. W. Sullivan. Physical controls on the development and characteristics of Antarctic sea ice biological communities—a review and synthesis. *Deep Sea Research Part I: Oceanographic Research Papers*, 41(10):1583–1604, 1994.

[3] A.-C. Alderkamp, M. M. Mills, G. L. van Dijken, P. Laan, C.-E. Thuróczy, L. J. Gerringa, H. J. W. de Baar, C. D. Payne, R. J. W. Visser, A. G. J. Buma, and K. R. Arrigo. Iron from melting glaciers fuels phytoplankton blooms in the Amundsen Sea (Southern Ocean): Phytoplankton characteristics and productivity. *Deep Sea Research Part II: Topical Studies in Oceanography*, 71–76(0):32–48, Sept. 2012.

[4] S. Andersen, R. Tonboe, L. Kaleschke, G. Heygster, and L. T. Pedersen. Intercomparison of passive microwave sea ice concentration retrievals over the high-concentration Arctic sea ice. *Journal Of Geophysical Research-Oceans*, 112(C8):C08004, Jan. 2007.

[5] F. A. J. Armstrong, C. R. Stearns, and J. D. H. Strickland. The measurement of upwelling and subsequent biological process by means of the Technicon Autoanalyzer® and associated equipment. *Deep Sea Research and Oceanographic Abstracts*, 14(3):381–389, June 1967.

[6] K. R. Arrigo, K. E. Lowry, and G. L. van Dijken. Annual changes in sea ice and phytoplankton in polynyas of the Amundsen Sea, Antarctica. *Deep-Sea Res Pt II: Topical Studies in Oceanography*, 71:5–15, 2012.

[7] K. R. Arrigo, D. H. Robinson, D. L. Worthen, R. B. Dunbar, G. R. DiTullio, M. VanWoert, and M. P. Lizotte. Phytoplankton Community Structure and the Drawdown of Nutrients and CO2 in the Southern Ocean. *Science*, 283(5400):365–367, Jan. 1999.

[8] K. R. Arrigo, G. van Dijken, and M. Long. Coastal Southern Ocean: A strong anthropogenic CO2 sink. *Geophysical Research Letters*, 35(21):L21602, Nov. 2008.

[9] K. R. Arrigo and G. L. van Dijken. Phytoplankton dynamics within 37 Antarctic coastal polynya systems. *Journal Of Geophysical Research-Oceans*, 108(C8):3271–, Jan. 2003.

[10] K. R. Arrigo, G. L. van Dijken, and S. Bushinsky. Primary production in the Southern Ocean, 1997–2006. *Journal Of Geophysical Research-Oceans*, 113(C8):C08004, Jan. 2008.

[11] K. R. Arrigo, A. M. Weiss, and W. O. Smith, Jr. Physical forcing of phytoplankton dynamics in the southwestern Ross Sea. *Journal Of Geophysical Research-Oceans*, 103(C1):1007–1021, 1998.

[12] K. R. Arrigo, D. Worthen, A. Schnell, and M. P. Lizotte. Primary production in Southern Ocean waters. *Journal Of Geophysical Research-Oceans*, 103(C8):15587–15600, Jan. 1998.

[13] E. L. Atlas, L. I. Gordon, S. W. Hager, and P. K. Park. A practical manual for the use of the Technicon Autoanalyzer in seawater nutrient analyses, rev. Technical Report 71-22, Oct. 1971.

[14] N. E. Barrand, D. G. Vaughan, N. Steiner, M. Tedesco, P. Kuipers Munneke, M. R. van den Broeke, and J. S. Hosking. Trends in Antarctic Peninsula surface melting conditions from observations and regional climate modeling. *Journal Of Geophysical Research-Earth Surface*, 118(1):315–330, Mar. 2013.

[15] M. Behrenfeld and P. Falkowski. Photosynthetic rates derived from satellite-based chlorophyll concentration. *Limnology And Oceanography*, 42(1):1–20, 1997.

[16] M. J. Behrenfeld. Climate-mediated dance of the plankton. *Nature Climate Change*, 4(10):880–887, Sept. 2014.

[17] D. W. Beran. Large Amplitude Lee Waves and Chinook Winds. *J. Appl. Meteor.*, 6(5):865–877, Jan. 2013.

[18] H. Bernhardt and A. Wilhelms. The Continuous determination of low level iron, soluble phosphate and total phosphate with the autoanalyzer. In *Technicon Symposium: Automation in Analytical Chemistry*, pages 385–389, Oct. 1967.

[19] E. Berthier, T. A. Scambos, and C. A. Shuman. Mass loss of Larsen B tributary glaciers (Antarctic Peninsula) unabated since 2002. *Geophysical Research Letters*, 39(13):L13501, Jan. 2012.

[20] M. L. Bertolin and I. Schloss. Phytoplankton production after the collapse of the Larsen A Ice Shelf, Antarctica. *Polar Biology*, 32(10):1435–1446–1446, 2009.

[21] M. P. Bhatia, E. B. Kujawinski, S. B. Das, C. F. Breier, P. B. Henderson, and M. A. Charette. Greenland meltwater as a significant and potentially bioavailable source of iron to the ocean. *Nature Geoscience*, 6(4):274–278, Apr. 2013.

[22] D. Blondeau-Patissier, J. F. R. Gower, A. G. Dekker, S. R. Phinn, and V. E. Brando. A review of ocean color remote sensing methods and statistical techniques for the detection, mapping and analysis of phytoplankton blooms in coastal and open oceans. *Progress In Oceanography*, 123:123–144, Apr. 2014.

[23] M. A. Bourassa, S. T. Gille, C. Bitz, D. Carlson, I. Cerovecki, C. A. Clayson, M. F. Cronin, W. M. Drennan, C. W. Fairall, R. N. Hoffman, G. Magnusdottir, R. T. Pinker, I. A. Renfrew, M. Serreze, K. Speer, L. D. Talley, and G. A. Wick. High-Latitude Ocean and Sea Ice Surface Fluxes: Challenges for Climate Research. *Bull. Amer. Meteor. Soc.*, 94(3):403–423, Jan. 2013.

[24] P. Boyd. Ironing Out Algal Issues in the Southern Ocean. *Science*, 304(5669):396–397, Jan. 2004.

[25] P. W. Boyd and M. J. Ellwood. The biogeochemical cycle of iron in the ocean. *Nature Geoscience*, 3(10):675–682, Sept. 2010.

[26] S. Brachfeld, E. Domack, C. Kissel, C. Laj, A. Leventer, S. Ishman, R. Gilbert, A. Camerlenghi, and L. B. Eglinton. Holocene history of the Larsen-A Ice Shelf constrained by geomagnetic paleointensity dating. *Geology*, 31(9):749–752, Jan. 2003.

[27] D. H. Bromwich and D. D. Kurtz. Katabatic wind forcing of the Terra Nova Bay polynya. *Journal Of Geophysical Research-Oceans*, 89(C3):3561–3572, Jan. 1984.

[28] D. H. Bromwich, J. P. Nicolas, A. J. Monaghan, M. A. Lazzara, L. M. Keller, G. A. Weidner, and A. B. Wilson. Central West Antarctica among the most rapidly warming regions on Earth. *Nature Geoscience*, 6(2):139–145, Feb. 2013.

[29] P. M. Bruchhausen, J. A. Raymond, S. S. Jacobs, A. L. DeVries, E. M. Thorndike, and H. H. DeWitt. Fish, Crustaceans, and the Sea Floor Under the Ross Ice Shelf. *ScienceNew Series*, 203(4379):449–451, Feb. 1979.

[30] J. Campbell, D. Antoine, R. Armstrong, K. Arrigo, W. Balch, R. Barber, M. Behrenfeld, R. Bidigare, J. Bishop, M.-E. Carr, W. Esaias, P. Falkowski, N. Hoepffner, R. Iverson, D. Kiefer, S. Lohrenz, J. Marra, A. Morel, J. Ryan, V. Vedernikov, K. Waters, C. Yentsch, and J. Yoder. Comparison of algorithms for estimating ocean primary production from surface chlorophyll, temperature, and irradiance. *Global Biogeochemical Cycles*, 16(3):9–1–9–15, July 2002.

[31] M. R. Cape, M. Vernet, M. Kahru, and G. Spreen. Polynya dynamics drive primary production in the Larsen A and B embayments following ice shelf collapse. *Journal Of Geophysical Research-Oceans*, 119(1):572–594, Jan. 2014.

[32] M.-E. Carr, M. A. M. Friedrichs, M. Schmeltz, M. Noguchi Aita, D. Antoine, K. R. Arrigo, I. Asanuma, O. Aumont, R. Barber, M. Behrenfeld, R. Bidigare, E. T. Buitenhuis, J. Campbell, A. Ciotti, H. Dierssen, M. Dowell, J. Dunne, W. Esaias, B. Gentili, W. Gregg, S. Groom, N. Hoepffner, J. Ishizaka, T. Kameda, C. Le Quere, S. Lohrenz, J. Marra, F. Mélin, K. Moore, A. Morel, T. E. Reddy, J. Ryan, M. Scardi, T. Smyth, K. Turpie, G. Tilstone, K. Waters, and Y. Yamanaka. A comparison of global estimates of marine primary production from ocean color. *Deep Sea Research Part II: Topical Studies in Oceanography*, 53(5–7):741–770, Apr. 2006.

[33] A. Cefarelli, M. Vernet, and M. Ferrario. Phytoplankton composition and abundance in relation to free-floating Antarctic icebergs. *Deep Sea Research Part II: Topical Studies in Oceanography*, 58(11-12):1436–1450, 2011.

[34] A. Clarke. Seasonality in the antarctic marine environment. *Comparative Biochemistry and Physiology Part B: Comparative Biochemistry*, 90(3):461–473, Jan. 1988.

[35] A. Clarke and N. M. Johnston. Antarctic marine benthic diversity. *Oceanography and Marine Biology*, 41:47–114, Oct. 2003.

[36] J. C. Comiso and C. L. Parkinson. Arctic sea ice parameters from AMSR-E data using two techniques and comparisons with sea ice from SSM/I. *Journal Of Geophysical Research-Oceans*, 113(C2):C02S05, 2008.

[37] A. Cook, A. Fox, D. Vaughan, and J. G. Ferrigno. Retreating glacier fronts on the Antarctic Peninsula over the past half-century. *Science*, 308(5721):541–544, 2005.

[38] A. J. Cook and D. G. Vaughan. Overview of areal changes of the ice shelves on the Antarctic Peninsula over the past 50 years. *The Cryosphere*, 4(1):77–98, 2010.

[39] A. Cooper. Historical observations of Prince Gustav Ice Shelf. *Polar Record*, 1997.

[40] J. J. Cullen and M. R. Lewis. The kinetics of algal photoadaptation in the context of vertical mixing. *Journal Of Plankton Research*, 10(5):1039–1063, 1988.

[41] P. K. Dayton and J. S. Oliver. Antarctic Soft-Bottom Benthos in Oligotrophic and Eutrophic Environments. *Science*, 197(4298):55–58, Jan. 1977.

[42] G. Deacon. *The hydrology of the southern ocean*. Cambridge University Press ; Macmillan, London; New York, 1937.

[43] F. Defant. Local winds. pages 655–672. Compendium of Meteorology, Boston, MA, Oct. 1951.

[44] H. Dierssen, R. Smith, and M. Vernet. Glacial meltwater dynamics in coastal waters west of the Antarctic peninsula. *Proceedings Of The National Academy Of Sciences Of The United States Of America*, 99(4):1790–1795, 2002.

[45] H. Dierssen, M. Vernet, and R. Smith. Optimizing models for remotely estimating primary production in Antarctic coastal waters. *Antarctic Science*, 12(1):20–32, 2000.

[46] Q. Ding and E. J. Steig. Temperature Change on the Antarctic Peninsula Linked to the Tropical Pacific*. *Journal Of Climate*, 26(19):7570–7585, Jan. 2013.

[47] M. S. Dinniman, J. M. Klinck, and W. O. J. Smith. A model study of Circumpolar Deep Water on the West Antarctic Peninsula and Ross Sea continental shelves. *Deep Sea Research Part II: Topical Studies in Oceanography*, 58:1508–1523, 2011.

[48] E. Domack, D. Duran, A. Leventer, S. Ishman, S. Doane, S. McCallum, D. Amblas, J. Ring, R. Gilbert, and M. Prentice. Stability of the Larsen B ice shelf on the Antarctic Peninsula during the Holocene epoch. *Nature*, 436(7051):681–685, 2005.

[49] H. W. Ducklow, K. Baker, D. G. Martinson, L. B. Quetin, R. M. Ross, R. C. Smith, S. E. Stammerjohn, M. Vernet, and W. Fraser. Marine Pelagic Ecosystems: The West Antarctic Peninsula. *Philosophical Transactions: Biological Sciences*, 362(1477):67–94, Jan. 2007.

[50] H. W. Ducklow, M. Erickson, J. Kelly, M. Montes-Hugo, C. A. Ribic, R. C. Smith, S. E. Stammerjohn, and D. M. Karl. Particle export from the upper ocean over the continental shelf of the west Antarctic Peninsula: A long-term record, 1992-2007. *Deep Sea Research Part II: Topical Studies in Oceanography*, 55:2118–2131, 2008.

[51] H. W. Ducklow, W. R. Fraser, M. P. Meredith, S. E. Stammerjohn, S. C. Doney, D. G. Martinson, S. F. Sailley, O. M. Schofield, D. K. Steinberg, H. J. Venables, and C. D. Amsler. West Antarctic Peninsula: An Ice-Dependent Coastal Marine Ecosystem in Transition. *Oceanography*, 26(3):190–203, Sept. 2013.

[52] D. R. Durran. Mountain Waves and Downslope Winds. *Meteorological Monographs*, 23(45):59–83, June 1990.

[53] D. R. Durran and J. B. Klemp. A Compressible Model for the Simulation of Moist Mountain Waves. *Monthly Weather Review*, 111(12):2341–2361, Dec. 1983.

[54] P. Dutrieux, J. De Rydt, A. Jenkins, P. R. Holland, H. K. Ha, S. H. Lee, E. J. Steig, Q. Ding, E. P. Abrahamsen, and M. Schröder. Strong Sensitivity of Pine Island Ice-Shelf Melting to Climatic Variability. *Science*, 343(6167):174–178, Jan. 2014.

[55] H. Eicken. The role of sea ice in structuring Antarctic ecosystems. *Polar Biology*, 12(1):3–13, Apr. 1992.

[56] S. El-Sayed and G. A. Fryxell. Phytoplankton. In E. I. Friedman, editor, *Antarctic Microbiology*, pages 62–122. John Wiley & Sons, Ltd., New York.

[57] S. Z. El-Sayed and S. Taguchi. Primary production and standing crop of phytoplankton along the ice-edge in the Weddell Sea. *Deep Sea Research Part A. Oceanographic Research Papers*, 28(9):1017–1032, Sept. 1981.

[58] A. D. Elvidge. *Polar föhn winds and warming over the Larsen C Ice Shelf, Antarctica*. PhD thesis, University of East Anglia, Sept. 2013.

[59] A. D. Elvidge, I. A. Renfrew, J. C. King, A. Orr, T. A. Lachlan-Cope, M. Weeks, and S. L. Gray. Foehn jets over the Larsen C Ice Shelf, Antarctica. *Quarterly Journal of the Royal Meteorological Society*, pages n/a–n/a, Apr. 2014.

[60] J. G. Ferrigno, A. Cook, A. M. Mathie, R. J. Williams, C. Swithinbank, K. M. Foley, A. Fox, J. W. Thomson, and J. Sievers. Coastal-Change and Glaciological Map of the Larsen Ice Shelf Area, Antarctica: 1940–2005. *U.S. Geological Survey Geologic Investigations Series Map I–2600–B*, (1 map sheet):28–p., Jan. 2008.

[61] J. G. Ferrigno, A. J. Cook, K. M. Foley, R. S. Williams, Jr, C. Swithinbank, A. Fox, J. W. Thomson, and J. Sievers. Coastal-change and glaciological map of the Trinity Peninsula area and South Shetland Islands, Antarctica – 1843–2001. *U.S. Geological Survey Geologic Investigations Series Map I–2600–A*, pages 32–p., Jan. 2008.

[62] G. Fischer, R. Gersonde, and G. Wefer. Organic carbon, biogenic silica and diatom fluxes in the marginal winter sea-ice zone and in the Polar Front Region: interannual variations and differences in composition. *Deep Sea Research Part II: Topical Studies in Oceanography*, 49(9–10):1721–1745, 2002.

[63] A. D. Fraser, R. A. Massom, K. J. Michael, B. K. Galton-Fenzi, and J. L. Lieser. East Antarctic Landfast Sea Ice Distribution and Variability, 2000–08. *Journal Of Climate*, 25(4):1137–1156, Jan. 2013.

[64] P. W. Froneman, E. A. Pakhomov, and M. G. Balarin. Size-fractionated phytoplankton biomass, production and biogenic carbon flux in the eastern Atlantic sector of the Southern Ocean in late austral summer 1997–1998. *Deep-Sea Research II: Topical Studies in Oceanography*, 51(22–24):2715–2729, Dec. 2004.

[65] A. Ganachaud and C. Wunsch. Improved estimates of global ocean circulation, heat transport and mixing from hydrographic data. *Nature*, 408(6811):453–457, Nov. 2000.

[66] I. A. Garibotti, M. Vernet, W. A. Kozlowski, and M. E. Ferrario. Composition and biomass of phytoplankton assemblages in coastal Antarctic waters: a comparison of chemotaxonomic and microscopic analyses. *Marine Ecology . . .* , 247:27–42, 2003.

[67] D. L. Garrison, K. N. Buck, and G. A. Fryxell. Algal assemblages in antarctic pack ice and in ice-edge plankton. *Journal Of Phycology*, 23(4):564–572, 1987.

[68] D. L. Garrison, C. W. Sullivan, and S. F. Ackley. Sea ice microbial communities in antarctica. *BioScience*, 36(4):243–250, 1986.

[69] L. J. Gerringa, A.-C. Alderkamp, P. Laan, C.-E. Thuróczy, H. J. W. de Baar, M. M. Mills, G. L. van Dijken, H. v. Haren, and K. R. Arrigo. Iron from melting glaciers fuels the phytoplankton blooms in Amundsen Sea (Southern Ocean): Iron biogeochemistry. *Deep Sea Research Part II: Topical Studies in Oceanography*, 71–76(0):16–31, Jan. 2012.

[70] N. F. Glasser, T. A. Scambos, J. Bohlander, M. Truffer, E. Pettit, and B. J. Davies. From ice-shelf tributary to tidewater glacier: continued rapid recession, acceleration and thinning of Rohss Glacier following the 1995 collapse of the Prince Gustav Ice Shelf, Antarctic Peninsula. *Journal Of Glaciology*, 57(203):397–406, 2011.

[71] A. G. Glover, C. R. Smith, S. L. Mincks, P. Y. G. Sumida, and A. R. Thurber. Macrofaunal abundance and composition on the West Antarctic Peninsula continental shelf: Evidence for a sediment 'food bank' and similarities to deep-sea habitats. *Deep Sea Research Part II: Topical Studies in Oceanography*, 55(22-23):2491–2501, Nov. 2008.

[72] K. Golden, S. F. Ackley, and V. I. Lytle. The percolation phase transition in sea ice. *Science*, 282(5397):2238–2241, 1998.

[73] A. Gordon. Western Weddell sea thermohaline stratification. *Antarctic Research Series*, 1998.

[74] A. L. Gordon and J. C. Comiso. Polynyas in the Southern Ocean. *Scientific American; (USA)*, 258:6, June 1988.

[75] L. J. Grange and C. R. Smith. Megafaunal Communities in Rapidly Warming Fjords along the West Antarctic Peninsula: Hotspots of Abundance and Beta Diversity. *PLoS ONE*, 8(12):e77917, Dec. 2013.

[76] D. P. Grosvenor, J. C. King, T. W. Choularton, and T. Lachlan-Cope. Downslope föhn winds over the Antarctic Peninsula and their effect on the Larsen ice shelves. *Atmospheric Chemistry and Physics*, 14(18):9481–9509, 2014.

[77] J. Gutt, I. Barratt, E. Domack, C. d'Udekem d'Acoz, W. Dimmler, A. Grémare, O. Heilmayer, E. Isla, D. Janussen, E. Jorgensen, K.-H. Kock, L. Sophia Lehnert, P. López-Gonzáles, S. Langner, K. Linse, M. Eugenia Manjón-Cabeza, M. Meißner, A. Montiel, M. Raes, H. Robert, A. Rose, E. Sañé Schepisi, T. Saucède, M. Scheidat, H.-W. Schenke, J. Seiler, and C. Smith. Biodiversity change after climate-induced ice-shelf collapse in the Antarctic. *Deep Sea Research Part II: Topical Studies in Oceanography*, 58(1–2):74–83, Jan. 2011.

[78] J. Gutt, M. Cape, W. Dimmler, L. Fillinger, E. Isla, V. Lieb, T. Lundälv, and C. Pulcher. Shifts in Antarctic megabenthic structure after ice-shelf disintegration in the Larsen area east of the Antarctic Peninsula. *Polar Biology*, 36(6):895–906, 2013.

[79] T. J. Hart. On the phytoplankton of the southwest Atlantic and the Bellingshausen Sea, 1929–1931. *Discovery Reports*, 8:1–286, 1934.

[80] L. R. Haury, J. McGowan, and P. H. Wiebe. Patterns and processes in the time-space scales of plankton distributions. In *NATO Conference Series IV Marine Sciences*, pages 277–327, Oct. 1978.

[81] J. R. Hawkings, J. L. Wadham, M. Tranter, R. Raiswell, L. G. Benning, P. J. Statham, A. Tedstone, P. Nienow, K. Lee, and J. Telling. Ice sheets as a significant source of highly reactive nanoparticulate iron to the oceans. *Nature Communications*, 5, May 2014.

[82] C. D. Hewes, O. Holm-Hansen, and E. Sakshaug. Alternate Carbon Pathways at Lower Trophic Levels in the Antarctic Food Web. In *Antarctic Nutrient Cycles and Food Webs*, pages 277–283. Springer Berlin Heidelberg, Berlin, Heidelberg, 1985.

[83] B. A. Hodges and D. L. Rudnick. Simple models of steady deep maxima in chlorophyll and biomass. *Deep Sea Research Part I: Oceanographic Research Papers*, 51(8):999–1015, Aug. 2004.

[84] O. Hoegh-Guldberg and J. F. Bruno. The Impact of Climate Change on the World's Marine Ecosystems. *Science*, 328(5985):1523–1528, June 2010.

[85] K. P. Hoinka. What is a Foehn Clearance? *Bulletin Of The American Meteorological Society*, 66(9):1123–1132, Sept. 1985.

[86] P. R. Holland. The seasonality of Antarctic sea ice trends. *Geophysical Research Letters*, 41(12):4230–4237, June 2014.

[87] P. R. Holland and R. Kwok. Wind-driven trends in Antarctic sea-ice drift. *Nature Geoscience*, 5(12):872–875, Nov. 2012.

[88] O. Holm-Hansen, C. J. Lorenzen, R. W. Holmes, and J. D. H. Strickland. Fluorometric Determination of Chlorophyll. *Ices Journal Of Marine Science*, 30(1):3–15, Dec. 1965.

[89] M. Hoppema, H. J. W. de Baar, R. G. J. Bellerby, E. Fahrbach, and K. Bakker. Annual export production in the interior Weddell Gyre estimated from a chemical mass balance of nutrients. *Deep Sea Research Part II: Topical Studies in Oceanography*, 49(9-10):1675–1689, Jan. 2002.

[90] M. Hoppema and L. Goeyens. Redfield behavior of carbon, nitrogen, and phosphorus depletions in Antarctic surface water. *Limnology And Oceanography*, 44(1):220–224, 1999.

[91] M. Hoppema, L. Goeyens, and E. Fahrbach. Intense nutrient removal in the remote area off Larsen Ice Shelf (Weddell Sea). *Polar Biology*, 23(2):85–94–94, 2000.

[92] M. Hoppema, R. Middag, H. J. W. de Baar, E. Fahrbach, E. M. van Weerlee, and H. Thomas. Whole season net community production in the Weddell Sea. *Polar Biology*, 31(1):101–111, July 2007.

[93] J. S. Hosking, A. Orr, G. J. Marshall, J. Turner, and T. Phillips. The Influence of the Amundsen–Bellingshausen Seas Low on the Climate of West Antarctica and Its Representation in Coupled Climate Model Simulations. *Journal Of Climate*, 26(17):6633–6648, Sept. 2013.

[94] C. Hsieh, S. Glaser, A. Lucas, and G. Sugihara. Distinguishing random environmental fluctuations from ecological catastrophes for the North Pacific Ocean. *Nature*, 435(7040):336–340, 2005.

[95] J. Huisman, N. N. P. Thi, D. M. Karl, and B. Sommeijer. Reduced mixing generates oscillations and chaos in the oceanic deep chlorophyll maximum. *Nature*, 439(7074):322–325, Jan. 2006.

[96] S. S. Jacobs, A. Jenkins, C. F. Giulivi, and P. Dutrieux. Stronger ocean circulation and increased melting under Pine Island Glacier ice shelf. *Nature Geoscience*, 4(8):519–523, June 2011.

[97] S. W. Jeffrey and G. F. Humphrey. New spectrophotometric equations for determining chlorophylls a, b, c1, c2 in higher plants, algae, and natural phytoplankton. *Biochem. Physiolo. Pflanzen*, 167:191–194.

[98] J. Jennings, L. Gordon, and D. Nelson. Nutrient depletion indicates high primary productivity in the Weddell Sea. *Nature*, 309(5963):51–54, May 1984.

[99] J. C. Jennings, L. I. Gordon, and D. Nelson. Nutrient depletion indicates high primary productivity in the weddell sea. *Nature*, 309(5963):51–54, 1984.

[100] R. Johnson, P. G. Strutton, S. W. Wright, A. McMinn, and K. M. Meiners. Three improved satellite chlorophyll algorithms for the Southern Ocean. *Journal Of Geophysical Research-Oceans*, 118(7):3694–3703, 2013.

[101] M. Kahru and B. G. Mitchell. Blending of ocean colour algorithms applied to the Southern Ocean. *Remote Sensing Letters*, 1(2):119–124, June 2010.

[102] L. Kaleschke, G. Heygster, C. Lupkes, A. Bochert, H. J. Hartmann, J. Haarpaintner, and T. Vihma. SSM/I sea ice remote sensing for mesoscale ocean-atmosphere interaction analysis. *Canadian Journal Of Remote Sensing*, 27(5):526–537, 2001.

[103] S. Kern, G. Spreen, L. Kaleschke, S. de La Rosa, and G. Heygster. Polynya Signature Simulation Method polynya area in comparison to AMSR-E 89 GHz sea-ice concentrations in the Ross Sea and off the Adelie Coast, Antarctica, for 2002-05: first results. *Annals of Glaciology*, 46(1):409–418, 2007.

[104] A. L. King and K. Barbeau. Evidence for phytoplankton iron limitation in the southern California Current System. *Marine Ecology Progress Series*, 342:91–103, July 2007.

[105] A. L. King and K. A. Barbeau. Dissolved iron and macronutrient distributions in the southern California Current System. *Journal Of Geophysical Research-Oceans*, 116:C03018, 2011.

[106] J. C. King and J. C. Comiso. The spatial coherence of interannual temperature variations in the Antarctic Peninsula. *Geophysical Research Letters*, 30(2):1040, Jan. 2003.

[107] J. C. King, T. A. Lachlan-Cope, R. S. Ladkin, and A. Weiss. Airborne Measurements in the Stable Boundary Layer over the Larsen Ice Shelf, Antarctica. *Boundary-Layer Meteorology*, 127(3):413–428, 2008.

[108] J. C. King and J. Turner. *Antarctic Meteorology and Climatology*. Cambridge University Press, Cambridge, 2009.

[109] J. Kirk. *Light and Photosynthesis in Aquatic Ecosystems*. Cambridge University Press, 3rd edition edition, Feb. 2011.

[110] J. M. Klinck. Heat and salt changes on the continental shelf west of the Antarctic Peninsula between January 1993 and January 1994. *Journal Of Geophysical Research-Oceans*, 103(C4):7617–7636, 1998.

[111] R. Kwok and J. Comiso. Southern Ocean climate and sea ice anomalies associated with the Southern Oscillation. *Journal Of Climate*, 15(5):487–501, 2002.

[112] R. Kwok and J. C. Comiso. Spatial patterns of variability in antarctic surface temperature: Connections to the Southern Hemisphere Annular Mode and the Southern Oscillation. *Geophysical Research Letters*, 29(14), 2002.

[113] C. Lancelot, S. Mathot, C. Veth, and H. Baar. Factors controlling phytoplankton ice-edge blooms in the marginal ice-zone of the northwestern Weddell Sea during sea ice retreat 1988: Field observations and mathematical modelling. *Polar Biology*, 13(6):377–387–387, 1993.

[114] P. Leavitt. A review of factors that regulate carotenoid and chlorophyll deposition and fossil pigment abundanc. *Journal Of Paleolimnology*, 1993.

[115] P. Leavitt and D. HODGSON. Sedimentary pigments. In J. Smol, H. J. Birks, and M. Williams, editors, *Tracking Environmental Change Using Lake Sediments*, page 371. Springer, 2001.

[116] L. Legendre, S. F. Ackley, G. S. Dieckmann, B. Gulliksen, R. Horner, T. Hoshiai, I. A. Melnikov, W. S. Reeburgh, M. Spindler, and C. W. Sullivan. Ecology of sea ice biota. 2. Global significance. *Polar Biology*, 12(3-4):429–444, 1992.

[117] S. A. Levin. The problem of pattern and scale in ecology. *Ecology*, 73(6):1943–1967, 1992.

[118] X. Li, D. M. Holland, E. P. Gerber, and C. Yoo. Impacts of the north and tropical Atlantic Ocean on the Antarctic Peninsula and sea ice. *Nature*, 505(7484):538–542.

[119] H. Lin and B. S. Twining. Chemical speciation of iron in Antarctic waters surrounding free-drifting icebergs. *Marine Chemistry*, 128:81–91, 2012.

[120] M. Lizotte. The contributions of sea ice algae to Antarctic marine primary production. *American Zoologist*, 41(1):57–73, 2001.

[121] D. G. Long and B. R. Hicks. Standard BYU QuikSCAT and Seawinds Land/Ice Image Products . Technical report, BYU Center for Remote Sensing, Provo, UT, Aug. 2010.

[122] J. F. Lübbecke, N. J. Burls, C. J. C. Reason, and M. J. McPhaden. Variability in the South Atlantic Anticyclone and the Atlantic Niño Mode. *Journal Of Climate*, 27(21):8135–8150, Aug. 2014.

[123] D. Lubin, R. A. Wittenmyer, D. H. Bromwich, and G. J. Marshall. Antarctic Peninsula mesoscale cyclone variability and climatic impacts influenced by the SAM. *Geophysical Research Letters*, 35(2):–, 2008.

[124] N. MAAß and L. Kaleschke. Improving passive microwave sea ice concentration algorithms for coastal areas: applications to the Baltic Sea. *Tellus Series A-Dynamic Meteorology And Oceanography*, 62(4):393–410, Jan. 2010.

[125] T. Maksym, S. Stammerjohn, S. Ackley, and R. Massom. Antarctic Sea Ice—A Polar Opposite? *Oceanography*, 25(3):140–151, Sept. 2012.

[126] M. Manizza, C. Le Quere, A. J. Watson, and E. T. Buitenhuis. Bio-optical feedbacks among phytoplankton, upper ocean physics and sea-ice in a global model. *Geophysical Research Letters*, 32(5):L05603, 2005.

[127] J. Marr. The natural history and geography of the Antarctic krill (Euphasia superba Dana). Technical report, Oct. 1962.

[128] G. J. Marshall. Trends in the Southern Annular Mode from Observations and Reanalyses. *Journal Of Climate*, 16(24):4134–4143, Dec. 2003.

[129] G. J. Marshall, A. Orr, N. P. M. van Lipzig, and J. C. King. The Impact of a Changing Southern Hemisphere Annular Mode on Antarctic Peninsula Summer Temperatures. *Journal Of Climate*, 19(20):5388–5404, Jan. 2006.

[130] J. H. Martin, S. E. Fitzwater, and R. M. Gordon. Iron deficiency limits phytoplankton growth in Antarctic waters. *Global Biogeochemical Cycles*, 4(1):5–12, Sept. 1990.

[131] J. H. Martin, R. M. Gordon, and S. E. Fitzwater. Iron in Antarctic waters. *Nature*, 345(6271):156–158, May 1990.

[132] P. J. Martin and D. A. Peel. The spatial distribution of 10 m temperatures in the Antarctic Peninsula. *Journal Of Glaciology*, 20:311–317, 1978.

[133] R. A. Massom, S. E. Stammerjohn, W. Lefebvre, S. A. Harangozo, N. Adams, T. A. Scambos, M. J. Pook, and C. Fowler. West Antarctic Peninsula sea ice in 2005: Extreme ice compaction and ice edge retreat due to strong anomaly with respect to climate. *Journal Of Geophysical Research-Oceans*, 113:–, 2008.

[134] R. A. Massom, S. E. Stammerjohn, R. C. Smith, M. J. Pook, R. A. Iannuzzi, N. Adams, D. G. Martinson, M. Vernet, W. R. Fraser, L. B. Quetin, R. M. Ross, Y. Massom, and H. R. Krouse. Extreme Anomalous Atmospheric Circulation in the West Antarctic Peninsula Region in Austral Spring and Summer 2001/02, and Its Profound Impact on Sea Ice and Biota*. *Journal Of Climate*, 19(15):3544–3571, 2006.

[135] M. A. McClintic, D. J. DeMaster, C. J. Thomas, and C. R. Smith. Testing the FOODBANCS hypothesis: Seasonal variations in near-bottom particle flux, bioturbation intensity, and deposit feeding based on Th-234 measurements. *Deep Sea Research Part II: Topical Studies in Oceanography*, 55(22-23):2425–2437, 2008.

[136] M. P. Meredith and J. C. King. Rapid climate change in the ocean west of the Antarctic Peninsula during the second half of the 20th century. *Geophysical Research Letters*, 32(19):L19604, 2005.

[137] M. P. Meredith, H. J. Venables, A. Clarke, H. W. Ducklow, M. Erickson, M. J. Leng, J. T. M. Lenaerts, and M. R. Van Den Broeke. The Freshwater System West of the Antarctic Peninsula: Spatial and Temporal Changes. *Journal Of Climate*, 26(5):1669–1684, Jan. 2013.

[138] B. G. Mitchell, E. A. Brody, O. Holm-Hansen, C. McClain, and J. Bishop. Light Limitation of Phytoplankton Biomass and Macronutrient Utilization in the Southern Ocean. *Limnology And Oceanography*, 36(8):1662–1677, Jan. 1991.

[139] B. G. Mitchell and O. Holm-Hansen. Observations of modeling of the Antartic phytoplankton crop in relation to mixing depth. *Deep Sea Research Part A. Oceanographic Research Papers*, 38(8-9):981–1007, Jan. 1991.

[140] M. Montes-Hugo, S. C. Doney, H. W. Ducklow, W. Fraser, D. Martinson, S. E. Stammerjohn, and O. Schofield. Recent Changes in Phytoplankton Communities Associated with Rapid Regional Climate Change Along the Western Antarctic Peninsula. *Science*, 323(5920):1470–1473, Mar. 2009.

[141] P. K. Munneke, M. R. van den Broeke, J. C. King, T. Gray, and C. H. Reijmer. Near-surface climate and surface energy budget of Larsen C ice shelf, Antarctic Peninsula. *Cryosphere*, 6(2):353–363, 2012.

[142] G. A. Nield, V. R. Barletta, A. Bordoni, M. A. King, P. L. Whitehouse, P. J. Clarke, E. Domack, T. A. Scambos, and E. Berthier. Rapid bedrock uplift in the Antarctic Peninsula explained by viscoelastic response to recent ice unloading. *Earth And Planetary Science Letters*, 397(0):32–41.

[143] D. Nowacek, A. Friedlaender, P. Halpin, E. Hazen, D. Johnston, A. Read, B. Espinasse, M. Zhou, and Y. Zhu. Super-Aggregations of Krill and Humpback Whales in Wilhelmina Bay, Antarctic Peninsula. *PLoS ONE*, 6(4):e19173 EP–, Apr. 2011.

[144] J. E. O'Reilly, S. Maritorena, B. G. Mitchell, D. A. Siegel, K. L. Carder, S. A. Garver, M. Kahru, and C. McClain. Ocean color chlorophyll algorithms for SeaWiFS. *Journal Of Geophysical Research-Oceans*, 103(C11):24937–24953, 1998.

[145] J. E. O'Reilly, S. Maritorena, D. A. Siegel, M. C. O'brien, D. A. Toole, B. G. Mitchell, M. Kahru, F. P. Chavez, P. Strutton, G. F. Cota, S. B. Hooker, C. R. McClain, K. L. Carder, F. E. Muller-Karger, L. Harding, A. Magnuson, D. Phinney, G. F. Moore, J. Aiken, K. R. Arrigo, R. Letelier, and M. Culver. Ocean Color Chlorophyll a Algorithms for SeaWiFS, OC2 and OC4: Version 4. *SeaWiFS Postlaunch Calibration and Validation Analyses*, 11(3):8–22, 2000.

[146] A. Orr, D. Cresswell, G. Marshall, J. Hunt, J. Sommeria, C. Wang, and M. Light. A 'low-level' explanation for the recent large warming trend over the western Antarctic Peninsula involving blocked winds and changes in zonal circulation. *Geophysical Research Letters*, 31(6):L06204, 2004.

[147] A. Orr, G. J. Marshall, J. C. R. Hunt, J. Sommeria, C.-G. Wang, N. P. M. van Lipzig, D. Cresswell, and J. C. King. Characteristics of summer airflow over the Antarctic Peninsula in response to recent strengthening of westerly circumpolar winds. *Journal of the Atmospheric Sciences*, 65(4):1396–1413, Apr. 2008.

[148] A. H. Orsi, G. C. Johnson, and J. L. Bullister. Circulation, mixing, and production of Antarctic Bottom Water. *Progress In Oceanography*, 43(1):55–109, Jan. 1999.

[149] L. S. Peck, D. K. A. Barnes, A. J. Cook, A. H. Fleming, and A. Clarke. Negative feedback in the cold: ice retreat produces new carbon sinks in Antarctica. *Global Change Biology*, 16(9):2614–2623, 2010.

[150] D. K. Perovich, J. A. Richter-Menge, K. F. Jones, and B. Light. Sunlight, water, and ice: Extreme Arctic sea ice melt during the summer of 2007. *Geophysical Research Letters*, 35(11):L11501, June 2008.

[151] C. Petrich, H. Eicken, J. Zhang, J. Krieger, Y. Fukamachi, and K. I. Ohshima. Coastal landfast sea ice decay and breakup in northern Alaska: Key processes and seasonal prediction. *Journal Of Geophysical Research-Oceans*, 117(C2):C02003, Jan. 2012.

[152] J. G. Powers, A. J. Monaghan, A. M. Cayette, D. H. Bromwich, Y.-H. Kuo, and K. W. Manning. Real-Time Mesoscale Modeling Over Antarctica: The Antarctic Mesoscale Prediction System*. *Bull. Amer. Meteor. Soc.*, 84(11):1533–1545, Nov. 2003.

[153] H. D. Pritchard, S. R. M. Ligtenberg, H. A. Fricker, D. G. Vaughan, M. R. van den Broeke, and L. Padman. Antarctic ice-sheet loss driven by basal melting of ice shelves. *Nature*, 484(7395):502–505, 2012.

[154] M. Rebesco, E. Domack, F. Zgur, C. Lavoie, A. Leventer, S. Brachfeld, V. Willmott, G. Halverson, M. Truffer, T. Scambos, J. Smith, and E. Pettit. Boundary condition of grounding lines prior to collapse, Larsen-B Ice Shelf, Antarctica. *Science*, 345(6202):1354–1358, Sept. 2014.

[155] A. C. Redfield. The biological control of chemical factors in the environment. *American Scientist*, 46(3):230A–221, Sept. 1958.

[156] N. Reuss and D. Conley. Effects of sediment storage conditions on pigment analyses. *Limnology And Oceanography-Methods*, 3:477–487, 2005.

[157] J. Reynolds. The distribution of mean annual temperatures in the Antarctic Peninsula. *British Antarctic Survey Bulletin*, 1981.

[158] E. Rignot, J. L. Bamber, M. R. Van Den Broeke, C. Davis, Y. Li, W. J. Van De Berg, and E. Van Meijgaard. Recent Antarctic ice mass loss from radar interferometry and regional climate modelling. *Nature Geoscience*, 1(2):106–110, 2008.

[159] E. Rignot, G. Casassa, P. Gogineni, W. Krabill, A. Rivera, and R. Thomas. Accelerated ice discharge from the Antarctic Peninsula following the collapse of Larsen B ice shelf. *Geophysical Research Letters*, 31(18):L18401, 2004.

[160] E. Rignot, J. Mouginot, M. Morlighem, H. Seroussi, and B. Scheuchl. Widespread, rapid grounding line retreat of Pine Island, Thwaites, Smith, and Kohler glaciers, West Antarctica, from 1992 to 2011. *Geophysical Research Letters*, 41(10):3502–3509, 2014.

[161] H. Rott, W. Rack, P. Skvarca, and H. De Angelis. Northern Larsen Ice Shelf, Antarctica: further retreat after collapse. In *Annals of Glaciology, Vol 34, 2002*, pages 277–282. Innsbruck Univ, Inst Meteorol & Geophys, A-6020 Innsbruck, Austria, 2002.

[162] H. Rott, P. Skvarca, and T. Nagler. Rapid collapse of northern Larsen Ice Shelf, Antarctica. *Science*, 271(5250):788–792, 1996.

[163] C. D. Rye, A. C. Naveira Garabato, P. R. Holland, M. P. Meredith, A. J. George Nurser, C. W. Hughes, A. C. Coward, and D. J. Webb. Rapid sea-level rise along the Antarctic margins in response to increased glacial discharge. 7(10):732–735, Aug. 2014.

[164] B. T. Saenz and K. R. Arrigo. Annual primary production in Antarctic sea ice during 2005-2006 from a sea ice state estimate. *Journal Of Geophysical Research-Oceans*, 119(6):3645–3678, June 2014.

[165] E. Sakshaug, D. Slagstad, and O. Holm-Hansen. Factors controlling the development of phytoplankton blooms in the Antarctic Ocean — a mathematical model. *Marine Chemistry*, 35(1-4):259–271, Nov. 1991.

[166] E. Sane, E. Isla, M. Angeles Barcena, and D. J. DeMaster. A Shift in the Biogenic Silica of Sediment in the Larsen B Continental Shelf, Off the Eastern Antarctic Peninsula, Resulting from Climate Change. *PLoS ONE*, 8(1), 2013.

[167] E. Sane, E. Isla, D. Gerdes, A. Montiel, and J. M. Gili. Benthic macrofauna assemblages and biochemical properties of sediments in two Antarctic regions differently affected by climate change. *Continental Shelf Research*, 35:53–63, 2012.

[168] E. Sane, E. Isla, A. Gremare, J. Gutt, G. Vetion, and D. J. DeMaster. Pigments in sediments beneath recently collapsed ice shelves: The case of Larsen A and B shelves, Antarctic Peninsula. *Journal Of Sea Research*, 65(1):94–102, 2011.

[169] E. Sane, E. Isla, A. M. Pruski, M. A. Barcena, G. Vetion, and D. DeMaster. Diatom valve distribution and sedimentary fatty acid composition in Larsen Bay, Eastern Antarctica Peninsula. *Continental Shelf Research*, 31(11):1161–1168, 2011.

[170] J. L. Sarmiento, R. Slater, R. Barber, L. Bopp, S. C. Doney, A. C. Hirst, J. Kleypas, R. Matear, U. Mikolajewicz, P. Monfray, V. Soldatov, S. A. Spall, and R. Stouffer. Response of ocean ecosystems to climate warming. *Global Biogeochemical Cycles*, 18(3):GB3003, 2004.

[171] T. Scambos, C. Hulbe, and M. Fahnestock. ClimateâĂŘinduced ice shelf disintegration in the Antarctic Peninsula. *Antarctic Peninsula Climate Variability: Historical and Paleoenvironmental Perspectives*, pages 79–92, 2003.

[172] T. A. Scambos. Climate, Sea Ice, and Ocean Precursors to the Larsen Ice Shelf Disintegrations. Dec. 2014.

[173] T. A. Scambos, E. Berthier, and C. A. Shuman. The triggering of subglacial lake drainage during rapid glacier drawdown: Crane Glacier, Antarctic Peninsula. *Annals of Glaciology*, 52(59):74–82, Dec. 2011.

[174] T. A. Scambos, J. A. Bohlander, C. A. Shuman, and P. Skvarca. Glacier acceleration and thinning after ice shelf collapse in the Larsen B embayment, Antarctica. *Geophysical Research Letters*, 31(18):L18402–, Jan. 2004.

[175] T. A. Scambos, T. M. Haran, M. A. Fahnestock, T. H. Painter, and J. Bohlander. MODIS-based Mosaic of Antarctica (MOA) data sets: Continent-wide surface morphology and snow grain size. *Remote Sensing Of Environment*, 111(2-3):242–257, 2007.

[176] T. A. Scambos, C. Hulbe, M. Fahnestock, and J. Bohlander. The link between climate warming and break-up of ice shelves in the Antarctic Peninsula. *Journal Of Glaciology*, 46(154):516–530, Aug. 2000.

[177] T. A. Scambos, R. Ross, T. Haran, R. Bauer, D. G. Ainley, K. W. Seo, M. D. Keyser, A. Behar, and D. R. MacAyeal. A camera and multisensor automated station design for polar physical and biological systems monitoring: AMIGOS. *Journal Of Glaciology*, 59(214):303–314, Apr. 2013.

[178] O. Schofield, H. W. Ducklow, D. G. Martinson, M. P. Meredith, M. A. Moline, and W. R. Fraser. How Do Polar Marine Ecosystems Respond to Rapid Climate Change? *Science*, 328(5985):1520–1523, Jan. 2010.

[179] W. Schwerdtfeger. The Effect of the Antarctic Peninsula on the Temperature Regime of the Weddell Sea. *Monthly Weather Review*, 103(1):45–51, Jan. 1975.

[180] W. Schwerdtfeger. Meteorological aspects of the drift of ice from the Weddell Sea toward the mid-latitude westerlies. *Journal of Geophysical Research*, 84(C10):6321, 1979.

[181] P. N. Sedwick and G. R. DiTullio. Regulation of algal blooms in Antarctic Shelf Waters by the release of iron from melting sea ice. *Geophysical Research Letters*, 24(20):2515–2518, Dec. 1997.

[182] P. N. Sedwick, G. R. DiTullio, and D. J. Mackey. Iron and manganese in the Ross Sea, Antarctica: Seasonal iron limitation in Antarctic shelf waters. *Journal Of Geophysical Research-Oceans*, 105(C5):11321–11336, Jan. 2000.

[183] E. H. Shadwick, S. R. Rintoul, B. Tilbrook, G. D. Williams, N. Young, A. D. Fraser, H. Marchant, J. Smith, and T. Tamura. Glacier tongue calving reduced dense water formation and enhanced carbon uptake. *Geophysical Research Letters*, 40(5):904–909, Jan. 2013.

[184] C. A. Shuman, E. Berthier, and T. A. Scambos. 2001-2009 elevation and mass losses in the Larsen A and B embayments, Antarctic Peninsula. *Journal Of Glaciology*, 57(204):737–754, 2011.

[185] D. A. Siegel, E. Fields, and K. O. Buesseler. A bottom-up view of the biological pump: Modeling source funnels above ocean sediment traps. *Deep Sea Research Part I: Oceanographic Research Papers*, 55(1):108–127, Jan. 2008.

[186] P. Skvarca, W. Rack, and H. Rott. 34 year satellite time series to monitor characteristics, extent and dynamics of Larsen B Ice Shelf, Antarctic Peninsula. *Annals of Glaciology*, 29(1):255–260, June 1999.

[187] P. Skvarca, W. Rack, H. Rott, and T. I. Donángelo. Climatic trend and the retreat and disintegration of ice shelves on the Antarctic Peninsula: an overview. *Polar Research*, 18(2):151–157, Jan. 1999.

[188] V. Smetacek and S. Nicol. Polar ocean ecosystems in a changing world. *Nature*, 437(7057):362–368, 2005.

[189] C. R. Smith, S. Mincks, and D. J. DeMaster. A synthesis of bentho-pelagic coupling on the Antarctic shelf: Food banks, ecosystem inertia and global climate change. *Deep Sea Research Part II: Topical Studies in Oceanography*, 53(8-10):875–894, 2006.

[190] C. R. Smith, S. Mincks, and D. J. DeMaster. The FOODBANCS project: Introduction and sinking fluxes of organic carbon, chlorophyll-a and phytodetritus on the

western Antarctic Peninsula continental shelf. *Deep Sea Research Part II: Topical Studies in Oceanography*, 55(22-23):2404–2414, 2008.

[191] R. Smith, K. Baker, W. Fraser, E. Hofmann, D. Karl, J. Klink, L. Quentin, B. Prezelin, R. Ross, W. Trivelpiece, and M. Vernet. The Palmer LTER: A Long-Term Ecological Research Program at Palmer Station, Antarctica. *Oceanography*, 8(3):77–86, 1995.

[192] R. C. Smith, D. Ainley, K. Baker, E. Domack, S. Emslie, B. Fraser, J. Kennett, A. Leventer, E. Mosley-Thompson, S. Stammerjohn, and M. Vernet. Marine ecosystem sensitivity to climate change. *BioScience*, 49(5):393–404, 1999.

[193] R. C. Smith, H. M. Dierssen, and M. Vernet. Phytoplankton Biomass and Productivity in the Western Antarctic Peninsula Region. In *Foundations for Ecological Research West of the Antarctic Peninsula*, pages 333–356. American Geophysical Union, Washington, D. C., 1996.

[194] S. D. Smith, R. D. Muench, and C. H. Pease. Polynyas and leads: An overview of physical processes and environment. *Journal of Geophysical Research*, 95(C6):9461–9479, Jan. 1990.

[195] W. O. Smith, V. Asper, S. Tozzi, X. Liu, and S. E. Stammerjohn. Surface layer variability in the Ross Sea, Antarctica as assessed by in situ fluorescence measurements. *Progress In Oceanography*, 88(1–4):28–45, Jan. 2011.

[196] W. O. Smith and D. M. Nelson. Phytoplankton Bloom Produced by a Receding Ice Edge in the Ross Sea: Spatial Coherence with the Density Field. *Science*, 227(4683):163–166, Jan. 1985.

[197] W. O. Smith, Jr and D. M. Nelson. Importance of Ice Edge Phytoplankton Production in the Southern Ocean. *BioScience*, 36(4):251–257, Apr. 1986.

[198] W. O. Smith, Jr and D. M. Nelson. Phytoplankton Growth and New Production in the Weddell Sea Marginal Ice Zone in the Austral Spring and Autumn. *Limnology And Oceanography*, 35(4):809–821, Jan. 1990.

[199] J. C. Speirs, H. A. McGowan, D. F. Steinhoff, and D. H. Bromwich. Regional climate variability driven by foehn winds in the McMurdo Dry Valleys, Antarctica. *International Journal Of Climatology*, 33(4):945–958, Jan. 2013.

[200] J. C. Speirs, D. F. Steinhoff, H. A. McGowan, D. H. Bromwich, and A. J. Monaghan. Foehn Winds in the McMurdo Dry Valleys, Antarctica: The Origin of Extreme Warming Events. *Journal Of Climate*, 23(13):3577–3598, 2010.

[201] G. Spreen, L. Kaleschke, and G. Heygster. Sea ice remote sensing using AMSR-E 89-GHz channels. *Journal Of Geophysical Research-Oceans*, 113(C2):C02S03, 2008.

[202] S. Stammerjohn, R. Massom, D. Rind, and D. Martinson. Regions of rapid sea ice change: An inter-hemispheric seasonal comparison. *Geophysical Research Letters*, 39(6):L06501–, Jan. 2012.

[203] S. E. Stammerjohn, D. G. Martinson, R. C. Smith, and R. A. Iannuzzi. Sea ice in the western Antarctic Peninsula region: Spatio-temporal variability from ecological and climate change perspectives. *Deep Sea Research Part II: Topical Studies in Oceanography*, 55:2041–2058, 2008.

[204] S. E. Stammerjohn, D. G. Martinson, R. C. Smith, X. Yuan, and D. Rind. Trends in Antarctic annual sea ice retreat and advance and their relation to El Nino-Southern Oscillation and Southern Annular Mode variability. *Journal Of Geophysical Research-Oceans*, 113:–, 2008.

[205] T. P. Stanton, W. J. Shaw, M. Truffer, H. F. J. Corr, L. E. Peters, K. L. Riverman, R. Bindschadler, D. M. Holland, and S. Anandakrishnan. Channelized Ice Melting in the Ocean Boundary Layer Beneath Pine Island Glacier, Antarctica. *Science*, 341(6151):1236–1239, Sept. 2013.

[206] E. J. Steig, D. P. Schneider, S. D. Rutherford, M. E. Mann, J. C. Comiso, and D. T. Shindell. Warming of the Antarctic ice-sheet surface since the 1957 International Geophysical Year. *Nature*, 457(7228):459–462, Jan. 2009.

[207] D. F. Steinhoff, D. H. Bromwich, and A. Monaghan. Dynamics of the Foehn Mechanism in the McMurdo Dry Valleys of Antarctica from Polar WRF. *Quarterly Journal of the Royal Meteorological Society*, 139(675):1615–1631, 2013.

[208] D. F. Steinhoff, D. H. Bromwich, J. C. Speirs, H. A. McGowan, and A. J. Monaghan. Austral summer foehn winds over the McMurdo dry valleys of Antarctica from Polar WRF. *Quarterly Journal of the Royal Meteorological Society*, 140(683):1825–1837, 2014.

[209] M. Stibal, M. Sabacka, and J. Zarsky. Biological processes on glacier and ice sheet surfaces. *Nature Geoscience*, 5(11):771–774, Nov. 2012.

[210] H. Sverdrup. On conditions for the vernal blooming of phytoplankton. *J. Cons. Int. Explor. Mer*, 18(3):287–295, 1953.

[211] T. Takahashi, S. C. Sutherland, C. Sweeney, A. Poisson, N. Metzl, B. Tilbrook, N. Bates, R. Wanninkhof, R. A. Feely, C. Sabine, J. Olafsson, and Y. Nojiri. Global sea–air CO2 flux based on climatological surface ocean pCO2, and seasonal biological and temperature effects. *Deep Sea Research Part II: Topical Studies in Oceanography*, 49(9-10):1601–1622, Jan. 2002.

[212] T. Takahashi, S. C. Sutherland, R. Wanninkhof, C. Sweeney, R. A. Feely, D. W. Chipman, B. Hales, G. Friederich, F. Chavez, C. Sabine, A. Watson, D. C. E.

Bakker, U. Schuster, N. Metzl, H. Yoshikawa-Inoue, M. Ishii, T. Midorikawa, Y. Nojiri, A. Koertzinger, T. Steinhoff, M. Hoppema, J. Olafsson, T. S. Arnarson, B. Tilbrook, T. Johannessen, A. Olsen, R. Bellerby, C. S. Wong, B. Delille, N. R. Bates, and H. J. W. de Baar. Climatological mean and decadal change in surface ocean pCO(2), and net sea-air CO2 flux over the global oceans. *Deep Sea Research Part II: Topical Studies in Oceanography*, 56(8-10):554–577, 2009.

[213] D. W. J. Thompson and S. Solomon. Interpretation of Recent Southern Hemisphere Climate Change. *Science*, 296(5569):895–899, May 2002.

[214] J. L. Tison, A. Worby, B. Delille, F. Brabant, S. Papadimitriou, D. Thomas, J. de Jong, D. Lannuzel, and C. Haas. Temporal evolution of decaying summer first-year sea ice in the Western Weddell Sea, Antarctica. *Deep Sea Research Part II: Topical Studies in Oceanography*, 55(8-9):975–987, Apr. 2008.

[215] P. Tréguer and G. Jacques. Dynamics of nutrients and phytoplankton, and fluxes of carbon, nitrogen and silicon in the Antarctic Ocean. *Polar Biology*, 12(2):149–162, 1992.

[216] J. Turner, G. J. Marshall, and T. A. Lachlan-Cope. Analysis of synoptic-scale low pressure systems within the Antarctic Peninsula sector of the circumpolar trough. *International Journal Of Climatology*, 18(3):253–280, Mar. 1998.

[217] R. E. Turner, N. Qureshi, N. N. Rabalais, Q. Dortch, D. Justic, R. F. Shaw, and J. Cope. Fluctuating silicate:nitrate ratios and coastal plankton food webs. *Proceedings of the National Academy of Sciences*, 95(22):13048–13051, Oct. 1998.

[218] J. Uitz, H. Claustre, B. Gentili, and D. Stramski. Phytoplankton class-specific primary production in the world's oceans: Seasonal and interannual variability from satellite observations. *Global Biogeochemical Cycles*, 24(3):n/a–n/a, Aug. 2010.

[219] R. D. Vaillancourt, R. N. Sambrotto, S. Green, and A. Matsuda. Phytoplankton biomass and photosynthetic competency in the summertime Mertz Glacier Region of East Antarctica. *Deep Sea Research Part II: Topical Studies in Oceanography*, 50(8-9):1415–1440, 2003.

[220] M. van den Broeke. Strong surface melting preceded collapse of Antarctic Peninsula ice shelf. *Geophysical Research Letters*, 32(12):L12815–, Jan. 2005.

[221] M. van den Broeke, C. Reijmer, and R. van de Wal. Surface radiation balance in Antarctica as measured with automatic weather stations. *Journal Of Geophysical Research-Solid Earth*, 109(D9):D09103, Jan. 2004.

[222] N. P. M. van Lipzig, G. J. Marshall, A. Orr, and J. C. King. The relationship between the southern hemisphere annular mode and Antarctic Peninsula summer temperatures: Analysis of a high-resolution model climatology. *Journal Of Climate*, 21(8):1649–1668, 2008.

[223] D. Vaughan, G. Marshall, W. Connolley, C. Parkinson, R. Mulvaney, D. Hodgson, J. King, C. Pudsey, and J. Turner. Recent rapid regional climate warming on the Antarctic Peninsula. *Climatic Change*, 60(3):243–274, 2003.

[224] D. G. Vaughan and C. S. M. Doake. Recent atmospheric warming and retreat of ice shelves on the Antarctic Peninsula. *Nature*, 379(6563):328–331, Jan. 1996.

[225] M. Vernet, W. A. Kozlowski, L. R. Yarmey, A. T. Lowe, R. M. Ross, L. B. Quetin, and C. H. Fritsen. Primary production throughout austral fall, during a time of decreasing daylength in the western Antarctic Peninsula. *Marine Ecology Progress Series*, 452:45–61, 2012.

[226] M. Vernet, D. Martinson, R. Iannuzzi, S. Stammerjohn, W. Kozlowski, K. Sines, R. Smith, and I. Garibotti. Primary production within the sea-ice zone west of the Antarctic Peninsula: I-Sea ice, summer mixed layer, and irradiance. *Deep Sea Research Part II: Topical Studies in Oceanography*, 55:2068–2085, 2008.

[227] J. J. Walsh, D. A. Dieterle, and J. Lenes. A numerical analysis of carbon dynamics of the Southern Ocean phytoplankton community: the roles of light and grazing in effecting both sequestration of atmospheric CO2 and food availability to larval krill. *Deep Sea Research Part I: Oceanographic Research Papers*, 48(1):1–48, Jan. 2001.

[228] S. Wang and J. K. Moore. Variability of primary production and air-sea CO2 flux in the Southern Ocean. *Global Biogeochemical Cycles*, 26:–, 2012.

[229] W. F. Weeks. *On Sea Ice*. University of Alaska Press, Fairbanks, AK, Oct. 2010.

[230] D. Yi, H. J. Zwally, and J. W. Robbins. ICESat observations of seasonal and interannual variations of sea-ice freeboard and estimated thickness in the Weddell Sea, Antarctica (2003-2009). *Annals of Glaciology*, 52(57):43–51, 2011.

[231] X. Yuan. ENSO-related impacts on Antarctic sea ice: a synthesis of phenomenon and mechanisms. *Antarctic Science*, 16(4):415–425, 2004.

[232] V. Zagorodnov, O. Nagornov, T. A. Scambos, A. Muto, E. Mosley-Thompson, E. C. Pettit, and S. Tyuflin. Borehole temperatures reveal details of 20th century warming at Bruce Plateau, Antarctic Peninsula. *The Cryosphere Discussions*, 5(6):3053–3084, 2011.